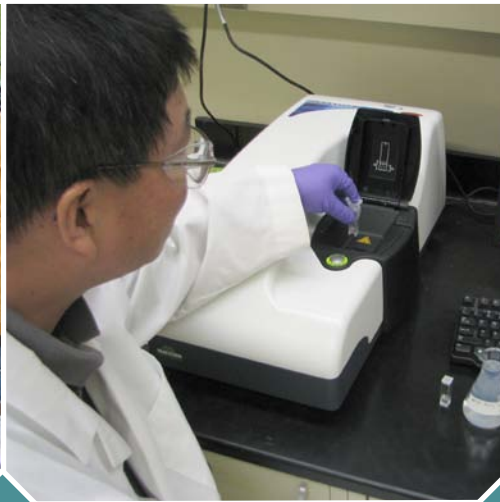


Identification and Characterization Methods for Reactive Minerals Responsible for Natural Attenuation of Chlorinated Organic Compounds in Ground Water



Identification and Characterization Methods for Reactive Minerals Responsible for Natural Attenuation of Chlorinated Organic Compounds in Ground Water

Yongtian He

National Research Council Research Associate

Chunming Su

John Wilson

Rick Wilkin

Cherri Adair

Tony Lee

*U.S. EPA/ORD Ground Water and Ecosystems
Restoration Division*

Paul Bradley

*U.S.G.S. South Carolina Water Science Center in
Columbia, SC*

Mark Ferrey

Minnesota Pollution Control Agency

Notice

The U.S. Environmental Protection Agency through its Office of Research and Development funded portions of the research described here. Mention of trade names and commercial products does not constitute endorsement or recommendation for use. All research projects making conclusions and recommendations based on environmentally related measurements and funded by the Environmental Protection Agency are required to participate in the Agency Quality Assurance Program. This project was conducted under a Quality Assurance Project Plan for Task 3674 and 19421. Work performed by U.S. EPA employees or by the U.S. EPA on-site analytical contractor followed procedures specified in these plans without exception. Information on the plans and documentation of the quality assurance activities and results are available from Cherri Adair or John Wilson.

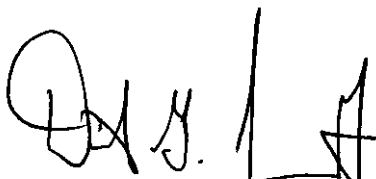
Foreword

The U.S. Environmental Protection Agency (EPA) is charged by Congress with protecting the Nation's land, air, and water resources. Under a mandate of national environmental laws, the Agency strives to formulate and implement actions leading to a compatible balance between human activities and the ability of natural systems to support and nurture life. To meet this mandate, EPA's research program is providing data and technical support for solving environmental problems today and building a science knowledge base necessary to manage our ecological resources wisely, understand how pollutants affect our health, and prevent or reduce environmental risks in the future.

The National Risk Management Research Laboratory (NRMRL) is the Agency's center for investigation of technological and management approaches for preventing and reducing risks from pollution that threatens human health and the environment. The focus of the Laboratory's research program is on methods and their cost-effectiveness for prevention and control of pollution to air, land, water, and subsurface resources; protection of water quality in public water systems; remediation of contaminated sites, sediments and ground water; prevention and control of indoor air pollution; and restoration of ecosystems. NRMRL collaborates with both public and private sector partners to foster technologies that reduce the cost of compliance and to anticipate emerging problems. NRMRL's research provides solutions to environmental problems by: developing and promoting technologies that protect and improve the environment; advancing scientific and engineering information to support regulatory and policy decisions; and providing the technical support and information transfer to ensure implementation of environmental regulations and strategies at the national, state, and community levels.

Monitored Natural Attenuation is widely used by U.S. EPA to manage risk associated with hazardous organic contaminants in soils and ground water. The Agency prefers attenuation mechanisms that destroy contaminants. As a result, site characterization at hazardous waste sites has focused on biological degradation of organic contaminants because biodegradation was the only mechanism that was widely acknowledged to destroy organic contaminants. In recent years it has become increasingly apparent that abiotic degradation mechanisms can make a substantial contribution to natural attenuation of a variety of halogenated organic compounds in soil, sediment and ground water.

This report provides a technical basis to evaluate the contribution of abiotic processes to MNA of halogenated organic compounds. The report reviews the current knowledge of the rate of transformation of halogenated organic compounds that is associated with reactive mineral phases in soil and aquifer sediment. The report also reviews the known transformation products.



David G. Jewett, Acting Director
Ground Water and Ecosystems Restoration Division
National Risk Management Research Laboratory

Contents

Notice	ii
Foreword	iii
Acknowledgements	xiii
Executive Summary	xv
Evolution of Applications for Abiotic Processes.	xvi
Important Reactive Iron Minerals.	xvii
Iron Sulfides.	xviii
Magnetite.	xix
Green Rust.	xx
Adsorbed Fe(II).	xx
Phyllosilicate Clays.	xxi
Iron Carbonates.	xxi
1.0 Formation and Stability of Reactive Iron and Sulfur Minerals Under Various Geochemical Conditions	1
1.1 Formation Processes of Reactive Minerals	3
1.1.1 Formation of Pyrite and Mackinawite	4
1.1.2 Formation of Siderite	6
1.1.3 Formation of Green Rusts	6
1.1.4 Formation and Transformation of Goethite and Ferrihydrite.	7
1.2 Geochemical Modeling.	7
2.0 Iron Sulfide Minerals	11
2.1 Applications of Iron Sulfide Minerals	11
2.2 Abiotic Transformation of Chlorinated Ethylenes	12
2.2.1 Transformation Products	12
2.2.2 Rates of Degradation on Iron Sulfide Minerals	15
2.2.3 Factors Affecting Degradation	15
2.2.3.1 Effect of Freeze Drying FeS on Rate Constants for Transformation of TCE	15
2.2.3.2 Effect of pH on the Rate of Transformation of TCE on FeS	16
2.2.3.3 Organic Molecules.	17
2.2.3.4 Metal Ions	17
2.2.3.5 Dissolved Oxygen (DO)	17
2.2.4 Degradation Mechanisms.	17
2.3 Abiotic Transformation of Chlorinated Alkanes	18
2.3.1 Degradation Products	18
2.3.2 Rates of Degradation on Iron Sulfide Minerals	19
2.3.3 Conditions Affecting Degradation	20
2.3.3.1 pH	20
2.3.3.2 Metals	21
2.3.3.3 Sulfide	21
2.3.3.4 Organic Molecules.	21
2.4 Abiotic Transformation of Chlorinated Methanes	22
2.4.1 Degradation Products	22
2.4.2 Rate Constants	22
2.4.3 Conditions Affecting Reactivity	24

2.4.3.1	pH	24
2.4.3.2	Sulfide	24
2.4.3.3	Organic Compounds	25
2.5	Abiotic Transformation of the Brominated Ethane EDB	25
2.5.1	Degradation Products	25
2.5.2	Rate Constants	25
2.5.3	Conditions That Affect Degradation	26
2.5.3.1	Sulfate and Sulfide	26
2.5.3.2	pH	26
2.6	Formation, Transformations, and Reactivity of Iron Sulfides	26
2.6.1	FeS Mineralogy and Reactivity	26
2.6.2	Formation of FeS Minerals	27
2.6.3	Transformation of FeS Minerals	28
2.6.4	Effect of Transformations of Iron Sulfides on Reactivity	29
2.6.5	Effect of Transition Metals on Degradation	30
2.7	Environmental Implications	30
2.7.1	Geochemical Parameters	30
2.7.2	Differentiating Biotic and Abiotic Degradation	31
2.7.3	Geochemical Modeling	31
3.0	Magnetite	33
3.1	Structure of Magnetite	33
3.2	Transformation Products of Chlorinated Organic Compounds on Magnetite	33
3.3	Effect of Properties of Magnetite on Rate of Transformation	34
3.3.1	Effect of Particle Size and Surface Area	34
3.3.2	Effect of pH	35
3.3.3	Effect of Fe ²⁺ Sorbed to the Surface of Magnetite	35
3.4	Rates of Transformation of Chlorinated Organic Compounds on Magnetite	36
3.4.1	Degradation of <i>cis</i> -DCE and Vinyl Chloride on Magnetite	36
3.4.2	Degradation of PCE and TCE on Magnetite	40
3.4.3	Degradation of Carbon Tetrachloride on Magnetite	42
3.5	Rates of Transformation Normalized to Magnetic Susceptibility	45
4.0	Transformation of Chlorinated Hydrocarbons by Green Rusts	47
4.1	Structure and Reactivity of Green Rusts	47
4.1.1	Chemical Composition and Crystal Structure of Green Rusts	47
4.1.2	Chemical Reactivity of Green Rusts	48
4.1.3	Abiotic Degradation of PCE and TCE by Green Rusts	49
4.1.3.1	Reports of Degradation of PCE and TCE in the Literature	49
4.1.3.2	Degradation of TCE in Studies Performed at Kerr Center (U.S. EPA)	49
4.1.4	Abiotic Degradation of Chlorinated Methanes and Alkanes by Green Rusts	51
4.1.4.1	Reports of Degradation of Chlorinated Methanes and Alkanes in the Literature	51
4.1.4.2	Degradation of Carbon Tetrachloride in the EPA Study	52
4.1.4.3	Reports of Degradation of Chlorinated Alkanes in the Literature	53
4.2	Occurrence and Determination of Green Rusts	55
4.2.1	Geochemical Conditions that Favor Green Rust Formation	55
4.2.2	Structural Stability of Carbonate Green Rust	56
5.0	Phyllosilicate Clays	59
5.1	Structural Iron in Phyllosilicate Clays	59
5.2	Degradation Processes on Phyllosilicate Clays	59
5.3	Rate Constants for Degradation of Chlorinated Alkenes	60
5.4	Rate Constants for Degradation of Carbon Tetrachloride and Chlorinated Alkanes	60

5.5	Effect of Sorbed Iron (II) on the Rate of Degradation	61
5.6	Extrapolation of Rate Constants to the Field	61
6.0	Methods to Characterize Sediments and Organic Contaminants	67
6.1	Isotopic Fractionation to Characterize Degradation of Organic Compounds	67
6.1.1	Isotopic Fractionation of Carbon Tetrachloride on Various Iron Minerals	67
6.1.2	Isotopic Fractionation of PCE and TCE on Iron(II) Monosulfide	68
6.1.3	Isotopic Fractionation of EDB on Iron(II) Monosulfide	68
6.1.4	Isotopic Fractionation of TCE on Green Rust	69
6.1.5	Isotopic Fractionation of TCE and <i>cis</i> -DCE on Magnetite	69
6.1.6	Isotopic Fractionation of Chlorinated Alkanes on Phyllosilicate Clay	70
6.2	Methods to Estimate the Quantity of Reactive Minerals	70
6.2.1	Characterization by Chemical Extraction Methods	71
6.2.1.1	Sulfur Minerals in Soil and Sediments	71
6.2.1.2	Interferences with Chemical Extraction Methods for Sulfur Minerals	72
6.2.2	Characterization of Chemical Identify by Spectroscopy or Diffraction	73
6.2.2.1	Characterization by X-ray Diffraction (XRD)	73
6.2.2.2	Characterization of Green Rusts by X-ray Diffraction (XRD) and Atomic Force Microscopy (AFM)	74
6.2.2.3	Characterization of Green Rusts by Infrared Spectroscopy (IR)	76
6.2.3	Estimating Magnetite in Sediment from Magnetic Susceptibility	76
6.3	Methods to Determine Oxidation Status	78
6.3.1	Characterization of Green Rusts by Mössbauer Spectroscopy	78
6.3.2	Characterization of Green Rust by X-ray Adsorption Near Edge Spectroscopy (XANES)	80
6.4	Methods to Estimate the Specific Surface Area of Minerals	82
6.4.1	Surface Area from Peak Broadening during X-ray Diffraction	82
6.4.2	Surface Area from Electron Microscopy	82
6.4.3	Characterization of Green Rusts by Scanning/Transmission Electron Microscopy	83
6.5	Collection and Handling of Samples	84
7.0	Recommendations for Future Research	85
7.1	Further Explore the Role of Phyllosilicate Clays	85
7.2	Reexamine the Role of Pyrite	85
7.3	Determine if Geochemical Models Can Be a Useful Surrogate to Predict the Rates of Abiotic Degradation at Field Scale	85
7.4	Use Geochemical Models to Improve Estimates of Degradation on Mineral Surfaces	85
7.5	Characterize Isotopic Fractionation of <i>cis</i> -DCE and Vinyl Chloride on Reactive Minerals	85
7.6	Characterize the Role of Manganese Oxides	86
8.0	References	87
Appendix A	Iron Sulfides	101
A.1	Experimental Details Related to TCE Degradation by FeS	101
A.2	Experimental Details Related to EDB Degradation by FeS	102
Appendix B	Magnetite	103
B.1	Building 102 Site and Site A on the TCAAP, North of St. Paul, Minnesota	103
B.2	Baytown Superfund Site, Minnesota	108
B.3	Thermo-Chem Site, East of Muskegon, Michigan	109
B.4	Products of Degradation of <i>cis</i> -DCE in Sediment from TCAAP Minnesota Site	111
B.5	Removal of Vinyl Chloride in Sediment from TCAAP Minnesota Site	112
Appendix C	Materials and Methods for Laboratory Studies of Abiotic Transformation of TCE and Carbon Tetrachloride by Green Rusts	113

Appendix D Quality Assurance Documentation	115
D.1 Analysis of Halogenated Organic Compounds in Water Samples	115
D.2 Analysis of Ratio of Stable Isotopes of Carbon in TCE and cis-DCE	119
D.3 Analysis of Total Iron in Sediment	122
D.4 Analysis of Sodium, Potassium, Calcium, Magnesium, and Iron in Water Samples	122
D.5 Analysis of Sulfate and Chloride in Water Samples	124
D.6 Analysis of Sulfide in Water Samples	124
D.7 Determination of Magnetic Susceptibility	124
D.8 Scintillation Counting	125

Figures

Figure 1.1. Mineral stability diagrams: a) Eh versus $\log a \text{H}_2\text{S}$ showing stability fields for goethite, magnetite, carbonate green rust, siderite, mackinawite, and pyrite ($\text{Fe}=10^{-4}$, $\text{C}=10^{-3}$, $\text{pH}=7.5$, hematite suppressed); b) Eh versus $\log a \text{HCO}_3^-$ showing stability fields for goethite, magnetite, carbonate green rust, and siderite ($\text{Fe}=10^{-4}$, $\text{pH}=7.5$, hematite suppressed).	4
Figure 1.2. Ternary diagram showing the importance of controlling factors on iron sulfide formation in natural aquifers and biowalls.	5
Figure 1.3. Saturation indices (SI) for a) disordered mackinawite and b) crystalline mackinawite as a function of pH and time (ground water from the biowall at OU-1 on Altus AFB, OK).	10
Figure 2.1. TCE degradation by chemically synthesized FeS at pH 7.2.	16
Figure 2.2. Effect of pH on the rate of TCE degradation on chemically synthesized FeS. The data series Not freeze dried [2] and Freeze dried [2] repeat data from Figure 2.1.	16
Figure 2.3. EDB degradation by FeS at pH 7.2.	26
Figure 2.4. Effect of pH on the first order rate constant for EDB degradation by FeS. The rate constant is normalized to the concentration of FeS in suspension.	26
Figure 3.1. Effect of solution pH on the rate constant for degradation of carbon tetrachloride on the surface of magnetite.	35
Figure 3.2. Effect of pH on the solution concentrations of Fe^{2+} in equilibrium with magnetite.	36
Figure 3.3. Sorption isotherms for Fe^{2+} on the surface of magnetite.	36
Figure 3.4. Removal of <i>cis</i> -DCE in aquifer sediment containing magnetite.	37
Figure 3.5. The surface area specific rate of degradation of <i>cis</i> -DCE on magnetite can explain the removal of <i>cis</i> -DCE in sediment from the TCAAP.	38
Figure 4.1. The crystal structure of green rust compounds consists of layers of $\text{Fe}(\text{II})(\text{OH})_6$ in which some of the $\text{Fe}(\text{II})$ is replaced by $\text{Fe}(\text{III})$	47
Figure 4.2. X-ray diffraction pattern of freshly synthesized carbonate green rust and sulfate green rust (less than 24 hours after synthesis) scanned as glycerol smears.	48
Figure 4.3. Removal of TCE in the presence of carbonate green rust as a function of reaction time, pH, and excess dissolved $\text{Fe}(\text{II})$	50
Figure 4.4. Removal of TCE in the presence of sulfate green rust as a function of reaction time with and without a 0.05 M pH 8 Trizma buffer.	50
Figure 4.5. Removal of TCE in the presence of sulfate green rust as a function of reaction time, concentration of added CuSO_4 , and presence or absence of 0.05 M Trizma buffer.	51
Figure 4.6. Removal of carbon tetrachloride in the presence of sulfate green rust as a function of reaction time and pH.	53
Figure 4.7. Proposed pathways for the reduction of chlorinated ethanes in aqueous suspensions of green rusts and in green rust suspensions spiked with $\text{Ag}(\text{I})$ (AgGR) or $\text{Cu}(\text{II})$ (CuGR); however, some elements of the pathways shown are not relevant to all experimental systems.	54
Figure 4.8. Adsorption of the phosphate on the lateral $\{10\bar{1}0\}$ face of the $\text{GR}(\text{CO}_3^{2-})$ crystal that stabilizes it (From Bocher et al., 2004).	57

Figure 6.1. Fractionation of stable isotopes of carbon during abiotic degradation of TCE in aquifer sediment containing magnetite (site at Building 102 at TCAAP).	69
Figure 6.2. Fractionation of stable isotopes of carbon during abiotic degradation of <i>cis</i> -DCE in aquifer sediment containing magnetite.	70
Figure 6.3. Powder X-ray diffraction scans of mixtures of magnetite and quartz.	74
Figure 6.4. Blow-up of the 2-theta region from 44 to 48°, showing the most intense diffraction peak for magnetite at 45.2°.	74
Figure 6.5. Relationship between the mass magnetic susceptibility of a sediment sample and the content of magnetic materials.	77
Figure 6.6. Mössbauer spectra of products obtained during reduction of γ -FeOOH (80 mM) with formate (75 mM) in the presence of AQDS (100 μ M) in bacterial cultures (initially 8×10^9 cells mL).	79
Figure 6.7. Total electron yield XANES measurements of the Fe-LII, III absorption edges for green rust and reference samples FeCl ₂ (II+) and goethite (III+).	81
Figure 6.8. TEM image and corresponding electron diffraction pattern of carbonate green rust hexagonal crystals mixed with a minor fine-grained phase (γ -FeOOH) obtained after 6 days of bacterial reduction of lepidocrocite (initially 80 mM γ -FeOOH, 75 mM formate, and 100 μ M AQDS).	83
Figure B.1. Orientation of monitoring wells at the Building 102 site on the TCAAP.	104
Figure B.2. Orientation of monitoring wells at Site A on the TCAAP.	105
Figure B.3. Removal of PCE in autoclaved sediment from the Building 102 Site and Site A on the former TCAAP, north of St. Paul, MN.	107
Figure B.4. Removal of TCE in autoclaved sediment from the Building 102 Site and Site A on the former TCAAP, north of St. Paul, MN.	107
Figure B.5. Removal of <i>cis</i> -DCE in autoclaved sediment from the Building 102 Site and Site A on the former TCAAP, north of St. Paul, MN.	108
Figure B.6. Relationship between monitoring wells in Table B.3 and TCE contamination in the underlying Prairie Du Chien Aquifer at Baytown Township, MN.	108
Figure B.7. Removal of TCE in sediment from the Baytown Site, north of St. Paul, Minnesota.	109
Figure B.8. Location of sediment used for microcosms in the plume of contamination at the Thermo-Chem site near Muskegon, Michigan.	110
Figure B.9. Removal of <i>cis</i> -DCE in sediment from the Thermo-Chem site, east of Muskegon, Michigan.	111
Figure B.10. Removal of <i>cis</i> -DCE in autoclaved sediment from the former TCAAP, north of St. Paul, MN.	112
Figure B.11. Removal of vinyl chloride in sediment from the former TCAAP, north of St. Paul, MN.	112

Tables

Table 1.	Degradation of carbon tetrachloride on reactive iron and sulfur minerals in laboratory experiments.	xviii
Table 1.1.	Mineralogical data for iron- and sulfur-bearing phases of interest.	1
Table 1.2.	Field data and results of geochemical speciation modeling of a biowall at the OU-1 site on Altus AFB, OK.	9
Table 2.1.	Rate Constants and products of abiotic degradation of chlorinated ethylenes by FeS minerals.	13
Table 2.2.	Rates and products of abiotic degradation of chlorinated alkanes on FeS minerals	19
Table 2.3.	Rates and products of abiotic degradation of chlorinated methanes on FeS minerals	23
Table 3.1.	Surface area specific rate constants for removal of <i>cis</i> -DCE and vinyl chloride on magnetite.	39
Table 3.2.	Surface area specific rates of removal of PCE and TCE on magnetite.	41
Table 3.3.	Surface area specific rate constants for removal of carbon tetrachloride on magnetite.	43
Table 3.4.	Relationship between the rate of removal of PCE, TCE, <i>cis</i> -DCE or vinyl chloride and the content of total iron, and the magnetic susceptibility of aquifer sediment.	44
Table 4.1.	Specific surface area values reported in the literature for synthetic green rusts	48
Table 4.2.	Rate constants for transformation of chlorinated hydrocarbons by green rusts.	55
Table 5.1.	Rate constants for degradation of chlorinated alkenes on phyllosilicate clay minerals.	63
Table 5.2.	Rate constants for degradation of carbon tetrachloride and chlorinated alkanes on phyllosilicate clay minerals.	65
Table 5.3.	Maximum quantity (C^0_{RC}) of chlorinated hydrocarbon that can be reduced by reactive iron in representative phyllosilicate clays.	66
Table B.1.	Distribution of chlorinated organic compounds and geochemical parameters in ground water at the Building 102 site on the TCAAP in 2005.	104
Table B.2.	Distribution of chlorinated organic compounds and geochemical parameters in ground water at Site A on the TCAAP in 1998.	105
Table B.3.	Distribution of chlorinated organics and dissolved oxygen in the ground water in the Baytown TCE plume.	109
Table B.4.	Distribution of chlorinated organic compounds and geochemical parameters in ground water on the bank of Black Creek at the Thermo-Chem site in Michigan.	110
Table B.5.	Distribution of ^{14}C from ^{14}C - <i>cis</i> -DCE in microcosms and container controls.	112
Table D.1.	Quality of Data on Concentrations of Halogenated Organic Compounds as Determined in Experiments Described in Section 2.	116
Table D.2.	Quality of Data on Concentrations of Acetylene as Determined in Experiments Described in Section 2.	117
Table D.3.	Quality of Data on Concentrations of Halogenated Organic Compounds as Determined in Experiments Described in Section 3 and Appendix B	118
Table D.4.	Quality of Data on Concentrations of Halogenated Organic Compounds as Determined in Experiments Described in Section 4.	119

Table D.5. Quality parameters for analysis of $\delta^{13}\text{C}$ in TCE and <i>cis</i> -DCE.	121
Table D.6. Quality of Data on Concentrations of Total Iron in Sediment as Determined in Experiments Described in Section 3	122
Table D.7. Quality of Data on Concentrations of Sodium, Potassium, Calcium, Magnesium and Iron used in the Geochemical Modeling in Section 1.	123
Table D.8. Quality of Data on Concentrations of Sulfate and Chloride used in the Geochemical Modeling in Section 1	124

Acknowledgements

Peer reviews for this document were provided by Bill Batchelor (Department of Civil Engineering, Texas A&M University), Dick Brown (a technical director for ERM, Inc. based in Ewing, New Jersey), James Henderson (a project director for the DuPont Corporate Remediation Group based in Charlotte, North Carolina), Romona Darlington (Research Scientist at Battelle Memorial Institute, Columbus, Ohio), J. Gillette (Air Force Center for Engineering and the Environment, San Antonio, Texas), Michael Barcelona (Department of Chemistry, Western Michigan University, Kalamazoo, Michigan) and Robert Ford (U.S. EPA National Risk Management Research Laboratory, Cincinnati, Ohio).

Significant technical support was provided by Tracy Pardue, Lisa Hudson, Sean Beach, Steve Markham, Vanessa Scroggins, Ying Wang, and John Cox (Shaw Environmental), Lynda Callaway and Kristie Hargrove (U.S. EPA), and Kevin Smith and John Skender (Student Contractors).

Pat Bush (an Information Coordinator with the Senior Environmental Employee Program, a grantee with U.S. EPA at the R.S. Kerr Environmental Research Center, Ada, Oklahoma) is acknowledged for her technical editing to provide consistency in formatting and grammar. Martha Williams (a Publication Editor for SRA, a contractor to U.S. EPA at the R.S. Kerr Environmental Research Center in Ada, Oklahoma) assisted with final editing and formatting for publication. Kathy Tynsky (a Graphics Designer for SRA, a contractor to U.S. EPA at the R.S. Kerr Environmental Research Center in Ada, Oklahoma) assisted with photos and proofing for this publication.

Executive Summary

This report is intended to facilitate the application of abiotic processes to remediate contamination from halogenated hydrocarbons in ground water. It is intended for scientists or engineers who design remedies for contaminated ground water, or who review the remedial proposals of others. It reviews the literature on the rate of degradation of particular halogenated hydrocarbons on particular reactive minerals, provides information on currently available techniques to characterize the reactive minerals that may be present in aquifer material, and it evaluates the prospects for applying the available analytical techniques to make a quantitative prediction of the rate or extent of degradation.

Ideally this report would identify appropriate analytical techniques that are appropriate and sensitive for each class of reactive mineral, and would provide equations that would relate the quantity or surface area of each mineral to the rate of degradation that might be expected. For iron(II) monosulfides, the current state of science approaches this expectation. For magnetite, the available technique is sensitive, but not particularly specific, and the predictions allowed by the current state of practice are only semi-qualitative. For green rusts, the kinetics of degradation are understood in simple laboratory systems, but the current state of science is not adequate to allow predictions of the rate of reaction in complex aquifer materials. For other reactive minerals, even less information is available.

This summary provides a brief review of previous research activity and engineering practice dealing with abiotic processes. It reviews the structure and reactivity of the major classes of reactive iron and sulfur minerals in ground water, and considers the efficacy of current approaches to characterize the reactive minerals.

Section 1 of this report reviews the structure and composition of the major classes of minerals that contribute to abiotic degradation of halogenated hydrocarbons in ground water. Section 1 also identifies the geochemical environments in which the various minerals are stable, and illustrates the use of geochemical modeling to predict the occurrence of reactive minerals in aquifer material from an analysis of relevant parameters in ground water.

Sections 2, 3, 4, and 5 deal in detail with the most common and well-studied reactive minerals; Section 2 deals with iron sulfides, Section 3 with magnetite, Section 4 with green rusts, and Section 5 with phyllosilicate clays. Each section in turn reviews the available literature on the rates of reaction of various halogenated hydrocarbons, the influence of geochemical parameters (such as pH) on the rate of reaction, describes the degradation products that can be expected from various halogenated hydrocarbons, and describes in detail the most appropriate analytical techniques to characterize the reactive mineral.

Section 6 describes the present state of practice for analysis of reactive minerals. The section discusses the sensitivity of and specificity of analytical methods that are available to determine reactive iron sulfur minerals in aquifer sediment. It describes precautions that are necessary to preserve the integrity of core samples that are collected for the analysis of reactive minerals. Section 6 also evaluates the use of stable isotope analyses to monitor the extent of degradation of the chlorinated hydrocarbons at field scale.

Section 7 provides recommendations for future research.

Evolution of Applications for Abiotic Processes

For many years, the only non-biological reactions that were considered to have application to the restoration of ground water contaminated with halogenated organic compounds were the reactions of 1,1,1-TCA to form 1,1-DCE or acetate (Vogel and McCarty, 1987; Vogel et al., 1987), and reactions that destroyed EDB in the presence of HS⁻ in solution (Barbash and Reinhard, 1989). Catalytic reactions on surfaces were generally ignored.

This situation changed with the successful application of permeable reactive barriers (PRBs) containing zero-valent iron to treat TCE in ground water (Gillham and O'Hannesin, 1994; Wilkin and Puls, 2003). Interest in the research community and the remediation community expanded out of a narrow focus on biological processes to include abiotic reactions on surfaces. Detailed and comprehensive studies compared the rates of reaction of chlorinated hydrocarbons on iron(II) monosulfides (Butler and Hayes, 1998, 1999, 2000, 2001), on magnetite (Lee and Batchelor, 2002a) and on green rusts (Lee and Batchelor, 2002b; O'Loughlin et al., 2003).

Kennedy et al. (2006b) applied the laboratory studies of Butler and Hayes (1999, 2001) on TCE degradation by iron(II) monosulfides to explain the removal of TCE that was observed in a PRB at Altus AFB, OK. The PRB was constructed with sand and shredded plant mulch. The sand contained iron in coatings on the quartz grains. Ambient concentrations of sulfate in the ground water were high, and large amounts of iron(II) monosulfide accumulated in the PRB. Kennedy et al. (2006b) attempted to treat TCE in ground water by injecting magnesium sulfate and lactate into a plume. Sulfate reduction produced large quantities of iron sulfides in the aquifer matrix.

Iron and sulfur minerals are common corrosion products in zero-valent iron reactive barriers,

and many of these minerals can transform or degrade chlorinated organic compounds. Until recently, the formation of secondary minerals has generally been viewed as an undesirable outcome that limits the long-term performance of reactive barriers. However, some of the corrosion products that are associated with granular or nano-sized iron particles may contribute to the overall treatment effectiveness of reactive barriers (Wilkin and Puls, 2003; Nooten et al., 2008).

If the ambient concentrations of sulfate are high, reactive iron and sulfur minerals can be expected to form during in situ anaerobic bioremediation of chlorinated hydrocarbons. Bioremediation involves the addition of a biodegradable carbon source to support biological reductive dechlorination. The same carbon source will support sulfate reduction to produce sulfide.

Abiotic processes also have a role in the natural attenuation of contaminants. Abiotic degradation of PCE and TCE tends to favor dichloro-elimination reactions to produce acetylene over a sequential hydrogenolysis reaction to produce *cis*-DCE and vinyl chloride (Butler and Hayes, 2000). Abiotic processes can also degrade chlorinated ethylenes to glycolate, acetate, formate, and carbon dioxide (Darlington et al., 2008). Anaerobic biological reactions follow the hydrogenolysis pathway exclusively. The removal or treatment of chlorinated hydrocarbons through abiotic reactions may avoid the production of toxic daughter products such as vinyl chloride.

Ferrey et al. (2004) applied the laboratory studies of Lee and Batchelor (2002a) with magnetite to explain the natural attenuation of *cis*-DCE in a plume of contaminated ground water. Despite the disappearance of *cis*-DCE, vinyl chloride or ethylene did not accumulate in the ground water.

Brown et al. (2007) suggested that a role for abiotic processes in natural attenuation could be demonstrated in four ways. First of all, abiotic processes are probably important in plumes of PCE or TCE when the concentrations of PCE and TCE decline with distance along the flow path, and there is no evidence of the accumulation of their chlorinated transformation products *cis*-DCE and vinyl chloride. Second, mineralogical analyses can be performed on aquifer sediments to recognize reactive minerals such as magnetite or iron monosulfides. Third, the ground water can be monitored for reaction products that are unique to abiotic reactions, such as acetylene. This line of evidence can be expanded to look at the fractionation of stable isotopes in the chlorinated hydrocarbons. Finally, protocols for microcosm studies should be modified or expanded to specifically examine abiotic reactions. Removal of contaminants in autoclaved controls should not be discounted as the trivial loss of material from the container.

Important Reactive Iron Minerals

A variety of iron-bearing soil minerals can degrade chlorinated hydrocarbons. Iron sulfides (disordered mackinawite, mackinawite, and pyrite), iron oxides (magnetite), green rust, and iron-bearing clays have been shown to support complete or nearly complete transformation of PCE, TCE, and carbon tetrachloride. These minerals have been identified in aquatic environments, typically in iron-reducing and/or sulfate-reducing environments. Mineral surfaces act as electron donors and/or reaction mediators to increase the rate of reductive dechlorination. Laboratory evidence suggests that the more thermodynamically stable phases (pyrite and magnetite) support comparatively slower rates of TCE reduction than metastable phases, such as mackinawite.

Table 1 compares the rates of degradation of carbon tetrachloride on mackinawite, magnetite, sulfate green rust, goethite, lepidocrocite, pyrite, siderite, and hematite in laboratory

studies. The reactions occur at the surfaces of minerals, and the rates of reaction should be proportional to the surface areas of the minerals presented to water. This information is easily attained for specific samples of pure minerals, but it is difficult to estimate the specific surface area of a particular mineral in soils and aquifer materials. As a consequence, Table 1 ranks the reactions on the minerals by the magnitude of their rate constants that have been normalized by the mass concentration of the mineral. Data on surface areas and surface-area normalized rate constants are presented for comparison.

Mackinawite was the most reactive mineral; magnetite was approximately tenfold less reactive than mackinawite, and sulfate green rust was approximately tenfold less reactive than magnetite.

Iron(II) sorbed to the surface of minerals contributes to the degradation of carbon tetrachloride. The rates of degradation for mackinawite, magnetite, goethite, lepidocrocite, siderite, and hematite were determined in the presence of 1 mM dissolved Fe^{2+} . The degradation of carbon tetrachloride by reactions on goethite, lepidocrocite, siderite, and hematite are probably carried out by iron(II) sorbed to the mineral surfaces. The rates on goethite and lepidocrocite are roughly comparable to the rate of degradation on magnetite. This might be expected for hematite. Hematite in the presence of iron(II) is transformed to magnetite (Behrends and Van Cappellen, 2007). The rates on siderite and hematite are much slower.

Table 1 lists the specific surface areas of the minerals used in the experiments. With the exception of pyrite, the minerals were synthesized by precipitation from solution and the particle size and specific surface area of the laboratory preparations were loosely comparable to the particle size and surface area of natural minerals in aquifer material. In contrast, pyrite was prepared by grinding a large specimen to a powder, and the specific surface

Table 1. Degradation of carbon tetrachloride on reactive iron and sulfur minerals in laboratory experiments. In some cases, Fe²⁺ was added to the reaction medium. The pseudo first order rate constant is normalized to the concentration of the mineral (units of L g⁻¹ day⁻¹) or to the surface area of the mineral presented to water (L m² day⁻¹).

Mineral	First Order Rate Constant		Specific Surface	Conc.	pH	Reference
	L g ⁻¹ day ⁻¹	L m ² day ⁻¹				
mackinawite with Fe ²⁺	15	1.1	13	4	7.2	Zwank et al. (2005)
magnetite with Fe ²⁺	2.3	0.12	19	2.6	7.3	Zwank et al. (2005)
sulfate green rust	0.30	0.021	14.1	5	7.6	O'Loughlin et al. (2003)
goethite with Fe ²⁺	0.18	0.010	17	3.1	7.2	Zwank et al. (2005)
lepidocrocite with Fe ²⁺	0.059	0.0033	18	2.8	7.2	Zwank et al. (2005)
pyrite	0.014	0.16	0.088	14.8	6.5	Kriegman-King and Reinhard (1994)
siderite with Fe ²⁺	0.0074	0.00019	38	1.3	7.1	Zwank et al. (2005)
hematite with Fe ²⁺	0.0067	0.00048	14	3.6	7.2	Zwank et al. (2005)

area of the pyrite was nearly one hundredfold lower than the other minerals. When the rate of degradation on pyrite is expressed on a mass basis, the rate is very low. When the rates are compared on a surface area basis, the degradation of carbon tetrachloride on pyrite is comparable to the rate on magnetite.

Because they are more reactive, mackinawite, magnetite, and green rusts have received the most attention, and more information is available in the literature on their behavior. This report will emphasize the degradation of chlorinated hydrocarbons on iron sulfides (including mackinawite), on magnetite, and on green rusts.

Iron Sulfides

Transition metal sulfides (e.g., FeS, NiS, CuS, ZnS, CdS) have exceedingly low solubility products and might be expected to form in sulfate-reducing environments. However,

transition metals other than iron are typically present in trace amounts in aquifer materials, which does not allow for any significant accumulation of sulfide minerals other than those of iron. Due in part to the fact that iron is the most abundant of these transition metals, iron sulfides are the only metal sulfides commonly recognized in soils and sediments. In contaminated systems with high metal loadings, sulfides of Hg, Zn, Cd, and Cu have been reported. Studies on FeS amended with other metals (e.g., Cr, Mn, Ni, Cu, Zn, Cd, and Hg) suggest that increased rates of transformation of chlorinated hydrocarbons may be achieved in systems containing FeS that have been substituted with Co, Ni, or Hg (Jeong and Hayes, 2003; 2007).

Several iron sulfide phases have been synthesized in the laboratory, either as transient intermediates or as stable end products, and

are therefore likely to form in subsurface environments. These phases are: disordered mackinawite, FeS; mackinawite, FeS; cubic iron sulfide, FeS; hexagonal pyrrhotite, Fe_{1-x}S; greigite, Fe₃S₄; smythite, Fe₉S₁₁; marcasite, orthorhombic FeS₂; and, pyrite, cubic FeS₂. Pyrrhotite and pyrite represent the thermodynamically stable phases at the temperatures and pressures characteristic of shallow ground water aquifers. Disordered mackinawite, mackinawite, and greigite are metastable with respect to pyrite and/or stoichiometric pyrrhotite but are considered to be the principal precursor phases to pyrite (Schoonen, 2004).

Laboratory studies have primarily focused on the reductive dechlorination ability of precipitated FeS (e.g., Butler and Hayes, 1998; 1999; 2000). Compounds investigated include hexachloroethane, PCE, TCE, 1,1-DCE, pentachloroethanes, tetrachloroethanes, trichloroethanes, dichloroethanes, carbon tetrachloride, and tribromomethane. No appreciable reaction was observed for 1,1-dichloroethane, 1,2-dichloroethane, and 1,1,2-trichloroethane, but all other compounds were transformed with half-lives of hours to days. There are several key observations from these lab-based studies. First, the degradation reactions occur at the mineral surface and not in aqueous solution. Second, the rate of FeS-mediated reductive dechlorination is a strong function of pH, with the rate increasing with increasing pH. Third, there is some evidence to suggest that the reaction mechanism may be associated with surface-bound Fe(II) and not surface-bound S(-II). Fourth, acetylene is a major reaction product for both PCE and TCE transformation. This contrasts with the sequential hydrogenolysis products such as *cis*-DCE and vinyl chloride that are produced in the microbiological transformation of these compounds. Finally, the oxidation or transformation of FeS in the environment will have a strong influence on the potential for sustained intrinsic remediation (Butler and Hayes, 2001; He et al., 2008).

Laboratory investigations with pyrite, an iron disulfide, are more limited compared to FeS, but include examinations of carbon tetrachloride transformation (Kriegman-King and Reinhard, 1994; Lipczynska-Kochany et al., 1994) and TCE transformation (Weerasooriya and Dharmasena, 2001; Lee and Batchelor, 2004; Pham et al., 2008). Kriegman-King and Reinhard (1994) proposed that electron transfer at the pyrite surface occurs at sulfur sites because carbon disulfide was detected as a reaction product and because the surfaces of the pyrite grains used in batch experiments were depleted in iron (based on X-ray photoelectron spectroscopy measurements). Pham et al. (2008) recently found that in the presence of pyrite and dissolved oxygen, TCE could be oxidized to organic acids, including dichloroacetic acid, glyoxylic acid, oxalic acid, and formic acid. It seems unlikely that this type of oxidative transformation could be sustained in natural systems where pyrite would be present in aquifer sediments. Extensive studies on acid mine drainage have documented the rapid oxidation of pyrite in oxidizing environments. Nevertheless, the results of Pham et al. (2008) are somewhat intriguing and indicate that multiple transformation pathways may be possible for trichloroethylene in the presence of iron sulfides like pyrite, and possibly mackinawite.

Consult Section 2 for more details on iron sulfides.

Magnetite

Magnetite, a mixed Fe(II)-Fe(III) iron oxide, is a widespread but typically minor component of aquifer sediments. The structure of magnetite is that of an inverse spinel, which can be expressed by rewriting the formula as Fe³⁺(Fe²⁺,Fe³⁺)O₄. It is usually present as a detrital phase derived from bedrock weathering. However, very fine-grained authigenic magnetite can be produced by iron-reducing bacteria or via the transformation of Fe(III) hydroxides under reducing conditions. Under sulfate-reducing conditions, magnetite will slowly

dissolve and react to form pyrite. This transformation of magnetite to pyrite is believed to be important under high sulfide concentrations (>1 mM) over several decades (Canfield and Berner, 1987). At lower concentrations of dissolved sulfide, magnetite dissolution without pyrite replacement is observed. Magnetite is also a common corrosion product in passive reactive barriers (PRBs) constructed with zero-valent iron. In PRBs, green rusts form as a corrosion product of zero-valent iron, then magnetite forms as a transformation product of the green rust.

Consult Section 3 for more details on magnetite.

Green Rust

Green rust compounds are compositionally variable, mixed valence Fe(II)/Fe(III) layered hydroxides (Hansen, 1989; Taylor, 1973). Green rust compounds have been identified in reducing soils and are sometimes corrosion products in iron-based reactive barriers. Green rust structural units consist of alternating positively charged tri-octahedral metal hydroxide sheets and negatively charged interlayers of anions. Anions present in the interlayer positions typically are Cl^- , CO_3^{2-} , or SO_4^{2-} . Laboratory experiments have revealed mixed results regarding the efficiency of dechlorination in the presence of green rust (Erbs et al., 1999; Lee and Batchelor, 2003; 2004). The reactivity of green rust can be enhanced by adding Cu^{2+} or Ag^+ ions during green rust synthesis (O'Loughlin et al., 2003). Addition of these metals may lead to a galvanic couple involving a zerovalent metal (i.e., Cu or Ag) and green rust, with contaminant reduction occurring on the surface of the metal and green rust providing the source of electrons for the electrochemical cell.

Consult Section 4 for more details on green rusts.

Adsorbed Fe(II)

The presence of mineral surfaces has been shown to dramatically increase rates of contaminant reduction by Fe(II). Amonette et al. (2000), Charlet et al. (2002), Pecher et al. (2002), Szecsody et al. (2004), and Elsner et al. (2004a) show that sorption of Fe(II) on the iron oxyhydroxide goethite led to high rates of carbon tetrachloride degradation.

Importantly, no reduction of carbon tetrachloride occurred in systems with Fe(II) but no goethite, indicating that the degradation processes were controlled at the mineral surface. In their review of reactions involving sorbed Fe(II) as an electron donor, Schoonen and Strongin (2005) postulate that this increase in reducing power on surfaces results from the formation of a $\text{Me-O-Fe}^{\text{II}}$ species, where Me is structural iron in the mineral crystal. The bond to the structural iron makes the sorbed Fe(II) a stronger electron donor, because of the electron density the structural iron is transferred through the bridging oxygen atom to the sorbed Fe(II). However, the mineral surface may also contribute by providing a sink for Fe(III) that otherwise would be in solution, thus changing the ratio of Fe(II) to Fe(III), which would affect the thermodynamics of the Fe(II)/Fe(III) couple and make Fe(II) in solution a stronger reductant (Bill Batchelor, Texas A&M University, College Station, Texas, personal communication).

In general, the rate of contaminant degradation determined in experimental studies is proportional to the concentration of Fe(II) adsorbed at the mineral surface as determined by chemical extraction or from the measured disappearance of Fe(II) from solution. Amonette et al. (2000) suggested that a simultaneous transfer of two electrons takes place from two adjacent Fe(II) surface sites that react with a sorbed carbon tetrachloride molecule, thus leading to a rate dependence that is second-order with respect to the concentration of carbon tetrachloride. Although the exact controls and mechanisms

of contaminant reduction are topics of continuing research, it is clear that the primary role of the goethite surface is to catalyze the reaction by fixing the position of the two charged reactants in a geometry that is suitable for reaction with carbon tetrachloride (Amonette et al., 2000). Mossbauer studies with ^{57}Fe and ^{56}Fe compounds have revealed interesting and unanticipated complexity; sorbed Fe(II) leads to electron transfer and reduction of structural Fe(III) near the mineral surface (Williams and Scherer, 2004).

Phyllosilicate Clays

Another class of iron-bearing minerals that are common components of aquifer sediments but have received less attention includes the iron-bearing clay minerals biotite, montmorillonite, and vermiculite (Lee and Batchelor, 2004) or smectite (Neumann et al., 2009). Because iron-bearing clays are often abundant soil components, these minerals could play a significant role in affecting the transport and fate of chlorinated organic compounds. Lee and Batchelor (2003) found that the reductive capacities of iron-bearing phyllosilicates were from one to three orders of magnitude less than those of other iron sulfides and oxides. Neumann et al. (2009) concluded that structural Fe^{2+} in smectites will become important in the subsurface only when the iron(hydr)oxides are reductively dissolved. Brown et al. (2007) presented data from a site (their Site A), where ground water in an aquifer containing glauconitic marine clay was contaminated with 1,1,1-TCA, 1,1-DCE, and 1,1-DCA. The sediments were naturally reducing. The concentrations of chlorinated hydrocarbons were reduced ten thousand fold as ground water moved 200 meters along the flow path.

Iron Carbonates

The iron carbonate siderite (FeCO_3) is closely related to the minerals rhodochrosite (MnCO_3), magnesite (MgCO_3), and calcite (CaCO_3). These minerals often have some substitution

of their metal ions. Siderite is a common mineral associated with sedimentary rocks, bog deposits, and coal fields, where it occurs as a reddish-brown mineral in shale layers, nodules, concretions, and fossil burrows. Although little work has been carried out on evaluating the reactivity of siderite with chlorinated compounds, it is included in this discussion because it is expected to form in reducing, nonsulfidic ground-water systems. Note that an iron hydroxycarbonate mineral appears to be a major species of carbonate precipitate within granular zerovalent iron PRBs (Wilkin and Puls, 2003). Studies to evaluate the controls on precipitation of this phase are underway at the Kerr Center (U.S. EPA/ORD) and it appears that elevated pH (~ 10) in zerovalent iron PRBs is an important factor.

Formation and Stability of Reactive Iron and Sulfur Minerals Under Various Geochemical Conditions

The minerals which support abiotic transformations of chlorinated compounds include mackinawite, pyrite, siderite, magnetite, green rust,

and goethite with adsorbed Fe(II). Table 1.1 describes the structure of these minerals.

Table 1.1 Mineralogical data for iron- and sulfur-bearing phases of interest.

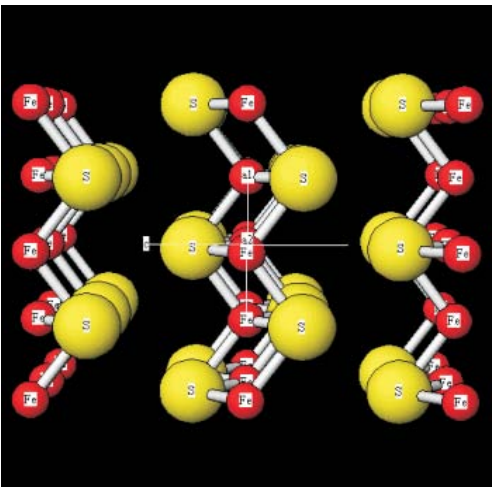
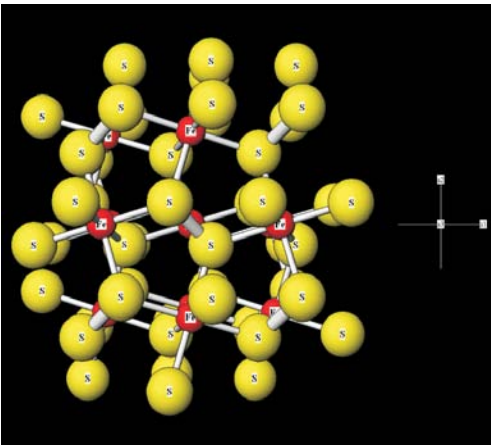
Reactive Mineral	General Description	Structural Image
Mackinawite	<p>FeS (Tetragonal) Specific gravity = 4.17 Each Fe(II) atom is bonded to four sulfur atoms. Tetrahedra share edges to form layers that are stacked and interact by van der Waals forces.</p> <p>Litharge (PbO) structure type.</p>	
Pyrite	<p>FeS₂ (Cubic) Specific gravity = 4.95-5.10 Each Fe(II) atom is in octahedral coordination with the center of a disulfide unit.</p> <p>NaCl structure type.</p>	

Table 1.1. (cont.) Mineralogical data for iron- and sulfur-bearing phases of interest.

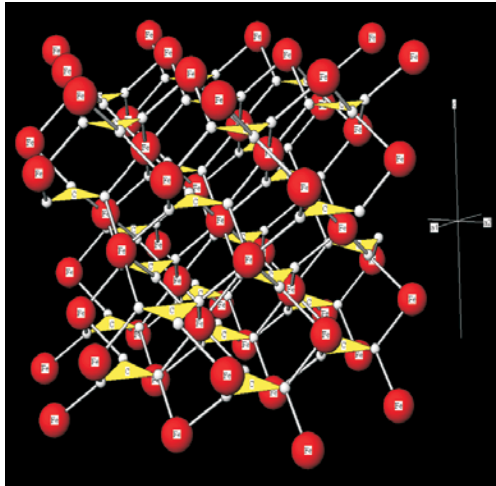
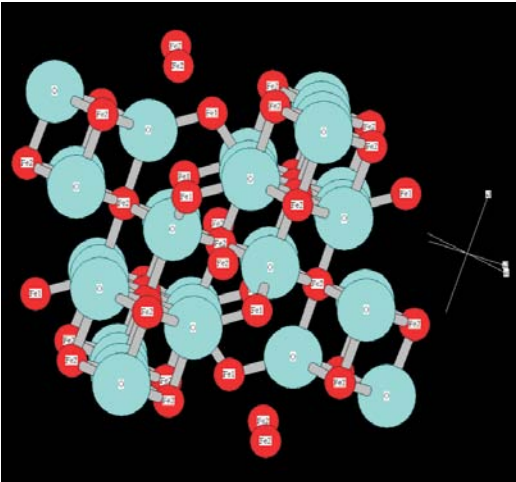
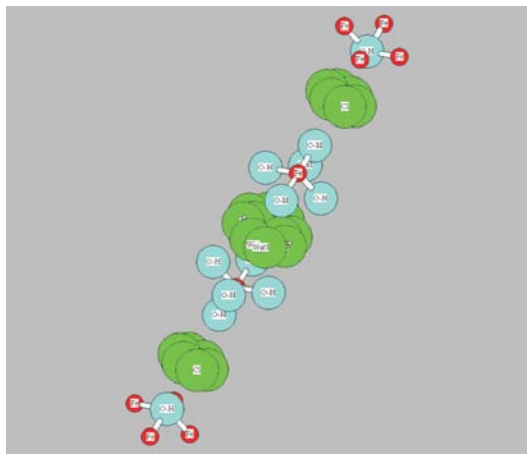
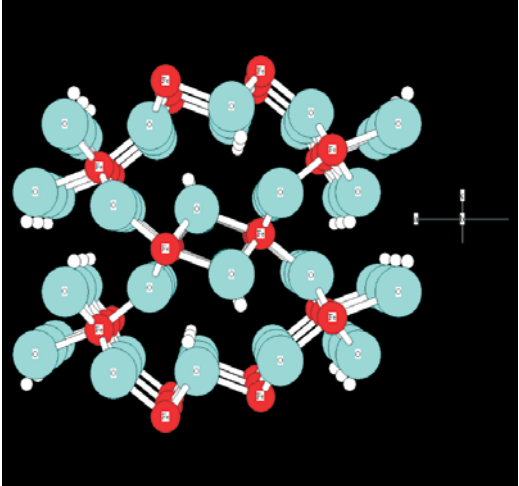
Reactive Mineral	General Description	Structural Image
Siderite	<p>FeCO_3 (Trigonal) Specific gravity = 3.96 Each Fe(II) atom is in octahedral coordination with $(\text{CO}_3)^{2-}$ ions. The unit cell is slightly distorted to accommodate large planar (CO_3) groups which contain carbon atoms at the center of an equilateral triangle of oxygen atoms. NaCl structure type.</p>	
Magnetite	<p>Fe_3O_4 (Cubic) Specific gravity = 5.2 One third of iron atoms are in tetrahedral coordination with oxygen; two thirds of the iron atoms are in octahedral coordination. One half of the six-fold coordination iron atoms are Fe(II). Spinel (inverse) structure type.</p>	
Green Rust	<p>$(\text{Fe}^{2+}, \text{Mg})_6 \text{Fe}_2^{3+}(\text{OH})_8 \cdot 4\text{H}_2\text{O}$ (Fougerite; Trigonal) Specific gravity = 3.5 (calc) $\text{Fe}(\text{OH})_2$ layers alternate with inter-layers of anions (chloride, sulfate, or carbonate) and water molecules.</p>	

Table 1.1. (cont.) Mineralogical data for iron- and sulfur-bearing phases of interest.

Reactive Mineral	General Description	Structural Image
Goethite	<p>FeOOH (Orthorhombic) Specific gravity = 4.27-4.29 Oxygen atoms are arranged in a sequence of hexagonal close-packed arrays with Fe(III) in octahedral interstices. Fe(II) adsorbed at the mineral-water interface.</p> <p>Diaspore structure type.</p>	

1.1 Formation Processes of Reactive Minerals

This section discusses the relative stability and conditions that are associated with the formation of the principal reactive iron minerals. Because iron exhibits two oxidation states, Fe²⁺ and Fe³⁺, the stability of iron-bearing minerals is a function of the redox state of the system, which can be expressed in terms of Eh. In addition, inclusion of several different elements in the structure of these minerals requires the consideration of other geochemical parameters, such as pH, dissolved CO₂, and dissolved H₂S.

Figure 1.1 presents mineral stability diagrams plotted using the geochemical parameters that were identified as being of importance. Mineral stability diagrams presented in Figure 1.1 were constructed with the EQ/36 thermodynamic database, modified to include data for green rust and iron sulfides. It is important to recognize that mineral stability diagrams, such as the one presented in Figure 1.1, are constructed assuming that equilibrium is established. Natural systems are typically not

at thermodynamic equilibrium, yet these types of diagrams are highly useful in linking specific geochemical conditions (e.g., pH, concentration of bicarbonate) with minerals that might be expected to precipitate from solution.

Two diagrams (Figure 1.1a and Figure 1.1b) are plotted, one for sulfidic environments where the activity of the HCO₃⁻ anion is taken to be 10⁻³, and the other for non-sulfidic environments where the concentrations of dissolved sulfide are so low that pyrite and mackinawite do not plot on the Eh-log HCO₃⁻ diagram. These diagrams represent a theoretical prediction of natural settings, yet they are in overall qualitative agreement with the results of experimental and natural measurements of mineral formation. In aerobic, high Eh environments, only Fe(III) oxyhydroxides (goethite) are expected to form. Siderite is expected to form only at low Eh, low H₂S, and high HCO₃⁻. Stability fields for the carbonate form of green rust and for magnetite are present in systems containing low concentrations of inorganic carbon and low Eh. At the specified conditions, green rust

appears to be a stable phase. Carbonate green rust occupies a redox region intermediate to siderite and magnetite. Pyrite occupies a wide stability field encompassing low Eh and low to moderate concentrations of dissolved sulfide.

1.1.1 Formation of Pyrite and Mackinawite

Examination of Figure 1.1a shows that pyrite is the stable iron mineral under low Eh and moderate to high concentrations of dissolved sulfide. Such conditions are characteristic of anaerobic ground-water systems where sulfate reduction is on-going. The occurrence of pyrite in aquifer sediments is nearly always due to precipitation in place (authigenic formation) because detrital pyrite is chemically and physically unstable. Discussion of iron sulfide formation may be divided into issues relating to the sources of iron and sulfur, the factors limiting formation, and the mechanism of formation.

The principal source of iron for pyrite formation in subsurface environments is detrital iron minerals. Surface waters contain almost no dissolved iron and biogenic materials are typically low in iron content. Detrital iron minerals can dissolve by bacterial or abiotic processes. The most common source of dissolved iron is from the chemical or biological reduction of iron(III) hydroxides to produce dissolved iron(II) (Poulton, 2003). However, not all detrital iron minerals react completely to form pyrite. The most reactive iron-bearing phases are those that are very fine grained, such as hydrous iron(III) oxide, fine-grained goethite, and iron-bearing clay minerals (e.g., Raiswell and Canfield, 1996; Poulton et al., 2004). These fine-grained minerals often occur as adsorbed coatings on detrital silicates. In contrast, sand- and silt-sized grains of magnetite and ferruginous silicates are comparatively unreactive and can often

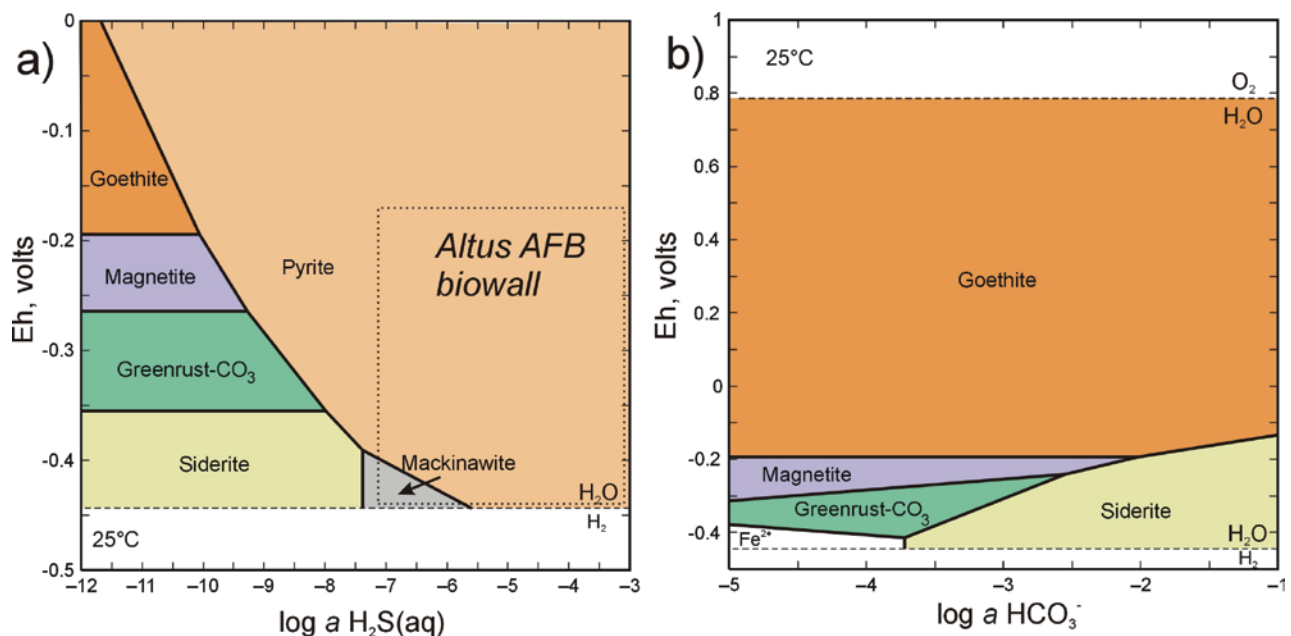


Figure 1.1. Mineral stability diagrams: a) Eh versus $\log a \text{H}_2\text{S}$ showing stability fields for goethite, magnetite, carbonate green rust, siderite, mackinawite, and pyrite ($\text{Fe}=10^{-4}$, $\text{C}=10^{-3}$, $\text{pH}=7.5$, hematite suppressed); b) Eh versus $\log a \text{HCO}_3^-$ showing stability fields for goethite, magnetite, carbonate green rust, and siderite ($\text{Fe}=10^{-4}$, $\text{pH}=7.5$, hematite suppressed). The $\log a \text{H}_2\text{S}$ and $\log a \text{HCO}_3^-$ refer to the common logarithm of the chemical activity of H_2S or HCO_3^- , as opposed to their concentration.

co-exist, in a metastable state in conditions that should support the precipitation of pyrite.

Pyrite forms as a result of a series of processes stemming from the initial reaction between dissolved sulfide and the iron released from detrital iron minerals. The major source of dissolved sulfide is bacterial reduction of sulfate. Sulfate in ground water is usually from dissolution of pyrite or other sulfides in aerobic environments or from the leaching of sulfate minerals that are components of certain sedimentary rocks. Consequently, the primary factors that limit the amount of pyrite, or any iron sulfide that forms, are: the concentration and reactivity of iron compounds, the availability of dissolved sulfate, and the concentration of organic carbon that acts as a carbon source for sulfate-reducing bacteria to produce dissolved sulfide. In natural systems, the concentration of reactive organic carbon is oftentimes found to be a limiting factor on the amount of bacterial sulfate reduction that occurs. In some organic-carbon-rich environments, where dissolved sulfide is abundant, the amount of iron sulfide precipitation is limited by the amount of reactive iron minerals. In ground-water systems, the concentration of dissolved sulfate, reactive carbon, or reactive iron can all be limiting factors for iron sulfide precipitation (Figure 1.2). In biowalls, the formation of iron sulfides is not limited by the abundance of organic carbon but can be limited by the availability of either sulfate or iron (Figure 1.2). Thus, understanding the primary controls on reactive mineral formation is essential for designing and implementing remedial systems in the field.

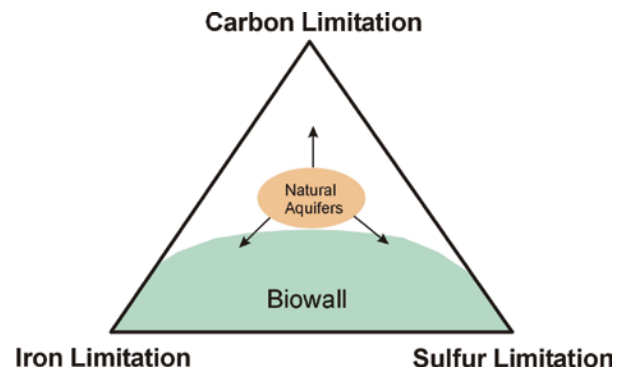


Figure 1.2. Ternary diagram showing the importance of controlling factors on iron sulfide formation in natural aquifers and biowalls.

It is now well known that pyrite formation proceeds through the formation of metastable iron monosulfide precursors. This has been shown by laboratory experimentation conducted to simulate a range of natural environments. Minerals that form initially at room temperature by the reaction of H_2S and HS^- with fine-grained goethite or dissolved ferrous iron are mackinawite (tetragonal FeS) and greigite (cubic Fe_3S_4). Both minerals are black and soluble in concentrated hydrochloric acid. Mackinawite and greigite are thermodynamically metastable relative to pyrite (and other iron sulfides such as troilite and pyrrhotite).

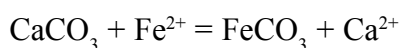
Although pyrite has a wide stability field on Figure 1.1a, its formation is impeded by relatively slow nucleation kinetics, unlike mackinawite which readily precipitates when solutions reach saturation. This fundamental difference in nucleation kinetics between mackinawite and pyrite represents one of the limitations of equilibrium diagrams such as Figure 1.1a to accurately depict mineral formation at low temperatures. The stability field of the thermodynamically stable phase, pyrite, is necessarily expanded over the metastable phase, mackinawite. The mechanism of the mackinawite-to-pyrite transformation has been the subject of many laboratory and field investigations (Schoonen, 2004;

Rickard and Luther, 2007). He et al. (2008) discuss the implication of this transformation process relative to dechlorination of TCE on iron sulfides. Pyrite is generally considered to be much less reactive toward chlorinated hydrocarbons than are iron(II) monosulfides.

He et al. (2008) measured Eh and dissolved sulfide concentrations in ground water from a plant mulch based passive reactive barrier (a biowall) at the OU-1 site at Altus AFB, OK. They also sampled and characterized iron and sulfur mineral phases that were accumulating in the biowall matrix. Iron and sulfur minerals were dominated by pyrite and mackinawite. The range of values for Eh and the chemical activity of H₂S in ground water in the OU-1 biowall are presented in Figure 1.1a. Consistent with the observed accumulation of pyrite and mackinawite, the Eh and chemical activity of H₂S in water in the biowall fall within the stability fields of pyrite and mackinawite in Figure 1.1a.

1.1.2 Formation of Siderite

The conditions under which siderite is stable are limited. Figure 1.1a and 1.1b show that Eh must be low (<0 mV) and dissolved sulfide concentrations must be low as well (<10^{-7.3} molar), a combination that would not be expected for reducing ground water systems that contain any appreciable concentrations of sulfate. Thus, siderite formation is expected in anaerobic environments only where sulfate is absent. In addition to waters containing dissolved sulfide, siderite is not expected from water rich in dissolved calcium. Following the reaction:



So that

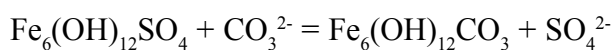
$$K = 158 = \{\text{Ca}^{2+}\} / \{\text{Fe}^{2+}\}$$

For siderite to be stable relative to calcite the concentration of iron must be greater than ~1% of the concentration of calcium (Wilkin and Puls, 2003). Substantial concentrations of calcium ion can prevent the precipitation of siderite in ground-water systems.

1.1.3 Formation of Green Rusts

Green rust is a mixed Fe(II)-Fe(III) hydroxide consisting of positively charged trioctahedral metal-hydroxide layers and negatively charged interlayer anions and water molecules (Table 1.1). It is believed to be an intermediate reaction product as reduced minerals oxidize to mixed ferric/ferrous or ferric minerals such as magnetite and goethite (Figure 1.1a). Green rust minerals have been prepared in the laboratory, using various chemical procedures, from solutions containing iron(II) and chloride ions, iron(II) and sulfate ions, and iron(II) and carbonate ions (e.g., Taylor et al., 1980; Hansen, 1989; Drissi et al., 1995; Ayala-Luis et al., 2008). Studies have shown that green rust minerals form from the bioreduction of hydrous iron(III) oxides by dissimilatory iron-reducing bacteria. Green rust has been identified using transmission electron microscopy as a corrosion product in zerovalent iron PRBs (Furukawa et al., 2002).

Two types of green rust (GR) minerals are distinguishable based upon X-ray diffraction analysis: GR1 in which the distance between hydroxide sheets is between about 0.75 and 0.80 nm (e.g., carbonate green rust) and GR2 in which the distance between sheets is about 1.1 nm (e.g., sulfate green rust). Solid-phase characterization and geochemical modeling studies of iron corrosion in zerovalent iron passive reactive barriers (PRBs) indicate that if the ground water is not impacted by mine waste, the carbonate forms of green rust will precipitate preferentially over the sulfate form in zerovalent iron systems (Wilkin and Puls, 2003). These observations can be understood by considering the following exchange equilibrium based upon the anhydrous components of green rust:



So that

$$K = \{\text{SO}_4^{2-}\} / \{\text{CO}_3^{2-}\}$$

Assuming ideal mixing relations in the solids (i.e., the activities of the solids are taken to be unity) and using available thermodynamic data from Bourrié et al., 1999, we estimate $K = 103.1$. Typically the $[\text{SO}_4^{2-} / \text{CO}_3^{2-}]$ ratio in ground water that has not been impacted by mine waste is less than 103.1, which is consistent with the predominance in aquifers and most reactive barriers of carbonate green rusts over sulfate green rusts.

1.1.4 Formation and Transformation of Goethite and Ferrihydrite

Goethite (FeOOH) and ferrihydrite ($\text{Fe}(\text{OH})_3$) are the most common Fe(III) (oxy)hydroxides in aquifers. Note that if the occurrence of goethite were to be suppressed from Figure 1.1b then $\text{Fe}(\text{OH})_3$ would occupy nearly the same region as goethite. These iron(III) minerals often have high surface area and intrinsic reactivity toward various metals and nutrients. Ferrihydrite is generally considered to be the most labile and most bioavailable Fe(III) hydroxide or Fe(III) oxide for dissimilatory iron-reducing bacteria. Ferrihydrite can undergo a number of transformation pathways leading to other minerals, some of which are of interest in the context of abiotic reductive dechlorination. Reaction of ferrihydrite with dissolved Fe(II), derived from the reductive dissolution of Fe(III) minerals, converts ferrihydrite to Fe phases such as goethite, lepidocrocite, green rust, and magnetite. The mineralization pathways are influenced by the concentration of dissolved Fe(II), pH, and concentration of ligands in solution. Magnetite formation from ferrihydrite is favored at high loadings of Fe(II) (>1 mmol Fe(II) per gram) and in the absence of bicarbonate. Magnetite precipitation is also favored at higher pH. At lower surface loadings of Fe(II), ferrihydrite converts to the oxyhydroxides, goethite and lepidocrocite depending on the presence or absence of ligands in solution (Hansel et al., 2005).

A geochemical environment of particular interest is the transitional redox regime where Fe(II) production occurs, but Fe(III)

oxyhydroxides still remain. The widespread occurrence of iron-reducing bacteria may provide a continuous supply of Fe(II) ions at the surface of minerals that may enhance the natural attenuation of ground-water contaminant plumes (Williams and Scherer, 2004; Tobler et al., 2007). This coupling of microbial respiration and abiotic reduction of organic compounds may allow for simultaneous natural attenuation of different chemical classes.

1.2 Geochemical Modeling

Reactive minerals can be unstable in the presence of oxygen in the atmosphere, and they may be present in aquifer sediments at low concentrations. As a consequence, the direct identification of reactive minerals in raw samples collected from the field is a difficult task. Most of the successful approaches to identify reactive minerals in aquifer material include a process to concentrate the reactive minerals through the use of density or sizing separations, followed by microscopy or other solid-phase analyses.

In some cases the presence or absence of reactive minerals can be predicted using thermodynamic calculations. Thermodynamic calculations based on measured concentrations of chemicals in ground water can provide clues to the potential occurrence of specific minerals in the aquifer sediment (Billon et al., 2003). Geochemical speciation modeling is a tool that can be used to constrain whether or not specific minerals that could support abiotic transformations are present in a system. In essence geochemical speciation models use water chemistry to constrain the mineralogical composition of the mineral phases present.

It is important to keep in mind that the results of geochemical modeling exercises are not definitive, but they can be used as supporting lines of evidence and provide important insight about the geochemical environment in the subsurface. The approach is more robust when the modeling encompasses water samples collected through time. Use of modeling is most successful

when specific questions are posed, i.e., is it possible that an iron sulfide is precipitating in a reactive barrier? It is imperative that models be supported with the appropriate field data and thermodynamic data. A specific example of modeling is presented here to explore the formation of reactive iron minerals in a plant mulch based passive reactive barrier (a biowall) that was installed at the OU-1 site on Altus AFB, Oklahoma, to treat TCE in ground water.

In this example, the equilibrium geochemical modeling software Geochemist's Workbench (Release 6.0, Rockware, Golden, CO) was used to model ground water chemical speciation. The "React" module was used to model chemical speciation in aqueous solutions and determine the saturation states of solutions with respect to selected iron sulfides and iron carbonates. The modeling provides a quantitative means of assessing whether or not solutions are undersaturated, oversaturated, or saturated with respect to specific mineral phases. Solutions that are at saturation (equilibrium) with respect to a specific mineral provide a case that the mineral could be present within the aquifer material (in this case the biowall) that is in contact with that water. Solutions that are undersaturated with respect to a particular mineral can be expected to dissolve that mineral into solution. Solutions that are oversaturated tend to precipitate, assuming that kinetic barriers of nucleation do not prevent mineral precipitation.

The standard database (thermo.dat) of Geochemist's Workbench was applied with important modifications to include thermodynamic data from Rickard (2006) for the solubility of crystalline mackinawite [FeS(c)] and Benning et al. (2000) for the solubility of disordered mackinawite [FeS(d)] following the reactions:



and



By examining both of these reactions, it is possible to compare the composition of ground water with solutions that are saturated against well-crystalline and freshly precipitated FeS. As shown in Table 1.2, inputs to the model were pH, and the concentrations of Na, K, Ca, Mg, Fe, Cl, SO_4^{2-} , $\text{H}_2\text{S(aq)}$, and HCO_3^- . It was found that the high concentrations of sulfide in the biowall necessarily drove the concentration of iron to very low levels. Non-detects cannot be used as model inputs. The concentrations in the water sample must be above the quantitation limit for the method used to analyze the samples. It was necessary to use inductively coupled plasma mass spectrometry (ICP-MS) to determine the concentrations of iron in ground water samples from the biowall. Note that the iron concentrations reported in Table 1.2 have units of parts per billion. These measurements are well below typical concentration ranges possible using spectrophotometric or emission-based ICP methods.

Based on the distribution of the measured concentrations of the major anions and cations, the charge balance was calculated and found to be generally better than 10% (which is suitable for the modeling). In this case, since we are interested in understanding the solution saturation states of the iron monosulfides and iron carbonate, the redox state was not fixed using the Eh value measured in the field. Instead, sulfate and sulfide were decoupled, i.e., not linked by redox equilibrium restrictions. In this way the field-determined Eh could be compared to a calculated Eh based on the measured concentrations of sulfide and sulfate and the pH following the reaction:



Comparing results for the measured and calculated Eh values shows fairly good agreement, particularly for samples containing high dissolved sulfide concentrations (>100 mg/L; Table 1.2). The platinum electrode response in this system is likely reflecting the sulfide/elemental sulfur pair (Berner, 1963).

Table 1.2. Field data and results of geochemical speciation modeling of a biowall at the OU-1 site on Altus AFB, OK.

Field Data											
Well	pH	Eh _m	Na	K	Ca	Mg	Fe	Cl ⁻	SO ₄ ²⁻	DIC	Σ H ₂ S
	SU	mV	ppm	ppm	ppm	ppm	ppb	ppm	ppm	ppm	ppm
EPA110	6.58	-171	428	32	386	119	48.7	289	27	523	164
EPA109	6.77	-206	389	9.0	333	112	11.3	299	89	398	344
EPA108	6.81	-209	396	6.8	353	107	27.5	298	355	336	208
EPA107	6.60	-194	366	16.2	373	93.9	4.60	264	67	414	188
EPA106	6.64	-185	383	19.9	407	145	170	308	686	325	88
EPA105	6.73	-185	346	3.9	396	138	19.2	293	1030	229	121
EPA104	6.77	-230	383	21.2	444	152	291	289	389	352	210
EPA103	6.75	-196	370	11.9	406	158	53.0	253	806	311	190
EPA102	6.70	-195	379	27.6	447	156	68.2	269	319	493	178
EPA101	6.98	-70	398	4.9	395	155	11.2	301	1600	96	1
Model Outputs											
Well	Eh _c	Charge Balance	Pyrite	Mackinawite (crystalline)	Mackinawite (disordered)	Gypsum	Siderite				
	mV	%	Saturation Index (SI)								
EPA110	-198	-8.4	9.42	-0.39	-0.87	-2.09	-2.46				
EPA109	-210	-11.5	9.03	-1.00	-1.48	-1.60	-3.57				
EPA108	-207	-6.8	9.37	-0.62	-1.09	-1.00	-3.06				
EPA107	-197	-7.1	8.53	-1.41	-1.89	-1.67	-3.65				
EPA106	-190	-3.3	10.0	0.13	-0.35	-0.71	-1.91				
EPA105	-196	-6.4	9.19	-0.79	-1.27	-0.55	-2.99				
EPA104	-202	-5.9	10.5	0.40	-0.08	-0.69	-2.02				
EPA103	-200	-5.8	9.75	-0.34	-0.82	-0.65	-2.76				
EPA102	-199	-7.5	9.77	-0.23	-0.72	-1.01	-2.61				
EPA101	-199	0.1	7.03	-1.45	-1.93	-0.40	-2.39				

Notes: All samples collected on 11/19 and 11/20, 2008. Samples for cations and anions were filtered through 0.45 μm disc-filters in the field. Samples for analysis of cations were acidified with HNO₃ for preservation. All samples were stored on ice or in a refrigerator prior to analysis. The saturation index (SI) is used to quantify the degree of saturation of a mineral and is defined as follows: $SI = \log(IAP/Ksp)$. Where IAP is the ion activity product and Ksp is the solubility product constant for the phase in question. For phases at saturation, $IAP=Ksp$ and $SI = 0$. A negative SI indicates that the phase is undersaturated ($IAP<Ksp$) while a positive SI ($IAP>Ksp$) indicates the phase is oversaturated. The analyses were checked for internal consistency using charge balance. The charge balance was calculated as follows: $(\sum(\text{meq/L positive charge}) - \sum(\text{meq/L negative charge})) / (\sum(\text{meq/L positive charge}) + \sum(\text{meq/L negative charge})) \times 100$. Eh_m and Eh_c are the field determined Eh and calculated Eh values, respectively. Calculated Eh values are based on the sulfate/sulfide redox pair.

The saturation states of the iron minerals were evaluated to determine if iron sulfides were likely to be forming within the biowall. We focused on the iron sulfides pyrite and mackinawite. Other iron sulfides, such as marcasite, troilite, and pyrrhotite are not likely candidates in this system. Marcasite often precipitates from low pH solutions. Troilite and pyrrhotite are simply not encountered as formation products in low-temperature systems. The results of the modeling for the iron minerals are provided in Table 1.2. Ground water within the biowall is nearly saturated with respect to iron monosulfide. Mean saturation indices for crystalline mackinawite and disordered mackinawite are -0.14 and -0.82, respectively (n=28). Figure 1.3 shows the SI values for crystalline mackinawite and disordered mackinawite as a function of pH. Notice that nearly half of the SI values calculated for crystalline mackinawite are >0, suggesting oversaturation and that SI=0 is a practical cap for values reflecting the saturation state of disordered mackinawite.

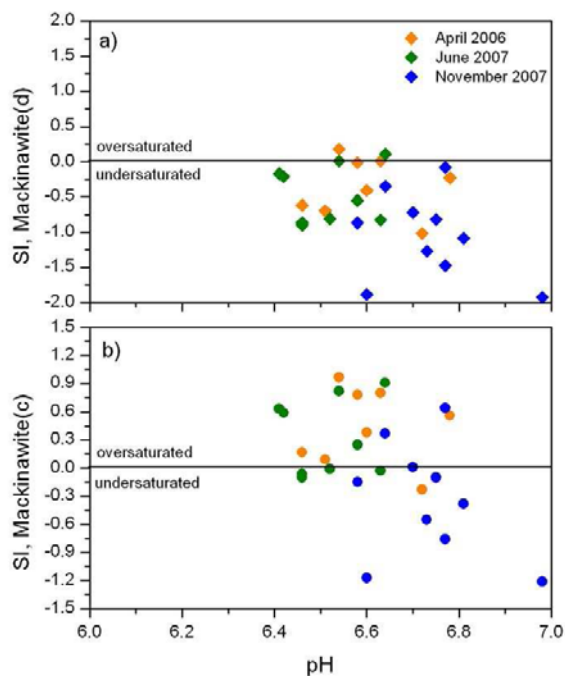


Figure 1.3. Saturation indices (SI) for a) disordered mackinawite and b) crystalline mackinawite as a function of pH and time (ground water from the biowall at OU-1 on Altus AFB, OK).

These features are consistent with the formation and aging of mackinawite in the biowall. The saturation state of freshly precipitated mackinawite (disordered) should not be exceeded because rapid precipitation kinetics are expected to drive solution concentrations down to the solubility limit. Clustering of SI values around SI=0 for crystalline mackinawite suggests that freshly precipitated and aged mackinawite may control the dissolved sulfide and iron concentrations in the biowall. Note that the disulfide pyrite is highly oversaturated in the biowall (mean SI= 9.6). This is expected because of kinetic barriers to direct precipitation of pyrite in aqueous solutions (Schoonen and Barnes, 1991). Even though the precipitation of pyrite does not regulate concentrations of sulfide and iron, there is a thermodynamic driving force for the mackinawite-to-pyrite transformation.

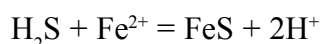
These interpretations reinforce the results of solid-phase investigations in the biowall reported by He et al. (2008). The important implication is that geochemical speciation modeling, based on water chemistry parameters, can be useful in evaluating whether or not potentially reactive phases are present in situations where solids cannot be collected and analyzed for mineral content.

The saturation states of the gypsum (calcium sulfate) and siderite phases were also evaluated in order to determine what reactions likely control the sulfate concentrations within the biowalls and whether iron carbonate formation was likely to compete with iron sulfide precipitation. Sulfate is important as an electron acceptor for sulfate-reducing bacteria (SRB). Ground water within the biowall is undersaturated in both gypsum and siderite. Consequently, precipitation of a calcium sulfate is not a sink for dissolved sulfate in the biowall; this may be linked to the fact that ground-water is likely supporting the precipitation of calcium carbonate (calcite or aragonite) which is oversaturated in the biowall. Siderite is highly undersaturated so the primary precipitation reactions involving iron are those that form iron sulfides.

2.1 Applications of Iron Sulfide Minerals

Iron sulfides are important redox active minerals that can form under anaerobic conditions. They are found in engineered systems such as zero valent iron passive reactive barriers, at contaminated sites that contain mixed wastes, and in natural sediments. Engineering systems where iron sulfide minerals are expected to play an important role in the abiotic degradation of chlorinated organic contaminants include permeable reactive barriers (PRBs), landfills, waste disposal facilities, and sites where chlorinated organic compounds are treated by anaerobic bioremediation. In addition, iron sulfide minerals may contribute to abiotic degradation of chlorinated organic contaminants in anaerobic sediments in natural wetlands and salt marsh environments.

In natural sediments, mixed plumes, and engineered systems, FeS is generally formed from Fe²⁺ and HS⁻ that is produced in these systems. Under anaerobic conditions, sulfate reducing bacteria (SRB) generate HS⁻. The Fe²⁺ can be produced by dissimilatory iron reducing bacteria or through reductive dissolution of hematite and other iron oxides by hydrogen sulfide (Pyzik and Sommer 1981). The production of dissolved sulfide species in the presence of dissolved metals can result in precipitation of metal sulfide mineral phases as shown in the following reaction:



Under ambient conditions, disordered mackinawite or FeS_{am} precipitate is usually the first iron sulfide phase formed (Rickard and Luther 2007; Rickard and Morse 2005). Amorphous FeS and poorly crystalline mackinawite (tetragonal structure) has been observed in PRB systems constructed with zero valent iron (ZVI) and in

biowall systems constructed with plant mulch (Benner et al. 1999; Phillips et al. 2000). In natural settings, iron monosulfide (FeS) formation is commonly observed in anoxic sediment environments. The HS⁻ produced by sulfate reducing bacteria may also directly react with iron oxides (e.g. hematite, goethite, ferrihydrite) and produce iron sulfides on the mineral surfaces.

Iron sulfide minerals mediate reductive transformation of a variety of halogenated organic compounds (Butler and Hayes 1998; Butler and Hayes 2000; Jeong and Hayes 2003; Jeong et al. 2007; Jeong et al. 2008). The transformation of chlorinated hydrocarbons such as TCE, PCE, carbon tetrachloride (CT), and trichloroethane (TCA) by a variety of FeS and FeS₂ minerals is well documented in the literature (Butler and Hayes 1999; Butler and Hayes 2001; Liang et al. 2007; Shen and Wilson 2007; Butler and Hayes 1998; Butler and Hayes 1999; Butler and Hayes 2000; Butler and Hayes 2001; Gander et al. 2002; Hansson et al. 2008). Degradation of hexachloroethane (HCA), tetrachloroethylene (PCE), and trichloroethylene (TCE) by nickel and copper sulfides has also been observed under certain conditions (Butler and Hayes 1998). Biotite and vermiculite (Kriegman-King and Reinhard 1992), and kaolinite (Hanoch et al. 2006) have been shown to enhance dechlorination by forming new FeS phases in the system.

This section reviews the abiotic degradation of different groups of halogenated aliphatic hydrocarbons by iron sulfide minerals, including discussion of the rate of degradation, the products of degradation, and the conditions associated with the degradation processes. The compounds will be discussed in four separate groups: (1) the chlorinated ethylenes

including PCE, TCE, *cis*-DCE, and vinyl chloride, (2) chlorinated alkanes including 1,1,1-TCA, 1,1,2-TCA, 1,1-DCA, and 1,2-DCA, (3) chlorinated methanes including carbon tetrachloride, chloroform, and dichloromethane and (4) EDB (1,2-dibromoethane).

2.2 Abiotic Transformation of Chlorinated Ethylenes

2.2.1 Transformation Products

Abiotic transformation kinetics are usually expressed in the literature as a first order rate constant or a surface area normalized first order rate constant. The first order rate constant or pseudo first order rate constant is obtained from fitting the experimental data to a first order rate law. A surface area normalized rate constant is calculated by dividing the first order rate constant by the surface area of the mineral (m^2/L) in suspension in the solution. The reactions occur on surfaces of the minerals, and the rate of reaction should be proportional to the surface area of the mineral presented to the water, and not to the bulk concentration of the mineral suspended in the water. The surface area normalized rate constants may provide a better comparison of rate constants, especially when the minerals vary widely in their specific surface area (m^2/g). However, information on specific surface area is not always readily available. Table 2.1 lists rates reported in the literature for abiotic degradation of chlorinated ethylenes by FeS phases. Most studies investigated the degradation of chlorinated ethylenes by FeS and pyrite; very few studies included other FeS phases such as troilite, or greigite. Most of these studies focus on PCE and TCE degradation; very few studies included DCE and vinyl chloride degradation by iron sulfide minerals.

Vogel et al. (1987) identified a variety of abiotic and biotic processes that could degrade chlorinated aliphatics, including hydrogenolysis, dihalo-elimination (loss of two adjacent chlorines forming a C-C bond), and coupling (loss of chlorines on two separate molecules forming a C-C bond, joining the two molecules). They

also identified other abiotic processes such as dehydrohalogenation and hydrolysis. For TCE, transformation by FeS or FeS_2 seems to occur via parallel reaction pathways. TCE is transformed by reductive elimination to acetylene via chloroacetylene as an intermediate, or by hydrogenolysis to *cis*-DCE (Butler and Hayes 1999; Jeong et al. 2007; Lee and Batchelor 2002a). Acetylene was reported to be the major reaction product in the reductive transformation of TCE by FeS (accounting for 70 to 80% of removed TCE), followed by *cis*-DCE (accounting for 7%), and ethylene, ethane, and other C_2 to C_6 hydrocarbons (accounting for 15 to 20%). The C_4 and C_6 minor products were attributed to coupling of radical intermediates formed in the TCE transformation process.

Sivavec and Horney (1997) reported a similar product distribution for transformation of TCE by the FeS mineral phase troilite. Acetylene was also detected as a product in the reaction of TCE and PCE with nickel and copper sulfides (Butler and Hayes 1999). Lee and Batchelor (2002a) found the main transformation product for TCE dechlorination by pyrite was acetylene, accounting for 86% of TCE that was removed. Minor products were *cis*-DCE (6.6% of TCE) and ethylene (4.4% of TCE).

Butler and Hayes (1999) proposed that PCE was transformed by FeS via parallel reaction pathways to acetylene, TCE, and *cis*-DCE. PCE was transformed to acetylene eight times faster than it was to TCE. No vinyl chloride was detected over the course of the experiment, which is likely due to only minimal accumulation of *cis*-DCE.

Lee and Batchelor (2002a) showed that the main transformation product of PCE on pyrite is acetylene, which accounted for 71.1% of PCE that was degraded. Minor products were ethylene (13.3%) and TCE (14.9%). Neither *cis*-DCE nor vinyl chloride was observed. PCE could be transformed to TCE, followed by the parallel transformation to acetylene and *cis*-DCE. The reductive dechlorination of

cis-DCE in pyrite suspension produced acetylene and ethylene, which accounted for 44.3% and 17.5% of removed *cis*-DCE, respectively. Neither vinyl chloride nor ethane was observed. However, a trace amount of vinyl chloride was detected as a transformation product of *cis*-DCE and *trans*-DCE by zerovalent Fe⁰ and Zn⁰ (Arnold and Roberts 2000). To our knowledge, there is no investigation of DCE degradation by FeS that has been reported to date.

Lee and Batchelor (2002a) proposed that dechlorination of vinyl chloride by pyrite followed a hydrogenolysis pathway to produce ethylene and ethane, with ethylene accounting for 77.3% of vinyl chloride that was removed. Ethylene was further reduced to ethane in the suspension, accounting for 11.4% of the target organic removed. Acetylene was not observed throughout the experiment.

No report on vinyl chloride degradation by FeS has been published.

Table 2.1. Rate Constants and products of abiotic degradation of chlorinated ethylenes by FeS minerals.

Chlorinated solvents	FeS mineral phases	Degradation product	Conditions	Rate constant	Reference
PCE	Fe ²⁺ and HS ⁻ in solution	None detected	pH 7.0, 0.1M NaHCO ₃ 1.85 mM FeCl ₂ 2.06 mM Na ₂ S	Not detected <10% in 33 days <10% in 33 days	Doong and Wu 1992
PCE	FeS (freeze dried)	TCE, acetylene via parallel reaction pathways, minor <i>cis</i> -DCE	pH 8.3, 10 g/L, 0.5m ² /L amended 10 ⁻³ M cysteine	(1.37±0.02)x10 ⁻² d ⁻¹ 2.74 x10 ⁻² L m ⁻² d ⁻¹ (3.67±0.08)x10 ⁻³ d ⁻¹ 7.34 x10 ⁻² L m ⁻³ d ⁻¹	Butler and Hayes 1999
PCE	Mackinawite (FeS)	Acetylene, TCE, <i>cis</i> -DCE, 1,1-DCE	pH 8.3, 10g/L FeS 0.1M tris buffer w/0.01M FeCl ₂ w/0.01M CoCl ₂ w/0.01M NiCl ₂ w/0.01M HgCl ₂	(1.82±0.24)x10 ⁻² d ⁻¹ (1.15±0.21)x10 ⁻² d ⁻¹ (2.13±0.18)x10 ⁻¹ d ⁻¹ (1.05±0.22)x10 ⁻² d ⁻¹ (3.69±0.38)x10 ⁻² d ⁻¹	Jeong and Hayes 2007
PCE	FeS	<i>cis</i> -DCE, TCE, ethylene	pH7, 10g/L pH8, 10g/L pH9, 10g/L	(6.3±1.6)x10 ⁻⁵ L m ² d ⁻¹ (5.3±0.51)x10 ⁻⁴ L m ² d ⁻¹ (1.21±0.12)x10 ⁻³ L m ⁻² d ⁻¹	Liang et al. 2007
PCE	Pyrite	TCE, acetylene, ethylene	pH8, 84 g/L 2340 m ² L ⁻¹	(1.01±0.02) d ⁻¹ 1.97x10 ⁻⁵ L m ⁻² d ⁻¹	Lee and Batchelor 2002a
TCE	FeS (freeze dried)	Acetylene, <i>cis</i> -DCE via parallel reaction pathways, minor amount of vinyl chloride	pH 8.3, 10 g/L, 0.5m ² /L amended 10 ⁻³ M cysteine	(3.58±0.34)x10 ⁻² d ⁻¹ 7.16 x10 ⁻² L m ² d ⁻¹ (1.03±0.12)x10 ⁻² d ⁻¹ 2.06 x10 ⁻² L m ² d ⁻¹	Butler and Hayes 1999
TCE	FeS (freeze dried)	Acetylene, <i>cis</i> -DCE, vinyl chloride	pH 7.3, 10g/L pH 9.3, 10g/L 1mM MnCl ₂ 2,2'-bipyridine 1% 2-propanol	(1.20±0.41)x10 ⁻² d ⁻¹ (4.80±1.03)x10 ⁻² d ⁻¹ (3.38±0.29)x10 ⁻² d ⁻¹ (3.02±0.21)x10 ⁻² d ⁻¹ (2.81±0.62)x10 ⁻² d ⁻¹	Butler and Hayes 2001

Table 2.1. Continued.

Chlorinated solvents	FeS mineral phases	Degradation product	Conditions	Rate constant	Reference
TCE	FeS	<i>cis</i> -DCE, vinyl chloride, ethylene	pH8, 10g/L FeS, HEPES buffer pH9, 10g/L, CHES buffer	$(1.61\pm 0.19)\times 10^{-4} \text{ L m}^{-2} \text{ d}^{-1}$ $(6.4\pm 0.81)\times 10^{-4} \text{ L m}^{-2} \text{ d}^{-1}$	Liang et al. 2007
TCE	Mackinawite	Acetylene, <i>cis</i> -DCE, 1,1-DCE	pH 8.3, 10g/L FeS, 0.1M tris buffer w/0.01M FeCl ₂ w/0.01M CoCl ₂ w/0.01M NiCl ₂ w/0.01M HgCl ₂	$(5.09\pm 0.24)\times 10^{-2} \text{ d}^{-1}$ $(2.01\pm 0.17)\times 10^{-2} \text{ d}^{-1}$ $(1.01\pm 0.09)\times 10^{-2} \text{ d}^{-1}$ $(3.43\pm 0.11)\times 10^{-2} \text{ d}^{-1}$ $(2.71\pm 0.17)\times 10^{-2} \text{ d}^{-1}$	Jeong and Hayes 2007
TCE	Pyrite	acetylene, ethylene	2 g/L ionic strength 0.01 M with NaClO ₄ , pH adjusted with NaOH or TRIS or PIPES buffer	pH 4.3, 0.182 d ⁻¹ , pH 5.3, 0.182 d ⁻¹ , pH 6.4, 0.293 d ⁻¹ pH 7.4, 0.552 d ⁻¹ pH 8.2, 0.866 d ⁻¹ pH 8.9, 1.21 d ⁻¹	Weerasooriya and Dharmasena 2001
TCE	Pyrite	Organic acid, CO ₂ , Cl ⁻	100 g/L pyrite, DO 0.54 to 8.6 mg/L	0.096 to 0.312 d ⁻¹	Pham et al. 2008
TCE	Pyrite	<i>cis</i> -DCE, acetylene, ethylene	pH 8, 84 g L ⁻¹ 2340 m ² L ⁻¹	$(1.60\pm 0.02) \text{ d}^{-1}$ $2.53\times 10^{-5} \text{ L m}^{-2} \text{ d}^{-1}$	Lee and Batchelor 2002a
TCE	FeS, not freeze dried	Acetylene, DCE	pH 7.2, 18 g/L FeS	$(1.52\pm 0.10)\times 10^{-1} \text{ d}^{-1}$	He et al. 2010
TCE	FeS, freeze dried	Acetylene, DCE	pH 7.2, 18 g/L FeS	$(7.18\pm 3.69)\times 10^{-3} \text{ d}^{-1}$	He et al. 2010
<i>cis</i> -DCE	FeS	none detected	pH 8.3, 10g/L FeS, 0.1M tris buffer	Degradation not detected	Jeong et al. 2007
1,1-DCE	FeS	none detected	pH 8.3, 10g/L FeS, 0.1M tris buffer	Degradation not detected	Jeong et al. 2007
<i>cis</i> -DCE	Pyrite	acetylene, ethylene	pH 8, 84 g L ⁻¹ 2340 m ² L ⁻¹	$(0.98\pm 0.02) \text{ d}^{-1}$ $1.32\times 10^{-5} \text{ L m}^{-2} \text{ d}^{-1}$	Lee and Batchelor 2002a
1,1-DCE	FeS (freeze dried)	none detected	pH 8.3, 10 g/L, 0.5m ² /L	Degradation not detected	Butler and Hayes 1999
Vinyl chloride	Pyrite	C ₂ H ₄ , C ₂ H ₆	pH 8, 84 g L ⁻¹ 2340 m ² L ⁻¹	$(1.71\pm 0.06) \text{ d}^{-1}$ $2.27\times 10^{-5} \text{ L m}^{-2} \text{ d}^{-1}$	Lee and Batchelor 2002a

2.2.2 Rates of Degradation on Iron Sulfide Minerals

Table 2.1 lists the rate constants for degradation of PCE, TCE, DCE, and vinyl chloride by common iron sulfide minerals under different conditions. The FeS used in most of these studies was chemically synthesized in the laboratory, while all FeS₂ used in the experiments was hydrothermal pyrite from natural deposits.

Previous studies established some general trends with regard to degradation of different compounds by iron sulfide minerals. TCE seems to be generally degraded faster than PCE. Butler and Hayes (1999) reported a corrected pseudo first order rate constant (k_{obs}') for PCE degradation by FeS of $(5.7 \pm 1.0) \times 10^{-4} \text{ h}^{-1}$. This value is lower than the k_{obs}' value for TCE of $(1.49 \pm 0.14) \times 10^{-3} \text{ h}^{-1}$. Pseudo first order rate constants for degradation of TCE and PCE, normalized for surface area of FeS (mackinawite) in suspension, were 7.16×10^{-2} and $2.74 \times 10^{-2} \text{ L m}^{-2} \text{ d}^{-1}$ respectively. Similar results for relative rates of degradation of chlorinated ethylenes have been reported on mackinawite (Butler and Hayes 1999) and zerovalent metals (Arnold and Roberts 1998).

Degradation of PCE and TCE on pyrite is slower than degradation by the other iron sulfide minerals. Lee and Batchelor (2002a) investigated abiotic dechlorination of chlorinated ethylenes by pyrite, and they found that rate constants for TCE were the highest, followed by those for vinyl chloride, PCE, and *cis*-DCE. Pseudo first order rate constants for degradation of TCE and PCE, normalized for surface area of FeS₂ (pyrite) in suspension, were $2.53 \times 10^{-5} \text{ L m}^{-2} \text{ d}^{-1}$ and $1.97 \times 10^{-5} \text{ L m}^{-2} \text{ d}^{-1}$. Rate constants for *cis*-DCE and vinyl chloride were $1.32 \times 10^{-5} \text{ L m}^{-2} \text{ d}^{-1}$ and $2.27 \times 10^{-5} \text{ L m}^{-2} \text{ d}^{-1}$. The rates of degradation by pyrite (Lee and Batchelor, 2002a) are from 1390 to 2900 times lower than those reported for degradation on mackinawite and troilite (Butler and Hayes 1999; Sivavec and Horney 1997). These results indicate that pyrite is less reactive than meta-stable iron

sulfides for the reductive dechlorination of chlorinated ethylenes in natural and engineered systems (Lee and Batchelor 2002a).

2.2.3 Factors Affecting Degradation

To understand how different experimental conditions affect degradation, earlier studies investigated the effect of a number of environmental parameters such as pH, the concentration of sulfide in solution, and the concentration of organic matter on the rates of degradation of chlorinated ethylenes. These observations may help identify and optimize conditions to attain efficient dechlorination at field scale.

2.2.3.1 Effect of Freeze Drying FeS on Rate Constants for Transformation of TCE.

Most of the studies in the literature were conducted with FeS that was freeze dried after it was prepared. Figure 2.1 presents data from He et al. (2010) that compares the degradation of TCE by freeze dried FeS (FD-TCE) and FeS that was not freeze dried (for experimental details, see Appendix A.1). In the presence of FeS that was not freeze dried, TCE degraded quickly and after 28 days almost all the TCE was gone. With freeze dried FeS, concentrations of TCE decreased steadily over time, but at a much slower rate than non-freeze dried FeS. Even after 56 days of incubation, over 60% of the TCE remained. Control experiments with 5 mg/L and 50 mg/L hydrogen sulfide but no FeS showed no evidence of TCE degradation.

The calculated pseudo first order rate constant for degradation of TCE by FeS that was not freeze dried, normalized to the concentration of FeS in suspension (moles per liter), was $(0.75 \pm 0.042) \text{ M}^{-1} \text{ d}^{-1}$. This is much faster than the corresponding rate constant for freeze dried FeS [$(0.036 \pm 0.018) \text{ M}^{-1} \text{ d}^{-1}$]. The rate of TCE degradation on freeze dried FeS in Figure 2.1 is generally consistent with rate constants obtained by Butler and Hayes (2001) and Jeong et al. (2007) using freeze dried FeS.

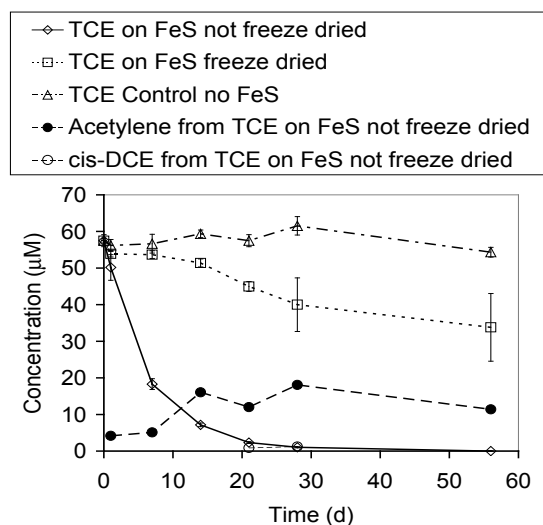


Figure 2.1. TCE degradation by chemically synthesized FeS at pH 7.2. Error bars are one standard deviation.

Shen and Wilson (2007) conducted column experiments to simulate TCE degradation in a mulch biowall, and the pseudo first order rate constant for TCE removal, normalized to the amount of biogenic FeS that formed in the system (0.53 to $2.3 \text{ M}^{-1} \text{ d}^{-1}$) was roughly equivalent to the rate constant obtained from non-freeze dried chemically synthesized FeS as presented in Figure 2.1. The rate of TCE degradation on FeS that is not freeze dried is from 20 to 50 times greater than the rate of degradation on freeze dried FeS.

2.2.3.2 Effect of pH on the Rate of Transformation of TCE on FeS

Figure 2.2 compares data from Butler and Hayes (2001) for the rate constant of TCE degradation on freeze dried FeS to data from He et al. (2010) for TCE degradation on both freeze dried FeS and FeS that was not freeze dried. The pseudo first order rate constants are normalized to the amount of FeS in the suspensions. Regardless of how the FeS was prepared, the rate of abiotic reaction of TCE on FeS increased with increasing pH.

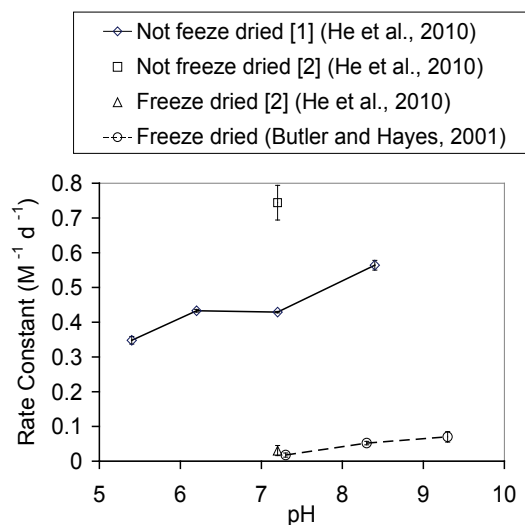


Figure 2.2. Effect of pH on the rate of TCE degradation on chemically synthesized FeS. The data series Not freeze dried [2] and freeze dried [2] repeat data from Figure 2.1.

Butler and Hayes (2001) showed that solution pH had a significant influence on both the overall rate constants for TCE transformation by FeS (k_{obs}) as well as the distribution of reaction products. A similar dependence of rate constants on pH was also observed in the transformation of TCE by pyrite (Lee and Batchelor 2002a; Weerasooriya and Dharmasena 2001).

The reason for the pH effect on TCE degradation by FeS remains unclear. One plausible explanation is that the reactive chemical species on the surface of the FeS changes as a function of pH. Bebie et al. (1998) have proposed that the surface chemistry of metal sulfides is dominated by sulfhydryl functional groups. An increase in pH would result in an increased concentration of deprotonated surface species. The difference in reactivity between the protonated and deprotonated forms of surface acid/conjugate base pairs can be explained by the greater driving force for electron donation by the more deprotonated ligands, which could cause an increased rate of reductive dechlorination at higher pH.

Butler and Hayes (2001) suggested surface functional groups that are more deprotonated would

also be better nucleophiles, which could increase the rate of formation of chloroacetylene and its degradation product (acetylene) by a nucleophile-induced dichloroelimination pathway. Similarly, Weerasooriya and Dharmasena (2001) explained the influence of pH on the transformation of TCE by pyrite on pH-dependent equilibria between pyrite surface functional group.

Alternatively, the pH effect on TCE degradation can be related to faster electron transfer at higher pH. Conway et al. (1980) use cyclic voltammetry to measure peak currents in FeS₂ (pyrite) and Fe_{1-x}S (pyrrhotite). Because the peak current is proportional to the rate of electron transfer at the electrode–solution interface, an increase in peak current with increasing pH implies a faster rate of electron transfer at higher pH values. Conway et al. (1980) suggested this pH-dependence of the peak current was greater as deprotonation of sulfide species increases in the interfacial region with increasing pH. As a result, electron transfer by FeS should increase at higher pH, leading to an increase in the rate of TCE degradation.

2.2.3.3 Organic Molecules

Organic molecules with strong affinities for the FeS surface may affect rate constants through surface electron transfer reactions. Butler and Hayes (1998) show that addition of cysteine significantly inhibits the rate of TCE reductive dechlorination by FeS. This rate reduction may be due to adsorption of cysteine or methionine to surface iron atoms in competition with HS⁻ or OH⁻, causing an energetic barrier or steric barrier to electron transfer (Butler and Hayes 2002). On the other hand, addition of 2,2-bipyridine and 2-propanol did not significantly affect pseudo first order rate constants or branching ratios for TCE transformation by FeS (Butler and Hayes 2001). However, unlike what they observed in the TCE system, Butler and Hayes (1998) found that 2,2'-bipyridine increased hexachloroethane degradation by FeS by an order of magnitude.

2.2.3.4 Metal Ions

Recently, Jeong and Hayes (2007) reported the impact of transition metals [Fe(II), Co(II), Ni(II), and Hg(II)] on the dechlorination rates of PCE and TCE. The impact of Fe(II) on the dechlorination rates varied with its concentration, due to the formation of several Fe sorption phases. Both Co(II) and Hg(II) enhanced the reductive dechlorination of PCE and TCE, but Ni(II) slowed the rate of dechlorination. Jeong and Hayes (2007) attributed their results to different dechlorination reactivities of new sulfide phases formed by interaction of the transition metals with FeS (See Section 2.3.3.2. for more discussion).

2.2.3.5 Dissolved Oxygen (DO)

Most of the past studies on degradation of chlorinated compounds by pyrite have been conducted under anaerobic conditions. The degradation of chlorinated compounds in pyrite suspension in the presence of O₂ has been less studied. Kriegman-King and Reinhard (1994) reported that oxygen inhibited carbon tetrachloride transformation by pyrite. In a more recent study, Pham et al. (2008) show that the rate of transformation of TCE on pyrite depended strongly on dissolved oxygen. The transformation rate increased with an increase in DO. The rate constant for degradation increased from 0.004 hr⁻¹ up to 0.013 hr⁻¹ as the DO increased from 0.017 to 0.268 mmol/L. In the more aerobic systems, TCE transformed to several organic acids including dichloroacetic acid, glyoxylic acid, oxalic acid, formic acid, and finally to CO₂ and chloride ion. Dichloroacetic acid was the only chlorinated degradation product of TCE that was observed in their experiments.

2.2.4 Degradation Mechanisms

The reductive dehalogenation of chlorinated compounds by the transfer of electrons from the mineral surface is similar to the mechanism of TCE dehalogenation on zerovalent iron (ZVI) (Liu et al. 2005; Pham et al. 2008). Two major pathways of reductive transformation of

TCE have previously been proposed (Butler and Hayes 2001; Lipczynska-Kochany et al. 1994). The first pathway, sometimes called β -elimination or dichloroelimination, results in the formation of an additional carbon-carbon bond with loss of two halogens on adjacent carbon atoms. TCE undergoes dichloroelimination to acetylene via the transient intermediate chloroacetylene (Arnold and Roberts 2000; Burris et al. 1996; Campbell et al. 1997; Roberts et al. 1996). Acetylene may undergo subsequent hydrogenation to ethylene and/or ethane under certain conditions (Arnold and Roberts 2000; Campbell et al. 1997), and it can also be hydrolyzed. Dichloroelimination results in the formation of relatively benign products.

In the second pathway TCE undergoes sequential hydrogenolysis, forming *cis*-DCE, vinyl chloride, and ethylene (Butler and Hayes 2001). Hydrogenolysis (replacement of a halogen by hydrogen) of both chloroethylenes leads to the formation of more toxic and recalcitrant chlorinated byproducts including the dichloroethylenes and vinyl chloride. Each of these reactions involves a net transfer of two electrons. Jeong et al. (2007) observed that acetylene was subsequently transformed in the presence of FeS, but little transformation of *cis*-DCE and 1,1-DCE was observed.

A third mechanism proposed by Pham et al. (2008) suggested that the transformation of TCE in aerobic pyrite suspension follows a Fenton-like mechanism, in which the reduction of O₂ at the pyrite surface can induce hydroxyl radical formation (Cohn et al. 2006; Pham et al. 2008; Rimstidt and Vaughan 2003).

The transformation of PCE and other contaminants by iron sulfide minerals is similar to the degradation of TCE. Jeong and Hayes (2007) proposed that PCE transforms to TCE via hydrogenolysis, to acetylene via β -elimination and to 1,1-DCE via α -elimination. The process of β -elimination results in loss of two halogens on the same carbon atom.

Lee and Batchelor (2002a) suggested that the main pathway for the reductive dechlorination of *cis*-DCE by pyrite is the reductive elimination pathway. They also proposed a sequential hydrogenolysis pathway to explain the reductive transformation of vinyl chloride in pyrite suspension (vinyl chloride \rightarrow ethylene \rightarrow ethane, which all involves 2 electron reductions).

2.3 Abiotic Transformation of Chlorinated Alkanes

2.3.1 Degradation Products

Based on the reaction pathway of 1,1,1-TCA proposed by Fennelly and Roberts (1998), 1,1,1-TCA can be initially transformed to 1,1-DCA through hydrogenolysis, to 1,1-dichloroethylene through dehydrochlorination, and to 2,2,3,3-tetrachlorobutane by coupling of two dichloroethyl radicals (H₃C- \dot{C} -Cl₂) that were produced by a one electron reduction of 1,1,1-TCA. In addition, it has been reported that carbene intermediates (H₃C-C-Cl) formed by two-electron reduction to 1,1,1-TCA triggered the formation of acetaldehyde and vinyl chloride (Butler and Hayes 2000; Choi et al. 2009).

Butler and Hayes (2002) showed that 1,1,1-TCA degraded on FeS, and that 1,1-DCA accounted for approximately 2% of 1,1,1-TCA that was degraded, however, 1,1-DCA, 1,2-DCA, and 1,1,2-TCA showed no appreciable transformation by FeS over approximately 120 days.

Gander et al. (2002) investigated 1,1,1-TCA transformation by iron sulfide and a methanogenic microbial consortium. In reactors containing FeS alone, minor amounts of 1,1-DCA (2%) and 2-butyne (4%) were observed as products, resulting in a carbon mass recovery of ~6% of the 1,1,1-TCA that was degraded. Other potential degradation products (1,2-dichloroethylene, acetic acid, acetylene, ethane, ethylene, acetaldehyde, *cis*-2-butene, and vinyl chloride) were not detected. In reactors containing LEC (a methanogenic culture of bacteria enriched on lactate) alone, the only identified product was 1,1-DCA, which accounted for 46 \pm 8% of the 1,1,1-TCA that was transformed (Gander et al. 2002).

2.3.2 Rates of Degradation on Iron Sulfide Minerals

Table 2.2 lists rates reported in the literature for degradation of chlorinated alkanes by FeS minerals. The rate constant for degradation of 1,1,1-TCA transformation by 10 g/L chemically synthesized FeS was $(0.28 \pm 0.03) \text{ d}^{-1}$, corresponding to a half-life of 2.5 days (Gander et al. 2002). Choi et al. (2009) show that 82% of initial 1,1,1-TCA (0.5 mM) was removed in contact with 33 g/L of FeS within 48 h, producing 1,1-DCA as the major transformation product. The rate constant for the reductive

dechlorination of 1,1,1-TCA was $(0.0375 \pm 0.0018) \text{ h}^{-1}$. Butler and Hayes (2000) reported a rate constant for degradation of 1,1,1-TCA on 10 g/L FeS of 0.235 d^{-1} , corresponding to a pseudo first order rate constant normalized to the surface area of FeS of $0.63 \text{ L m}^{-2} \text{ d}^{-1}$. This is approximately tenfold faster than the pseudo first order rate constant for degradation of TCE on FeS, which was $0.0716 \text{ L m}^{-2} \text{ d}^{-1}$ (Butler and Hayes, 1999, see Table 2.1).

Wilson et al. (2008) investigated 1,2-DCA degradation by biogenic FeS. They extracted

Table 2.2. Rates and products of abiotic degradation of chlorinated alkanes on FeS minerals.

Chlorinated solvents	FeS mineral phases	Degradation product	Conditions	Rate constant	Reference
1,1-DCA	FeS	None detected	Same as above	Rate not significant at 95% confidence	Butler and Hayes 2000
1,2-DCA	FeS	None detected	Same as above	Rate not significant at 95% confidence	Butler and Hayes 2000
1,2-DCA	Biogenic FeS	Not monitored	pH 7, 26 g/L FeS	$2.8 \times 10^{-2} \text{ d}^{-1}$	Wilson et al. 2008
1,1,1-TCA	Fe ²⁺ and HS ⁻ in solution	None detected	pH 7.0, 0.1M NaHCO ₃ and 1.85 mM FeCl ₂ 2.06 mM Na ₂ S	<10% in 33 days <10% in 33 days	Doong and Wu 1992
1,1,1-TCA	FeS, freeze dried	1,1-DCA, 2-butyne	pH 7.5, 10 g/L FeS, 100 mM NaHCO ₃	$0.28 \pm 0.03 \text{ d}^{-1}$	Gander et al. 2002
1,1,1-TCA	FeS	1,1-DCA	pH 8.3, 10 g /L FeS, 0.05 m ² /g, ionic strength 0.1M	$(2.35 \pm 0.34) \times 10^{-1} \text{ d}^{-1}$ $(0.63 \pm 0.09) \text{ L m}^{-2} \text{ d}^{-1}$	Butler and Hayes 2000
1,1,1-TCA	FeS	1,1-DCA, ethylene	pH 7.5, 33 g/L FeS, Tris buffer	$(9.0 \pm 0.043) \times 10^{-1} \text{ d}^{-1}$	Choi et al. 2009
1,1,2-TCA	FeS	1,1-DCE, vinyl chloride	pH 8.3, 10 g /L FeS, 0.05 m ² /g, ionic strength 0.1M	Rate not significant at 95% confidence	Butler and Hayes 2000
1,1,1,2-TeCA	FeS	1,1-DCE	Same as above	$(0.73 \pm 0.12) \text{ d}^{-1}$ $(1.46 \pm 0.24) \text{ L m}^{-2} \text{ d}^{-1}$	Butler and Hayes 2000
1,1,1,2,2-TeCA	FeS	TCE, <i>cis</i> -DCE, <i>trans</i> -DCE, acetylene	Same as above	$(4.56 \pm 9.6) \times 10^{-2} \text{ d}^{-1}$ $(9.12 \pm 19) \times 10^{-2} \text{ L m}^{-2} \text{ d}^{-1}$	Butler and Hayes 2000
PCA Pentachloroethane	FeS	PCE, TCE	pH 8.3, 10 g /L FeS, 0.05 m ² /g, ionic strength 0.1M	$(2.28 \pm 1.03) \text{ d}^{-1}$ $(4.6 \pm 2.1) \text{ L m}^{-2} \text{ d}^{-1}$	Butler and Hayes 2000

Table 2.2. Continued.

Chlorinated solvents	FeS mineral phases	Degradation product	Conditions	Rate constant	Reference
HCA Hexachloroethane	FeS, freeze dried	PCE, PCA, TCE, <i>cis</i> -DCE, acetylene	pH 7.8, 10 g /L FeS, 0.05 m ² /g, ionic strength 0.1M	(1.74±0.19) d ⁻¹ (3.5±0.38) L m ⁻² d ⁻¹	Butler and Hayes 1998
HCA	FeS, freeze dried	PCE, PCA, TCE, <i>cis</i> -DCE, acetylene	Same as above	(2.97±0.18) d ⁻¹ (5.9±0.36) L m ⁻² d ⁻¹	Butler and Hayes 2000
HCA	FeS, freeze dried	PCE	pH 8.3, 10 g /L FeS, 0.05 m ² /g, ionic strength 0.1M	(1.80±0.08) d ⁻¹ (3.61±0.16) L m ⁻² d ⁻¹	Jeong and Hayes 2003
HCA	FeS	Not monitored	pH 7.2, 2.0 g/L, 25 m ² /L, 1 mM Fe ²⁺	0.38 L m ⁻² d ⁻¹	Elsner et al. 2004b
HCA	FeS ₂ pyrite	Not monitored	pH 7.2, 28 g/L, 25 m ² /L, 1 mM Fe ²⁺	0.38 L m ⁻² d ⁻¹	Elsner et al. 2004b
γ-HCH hexachloro-cyclohexane	FeS, freeze dried	pentachloro-cyclohexene, tetrachloro-cyclohexene, dichlorocyclohexadiene, dichlorobenzenes, chlorobenzene	pH 8.3, tris-HCl, 10 g/L, 10 m ² /g ionic strength 0.1M	(1.1×10 ⁻²) d ⁻¹ (1.1×10 ⁻⁴) L m ⁻² d ⁻¹	Liu et al. 2003

a rate constant of 0.028 d⁻¹ in contact with 26 g/L FeS. This rate constant was an order of magnitude lower than rate constants for TCE and EDB degradation under similar conditions.

Butler and Hayes (2000) reported first order rate constants for degradation of hexachloroethane, pentachloroethane, 1,1,2,2-tetrachloroethane, 1,1,1,2-tetrachloroethane, and 1,1,1-trichloroethane in water containing 0.5 m² L⁻¹ FeS as poorly crystalline mackinawite. Table 2.2 expresses their data as a first order rate constant, and as a first order rate normalized to the surface area of FeS exposed to water. The surface area specific rates varied from a high of (28 ± 1.5) m² L⁻¹ d⁻¹ for pentachloroethane to a low of (5.9 ± 0.36) m² L⁻¹ d⁻¹ for hexachloroethane.

2.3.3 Conditions Affecting Degradation

Similar to other groups of halogenated aliphatic compounds, TCA degradation is affected by solution composition and environmental conditions.

2.3.3.1 pH

Previous studies demonstrated that the reductive dechlorination of TCE by FeS was strongly dependent on the suspension pH and generally increased with increasing pH (Butler and Hayes 1998; Butler and Hayes 2001). There is no report available in the literature concerning the effect of pH on TCA degradation by FeS. However, an effect similar to the effect on degradation of TCE would be expected because the FeS surface will be affected by changes in pH in a similar way.

Butler and Hayes (1998) investigated the influence of pH on the reductive dechlorination of hexachloroethane (HCA) by FeS occurring as poorly crystalline mackinawite. Increasing the solution pH from 7.1 to 9.5 caused a significant increase in the rate of reductive dechlorination of HCA by FeS. They proposed that a pH-dependent equilibrium between the protonated and deprotonated forms of FeS surface species is responsible for the pH dependence of the rate of reductive dechlorination of HCA by FeS, with the deprotonated species having greater reactivity.

2.3.3.2 Metals

Metal ions may be characterized as “hard” or “soft” depending on the Lewis acid base principle. Metal ions in water impact the dechlorination rates of hexachloroethane depending on their relative hardness. While hard metals decrease the dechlorination rates, intermediate to soft metals enhance the rates (Butler and Hayes 1998; Jeong and Hayes 2007). Choi et al. (2009) show that the reduction rate of 1,1,1-TCA by FeS increased with increasing concentration of transition metals. The rate constants in the presence of 10 mM Co(II) and Ni(II) were 0.06 and 0.11 h⁻¹, approximately 1.3 and 3.0 times greater than those by FeS alone.

Jeong and Hayes (2003) investigated the impact of various transition metals on the reductive dechlorination by mackinawite using a readily degradable chlorinated organic compound, hexachloroethane (HCA). They found that 10⁻³ M Cr(III) and Mn(II) (hard metal ions) decreased the dechlorination rates. These hard metal ions, due to their weak affinity for sulfides, are thought to form surface precipitates of hydroxides around FeS under the experimental conditions. These hydroxide precipitates should hinder the electron transfer between FeS and HCA (Butler and Hayes 1998; Jeong and Hayes 2003). In contrast, Co(II), Ni(II), Cu(II), Zn(II), Cd(II), and Hg(II) (intermediate/soft metal ions) at concentrations of 10⁻⁴, 10⁻³, and 10⁻² M increased the rates of HCA degradation on FeS (Jeong and Hayes 2003).

2.3.3.3 Sulfide

Choi et al. (2009) evaluated the effect of HS⁻ in solution on the rate of degradation of 1,1,1-TCA by FeS. Although 1,1,1-TCA was reductively degraded by HS⁻ in homogeneous solution to a certain extent, the rate of reaction was enhanced in the presence of FeS. Reductive dechlorination of 1,1,1-TCA by FeS increases with HS⁻ concentrations. The rate of 1,1,1-TCA degradation on FeS was 0.0375 ± 0.0018 h⁻¹. The rate in the presence of 5 mM HS⁻ was three times greater, and the rate in the presence of 20 mM HS⁻ was ten times greater than degradation by FeS without HS⁻ (Choi et al. 2009). The HS⁻ added to the suspension of FeS may bind to the surface of FeS and enhance the reaction rate of 1,1,1-TCA by facilitating the electron transfer or by forming reactive iron sulfide species on the surface of FeS (Choi et al. 2009).

Sulfide may also enhance dechlorination through formation of new FeS phases. Choi et al. (2009) show that iron sulfide can be deposited on the surface of iron metal and facilitate the electron transfer from iron metal to chlorinated organic compounds. Kriegman-King and Reinhard (1992) found that the rates of transformation of HCA by biotite or vermiculite increased significantly when HS⁻ was added to the experimental system. The increase in reactivity may have been due to the formation of a secondary iron sulfide phase upon reaction of HS⁻ with Fe²⁺ associated with the clay minerals (Kriegman-King and Reinhard 1992).

2.3.3.4 Organic Molecules

No experiment has been conducted to investigate the effect of natural organic matter (NOM) on 1,1,1-TCA degradation. However, several studies investigated the effect of NOM on HCA degradation. These studies indicate that organic compounds with strong metal chelating properties and delocalized π* electrons significantly increase the rate of HCA dechlorination (Jeong and Hayes 2003).

Butler and Hayes (1998) found that compounds with a bidentate chelating functional group,

including 2,2'-bipyridine, 1,10-phenanthroline, and EDTA, could significantly increase the rate of HCA reductive dechlorination. The presence of this functional group likely increased the driving force for adsorption of these compounds to the mineral surface (Butler and Hayes 1998). On the other hand, oxalate, succinate, and hydroquinone, which contain phenolic and carboxylic functional groups, had no significant effect on the HCA dechlorination rate (Butler and Hayes 1998). Addition of 1 mM cysteine, a thiol-containing amino acid, to the FeS reaction mixture reduced the rate of reductive dechlorination of HCA by almost one-half, and the addition of 1 mM methionine, an alkylthio amino acid, only slightly depressed the rate. This rate reduction may be due to adsorption of cysteine or methionine to surface iron atoms in competition with HS⁻ or OH⁻, causing an energetic or steric barrier to electron transfer (Butler and Hayes 1998).

2.4 Abiotic Transformation of Chlorinated Methanes

2.4.1 Degradation Products

Hanoch et al. (2006) has reviewed the capacity of common soil minerals to degrade carbon tetrachloride. Carbon tetrachloride can be reductively dechlorinated by pyrite (FeS₂) and FeS (Assaf-Anid and Lin 2002; Kenneke and Webber 2003; Lee and Batchelor 2002a; Pham et al. 2008) and by marcasite, which is also a form of FeS₂ (Butler and Hayes 1998; Kriegman-King and Reinhard 1994). There is one study on the degradation of chloroform on FeS (Kenneke and Webber 2003). To our knowledge, no information is available on degradation of dichloromethane by FeS or FeS₂ minerals.

Laboratory investigations have demonstrated that carbon tetrachloride can be degraded along two competing pathways: through hydrogenolysis to chloroform, and through hydrolysis to carbon dioxide (Criddle and McCarty 1991).

The iron sulfide minerals pyrite and marcasite were shown to reduce carbon tetrachloride to chloroform (Kriegman-King and Reinhard

1994). Kenneke and Webber (2003) reported 69% conversion of carbon tetrachloride to chloroform in the presence of FeS. Devlin and Müller (1999) reported that the principal product of carbon tetrachloride reduction by FeS was chloroform (48%) followed by carbon dioxide (10%), formate (5%), and carbon disulfide (2%). In addition, formation of non-chlorinated products such as carbon monoxide, methane, acetylene, ethylene, and ethane was also observed during abiotic degradation of carbon tetrachloride by various minerals (Criddle and McCarty 1991; Devlin and Müller 1999; Elsner 2004a; Kenneke and Webber 2003; Kriegman-King and Reinhard 1992; Maithreepala and Doong 2005; O'Loughlin et al. 2003).

Kriegman-King and Reinhard (1994) show that the product distribution of carbon tetrachloride degradation varies greatly depending on the reaction conditions. Under aerobic conditions, the major product was carbon dioxide which could account for 70% to 80% of the carbon tetrachloride transformed. In contrast, the anaerobic system forms approximately 50% chloroform and only 10% to 20% carbon dioxide.

2.4.2 Rate Constants

Hanoch et al. (2006) reviewed carbon tetrachloride dechlorination by some common soil minerals. In general, the rate of degradation on FeS minerals was the fastest among all the minerals that were tested. The rate of degradation on pyrite was slower than on FeS, but still faster than the other Fe(II) containing minerals.

Table 2.3 lists rate constants reported in the literature for degradation of chlorinated methanes by FeS minerals. Butler and Hayes (2000) reported rapid degradation of carbon tetrachloride in the presence of FeS, with an observed first order rate constant of $(6.39 \pm 0.79) \times 10^{-2} \text{ h}^{-1}$. Table 2.3 expresses their data as this first order rate, and as a first order rate normalized to the surface area of FeS exposed to water. The surface area specific rate of degradation of carbon tetrachloride was $(5.2 \pm 0.6) \text{ m}^2 \text{ L}^{-1} \text{ d}^{-1}$.

Table 2.3. Rates and products of abiotic degradation of chlorinated methanes on FeS minerals

Chlorinated solvents	FeS mineral phases	Degradation product	Conditions	Rate constant	Reference
CCl ₄	Fe ²⁺ or HS ⁻ in solution	CHCl ₃	pH 7.0, 0.1M NaHCO ₃ and 1.85 mM FeCl ₂ 2.06 mM Na ₂ S	90% removal in 10 days 0.23 d ⁻¹ <10% removal in 33 days	Doong and Wu 1992
CCl ₄ Carbon Tetrachloride	Mackinawite 1 Mackinawite 2	CHCl ₃ Chloroform	4 g/L FeS, 13 m ² /g pH 7.2, 0.6 g/L FeS, 77 m ² /g, pH 7.2	(5.84±0.31)×10 ¹ d ⁻¹ (1.2±0.06) L m ⁻² d ⁻¹ (1.52±0.11) d ⁻¹ (3.0±0.22)×10 ⁻² L m ⁻² d ⁻¹	Zwank et al. 2005
CCl ₄	FeS	CHCl ₃ , possibly CH ₄ , C ₂ H ₄ , C ₂ H ₆	FeS 33 g/L, Tris buffer, pH 7.5	(2.98±0.22)×10 ¹ d ⁻¹	Choi et al. 2009
CCl ₄	FeS	Not monitored	200g/L FeS, 0.05M I, pH 6.5	(4.15±0.12)×10 ¹ d ⁻¹	Lipczynska-Kochany et al. 1994
CCl ₄	FeS ₂	Not monitored	200g/L FeS ₂ , 0.05M I, pH 6.5	(4.15±0.19)×10 ¹ d ⁻¹	Lipczynska-Kochany et al. 1994
CCl ₄	FeS, fresh FeS, aged	CHCl ₃ , CS ₂ CHCl ₃ , CS ₂	0.73 g/L FeS 0.73 g/L FeS	66% removed in one day 1.07 d ⁻¹ 72% removed in one day 1.27 d ⁻¹	Devlin and Müller 1999
CCl ₄	FeS	CHCl ₃ , CH ₂ Cl ₂	pH 8, 18 g/L FeS	80% removed in 2.5 hours 9.7×10 ¹ d ⁻¹	Assaf-Anid and Lin 2002
CCl ₄	FeS, freeze dried	CHCl ₃	10g/L FeS, 0.05 m ² /g, pH 8.3, 0.1M Tris	(2.6±0.31) d ⁻¹ (5.2±0.62) L m ⁻² d ⁻¹	Butler and Hayes 2000
CCl ₄	FeS coating on Iron oxides formed by treating with HS ⁻	CHCl ₃	pH 8, 0.1M tris 0.13 g/L FeS on goethite 0.20 g/L FeS on hematite	(0.28±0.14) d ⁻¹ (0.22±0.12) d ⁻¹	Hanoch et al. 2006
CCl ₄	Pyrite	CHCl ₃ , CO ₂ , CS ₂ , formate	pH 6.5, fresh ground pyrite, 14.8 g/L, 0.01 m ² /g, anaerobic conditions	zero order kinetics 0.053 mol m ⁻² d ⁻¹ first order kinetics 0.12 d ⁻¹ 0.16 L m ⁻² d ⁻¹	Kriegman-King and Reinhard 1994

Table 2.3. Continued.

Chlorinated solvents	FeS mineral phases	Degradation product	Conditions	Rate constant	Reference
CCl ₄	Pyrite	CHCl ₃	6 g/L FeS	20% removed in one day 0.22 d ⁻¹	Devlin and Müller 1999
CCl ₄	Pyrrhotite	CHCl ₃	6 g/L FeS	60% removed in one day 0.91 d ⁻¹	Devlin and Müller 1999
CCl ₃ Chloroform	FeS coating on Iron oxides formed by treating with HS ⁻		pH 8, 0.1M tris 0.13 g/L FeS on goethite 0.20 g/L FeS on hematite	 (2.23±0.29) × 10 ⁻³ d ⁻¹ (9.37±0.98) × 10 ⁻³ d ⁻¹	Hanoch et al. 2006
CHCl ₃	FeS	Not monitored	pH 7.8, 0.044 g/L, 0.14 m ² /g	0.717 m ⁻² min ⁻¹ in 0.059 L 6.1 × 10 ¹ L m ⁻² d ⁻¹	Kenneke and Weber 2003

2.4.3 Conditions Affecting Reactivity

2.4.3.1 pH

Similar to PCE and TCE degradation, pH could have important effects on carbon tetrachloride degradation. This is because pH may affect the surface properties of the minerals, the aqueous speciation of sulfide, and probably the surface speciation of sulfide (Kriegman-King and Reinhard 1992). However, Kriegman-King and Reinhard (1992) didn't find a strong effect of solution pH on the degradation of carbon tetrachloride by biotite and vermiculite over a pH range of 6 to 10 standard units. We are not aware of any studies investigating the effect of pH on carbon tetrachloride degradation in the presence of iron sulfide minerals. Based on the discussion in section 2.2.3.2, we would expect pH to have a similar effect on carbon tetrachloride degradation by FeS as on degradation of TCE by FeS.

2.4.3.2 Sulfide

Sulfide was expected to play an important role in the kinetics because it could act as either

an electron donor or a nucleophile. Another major role sulfide could play is to form new FeS phases that could significantly enhance dechlorination. The reductive dechlorination of carbon tetrachloride to chloroform by dissolved hydrogen sulfide was reported to occur more rapidly when biotite and vermiculite were present, and the reaction was suggested to take place at the mineral surface (Kriegman-King and Reinhard 1992). Carbon tetrachloride was also shown to be reduced to chloroform by a sodium sulfide solution containing hematin (Assaf-Anid and Lin, 2002) and in water containing free Fe²⁺ and HS⁻ (Doong and Wu 1992). The reductive dechlorination of carbon tetrachloride to chloroform by dissolved hydrogen sulfide in the presence of the clay minerals could be due to the fact that sulfide can react with dissolved iron (released to solution from mineral dissolution) to form iron sulfide minerals, which can then react with carbon tetrachloride (Kriegman-King and Reinhard 1992).

2.4.3.3 Organic Compounds

Organic compounds representative of natural organic matter (NOM) affect the FeS-mediated reductive dechlorination of carbon tetrachloride to a greater or lesser extent, depending on their structure (Hanoch et al., 2006; Assaf-Anid and Lin, 2002; Butler and Hayes, 1998). These effects have been attributed to the formation of electron donating or electron withdrawing surface complexes (Butler and Hayes 1998). Devlin and Müller (1999) found that in the presence of humic acid, which acted as an electron mediator, the reduction of carbon tetrachloride was accelerated by a factor of ten. Addition of vitamin B₁₂ to aqueous FeS systems not only enhanced the rate of degradation of carbon tetrachloride, but also increased the yields of the hydrogenolysis products chloroform and dichloromethane (Assaf-Anid and Lin 2002). This indicates that organic co-solutes can influence the carbon tetrachloride product distribution, perhaps by acting as hydrogen atom donors. Hashsham et al. (1995) found that the addition of cobalamine to their microcosms increased the rate of transformation of ¹⁴C-labelled carbon tetrachloride one hundred-fold and resulted in 73% of carbon tetrachloride conversion to ¹⁴C-labelled carbon disulfide.

2.5 Abiotic Transformation of the Brominated Ethane EDB

2.5.1 Degradation Products

There is little information about ethylene dibromide (EDB) degradation in the literature. Several earlier studies investigated biological degradation of EDB (Bouwer and McCarty 1985; Henderson et al. 2008; Tandoi et al. 1994). These studies showed that EDB was biodegradable under aerobic and anaerobic conditions. EDB can be degraded through three potential pathways: through hydrolytic debromination to form 2-bromoethanol; through hydrogenolysis (reductive dehalogenation) to form bromoethane; and through dibromoelimination (dihaloelimination) to form ethylene (Wilson et al. 2008).

The only study of abiotic degradation of EDB by FeS to date was conducted by Wilson et al. (2008). In experiments on EDB degradation by laboratory synthesized FeS, ethylene was the major degradation product. Methane was detected but only at background levels, and ethane and acetylene were not detected (personal communication Yongtian He and John T. Wilson, unpublished data).

2.5.2 Rate Constants

The microcosm study by Wilson et al. (2008) shows that the removal of EDB followed first order kinetics without a lag, indicating that removal was an abiotic process that did not require acclimation of an active biological process. However, the study was conducted with biogenic FeS isolated from laboratory columns that simulated a plant mulch based passive reactive barrier. The biogenic FeS used in the study still contained small amounts of residual plant material, and was actively methanogenic and sulfate reducing. To confirm that the removal was truly an abiotic process, the experiment was repeated with chemically synthesized FeS. The FeS was not freeze dried. Details of the procedure are provided in Appendix A.2. The rate constant for degradation of EDB in the microcosm study of Wilson et al. (2008), normalized to the amount of biogenic FeS exposed to the porewater (moles FeS per liter porewater), was $0.781 \pm 0.249 \text{ M}^{-1} \text{ d}^{-1}$.

Figure 2.3 depicts the abiotic degradation of EDB by chemically synthesized FeS at pH 7.2. The rate constant of EDB degradation by synthesized FeS at pH 7.2 was $0.833 \pm 0.004 \text{ M}^{-1} \text{ d}^{-1}$. There was good agreement between the rate of degradation on biogenic FeS and chemically synthesized FeS.

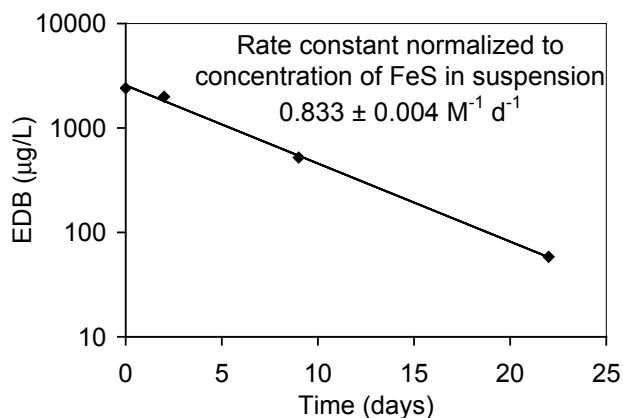


Figure 2.3. EDB degradation by FeS at pH 7.2.

2.5.3 Conditions That Affect Degradation

Wilson et al. (2008) summarized major factors that could be associated with EDB degradation in gasoline release sites.

2.5.3.1 Sulfate and Sulfide

The consumption of sulfate during sulfate reduction produces reactive HS^- that can destroy EDB, or can react with iron(III) minerals to produce FeS which also reacts to degrade EDB. The rate of reactions with HS^- in solution only becomes important to the abiotic degradation of EDB at HS^- concentrations above 0.2 mg/L. At lower concentrations of HS^- in solution, aqueous hydrolysis is faster than reaction with HS^- .

EDB can also react with H_2S and HS^- to produce a variety of thiols and thioethers (Schwarzenbach et al. 1985).

2.5.3.2 pH

Figure 2.4 depicts the effect of pH on the rate of EDB degradation by chemically synthesized FeS. There was a linear increase in the rate of degradation with pH in the range from pH 5 to 9 (Kuder et al., In prep.).

As discussed in Section 2.2.3.2, the rate of abiotic transformation of TCE by iron(II) sulfide also increases as the pH increases. Based on the data for TCE and EDB, pH seems to have a

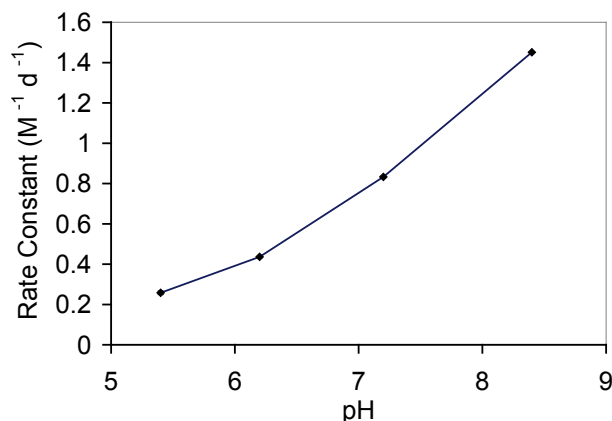


Figure 2.4. Effect of pH on the first order rate constant for EDB degradation by FeS. The rate constant is normalized to the concentration of FeS in suspension.

greater impact on rate of EDB degradation than on TCE degradation. The greater impact may be a composite of the direct effect of pH and the effect of pH on the concentration of sulfide in solution. As pH increases, the deprotonation of the surface of the FeS increases, which should increase its reactivity toward EDB. In experiments with chemically synthesized FeS, the measured concentration of sulfide also increases with pH (2, 9, 26, 40 mg/L at pH 5.4, 6.4, 7.2, 8.4, respectively). Previous studies by Wilson et al. (2008) showed that the presence of sulfide in solution can contribute to EDB degradation. In contrast to EDB, sulfide doesn't seem to have significant impact on TCE degradation rate.

2.6 Formation, Transformations, and Reactivity of Iron Sulfides

2.6.1 FeS Mineralogy and Reactivity

Mackinawite belongs to the P4/nmm space group (Taylor and Finger 1970). Mackinawite possesses a tetragonal layer structure (Wolthers et al. 2003), where the iron atoms are linked in a tetrahedral coordination to four equidistant sulfur atoms. These tetrahedrons share edges to form a layer structure. These layers are stacked along the c-axis and held together by weak van der Waals forces (Vaughan and Craig 1978). Within the layers, each Fe atom is in a

square planar coordination with four Fe atoms with an Fe-Fe distance of 2.5967 Å (Lennie et al. 1995). This is similar to the Fe-Fe distance in α -iron. The Fe-Fe bonding in mackinawite allows it to conduct electricity like a metal (Jeong et al. 2008; Taylor and Finger 1970; Vaughan and Ridout 1971; Wolthers et al. 2003).

The high reactivity of iron sulfide minerals in degrading chlorinated solvents may be related to the following unique properties of FeS:

- (1) The high electron transfer capability of mackinawite. As discussed above, mackinawite is a metallic conductor with the delocalized electrons in the plane of the mackinawite layers (Vaughan and Ridout 1971).
- (2) The hydrophobic character of mackinawite enhances sorption of TCE and other halogenated aliphatic compounds. Weerasooriya and Dharmasena (2001) suggest that TCE may be readily attracted to pyrite by hydrophobic interactions, thus facilitating the surface mediated electron transfer process. Park et al. (2006) suggest that FeS is more hydrophobic than FeS₂ and that the hydrophobicity of the particle surface is a critical factor in surface-mediated dehalogenation of chlorinated compounds.
- (3) FeS is a hydrate with an expanded lattice. Morse and Cornwell (1987) proposed that disordered mackinawite may be a hydrate. Mackinawite has an expanded lattice, in particular along the c axis, with intercalated water molecules between the tetrahedral sheets and possibly intercalated hydroxyl groups with associated protons, cations, or sulfide vacancies to balance charge (Wolthers et al. 2003).

- (4) FeS has a high reduction potential and chalcophilic (sulfur-loving) nature. Both Fe²⁺ and HS⁻ are strong reductants, which contributes to the high reduction potential of FeS phases. Several experimental studies have shown that iron sulfides are more reactive and effective in degradation of the chlorinated compounds than other Fe(II) containing minerals and Fe⁰ in PRB treatment systems. Elsner et al. (2004b) showed a general trend of reaction rates for hexachloroethane and 4-chloronitrobenzene where the rate of degradation increases in the order of Fe(II)+siderite < Fe(II)+iron oxides < Fe(II)+iron sulfides. Newly formed FeS phases have been reported to be significantly more reactive than iron metal in TCE transformation (Butler and Hayes 2001). Jeong and Hayes (2007) showed that in the presence of metals, the chalcophilic nature of FeS facilitated the formation of secondary sulfide phases such as CoS, which increases TCE degradation.

2.6.2 Formation of FeS Minerals

The formation of iron monosulfide (FeS) in a natural environment typically begins with biologically produced Fe²⁺ and HS⁻. Another possible mechanism is to proceed with reductive dissolution of Fe³⁺ oxide by HS⁻ that is generated by sulfate reducing bacteria. Reductive dissolution of goethite by HS⁻ can be described with the following reaction (Pyzik and Sommer 1981):



The Fe²⁺ formed via reductive dissolution then precipitates with aqueous H₂S or HS⁻ to form FeS (Devlin and Müller 1999; Neal et al. 2001; Pyzik and Sommer 1981). This FeS may take the form of mackinawite (FeS_{1-x}, where x = 0.025) (Berner 1970; Taylor and Finger

1970), amorphous phases (Berner 1970; Neal et al. 2001), and a phase tentatively identified by Neal et al. (2001) as hexagonal pyrrhotite (Fe_{1-x}S). While H_2S and HS^- are generated by sulfate reducing bacteria in natural systems, FeS can also form under strictly abiotic conditions (Benning et al. 2000; Hanoch et al. 2006; Herbert et al. 1998; Pyzik and Sommer 1981). In typical anoxic aquatic and sedimentary systems, the FeS concentration ranges from 1-100 mMol /kg (Rickard, 1997).

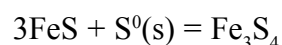
Sulfide mediated reductive dissolution of iron oxides can also lead to formation of elemental sulfur (Pyzik and Sommer 1981), polysulfides (S_4^{2-} or S_5^{2-}) (Pyzik and Sommer 1981), thiosulfate ($\text{S}_2\text{O}_3^{2-}$) (dos Santos Afonso and Stumm 1992; Pyzik and Sommer 1981), sulfite (SO_3^{2-}) (dos Santos Afonso and Stumm 1992), and sulfate (SO_4^{2-}) (dos Santos Afonso and Stumm 1992; Hanoch et al. 2006). These intermediate sulfur species could play an important role in FeS transformation.

2.6.3 Transformation of FeS Minerals

The most abundant iron sulfide phases in natural environments are amorphous iron (II) monosulfide (FeS_{am}), mackinawite (tetragonal FeS), greigite (Fe_3S_4), and pyrite (FeS_2). Most of these iron sulfide phases are metastable at ambient temperatures. FeS can transform to Fe_3S_4 and FeS_2 through biotic and/or abiotic pathways (Butler and Hayes 2001; Hanoch et al. 2006; Jeong and Hayes 2003). It is generally accepted that the reaction sequence $\text{FeS}_{\text{am}} \rightarrow$ mackinawite \rightarrow greigite \rightarrow pyrite is involved in pyrite formation (Lennie et al. 1997).

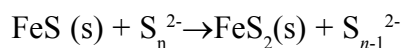
Greigite is the sulfur analogue of magnetite and has a similar inverse spinel structure. The greigite structure can be regarded as a cubic, close-packed array of sulfur atoms linked by smaller iron atoms (Rickard and Luther 2007). The mackinawite to greigite transformation occurs through an oxidation process (Boursiquot et al. 2001). Posfai et al. (1998) showed that some bacteria form intracellular nanometer-scale

crystals of greigite (Fe_3S_4) from nonmagnetic mackinawite (tetragonal FeS) and possibly from cubic FeS. Rickard (1997) proposed that the oxidation of FeS to Fe_3S_4 is a solid state reaction, which is supported by several other studies (Boursiquot et al. 2001; Jeong et al. 2008; Lennie et al. 1997; Posfai et al. 1998a,b). In this process, two thirds of Fe(II) are oxidized to Fe(III) and the S(-II) remains unoxidized. Transformation of mackinawite to greigite can be generally described by the following reaction:



FeS may be transformed to FeS_2 based on three different mechanisms.

- (1) A polysulfide pathway is proposed to be the primary pathway for $\text{FeS}_2(\text{s})$ formation. In this process, iron sulfide precursors react with S^0 , polysulfides, or other S intermediates to form pyrite through the following reactions:



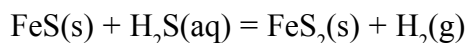
Production of intermediate sulfur species [for example, elemental sulfur, polysulfides, and thiosulfate ($\text{S}_2\text{O}_3^{2-}$)] is initiated through H_2S oxidation by oxidants such as O_2 , NO_3^- , Fe oxides, and manganese oxides (Butler and Hayes 2000; Butler and Rickard 2000; Henneke et al. 1997; Schoonen and Barnes 1991).

- (2) Another potential transformation mechanism is through greigite formation. Hunger and Benning (2007) show strong evidence for greigite being an intermediate on the formation pathway of pyrite, and that pyrite did not form directly from mackinawite. Their data show mackinawite disappeared as greigite was produced, and that pyrite was

produced as greigite disappeared. Benning et al. (2000) conducted experiments with ex-situ, freeze-dried mackinawite that show that at 25°C, 78% of mackinawite was transformed to pyrite, via greigite, within 24 h. Wang and Morse (1996) provided experimental evidence that the formation of pyrite is most rapid in the presence of greigite. The transformation of greigite to pyrite can be described as:



- (3) Under strictly anoxic conditions, H_2S can act as an oxidant. $\text{FeS}_2(\text{s})$ has been shown to form via the “ H_2S oxidation pathway” (Rickard 1997; Rickard and Luther 1997):



Rickard (1997) showed that the H_2S pathway proceeded more rapidly than the polysulfide pathway and all other pathways involving intermediate sulfur species. Hurtgen et al. (1999) suggested that the accumulation of H_2S in pore waters may promote pyrite formation. In an anoxic system with excess sulfide, sulfide could mediate the partial oxidation of mackinawite to greigite (Jeong et al. 2008; Rickard 1997; Vaughan and Ridout 1971). In addition, water has also been proposed as an oxidizing agent for this transformation process (Jeong et al. 2008; Rickard and Morse 2005).

For the first two pathways, intermediate sulfur species are critical in pyrite formation. Thus the availability of an oxidant to produce sulfur species with intermediate oxidation states controls the transformation of FeS to pyrite. Pyrite is frequently found at the interface between oxidizing and reducing conditions in the environment and the occurrence of pyrite is closely related to the oxidation of sulfide (Hurtgen et al. 1999). In a PRB field study, Herbert et al. (2000) observed a greater accumulation of mildly oxidized sulfur

species (pyrite, S_0) at the front end of the barrier. This observation suggests that oxidizing agents may be present at low concentrations in the ground water that enters the PRB from up gradient, but the oxidizing agents are consumed as groundwater passes through the reactive barrier.

2.6.4 Effect of Transformations of Iron Sulfides on Reactivity

Butler and Hayes (2001) suggested that the oxidation of mackinawite to greigite is faster at acidic versus alkaline pH, and that mineral aging in low pH groundwaters may eventually result in the deactivation of iron sulfide mineral surfaces with respect to reductive dechlorination. Butler and Hayes (2001) have observed that aged FeS at 76°C becomes completely unreactive to TCE over 6 months. They detected greigite formation by XRD in aged FeS. Lee and Batchelor (2002a) showed that the rate constant for degradation of TCE on pyrite was 1390 to 2900 times slower than rate constants of degradation reported for mackinawite and troilite. Devlin and Müller (1999) showed that FeS is more reactive than FeS_2 in degrading carbon tetrachloride. Shao and Butler (2009) had a similar observation in their microcosm study, which showed the decline in the rate of degradation of carbon tetrachloride corresponded to a decrease in the abundance of FeS and an increase in the abundance of pyrite. Kriegman-King and Reinhard (1994) showed that the condition of the pyrite surface was found to be an important factor in determining both the rates of reaction and the product distributions of carbon tetrachloride degradation. Pseudo zero order kinetics was observed with the fastest rates recorded for acid-washed and freshly exposed pyrite surfaces in anaerobic solutions. The slowest rates corresponded to reactions on pyrite in aerobic solutions (Devlin and Müller 1999; Hansson et al. 2008).

These observations show that different mineral phases have different reactivity. The transformation of iron sulfide minerals is expected to play a significant role in determining their reactivity. Because the iron sulfide minerals

are metastable at ambient conditions in the environment, understanding the reactivity of different iron sulfide phases and their transformation under different geochemical conditions is important in understanding their role in engineering remediation and natural attenuation.

2.6.5 Effect of Transition Metals on Degradation

The presence of transition metals is common as a constituent in mixed wastes with chlorinated organic solvents. In addition, transition metals can also be released under reducing conditions where FeS typically forms. Through their various interactions with FeS, transition metals can change the efficiency of FeS in the reductive dechlorination of chlorinated organic compounds.

Metal ions are characterized as hard or soft depending on the Lewis acid base principle. Due to their high affinity for sulfides, however, intermediate to soft metal ions can react with FeS in various ways: precipitation of pure metal sulfides (MS), formation of metal-substituted FeS by lattice exchange, and coprecipitation of the mixed sulfides in a Fe–M–S system (Jeong and Hayes 2003). Evidence of the incorporation of metal impurities into iron sulfides has been previously reported. For example, chemical analyses of natural mackinawite by Ostwald (1978) show that this mineral commonly contains nickel, cobalt, and copper in its lattice.

Di Toro et al. (1990) found that metals with lower sulfide solubility in general show a greater tendency to replace iron atoms. In contrast, Mn(II), whose sulfide is more soluble than mackinawite, was not found to form any sulfide precipitates in a suspension of mackinawite (Arakaki and Morse 1993).

Choi et al. (2009) showed that the addition of the transition metal Ni(II) and HS⁻ caused a noticeable morphologic change of the surface of FeS. The transition metal was substituted for structural iron resulting in a decrease in

the iron content of the FeS (from 52.6% down to 46.9%). They found that one third of the transition metal in a suspension of FeS existed in the zerovalent form. The zerovalent form acts as a catalyst to accelerate degradation of carbon tetrachloride and 1,1,1-TCA.

Depending on how metal ions interact with FeS, transition metals can either inhibit or stimulate the degradation of chlorinated organic compounds. Fe(II) released as a result of the interaction of FeS with intermediate/soft metals, enhances the dechlorination of HCA at concentrations of 10⁻⁴ and 10⁻³ M through sorbed or dissolved Fe(II) species, while Fe(OH)₂(s) formed at a higher concentration (10⁻² M) also enhances reductive dechlorination. Co(II) and Hg(II) enhanced the reductive dechlorination of PCE and TCE, but Ni(II) slowed dechlorination (Jeong and Hayes 2007). Choi et al. (2009) showed that the reduction rate of 1,1,1-TCA increased with increasing concentration of transition metals. The rate constants with 10 mM Co(II) and Ni(II) were 0.06 and 0.11 h⁻¹, approximately 1.3 and 3.0 times greater than rates with FeS alone. Jeong and Hayes (2003) showed that metal ions impacted the dechlorination rate of HCA by FeS as a result of formation of secondary phases. Rate increases observed in systems amended with Co(II), Ni(II), and Hg(II) were not simply explained by the formation of pure metal sulfide. Instead, metal-substituted FeS or coprecipitated sulfides are thought to be responsible for the significantly increased rates observed in these systems (Jeong and Hayes 2003).

2.7 Environmental Implications

2.7.1 Geochemical Parameters

Previous studies have investigated a series of environmental factors that could affect the abiotic degradation of halogenated aliphatic compounds. It may be possible to use these geochemical parameters to identify environments where processes that degrade these organic compounds are favored. Parameters such as

transition metals, sulfide concentration, and natural organic matter have different effects on the degradation of halogenated aliphatic compounds depending on the specific compounds and specific conditions involved. At the current state of knowledge, it is difficult to use these parameters as reliable indicators of the degradation of chlorinated organic compounds. However, pH and the presence of anaerobic conditions seem to affect the transformation of halogenated compounds in a more consistent and predictable way. Under iron and sulfur reducing conditions, the formation of FeS can be expected. An increase in pH will generally increase the rate of degradation of chlorinated organic compounds on FeS.

2.7.2 Differentiating Biotic and Abiotic Degradation

Several approaches have been proposed to differentiate abiotic degradation from biological degradation of chlorinated hydrocarbon compounds. Because biotic and abiotic degradation follow different mechanisms and have different degradation products, it may be possible to differentiate biological degradation from abiotic degradation based on the distribution of products. Acetylene has been proposed as a product from abiotic degradation pathways (Butler and Hayes 1999).

Devlin and Müller (1999) noticed that when carbon tetrachloride reacted with freshly precipitated, amorphous FeS at near neutral pH, the ratio of the concentrations of chloroform and carbon disulfide produced from the reaction was $2:1 \pm 0.4$. They proposed that the 2:1 ratio may be a useful tool for distinguishing abiotic transformations from biodegradation in sulfate reducing environments where FeS is actively precipitated.

Abiotic processes may fractionate stable carbon isotopes of carbon more strongly than biodegradation. An analysis of stable isotope ratios can be used as a tool to differentiate biotic vs. abiotic degradation of TCE and PCE (Liang et al. 2007; Zwank et al. 2005). More importantly, stable

isotope ratios can be used to recognize transformation of chlorinated organic compounds when it is difficult or impossible to characterize degradation from the production or accumulation of degradation products. As an example, acetylene can be biologically degraded under anaerobic conditions, and may not accumulate in ground water where it is being produced.

2.7.3 Geochemical Modeling

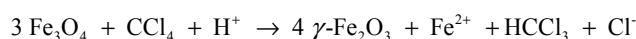
When comprehensive data is available on water chemistry, geochemical modeling may be used as a technique to predict the formation of FeS and other sulfides through the calculation of saturation indices. Geochemical models, based on water chemistry parameters, are useful in evaluating whether or not potentially reactive phases are present in situations where solids cannot be collected and analyzed for their mineral content.

3.1 Structure of Magnetite

Magnetite (Fe_3O_4) is a mixed valence iron mineral, containing roughly twice as much Fe^{3+} as Fe^{2+} . The formula can be expressed as $(\text{Fe}^{3+}(\text{Fe}^{2+}, \text{Fe}^{3+})\text{O}_4$ or as $\text{FeO}\cdot\text{Fe}_2\text{O}_3$. See Table 1.1 for a depiction of the three dimensional structure. Halogenated organic compounds can react with structural Fe^{2+} in magnetite, or with Fe^{2+} species sorbed to the surface of magnetite. One third of the iron is in a tetrahedral coordination with oxygen. All of the iron in the tetrahedral layer is Fe^{3+} . Two thirds of the iron is in an octahedral coordination with oxygen. Half of the iron in the octahedral layer is Fe^{3+} and half is Fe^{2+} . Danielsen and Hayes (2004) and McCormick and Adriaens (2004) note that electrons can “hop” between atoms of iron in the octahedral layer, making iron in this layer, or Fe^{2+} sorbed to this layer, more reactive.

3.2 Transformation Products of Chlorinated Organic Compounds on Magnetite

Vikesland et al. (2007) described the reaction of carbon tetrachloride (CCl_4) with magnetite as the transfer of one electron, with simultaneous cleavage of a C-Cl bond. The transfer of one electron produces the trichloromethyl radical ($\cdot\text{CCl}_3$) which can react with hydrogen donors to produce chloroform (HCCl_3) in the following reaction:



The trichloromethyl radical can also react to form other intermediates that finally decay or react to form carbon monoxide, methane, or formate (McCormick and Adriaens, 2004; Vikesland et al., 2007). The final distribution of products depends on pH and availability of hydrogen donors.

Less is known of the reactions of alkenes with magnetite. At this writing, the authors are not aware of any published study that identifies transformation products of PCE, TCE, *cis*-DCE or vinyl chloride on magnetite. The only transformation product identified by Lee and Batchelor (2002a) on magnetite was chloride. Ferrey et al. (2004) analyzed pore water in microcosms for reductive dechlorination products of *cis*-DCE, such as vinyl chloride and ethylene and ethane, and did not find them.

Darlington et al. (2008) followed the evolution of labeled carbon from ^{14}C -TCE that was incubated with samples of material from a sandstone aquifer that had been contaminated with chlorinated solvents. The aquifer matrix contained a variety of potentially reactive minerals including iron sulfides, pyrite, fougurite, magnetite, biotite, and vermiculite. The ground water was predominantly anaerobic. In some of the living microcosms, there was extensive transformation of the TCE to *cis*-DCE. Within 15 to 16 months, up to 10% of the label accumulated as ^{14}C - CO_2 . In sterile samples (autoclaved controls), the majority of label accumulated in a fraction that was water soluble, but was not stripped from the water by gas sparging after the pH had been adjusted with HCl. Further analysis indicated that this non-strippable fraction included glycolate, formate, and acetate. The only degradation products that were identified are carbon dioxide and organic compounds that can be readily biodegraded to carbon dioxide.

Ferrey et al. (2004) described the degradation of *cis*-DCE in sediment from the site of the former Twin Cities Army Ammunition Plant (TCAAP) in Minnesota. The primary reactive mineral in the sediment was magnetite. The surface area of magnetite in the sediment, together with the surface area specific rates of *cis*-DCE degradation

on magnetite published by Lee and Batchelor (2002a), could explain the removal of *cis*-DCE in the sediment. Ferrey, Wilson, Lee, and Bradley (Section B.4 of Appendix B) compared the evolution of label from ^{14}C -*cis*-DCE that was incubated in sediment from TCAAP that had been autoclaved. The only transformation product that could be identified was ^{14}C - CO_2 .

Danielsen and Hayes (2004) and McCormick and Adriaens (2004) speculated that Fe^{2+} sorbed to the octahedral layer of magnetite would stabilize the trichlorocarbene ion, and shift the products of carbon tetrachloride degradation away from chloroform toward carbon monoxide, formate, and methane. If a similar mechanism controls degradation of alkenes, then carbon dioxide would be the ultimate degradation product of *cis*-DCE on magnetite.

Little is known of reactions of chlorinated alkanes on magnetite. Elsner et al. (2004b) evaluated the degradation of hexachloroethane by Fe^{2+} sorbed to the surface of a series of minerals including magnetite. The primary transformation product recovered was PCE. Degradation of hexachloroethane on magnetite proceeded through beta elimination, also called dihaloelimination, where two chlorine atoms were removed from adjacent carbon atoms. This pathway is also an important pathway for reaction of alkenes on pyrite (Lee and Batchelor, 2002a) and on iron sulfides (Butler and Hayes, 1998).

3.3 Effect of Properties of Magnetite on Rate of Transformation

3.3.1 Effect of Particle Size and Surface Area

The rate of degradation of a chlorinated organic compound on magnetite depends on a number of factors. Because the reaction occurs at the solid surface, the rate is proportional to the surface area of magnetite presented to the pore water in the aquifer sediment, and rates in laboratory studies are conventionally normalized to the surface area of magnetite in the experimental system (Lee and Batchelor, 2002a). Because volume

varies as the cube of the linear dimension, while surface area varies as the square, finely divided magnetite has much greater surface area for a given mass of magnetite.

Vikesland et al. (2007) compared the rate of degradation of carbon tetrachloride on magnetite with an average particle size of 9 nm to degradation on magnetite with an average particle size of 80 nm. The rate of carbon tetrachloride degradation in the 9 nm preparation was $1.4 \text{ L g}^{-1} \text{ day}^{-1}$ at $\text{pH} = 7.8$, while the rate in the 80 nm preparation was $0.014 \text{ L g}^{-1} \text{ day}^{-1}$. When the rates were normalized to the surface area of the magnetite, the rate of degradation of carbon tetrachloride was still significantly faster in the 9 nm preparation. The specific surface areas of the 9 nm and 80 nm preparations were 63.5 and $14.5 \text{ m}^2 \text{ g}^{-1}$ respectively. The surface area normalized rate constants were 2.2×10^{-2} and $0.099 \times 10^{-2} \text{ L m}^{-2} \text{ day}^{-1}$, respectively. Vikesland et al. (2007) attributed the faster degradation in the preparation having an average particle size of 9 nm and specific surface area of $63.5 \text{ m}^2 \text{ g}^{-1}$ to quantum confinement effects. These effects become important at particle sizes less than approximately 20 nm.

The most detailed laboratory evaluations of the degradation of chlorinated organic compounds on magnetite are provided in McCormick et al. (2002) and Lee and Batchelor (2002a). For the laboratory studies to extrapolate to field conditions, the particle size distribution of magnetite should be similar. McCormick et al. (2002) prepared biogenic magnetite from a culture of iron reducing bacteria. Their preparation of magnetite had a specific surface area of $77.5 \text{ m}^2 \text{ g}^{-1}$. Lee and Batchelor (2002a) synthesized magnetite by mixing solutions of iron(II) chloride and iron(III) nitrate, then precipitating magnetite by adjusting the pH with NaOH. The specific surface area of the magnetite was $57.2 \text{ m}^2 \text{ g}^{-1}$. As discussed in Section 3.4.1, the average specific surface area of magnetite isolated from aquifer sediment at the TCAAP in Minnesota was $24 \text{ m}^2 \text{ g}^{-1}$. The

specific surface of these laboratory preparations of magnetite compare well with the average specific surface area of magnetite isolated from aquifer sediment at the TCAAP in Minnesota.

3.3.2 Effect of pH

The rate of degradation of a variety of organic compounds on magnetite increases as the pH increases. This effect has been shown for carbon tetrachloride by Danielsen and Hayes (2004) and Vikesland et al. (2007), and for RDX (hexahydro-1,3,5-trinitro-1,3,5-triazine) by Gregory et al. (2004). Danielsen and Hayes (2004) attributed the increase in reactivity to the degree of protonation of sites on the mineral surface. The rate of carbon tetrachloride degradation on deprotonated sites in their preparation of magnetite was approximately ten times greater than the rate of degradation on protonated sites.

As the solution pH increased, the fraction of sites which were deprotonated increased. Ferrous iron sorbed to the surface of iron minerals is postulated to form a $\equiv\text{Fe}-\text{O}-\text{Fe}^{\text{II}}$ species where $\equiv\text{Fe}$ refers to iron in the structure of the mineral (Schoonen and Strongin, 2005). Danielsen and Hayes (2004) describe the protonation reaction with the following equation:

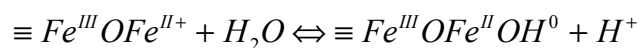


Figure 3.1 presents data from Danielsen and Hayes (2004) on the effect of pH on the rate of degradation of carbon tetrachloride on magnetite. They did not add additional Fe^{2+} to their preparation of magnetite, and their preparation of magnetite did not contain other iron minerals such as siderite [Iron(II) Carbonate] that would poison the concentration of Fe^{2+} in solution. As a result, Figure 3.1 presents the effect of solution pH on carbon tetrachloride degradation by structural iron in magnetite. There was a steady increase in the rate constant for degradation with increased pH. In general, the rate constant increases approximately 2.7 fold for each ten-fold increase in $[\text{OH}^-]$, up to pH 8.0.

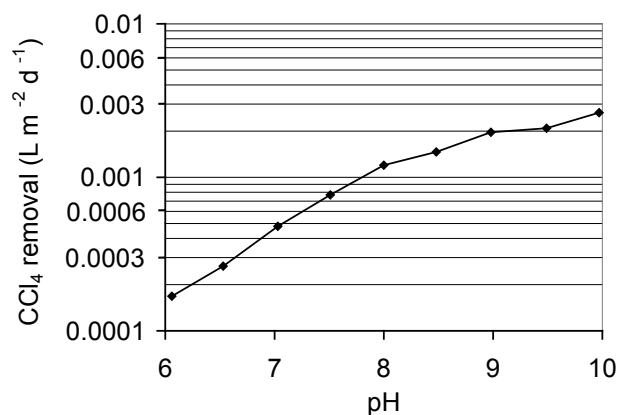


Figure 3.1. Effect of solution pH on the rate constant for degradation of carbon tetrachloride on the surface of magnetite. Redrawn from Danielsen and Hayes (2004).

3.3.3 Effect of Fe^{2+} Sorbed to the Surface of Magnetite

Lee and Batchelor (2002a) compared the rates of degradation of *cis*-DCE and vinyl chloride on magnetite as prepared, and in the presence of 2.4 g/L Fe^{2+} . In the presence of a high concentration of Fe^{2+} in solution (2,400 mg/L), the rates of degradation of *cis*-DCE and vinyl chloride were tenfold higher. Presumably, high concentrations of Fe^{2+} in solution increased the concentration of Fe^{2+} that was sorbed to the surface of the magnetite and was available to provide electrons for reaction with *cis*-DCE and vinyl chloride.

Amonette et al. (2000) compared the effect of sorbed Fe^{2+} on the rate of carbon tetrachloride degradation on goethite. When the pH was fixed at 7.0, the rate of carbon tetrachloride degradation was directly proportional to the density of Fe^{2+} sorbed to the goethite (mmol g^{-1}). Klausen et al. (1995) compared the effect of sorbed Fe^{2+} on the rate of nitrobenzene degradation on magnetite. At pH 7.0, the rate increased concomitant with the amount of sorbed Fe^{2+} . Gregory et al. (2004) compared the effect of sorbed Fe^{2+} on the rate of RDX degradation on magnetite. The rate increased

with the amount of sorbed Fe^{2+} ; however, the increased rate was not directly proportional to the increase in sorbed Fe^{2+} . The apparent order of the reaction with RDX with respect to the concentration of sorbed Fe^{2+} was 1.8 ± 0.3 .

The concentration of sorbed Fe^{2+} on the surface of magnetite should be related to the concentration of Fe^{2+} in solution. Danielsen and Hayes (2004) determined the concentration of iron in solution that would be in equilibrium with their preparation of magnetite. The iron was provided by dissolution of structural iron in magnetite. Their data are presented in Figure 3.2. If the concentration of total iron exceeded the equilibrium concentration, some other process such as biological iron reduction must have contributed to iron in solution. If the concentration of total iron was lower than the values in Figure 3.2, some other process must have removed the iron from solution, such as sorption of iron to the surface of the magnetite.

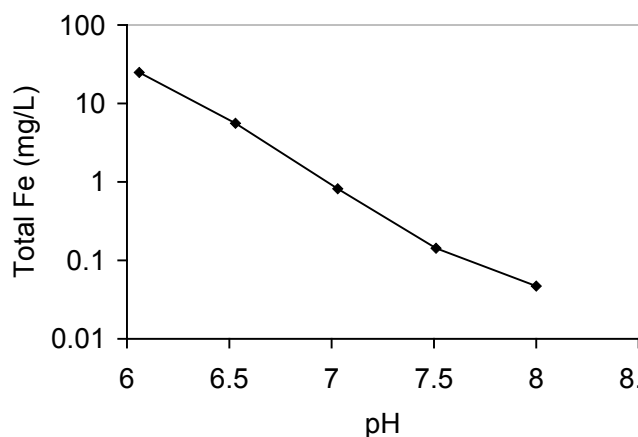


Figure 3.2. Effect of pH on the solution concentrations of Fe^{2+} in equilibrium with magnetite. Redrawn from Danielsen and Hayes (2004).

There are two sorption isotherms available in the literature (Gregory et al., 2004; Klausen et al., 1995). Gregory et al. (2004) purchased their magnetite, while Klausen et al. (1995) prepared theirs in the laboratory. The preparations differed in particle size, and thus in specific surface

area. Figure 3.3 presents the two isotherms. To facilitate comparison, the sorption of Fe^{2+} is normalized to the surface area of magnetite in the experimental systems (mmole m^{-2}). Both isotherms seemed to plateau at Fe^{2+} concentrations above 100 mg/L. However the concentrations of sorbed Fe^{2+} varied widely between the two preparations. Any attempt to predict the quantity of iron sorbed to the surface of magnetite in aquifer sediment will be at best semi-quantitative.

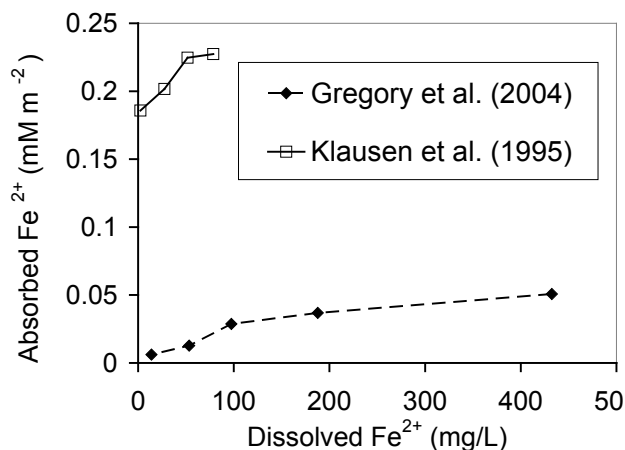


Figure 3.3. Sorption isotherms for Fe^{2+} on the surface of magnetite. Redrawn from Klausen et al. (1995) and Gregory et al. (2004).

3.4 Rates of Transformation of Chlorinated Organic Compounds on Magnetite

3.4.1 Degradation of *cis*-DCE and Vinyl Chloride on Magnetite

At the Twin Cities Army Ammunition Plant (TCAAP) north of St. Paul, Minnesota, a large plume of TCE had moved beyond the plant boundary and impacted municipal water supply wells down gradient of the plant. In response, the Army installed a series of pump-and-treat wells that intercepted the plume near the plume boundary. Based on a ground water transport and fate model, the concentrations of TCE in the plume were more than an order of magnitude lower than concentrations that would be expected if there were no degradation of TCE. Because of this discrepancy between measured

and expected concentrations of TCE, the site was proposed for a retrospective evaluation of the U.S. EPA Technical protocol for evaluating natural attenuation of chlorinated solvents in ground water (Wiedemeier et al., 1998).

Although TCE disappeared in the down gradient portion of the plume, there was very little *cis*-DCE, and no vinyl chloride or ethylene in the ground water. Low concentrations of *cis*-DCE would be expected if *cis*-DCE were being removed by natural biodegradation. However, the retrospective evaluation found that the geochemical environment in the plume was not consistent with natural anaerobic biological degradation of *cis*-DCE (Wilson et al., 2001).

In an attempt to identify the processes that were removing chlorinated solvents, a microcosm study was constructed with sediment from the site (Ferrey et al., 2004). Ferrey et al. (2004) selected sediment from an anaerobic, heavily contaminated zone in the middle of the plume with measureable Fe^{2+} in ground water, a less contaminated zone at the water table, and a marginally contaminated zone in oxygenated ground water below the plume. The microcosm study documented rates of removal of *cis*-DCE in the sediment (Figure 3.4) that were consistent with and would explain the low concentrations of *cis*-DCE in the field scale plume. Further, the microcosm study showed that the removal process was indifferent to sterilizing the sediment in an autoclave. Because sterilizing the sediment did not affect removal, natural biodegradation could not explain the removal of *cis*-DCE. The rates of removal in the microcosm study were also consistent with the rate of decline in concentrations of *cis*-DCE over time in monitoring wells at the site.

Working with magnetite that was chemically synthesized in their laboratory, Lee and Batchelor (2002a) showed that magnetite could degrade a variety of chlorinated alkenes including PCE, TCE, *cis*-DCE, and vinyl chloride. To determine whether magnetite in the aquifer

sediment could explain the removal of *cis*-DCE in ground water at the TCAAP, Ferrey et al. (2004) isolated the magnetic fraction from the sediment used for their microcosm study, used electron microscopy to estimate the distribution of particle sizes, and used X-ray diffraction analysis to estimate the mean particle size for magnetite. They used the magnetic susceptibility of the sediment to estimate the content of magnetite in the sediment, and from the content and specific surface area of magnetite they estimated the surface area of magnetite exposed to water in the sediment from TCAAP. Lee and Batchelor (2002a) had published two surface area specific rate constants for degradation of *cis*-DCE on magnetite, one for magnetite by itself, and a faster rate for magnetite in the presence of high concentrations of Fe^{2+} in solution. A model assuming a specific surface area for magnetite of $100 \text{ m}^2 \text{ g}^{-1}$, and the higher rate of degradation most closely matched the experimental data.

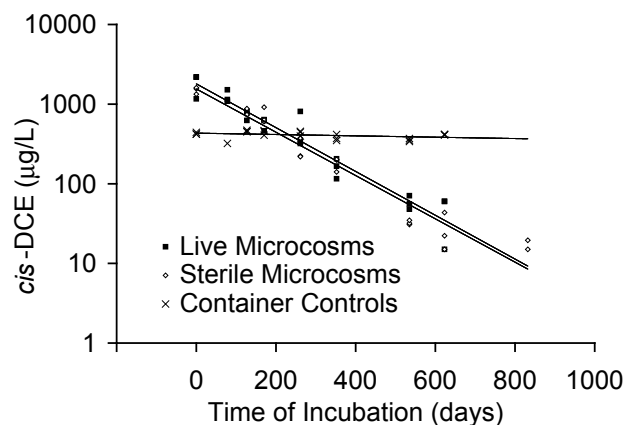


Figure 3.4. Removal of *cis*-DCE in aquifer sediment containing magnetite. Redrawn from Ferrey et al. (2004).

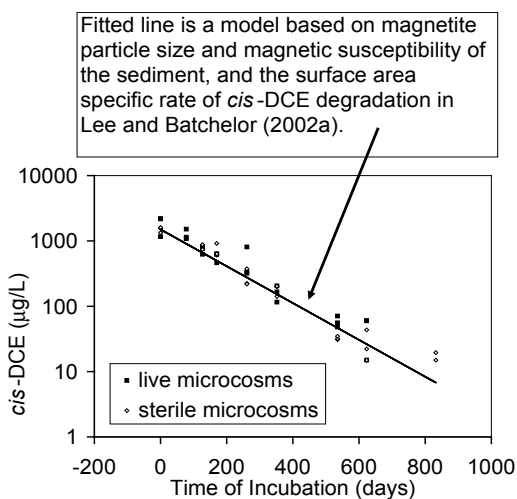


Figure 3.5. *The surface area specific rate of degradation of cis-DCE on magnetite can explain the removal of cis-DCE in sediment from the TCAAP. Redrawn from Ferrey et al. (2004).*

Figure 3.5 presents a further elaboration on the model of *cis*-DCE degradation presented in Ferrey et al. (2004). Ferrey et al. (2004) used the peak broadening of the strongest magnetite reflections at d spacings of 2.97, 2.53, and 1.48 Å to estimate the mean particle size. They reported a mean magnetite crystal size of 100 nm. The actual best estimate of the particle size was 46 nm (Robert Ford, U.S. EPA, personal communication). Assuming a crystal of magnetite is a cube, this would correspond to specific surface area of 24 m² g⁻¹. In the model presented in Figure 3.5, the amount of magnetite in the sediment was estimated from the magnetic susceptibility of sediment (1.6×10^{-6} m³ kg⁻¹) assuming that the quantity of magnetite is proportional to the mass magnetic susceptibility, and that a mass magnetic susceptibility of 2.7×10^{-6} m³ kg⁻¹ is equivalent to 1% by weight magnetite in silica sand. The relationship between mass magnetic susceptibility and the content of magnetite is described in more detail in Section 3.5.1. The model further assumed that the water filled porosity of the sediment was 0.25. The model projection

and the experimental data from the microcosm study were in good agreement (Figure 3.5).

Following the assumption in the model above, the mass magnetic susceptibility of the sediment used in the experimental treatments in Ferrey et al. (2004) was used to estimate the concentration of magnetite in the sediments. The concentration of magnetite in the laboratory experiments of Lee and Batchelor (2002a) were similar to the natural concentration of magnetite in the sediment from the TCAAP, and the specific surface area of the magnetite that was chemically synthesized by Lee and Batchelor (2002a) was similar to the specific surface area of magnetite isolated from the TCAAP sediment.

Table 3.1. Surface area specific rate constants for removal of *cis*-DCE and vinyl chloride on magnetite.

Reference	Source of Magnetite	First-Order Rate Constant ± 95% Confidence Interval Microcosm <i>Container Control</i>	Magnetite exposed to pore water	Specific Surface Area Magnetite	Surface Area Specific Rate Constant for Transformation
		year ⁻¹	g L ⁻¹	m ² g ⁻¹	L m ⁻² day ⁻¹
Removal of <i>cis</i> -DCE					
Lee and Batchelor (2002a)	Chemically synthesized		63	57.2	0.560 × 10 ⁻⁶
Lee and Batchelor (2002a)	Chemically synthesized, 2400 mg/L Fe ²⁺		63	57.2	5.74 × 10 ⁻⁶
Ferrey et al. (2004)	Natural in TCAAP shallow Fe ²⁺ ≤ 2.5 mg/L	0.58 ± 0.090 <i>0.071 ± 0.082</i>	27	24	1.32 × 10 ⁻⁶
Ferrey et al. (2004)	Natural in TCAAP Intermediate Fe ²⁺ ≤ 2.5 mg/L	2.29 ± 0.25 <i>0.071 ± 0.082</i>	47	24	2.8 × 10 ⁻⁶
Ferrey et al. (2004)	Natural in TCAAP Deep oxic	0.31 ± 0.08 <i>0.071 ± 0.082</i>	41	24	0.44 × 10 ⁻⁶
This study	Natural in TCAAP T5 shallow	0.82 ± 0.39 <i>0.26 ± 0.08</i>	25	24	1.97 × 10 ⁻⁶
This study	Natural in TCAAP Site A anoxic	0.73 ± 0.18 <i>0.21 ± 0.04</i>	29	24	1.47 × 10 ⁻⁶
This study	Natural in TCAAP Site 102 oxic	0.65 ± 0.20 <i>0.21 ± 0.04</i>	27	24	1.46 × 10 ⁻⁶
Removal of vinyl chloride					
Lee and Batchelor (2002a)	Chemically synthesized		63	57.2	0.564 × 10 ⁻⁶
Lee and Batchelor (2002a)	Chemically synthesized, 2400 mg/L Fe ²⁺		63	57.2	5.78 × 10 ⁻⁶
Ferrey et al. (2004) and This study	Natural in TCAAP Deep sediment, oxidized	0.311 ± 0.12	41	24	0.44 × 10 ⁻⁶

To extract a surface area specific rate constant from the data published by Ferrey et al. (2004), the rate constant for removal of the chlorinated organic contaminants in the sediment was divided by the surface area of magnetite exposed to ground water in the sediment. Table 3.1 compares the surface-area specific rate constants for removal of *cis*-DCE and vinyl chloride in the experiments of Lee and Batchelor (2002a) to rate constants calculated from the data on aquifer sediment presented in Ferrey et al. (2004).

As mentioned above, Lee and Batchelor (2002a) determined rate constants for *cis*-DCE removal for their magnetite as synthesized, and for magnetite that was incubated with high concentrations of Fe^{2+} in solution to maximize sorption of Fe^{2+} to the surface of their magnetite preparation. The rate constant for *cis*-DCE degradation was tenfold higher on magnetite in the Fe^{2+} solution. As mentioned previously, Ferrey et al. (2004) selected sediment from an anaerobic, heavily contaminated zone in the middle of the plume with measureable Fe^{2+} in ground water, a less contaminated zone at the water table, and a marginally contaminated zone in ground water from the bottom of the plume. There was a six-fold difference in the rates of *cis*-DCE degradation. Degradation was faster in the more contaminated, reduced sediment. The rate of *cis*-DCE degradation in sediment from the contaminated intermediate depth was comparable to the rate of removal on chemically synthesized magnetite incubated with high concentrations of Fe^{2+} , while the rate of degradation in the oxic sediment was comparable to removal on chemically synthesized magnetite without added Fe^{2+} .

Table 3.1 compares rate constants from published microcosm studies to rate constants from microcosm studies that were conducted as part of this study. Details of the microcosm studies are presented in Appendix B. The microcosm study described as TCAAP T5 in Table 3.1 used material from the same location as used for Ferrey et al. (2004). The experimental procedures followed Ferrey et al. (2004). In

contrast, the microcosm studies described as TCAAP Site A and TCAAP Site 102 are from two other sites on the TCAAP. These studies were designed to strictly exclude any biological activity from either *Dehalococcoides* strains that could use *cis*-DCE as an electron acceptor, or iron-reducing bacteria that can use *cis*-DCE as an electron donor or carbon source (Bradley, 2003). The sediment was dried to a powder, autoclaved, and made into microcosms with sterile oxygenated water. The microcosms were incubated in a dark cabinet exposed to air. The sediment or microcosms were never exposed to hydrogen in an anaerobic glove box. The surface area specific rates of removal of *cis*-DCE in these microcosms were comparable to the rates of removal of *cis*-DCE in the microcosm studies that were constructed and incubated in an anaerobic glove box.

Table 3.1 also compares the rate constants for removal of vinyl chloride in the experiments of Lee and Batchelor (2002a) to unpublished data from the experiment described in Ferrey et al. (2004). The data and experimental details are provided in Appendix B. As was the case for *cis*-DCE, the rate of degradation of vinyl chloride was ten times faster on the chemically synthesized magnetite incubated with Fe^{2+} , and the rate of removal of vinyl chloride in the oxic sediment was very similar to the rate on the chemically synthesized magnetite without additional Fe^{2+} .

3.4.2 Degradation of PCE and TCE on Magnetite

Surface area specific rate constants for removal of PCE and TCE are presented in Table 3.2. The rate constants for PCE and TCE degradation reported by Lee and Batchelor (2002a) on chemically synthesized magnetite were very similar to their rates for degradation of *cis*-DCE and vinyl chloride. The rates of degradation of PCE or TCE in oxidized natural sediment from the TCAAP, or from the nearby Baytown Superfund site in Minnesota, are fivefold to tenfold higher than the rates on the chemically synthesized

magnetite. Lee and Batchelor (2002a) did not report experiments on the effects of Fe²⁺ on rates of degradation of PCE and TCE on magnetite. If the rates in the presence of Fe²⁺ are enhanced tenfold, as was the case with *cis*-DCE and vinyl chloride, the rates of degradation of PCE or TCE on the chemically synthesized magnetite would compare closely with the rates of PCE or TCE degradation in the sediment from the TCAAP.

The rates of degradation of PCE, TCE, *cis*-DCE, and vinyl chloride on chemically synthesized magnetite as reported by Lee and Batchelor (2002a), on aquifer sediment from the TCAAP as reported by Ferrey et al. (2004), and this study all fall into a fairly narrow range (0.56 to 8.6 × 10⁻⁶ L m⁻¹ day⁻¹). If the surface area of magnetite in a sediment sample can be determined, it may be possible to estimate the rate of degradation of PCE, TCE, *cis*-DCE, or vinyl chloride within an order of magnitude.

Table 3.2. Surface area specific rates of removal of PCE and TCE on magnetite.

Reference	Source of Magnetite	First-Order Rate Constant ± 95% Confidence Interval Microcosm <i>Container Control</i>	Magnetite exposed to pore water	Specific Surface Area Magnetite	Surface Area Specific Rate Constant for Transformation
		yr ⁻¹	g L ⁻¹	m ² g ⁻¹	L m ⁻² day ⁻¹
Removal of PCE					
Lee and Batchelor (2002a)	Chemically synthesized		63	57.2	0.84 × 10 ⁻⁶
This study	Component TCAAP Site A sediment	0.20 ± 0.15 <i>0.83 ± 0.23</i>			
This study	Component TCAAP Site 102 sediment	1.32 ± 0.45 <i>0.83 ± 0.23</i>	51	24	5.6 × 10 ⁻⁶
Removal of TCE					
Lee and Batchelor (2002a)	Chemically synthesized		63	57.2	0.72 × 10 ⁻⁶
This study	Component TCAAP Site A sediment	0.32 ± 0.11 <i>0.51 ± 0.13</i>			
This study	Component TCAAP Site 102 sediment	0.95 ± 0.31 <i>0.51 ± 0.13</i>	51	24	4.1 × 10 ⁻⁶
This study	Component Baytown sediment	0.98 ± 0.49 <i>0.45 ± 0.11</i>	21	24	9.3 × 10 ⁻⁶

As mentioned above, the sediment from TCAAP Site A and Site 102 received special treatment to preclude any possibility of biodegradation of chlorinated organic compounds. The sediments were dried to a powder before they were autoclaved, and were resuspended in oxygenated water. The removal of TCE and PCE in microcosms constructed with sediment from Site A and Site 102 was compared to loss from container controls that were filled with sterile water but no sediment (Table 3.2). Both sediments removed *cis*-DCE at the same rate (Table 3.1), but the sediment from Site A did not remove TCE or PCE any faster than the loss from the container controls, while the sediment from Site 102 removed TCE and PCE at rates that were equivalent to the removal of *cis*-DCE.

It is difficult to explain the behavior of PCE and TCE in the sediment from Site A. There was no treatment in the study with a “living” microcosm. As a result, there is no way to determine whether the lack of activity was a property of the sediment as collected, or whether the magnetite was altered when the sediment was dried and autoclaved. The aquifer at Site A was anoxic with undetectable concentrations of dissolved oxygen and measurable concentrations of Fe²⁺ and Mn²⁺, while the aquifer at Site 102 often had measureable concentrations of dissolved oxygen in addition to Fe²⁺ and Mn²⁺.

Notice that the rate of removal of PCE and TCE in the microcosms constructed with sediment from Site A was significantly slower than the removal in the container controls that were only filled with sterile water. The sediment in the microcosms may have restricted exchange of water in the microcosms with the face of the Teflon-faced septum that sealed the microcosm, and thus imposed a mass transfer limitation on escape of PCE or TCE from the container. The removal of PCE or TCE in the Site A microcosms is probably a better control on losses of PCE and TCE from the Site 102

microcosms or the Baytown microcosms than is the removal in the container controls. Because the removal in the Site A microcosms was slow (0.2 to 0.3 per year) compared to the removal in the other microcosms, the removal in the other microcosms was not corrected for removal in the container controls.

3.4.3 Degradation of Carbon Tetrachloride on Magnetite

The rate of carbon tetrachloride degradation on magnetite was at least one hundredfold faster than the rate of degradation of the chlorinated alkenes (Compare Table 3.2 and 3.3). In the presence of Fe²⁺, the rates of degradation of carbon tetrachloride were roughly similar on magnetite produced by a culture of iron reducing bacteria (McCormick et al., 2002) or magnetite synthesized in the laboratory (Danielsen and Hayes, 2004; Zwank et al., 2005).

Vikesland et al. (2007 and Supporting Information) compared the rate of degradation of carbon tetrachloride on chemically synthesized nano-iron (particle size 9 nm) with a specific surface area of 63.5 m² g⁻¹ and “conventional” iron (particle size 80 nm) with a specific surface area of 14.5 m² g⁻¹. The surface area specific rate constant for degradation of carbon tetrachloride was 22 times faster with nano-iron. Vikesland et al. (2007) attributed the faster rate to quantum confinement in the nano-scale particles. They also showed that aggregation of the magnetite particles relieved the quantum confinement, and produced lower rates of degradation. The biogenic magnetite particles produced in the iron-reducing culture of McCormick et al. (2002) had a specific surface area of 68.9 m² g⁻¹, indicating that they were also nano-scale, yet the rate of carbon tetrachloride degradation was similar to conventional magnetite. Perhaps aggregation reduced the rate of degradation in their experimental system.

Table 3.3. Surface area specific rate constants for removal of carbon tetrachloride on magnetite.

Reference	Source of Magnetite	Magnetite exposed to pore water	Specific Surface Area Magnetite	Surface Area Specific Rate Constant for Transformation
		g L ⁻¹	m ² g ⁻¹	L m ⁻² day ⁻¹
Removal of carbon tetrachloride				
McCormick et al. (2002)	Separated from a culture of iron reducing bacteria 32 to 37 mg/L Fe ²⁺	7.3 to 26	77.5 or 68.9	8.9 × 10 ⁻⁴
Danielsen and Hayes (2004)	Chemically synthesized pH 7.03 0.82 mg/L Fe ²⁺	25	18	4.8 × 10 ⁻⁴
Zwank et al. (2005)	Chemically synthesized pH 7.2, 57 mg/L Fe ²⁺	2.6	19	1.2 × 10 ⁻¹
Vikesland et al. (2007) and SI	Chemically synthesized pH 7.8, 9 nm	5	63.5	2.2 × 10 ⁻²
Vikesland et al. (2007) and SI	Chemically synthesized pH 7.8, 80 nm	5	14.5	9.9 × 10 ⁻⁴

Table 3.4. Relationship between the rate of removal of PCE, TCE, *cis*-DCE or vinyl chloride and the content of total iron, and the magnetic susceptibility of aquifer sediment.

Source of Sediment	First-Order Rate Constant for Removal in Sediment \pm 95% Confidence Interval <i>Microcosm Container Control</i>	Mass Magnetic Susceptibility SI Units	First-Order Rate Constant Normalized by Mass Magnetic Susceptibility	Iron Expected From magnetite	Total Iron Nitric Acid extract
	yr ⁻¹	m ³ kg ⁻¹	yr ⁻¹ m ⁻³ kg	mg kg ⁻¹	mg kg ⁻¹
Removal of PCE in sediment					
TCAAP Site A	0.20 \pm 0.15 <i>0.83 \pm 0.23</i>	1.0 \times 10 ⁻⁶		5,090	7,780
TCAAP 102	1.32 \pm 0.45 <i>0.83 \pm 0.23</i>	0.91 \times 10 ⁻⁶	1.4 \times 10 ⁶	4,600	5,520
Removal of TCE in sediment					
TCAAP Site A	0.32 \pm 0.11 <i>0.51 \pm 0.13</i>	1.0 \times 10 ⁻⁶		5,090	7,780
TCAAP 102	0.95 \pm 0.31 <i>0.51 \pm 0.13</i>	0.91 \times 10 ⁻⁶	1.1 \times 10 ⁶	4,600	5,520
Baytown	0.98 \pm 0.49 <i>0.45 \pm 0.11</i>	0.41 \times 10 ⁻⁶	2.4 \times 10 ⁶	1,940	12,100
Removal of <i>cis</i> -DCE in sediment					
TCAAP shallow (Ferrey et al., 2004)	0.58 \pm 0.090 <i>0.071 \pm 0.082</i>	0.9 \times 10 ⁻⁶	0.64 \times 10 ⁶	4,540	6,520
TCAAP intermediate (Ferrey et al., 2004)	2.29 \pm 0.25 <i>0.071 \pm 0.082</i>	1.6 \times 10 ⁻⁶	1.4 \times 10 ⁶	8,460	10,300
TCAAP deep (Ferrey et al., 2004)	0.31 \pm 0.08 <i>0.071 \pm 0.082</i>	1.4 \times 10 ⁻⁶	0.22 \times 10 ⁶	7,320	9,160
TCAAP shallow T5	0.82 \pm 0.39 <i>0.26 \pm 0.08</i>	0.86 \times 10 ⁻⁶	0.95 \times 10 ⁶	4,309	Not done
TCAAP Site A	0.73 \pm 0.18 <i>0.21 \pm 0.04</i>	1.0 \times 10 ⁻⁶	0.73 \times 10 ⁶	5,090	7,780
TCAAP 102	0.65 \pm 0.20 <i>0.21 \pm 0.04</i>	0.91 \times 10 ⁻⁶	0.71 \times 10 ⁶	4,600	5,520
Thermo-Chem	0.58 \pm 0.39 <i>0.26 \pm 0.08</i>	0.15 \times 10 ⁻⁶	3.9 \times 10 ⁶	656	1,500
Removal of vinyl chloride in sediment					
TCAAP deep (Ferrey et al., 2004)	0.311 \pm 0.12	1.4 \times 10 ⁻⁶	0.22 \times 10 ⁶	7,320	9,160

3.5 Rates of Transformation Normalized to Magnetic Susceptibility

A determination of mass magnetic susceptibility is a useful tool for screening sediment for the presence of magnetite, and thus for the possibility of abiotic degradation of chlorinated organic compounds on magnetite. Table 3.4 compares the abiotic rate of removal of PCE, TCE, *cis*-DCE and vinyl chloride normalized to the mass magnetic susceptibility. The normalized rate of removal should be influenced by the effect of pH, the specific surface area of the magnetite, the presence or absence of sorbed Fe²⁺, and variations in the mass magnetic susceptibility of the magnetite in the sediment samples. Despite all these influences, and the uncertainty associated with the estimate of the rate of removal and the mass magnetic susceptibility, the normalized rates extend over little more than an order of magnitude. The rates were higher in the sediments that were anoxic based on measured concentrations of Fe²⁺ in ground water (TCAAP intermediate, or Thermo-Chem). Presumably the magnetite in sediment in contact with Fe²⁺ in ground water had higher concentrations of Fe²⁺ sorbed or precipitated on the surface.

Note in Table 3.4 that no rates are reported for removal of PCE or TCE in sediment from the TCAAP Site A. Although a mass magnetic susceptibility in the range of 1×10^{-6} m³ kg⁻¹ may indicate that degradation of PCE or TCE at rates near 0.3 to 2 per year is possible, but should not be taken as proof that abiotic degradation will occur at those rates.

Transformation of Chlorinated Hydrocarbons by Green Rusts

4.1 Structure and Reactivity of Green Rusts

4.1.1 Chemical Composition and Crystal Structure of Green Rusts

Green rusts are Fe(II)-Fe(III) hydroxysalts belonging to the general class of layered double hydroxides (Hansen, 2001). They consist of ordered layers of Fe(II)/Fe(III) hydroxides carrying positive charges, and interlayers containing anions and water molecules (Figure 4.1). Green rusts have a general formula $[\text{Fe(II)}_{1-x}\text{Fe(III)}_x(\text{OH})_2]^{x+} [(x/n)\text{A}^{n-} \cdot m\text{H}_2\text{O}]^{x-}$ where A^{n-} is the intercalated anions ($\text{A}^{n-} = \text{Cl}^-, \text{SO}_4^{2-}, \text{CO}_3^{2-} \dots$) and x is the Fe(III) molar fraction ($x = 0.25$ to 0.33) (Génin et al., 1998; Hansen, 2001). The type of anion (charge, shape, and size) defines the crystal structure, which gives a distinct X-ray diffraction pattern for green rusts (Figure 4.2).

Green rusts can exchange counter ions, so if a sulfate green rust were prepared and added to a solution of bicarbonate, it might well be converted to carbonate green rust, depending on the relative concentrations of the two anions. The carbonate green rust would be favored over sulfate green rust when $[\text{SO}_4^{2-}]/[\text{CO}_3^{2-}] < 1259$ (Su and Puls, 2004) based on thermodynamic calculations. Such a conversion may not be assured due to possible slow kinetics, but it is a possibility. It is expected that carbonate green rust should be the dominant form of green rusts that could be formed in non-mining impacted sites. Green rusts can be readily synthesized in a laboratory. Green rusts have been reportedly found in soils and sediments under suboxic and anoxic conditions (Génin et al., 1998; Refait et al., 2001; Bearcock et al., 2006).

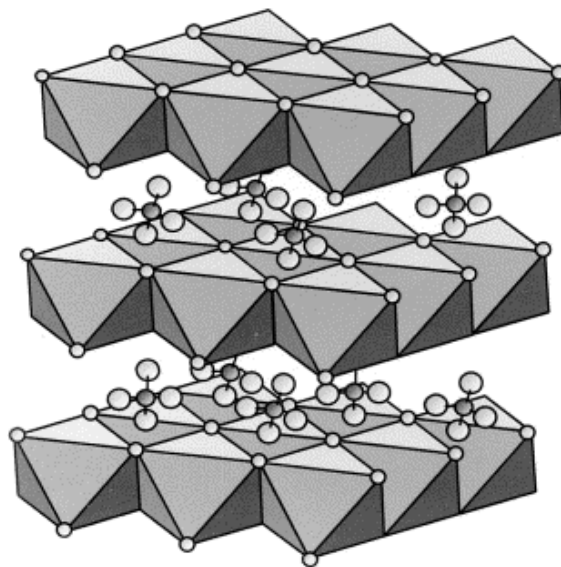


Figure 4.1. *The crystal structure of green rust compounds consists of layers of Fe(II)(OH)_6 in which some of the Fe(II) is replaced by Fe(III) . These alternate with layers of anions (SO_4^{2-} , CO_3^{2-} , and Cl^-) and water which bind the Fe(OH)_6 layers via hydrogen bonding (From Randall et al., 2001). If the interlayer is dominated by sulfate, carbonate, or chloride, then the material is described as sulfate green rust, carbonate green rust, or chloride green rust.*

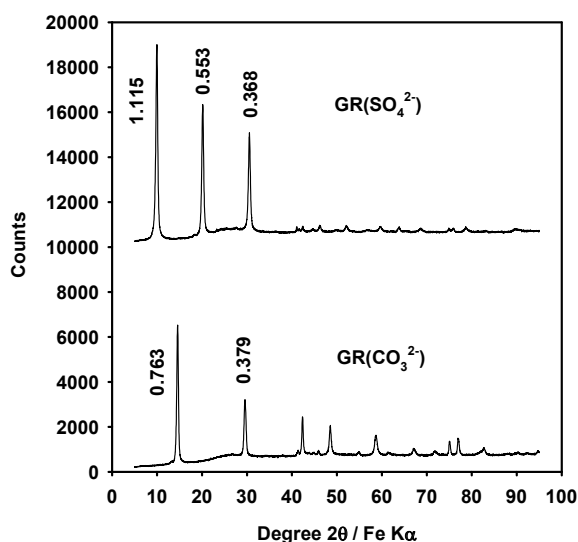


Figure 4.2. X-ray diffraction pattern of freshly synthesized carbonate green rust and sulfate green rust (less than 24 hours after synthesis) scanned as glycerol smears. Only d-spacings for basal reflections are shown (nm).

4.1.2 Chemical Reactivity of Green Rusts

Green rusts are very reactive minerals involved in the redox cycling of iron in both aquatic and terrestrial environments. Green rusts react readily with redox sensitive contaminants due to the iron in the layered structure. Their large external and internal surface area promotes the adsorption of contaminants and facilitates the association of contaminants with the reactive sites. They have been shown to chemically reduce a range of organic and inorganic contaminants such as nitrates (Hansen et al., 2001), Cr(VI) (Loyaux-Lawniczak et al., 2000), Se(IV) (Myneni et al., 1997), Ag(I), Au(III), Cu(II), and U(VI) (O’Loughlin et al., 2003; Suzuki et al., 2008), as well as chlorinated hydrocarbons (Erbs et al., 1999; Lee and Batchelor, 2002b; O’Loughlin and Burris, 2004; Scherer et al., 2007; Chun et al., 2007; Choi and Lee, 2008). Green rusts also adsorb contaminants such as As(V) and As(III) via surface complexations (Randall et al., 2001; Su and Wilkin, 2005). Carbonate green rust partially oxidizes As(III) to form As(V) (Su and Wilkin, 2005).

The rates of degradation of chlorinated hydrocarbons on the surface of green rusts should be a function of their surface area that is presented to the chlorinated hydrocarbons in water solution. Table 4.1 presents data on the specific surface area of a variety of forms of green rust. The specific surface area varies by almost two orders of magnitude. Bond and Fendorf (2003) reported values of 30.1 m² g⁻¹ for carbonate green rusts GR(CO₃²⁻), 19.0 m² g⁻¹ for chloride green rusts GR(Cl) and 3.6 m² g⁻¹ for sulfate green rusts GR(SO₄²⁻) using the BET N₂ adsorption method on a Coulter SA 3100 surface area analyzer. Samples were dried in the glove box by vacuum desiccation for 1 week prior to analysis. They claim that exposure to air during transfer to the instrument was minimal as evidenced by the lack of color change even in the most sensitive green rust sample, GR(CO₃²⁻). The highest specific surface area (86.3 m² g⁻¹) was reported by Lee and Batchelor (2002b) for sulfate green rust using EGME adsorption. To date, to the best of our knowledge, there is no report in the literature on the specific surface area of naturally occurring green rusts.

Table 4.1. Specific surface area values reported in the literature for synthetic green rusts

Green Rust	Surface area m ² g ⁻¹	Method	Reference
GR(Cl)	19.0	BET N ₂	Bond and Fendorf (2003)
GR(CO ₃ ²⁻)	30.1	BET N ₂	Bond and Fendorf (2003)
GR(CO ₃ ²⁻)	37.1 ± 9.4	BET N ₂	Chun et al. (2007)
GR(CO ₃ ²⁻)	47 ± 7 (n = 5)	BET N ₂	Williams and Scherer (2001)
GR(SO ₄ ²⁻)	3.6	BET N ₂	Bond and Fendorf (2003)
GR(SO ₄ ²⁻)	14.1	BET N ₂	O’Loughlin et al. (2003)
GR(SO ₄ ²⁻)	28.4	BET N ₂	This study
GR(SO ₄ ²⁻)	86.3	EGME	Lee and Batchelor (2002b)

4.1.3 Abiotic Degradation of PCE and TCE by Green Rusts

4.1.3.1 Reports of Degradation of PCE and TCE in the Literature

Earlier reports show that abiotic transformation of PCE and TCE by sulfate green rusts occur via reductive β -elimination to produce acetylene and other completely dechlorinated products (Lee and Batchelor, 2002b; Scherer et al., 2007). In contrast, microbial reductive dechlorination of PCE takes place via sequential hydrogenolysis to yield less chlorinated ethenes along the sequence TCE, *cis*-DCE, vinyl chloride, ethene, and ethane.

In contrast to the reports of Lee and Batchelor (2002b, 2003), Scherer et al. (2007) reported little reduction of 17 mg/L PCE or 13 mg/L TCE by chloride green rust, sulfate green rust, or carbonate green rust at concentrations of 5 or 7 g/L at pH 7.0 to 8.3. However, they did report substantial TCE degradation after 60 days of incubation when TCE was reacted with 10 g/L sulfate green rust at pH 8.2 in 0.02 M NaHCO₃.

Choi and Lee (2008) did not detect PCE degradation when PCE was reacted with sulfate green rust for 2 days. PCE only degraded if platinum chloride (0.5 mM) was added to the reaction mixture. This seems to be in contradiction to the data presented in Figure 1 of Lee and Batchelor (2002b), where approximately 20% of PCE disappeared after 2 days of reaction. But that decrease in concentration was only partly due to degradation. As indicated by the control, much of the reduction was due to rapid partitioning of PCE from the water to the container. The concentration in the control was decreased to about 90% of the original value in the first sample taken. Therefore, it would be more reasonable to say that 5 to 10% of PCE was degraded in 2 days. A difference in experimental procedures might explain the difference in behavior of green rust in these experiments; the green rust used in Lee and Batchelor (2002b) was dried before it was used in the experiment, but the green rust used in Choi and Lee (2008) was never dried.

Data from the unpublished dissertation of Choi (2005) supports the lack of reactivity of sulfate green rust with PCE when sulfate green rust is not dried (See Table 4.2, p 50 in Choi, 2005). It is unclear why drying of sulfate green rust would enhance its reactivity.

Reactive metal ions may be important to understanding the degradation of chlorinated hydrocarbons by green rusts. Maithreepala and Doong (2005), found that Cu(II) in chloride green rust enhanced the degradation of PCE, TCE, and carbon tetrachloride.

4.1.3.2 Degradation of TCE in Studies Performed at Kerr Center (U.S. EPA)

In an effort to verify the earlier findings, researchers in EPA's Ground Water and Ecosystems Research Division (GWERD) conducted batch tests on the abiotic degradation of TCE and carbon tetrachloride by synthetic green rusts. The concentrations of chlorinated compounds (2 – 10 mg/L) used in this study are comparable to those found in the plume areas of contaminated sites. Freshly synthesized green rusts were used to ensure material integrity. The concentration of green rusts in water (4.17 g/L) would correspond to a concentration of iron in aquifer sediment of approximately 0.03%. Calculations assume a water filled porosity of 30% and a density of 2.65 g/cm³ for aquifer sediment. Experimental details are provided in Appendix C.

Figure 4.3 depicts the degradation of TCE at a nominal concentration of 10 mg/L in suspensions containing 4.17 g/L of carbonate green rust. Over 31 days of incubation, there was no significant degradation of TCE at pH 10.3, or pH 8.8 or pH 7.0. None of the expected reaction products of TCE (*cis*-DCE, 1,1-DCE, *trans*-DCE, vinyl chloride, acetylene, ethene, ethane) were detected at quantifiable concentrations. Because this type of green rust is likely the most common green rust in ground waters contaminated with chlorinated hydrocarbons, these results would suggest that the potential for

degradation of TCE by green rusts may not be as great as previously believed.

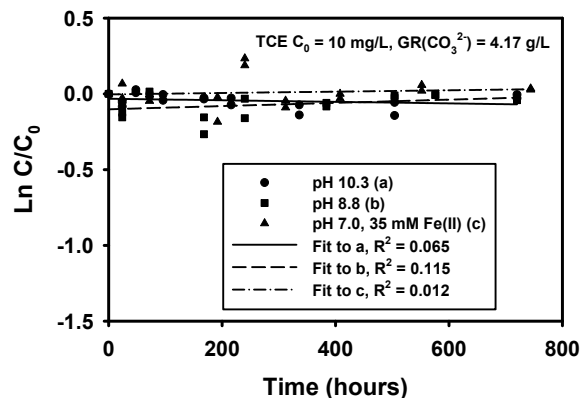


Figure 4.3. Removal of TCE in the presence of carbonate green rust as a function of reaction time, pH, and excess dissolved Fe(II). TCE was reacted with carbonate green rust in $0.037\text{ M Na}_2\text{SO}_4 + 0.030\text{ M Na}_2\text{CO}_3$.

Lee and Batchelor (2002b) reported a surface-area-normalized pseudo first order initial rate constant (k_{sa}) value of $8.55 \times 10^{-5}\text{ L m}^{-2}\text{ day}^{-1}$ for TCE degradation by sulfate green rust at pH 7. Over a pH range from 6.8 to 10.1, Lee and Batchelor (2002b) showed that as the pH increased from 6.8, the initial k_{sa} values were 1.64 fold higher at 7.3; 2.16 fold higher at pH 8.1; 3.05 fold higher at pH 9.2; and 3.96 fold higher at pH 10.1.

In the experiments at Kerr Center, TCE was not degraded in a suspension of sulfate green rust at pH 8.2 or at pH 8.0 (Figure 4.4). No detectable products were found.

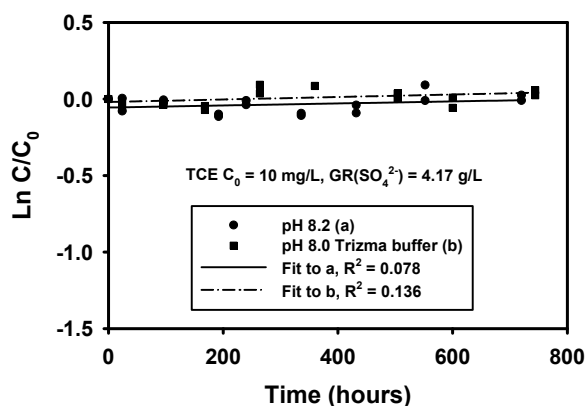


Figure 4.4. Removal of TCE in the presence of sulfate green rust as a function of reaction time with and without a 0.05 M pH 8 Trizma buffer. TCE was reacted with sulfate green rust in $0.074\text{ M Na}_2\text{SO}_4$.

In the EPA study, TCE degraded when 0.5 mM CuSO_4 was present in the suspensions of sulfate green rust. The average final equilibrium pH was 7.9. After 30 days of incubation, 42% of the TCE disappeared, yielding a value of $1.36 \times 10^{-4}\text{ L m}^{-2}\text{ day}^{-1}$ for the k_{sa} . This value is slightly larger than the initial k_{sa} value of $8.55 \times 10^{-5}\text{ L m}^{-2}\text{ day}^{-1}$ reported by Lee and Batchelor (2002b) for TCE degradation by sulfate green rust at pH 7 without a catalyst such as Cu(II).

Reaction products included *cis*-DCE, 1,1-DCE, *trans*-DCE, methylene chloride, ethene, and ethane. Addition of both 0.5 mM Cu(II) and $0.05\text{ M Trizma buffer (pH 8.0)}$ did not produce detectable TCE transformation. Addition of 2.0 mM Cu(II) without a buffer also did not produce measurable TCE degradation (Figure 4.5); however, trace amounts of ethene and ethane were detected in these two treatments. This implies that there is an optimal concentration of Cu(II) at which the reaction is catalyzed. Even in the presence of the optimal concentration of Cu(II), TCE degradation was not great and there was more scatter in the data with Cu(II) than without Cu(II).

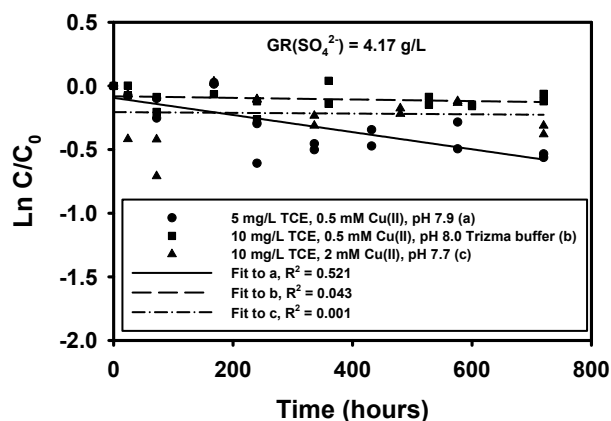


Figure 4.5. Removal of TCE in the presence of sulfate green rust as a function of reaction time, concentration of added CuSO_4 , and presence or absence of 0.05 M Trizma buffer. TCE was reacted with sulfate green rust in 0.074 M Na_2SO_4 .

The differences in results between the EPA study and the study of Lee and Batchelor (2002b) may be explained by differences in experimental procedures. The ratios of the mass of sulfate green rust to the mass of TCE in both studies were similar; however, the preparation of sulfate green rust used by Lee and Batchelor (2002b) had a specific surface area that was three times greater than the sulfate green rust used in the EPA study (Table 1). The higher surface area may have resulted in enhanced dechlorination. Also, drying of green rust may have had an effect. Further work is needed to provide a useful understanding of the role of green rusts in the abiotic degradation of PCE and TCE in contaminated ground water.

4.1.4 Abiotic Degradation of Chlorinated Methanes and Alkanes by Green Rusts

4.1.4.1 Reports of Degradation of Chlorinated Methanes and Alkanes in the Literature

Chun et al. (2007) studied the kinetics and pathways of the degradation of selected halogenated disinfection byproducts (DBPs) in the presence of carbonate green rust. Trichloronitromethane was rapidly degraded to methylamine via sequential hydrogenolysis followed by nitroreduction. Haloacetic acids reacted solely via sequential hydrogenolysis.

Trichloroacetonitrile, 1,1,1-trichloropropanone, and trichloroacetaldehyde hydrate were transformed via hydrolysis and hydrogenolysis. In contrast, chloroform was unreactive over 300 hours of incubation.

The chemical nature of the pH buffer affected the rates of reductive dehalogenation of disinfection byproducts, with faster rates in MOPS buffer than in carbonate buffer, the latter being representative of the buffer in drinking water systems. Carbonate green rust was unstable in both buffers and transformed to magnetite within 48 hours.

O'Loughlin et al. (2003) reported a k_{sa} value of $2.07 \times 10^{-2} \text{ L m}^{-2} \text{ day}^{-1}$ at pH 7.6 for the reduction of carbon tetrachloride by sulfate green rust within the first 6 hours of the reaction. Overall, the reaction was not well described by first-order kinetics. The authors demonstrated the catalytic activity of transition metal species in the reduction of chlorinated hydrocarbons, suggesting the potential for enhanced reduction by green rusts in the presence of an appropriate transition metal catalyst. The rates of reduction of carbon tetrachloride were greatly increased in systems amended with Cu(II), Au(III), and Ag(I) (listed in order of increasing rates) relative to green rust alone.

Erbs et al. (1999) reported values of 0.41 to 1.88 day^{-1} for degradation of carbon tetrachloride by sulfate green rust at pH ≈ 8 . They provided no information on the concentration of sulfate green rust or the total surface area of the sulfate green rust.

Various degradation products have been reported for carbon tetrachloride. Erbs et al. (1999) showed that reduction of carbon tetrachloride by sulfate green rust at pH 8 produced chloroform (CHCl_3) and hexachloroethane (C_2Cl_6) as the main chloroaliphatic products, while the sulfate green rust was oxidized to magnetite (Fe_3O_4). The formation of C_2Cl_6 indicates a coupling reaction between trichloromethyl radicals in the suspension.

The first-order rate constants for transformation of carbon tetrachloride with zerovalent iron and with sulfate green rust were in the same range. Thus, green rusts formed during corrosion of iron(0) under nonacid conditions may make a substantial contribution to the total reduction of carbon tetrachloride measured in iron(0) systems.

Chloroform was much less susceptible than carbon tetrachloride to reductive dechlorination by sulfate green rust. Rates of degradation for chloroform were approximately 100 times less than rates for carbon tetrachloride.

O'Loughlin et al. (2003) observed a variety of intermediates and products of carbon tetrachloride degradation, including chloroform, dichloromethane, chloromethane, methane, acetylene, ethene, ethane, carbon monoxide, tetrachloroethene, and various nonchlorinated C₃ and C₄ compounds. The distribution of products during the reductive dechlorination of carbon tetrachloride was highly dependent on the transition metal used.

Recently, X-ray absorption fine structure analysis of aqueous green rust suspensions amended with Ag(I), Au(III), or Cu(II) showed that the metals were reduced to their zerovalent forms. A possible mechanism for carbon tetrachloride reduction is the formation of a galvanic couple involving the zerovalent metal and green rust, with reduction of carbon tetrachloride occurring on the surface of the metal and green rust serving as the bulk electron source. The enhanced reduction of carbon tetrachloride by suspensions of green rust amended with Ag(I), Au(III), or Cu(II) may prove useful in the development of improved materials for remediation of chlorinated organic contaminants.

No evidence in the study of O'Loughlin et al. (2003) showed that the reduction of carbon tetrachloride and chloroform to methane can be envisioned as resulting from a series of sequential hydrogenolysis reactions (i.e., the stepwise replacement of hydrogen for chlorine), such that

carbon tetrachloride → chloroform → dichloromethane → chloromethane → methane. Results suggest that the reduction of carbon tetrachloride by green rust, silver green rust, gold green rust, and copper green rust involves processes other than sequential hydrogenolysis. In this reaction sequence, carbon tetrachloride is reduced primarily to methane and other non-chlorinated end products, largely through a series of one-electron reductions forming radicals and carbenes or carbenoids.

4.1.4.2 Degradation of Carbon Tetrachloride in the EPA Study

The degradation of carbon tetrachloride by sulfate green rust was pH dependent (Figure 4.6). At low pH, only limited degradation of carbon tetrachloride was observed; the k_{sa} was $1.58 \times 10^{-6} \text{ L m}^{-2} \text{ day}^{-1}$ at pH 4.45 and $3.20 \times 10^{-4} \text{ L m}^{-2} \text{ day}^{-1}$ at pH 6.05. The k_{sa} values ranged from $2.02 \times 10^{-3} \text{ L m}^{-2} \text{ day}^{-1}$ at pH 6.64 to $3.87 \times 10^{-3} \text{ L m}^{-2} \text{ day}^{-1}$ at pH 9.80, suggesting that in this pH range the reaction rates are not strongly influenced by changes in pH. The highest k_{sa} value of $5.61 \times 10^{-3} \text{ L m}^{-2} \text{ day}^{-1}$ was observed at pH 11.16. In the EPA study, chloroform, methylene chloride, methane, and ethylene were detected as reaction products.

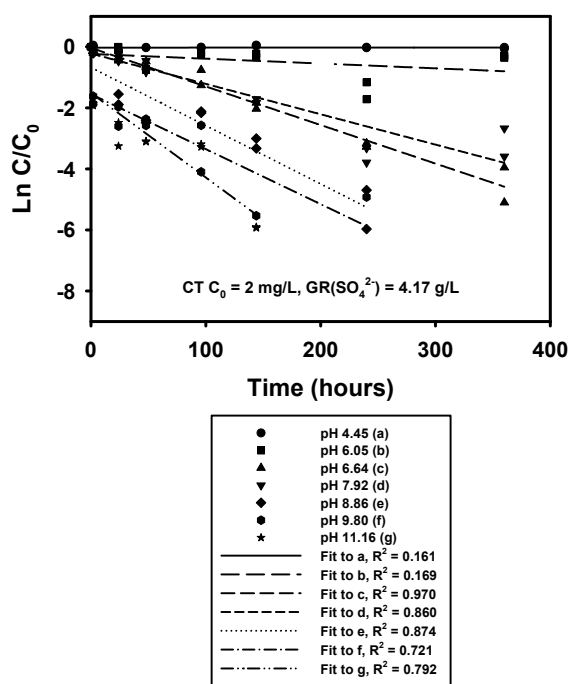


Figure 4.6. Removal of carbon tetrachloride in the presence of sulfate green rust as a function of reaction time and pH. Carbon tetrachloride was reacted with sulfate green rust in 0.074 M Na₂SO₄.

4.1.4.3 Reports of Degradation of Chlorinated Alkanes in the Literature

O'Loughlin and Burris (2004) examined reduction of halogenated ethanes in aqueous suspensions of sulfate green rusts, both alone and with the addition of Ag(I)(AgGR) and Cu(II) (CuGR). Hexachloroethane (HCA), pentachloroethane (PCA), 1,1,1,2-tetrachloroethane (1,1,1,2-TeCA), 1,1,2,2-tetrachloroethane (1,1,2,2-TeCA), 1,1,1-trichloroethane (1,1,1-TCA), 1,1,2-trichloroethane (1,1,2-TCA), 1,1-dichloroethane (1,1-DCA), and 1,2-dibromoethane were reduced in the presence of green rust alone, AgGR, or CuGR. Only 1,2-dichloroethane and chloroethane were nonreactive. The reduction was generally more rapid for more highly substituted ethanes than for ethanes having fewer halogen groups (HCA > PCA > 1,1,1,2-TeCA > 1,1,1-TCA > 1,1,2,2-TeCA > 1,1,2-TCA > 1,1-DCA), and isomers with the more asymmetric distributions of halogen groups were more rapidly

reduced than the isomer with greater symmetry (e.g., 1,1,1-TCA > 1,1,2-TCA). The addition of Ag(I) or Cu(II) to suspensions of green rust resulted in a substantial increase in the rate of reduction of halogenated ethanes as well as significant differences in the product distributions with respect to green rust alone.

Dechlorination of most chlorinated ethanes was through reductive β-elimination to produce vinyl chloride, ethene, and ethane, and/or through dehydrochlorination to produce DCE isomers (Figure 4.7). The reaction mechanism for dechlorination of 1,1,1-TCA by sulfate green rust is uncertain.

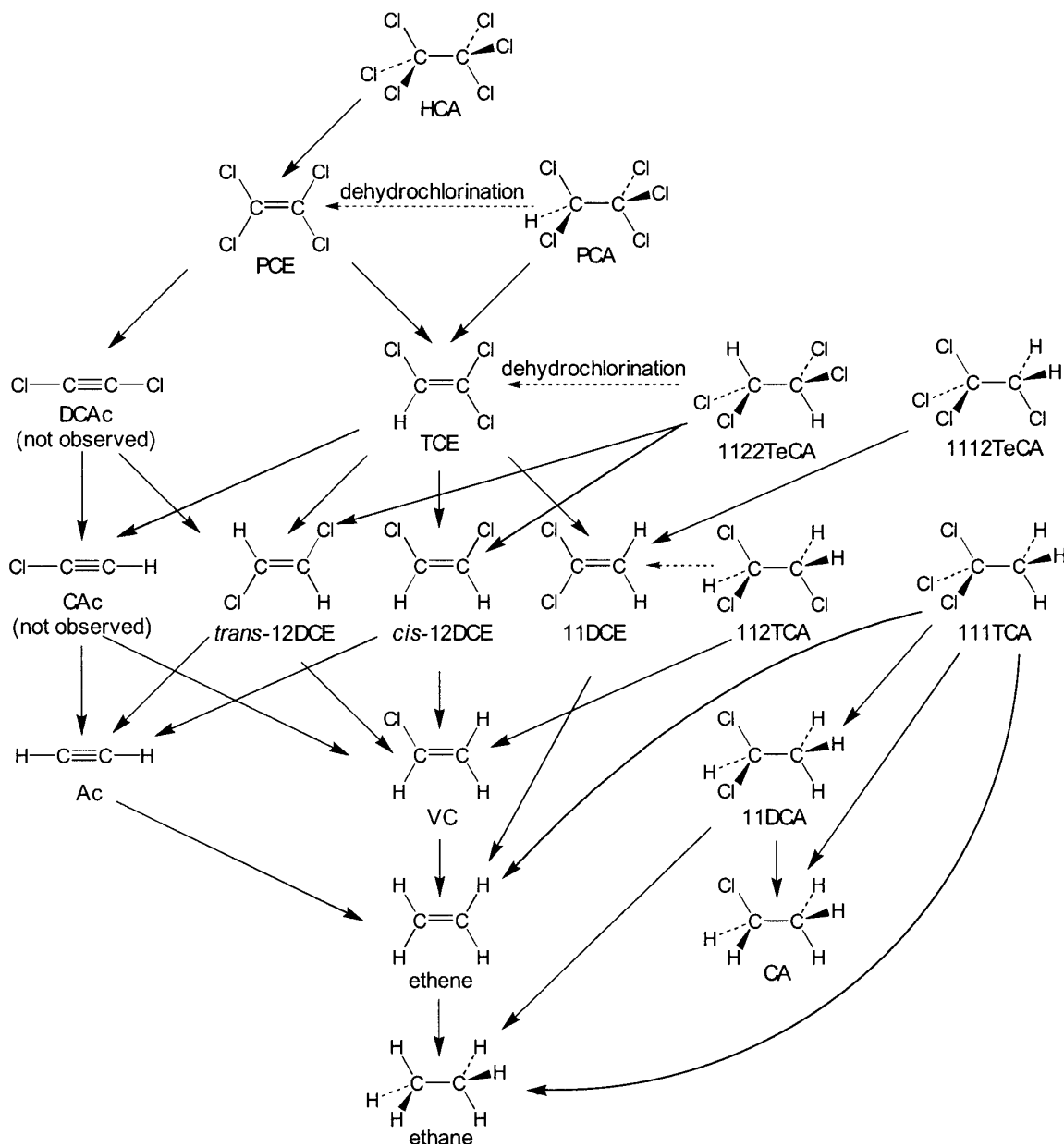


Figure 4.7. Proposed pathways for the reduction of chlorinated ethanes in aqueous suspensions of green rusts and in green rust suspensions spiked with Ag(I) (AgGR) or Cu(II) (CuGR); however, some elements of the pathways shown are not relevant to all experimental systems. Pathways leading to the formation of the C₄ hydrocarbons observed as products of the reduction of 1,1,1-trichloroethane (1,1,1-TCA) by AgGR or 1,1,2-trichloroethane (1,1,2-TCA) and pentachloroethane (PCA) by CuGR are not shown. HCA = hexachloroethane; 1,1,1,2-TeCA = 1,1,1,2-tetrachloroethane; 1,1,2,2-TeCA = 1,1,2,2-tetrachloroethane; 1,1-DCE = 1,1-dichloroethene; cis-1,2-DCE = cis-1,2-dichloroethene; trans-1,2-DCE = trans-1,2-dichloroethene; VC = vinyl chloride; DCAc = dichloroacetylene; CAc = chloroacetylene; Ac = acetylene (From O'Loughlin and Burris, 2004).

Table 4.2 summarizes the available information on the rate constants for abiotic degradation of chlorinated hydrocarbons by green rusts.

Table 4.2. Rate constants for transformation of chlorinated hydrocarbons by green rusts. Rate constants are quoted or converted to surface-area-normalized pseudo-first-order initial rate constant (k_{sa}) when information is available.

Compound	Mineral	pH	Rate Constant k_{sa} L m ⁻² day ⁻¹	Reference
PCE	GR(SO ₄ ²⁻)	7.0	1.62×10^{-4}	Lee and Batchelor (2002b)
TCE	GR(SO ₄ ²⁻)	7.0	8.55×10^{-5}	Lee and Batchelor (2002b)
TCE	GR(CO ₃ ²⁻)	10.3	No reaction	This Report
TCE	GR(CO ₃ ²⁻)	8.8	No reaction	This Report
TCE	GR(CO ₃ ²⁻)	7.0	No reaction	This Report (35 mM Fe(II))
TCE	GR(SO ₄ ²⁻)	8.0	No reaction	This Report
TCE	GR(SO ₄ ²⁻)	8.2 Trizma	No reaction	This Report
TCE	GR(SO ₄ ²⁻)	7.9	1.36×10^{-4}	This Report (0.5 mM Cu(II))
TCE	GR(SO ₄ ²⁻)	8.0 Trizma	No reaction	This Report (0.5 mM Cu(II))
TCE	GR(SO ₄ ²⁻)	7.7	No reaction	This Report (2.0 mM Cu(II))
CT	GR(SO ₄ ²⁻)	7.6	2.07×10^{-2}	O'Loughlin et al. (2003)*
CT	GR(SO ₄ ²⁻)	4.45	1.58×10^{-6}	This Report
CT	GR(SO ₄ ²⁻)	6.05	3.20×10^{-4}	This Report
CT	GR(SO ₄ ²⁻)	6.64	2.56×10^{-3}	This Report
CT	GR(SO ₄ ²⁻)	7.92	2.02×10^{-3}	This Report
CT	GR(SO ₄ ²⁻)	8.86	3.87×10^{-3}	This Report
CT	GR(SO ₄ ²⁻)	9.80	3.65×10^{-3}	This Report
CT	GR(SO ₄ ²⁻)	11.16	5.61×10^{-3}	This Report
<i>cis</i> -DCE	GR(SO ₄ ²⁻)	7.0	5.19×10^{-5}	Lee and Batchelor (2002b)
VC	GR(SO ₄ ²⁻)	7.0	7.77×10^{-5}	Lee and Batchelor (2002b)

*for the data of first 6 hours of reaction only.

4.2 Occurrence and Determination of Green Rusts

Our current knowledge on the occurrence and distribution of green rusts in contaminated sites is not adequate to evaluate their contribution to the abiotic transformation of chlorinated hydrocarbons in ground water. More work is needed to attain a practical capability to predict how and when green rust may form at a site and to quantitatively predict their capacity to degrade chlorinated hydrocarbons.

4.2.1 Geochemical Conditions that Favor Green Rust Formation

Green rusts can form from partial oxidation of Fe²⁺ in the groundwater or directly from corrosion of metallic iron that is used in reactive barriers and for reinforcement of underground radioactive waste repositories. The name “fougerite” has been formally approved by the Commission on New Minerals and Mineral Names of the International Mineralogical Association (IMA) (number

2003-057), on January 29, 2004 (Feder et al., 2005). The mixed valence compound fougérite (IMA 2003-057), a layered Fe(II)–Fe(III) hydroxysalt, is found in transitionally oxic and anoxic environments like hydromorphic soils (Génin et al. 1998; Trolard et al. 2007). Fougérite (IMA 2003-057) is a mixed $M(\text{II})$ - $M(\text{III})$ hydroxysalt of the green rust group, where $M(\text{II})$ can be Fe or Mg, and $M(\text{III})$ is Fe. The general structural formula is: $[\text{Fe}_{1-x}^{2+}\text{Fe}_x^{3+}\text{Mg}_y(\text{OH})_{2+2y}]^{+x}[x/nA^{-n} \bullet m\text{H}_2\text{O}]^{-x}$ where A is the interlayer anion and n its valency, with $1/4 \leq x/(1+y) \leq 1/3$ and $m \leq (1-x+y)$. The mineral forms by partial oxidation and hydrolysis of aqueous Fe^{2+} , to give small crystals (400–500 nm) in the form of hexagonal plates. The mineral is unstable in air and transforms to lepidocrocite or goethite. The name is for the locality of the occurrence, a forested Gleysol near Fougères, Brittany, France. Its characteristic blue-green color (5BG6/1 in the Munsell system) has long been used as a universal criterion in soil classification to identify Gleysols.

Dissolved silicon affects phase formation during neutralization and partial oxidation of iron(II) chloride solutions. In the absence of Si, the initial phase further reacts to form green rust, presumably a double hydroxide of Fe^{2+} and Fe^{3+} iron which ultimately forms lepidocrocite. In the presence of Si, the formation of green rust structure from the initial phase is inhibited, as evidenced by symmetrical basal and asymmetrical hk x-ray diffraction (XRD) lines, and ferrihydrite is the ultimate oxidation product (Karim, 1986).

Biogenic formation of carbonate green rust was observed in well controlled laboratory experiments (Ona-Nguema et al., 2002a; Ona-Nguema et al., 2002b). They confirmed that carbonate green rust is metastable with respect to magnetite in the presence of $\gamma\text{-FeOOH}$.

The competitive formation of carbonate green rust and sulfate green rust in bacterial cultures is dependent on the relative ratio (R) of bicarbonate

and sulfate concentrations (Ona-Nguema et al., 2004). When $R \geq 0.17$, only carbonate green rust was formed whereas when $R < 0.17$, a mixture of sulfate green rust and carbonate green rust was obtained. Ona-Nguema et al. (2004) used *Shewanella putrefaciens*, a dissimilatory iron-reducing bacterium (DIRB) to anaerobically catalyze the transformation of a ferric oxyhydroxide, lepidocrocite ($\gamma\text{-FeOOH}$), into Fe(II) in the presence of various sulfate concentrations. These results demonstrated that the sulfate green rust can originate from the microbial reduction of $\gamma\text{-FeOOH}$ and confirmed the preference for carbonate over sulfate during green rust precipitation.

Zegeye et al. (2005) investigated the formation of only sulfate green rust during the reduction of $\gamma\text{-FeOOH}$ by a DIRB. Their experimental study demonstrated that, under a H_2 atmosphere, the biogenic solid that was produced was a sulfate green rust and it was the sole iron(II-III) bearing mineral, regardless of the initial lepidocrocite concentration. The crystals of the biotically formed sulfate green rust were significantly larger than those observed for sulfate green rust obtained through abiotic preparation. The formation of green rust by *Shewanella* species isolated from a wide range of habitats and possessing varied metabolic capabilities suggests that under favorable conditions biogenic green rusts may be formed by a diverse array of DIRB (O'Loughlin et al., 2007; Zegeye et al., 2007).

4.2.2 Structural Stability of Carbonate Green Rust

Synthetic carbonate green rust is not stable; it quickly changes to magnetite and $\text{Fe}(\text{OH})_2$. No information is available on the potential for degradation of chlorinated solvents by $\text{Fe}(\text{OH})_2$. Studies have shown that the presence of certain anions help stabilize the crystal structure from degradation. These anions include phosphate (Bocher et al., 2004) and arsenate or arsenite (Su and Wilkin, 2005). Bocher et al. (2004) showed that in the presence of phosphate as low as $\{[\text{PO}_4]_{\text{min}}^0 / [\text{Fe}]\} \approx 1\%$, carbonate green rust is

stable. No P was detected by TEM-EDX when the basal (0001) crystal faces were analyzed, showing that no P was inserted in the GR inter-layers. In contrast, very low quantities of P were detected when the analyses were performed on the lateral faces of the green rust crystals. The preference of phosphate species for lateral faces is due to the fact that the $\{10\bar{1}0\}$ faces contain mono- and di-coordinated OH-surface groups. The PO_4^{3-} adsorbed on the lateral faces may act as a barrier that slows down the release in solution of the CO_3^{2-} species preventing carbonate green rust from transforming into a mixture of Fe_3O_4 and $\text{Fe}(\text{OH})_2$. See Figure 4.8.

Since carbonate green rust has been found to form in the natural environment by coprecipitation, some kind of stabilization agents (phosphate, silicate, etc.) may play a role.

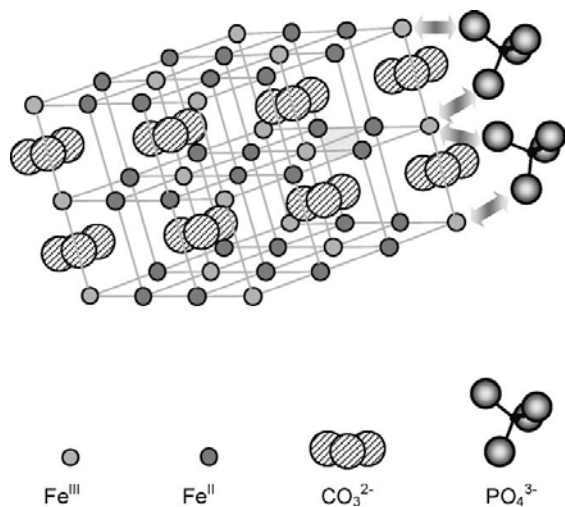


Figure 4.8. Adsorption of the phosphate on the lateral $\{10\bar{1}0\}$ face of the $\text{GR}(\text{CO}_3^{2-})$ crystal that stabilizes it (From Bocher et al., 2004).

Phyllosilicate Clays

5.1 Structural Iron in Phyllosilicate Clays

Phyllosilicate clays are composed of sheets of SiO_4 and AlO_4 tetrahedra with an approximate chemical formula of $(\text{Al},\text{Si})_3\text{O}_4$. Other elements such as iron can replace silicon or aluminum in the sheets. This iron is incorporated into the structure of the clay with co-valent bonds, and is referred to as structural iron. The structural iron can be iron(II) or iron(III), and its oxidation state can change as the clay interacts with oxidizing or reducing agents. The structural iron can also interact through shared oxygen atoms with iron(II) sorbed to the surface of the clay.

In experimental systems, the rate law for the degradation of the organic compound will frequently change over time. Lee and Batchelor (2004) described the kinetics of degradation of PCE, TCE, *cis*-DCE, and vinyl chloride on biotite, vermiculite, and montmorillonite with a model that contained two reactive sites. One type of reactive site was present at lower concentrations than the other type of site, but was much more reactive than the second type of site. Over time, the more reactive type of site is consumed, and the overall rate of degradation slows. Neumann et al. (2008) used nitroaromatic compounds as probes to characterize and compare two preparations of montmorillonite clay and a ferruginous smectite that had different proportions of iron(II) and iron(III) and different concentrations of total iron. They could explain the contrasting behavior of the probes on the clays by associating more reactive and less reactive sites with Fe(III)-O-Fe(II) entities and Fe(II)-O-Fe(II) entities in the crystal structure of the clays.

5.2 Degradation Processes on Phyllosilicate Clays

Kriegman-King and Reinhard (1992) examined the degradation products of carbon tetrachloride on biotite in the presence of HS^- . The primary products were chloroform, carbon disulfide, and carbon dioxide. The pH of the water had little effect on the rate of degradation, or the relative concentration of the degradation products.

Cervini-Silva et al. (2001) found that 1,1,2,2-tetrachloroethane degraded to TCE on ferruginous smectite. Neumann et al. (2009) also compared degradation of carbon tetrachloride, 1,1,1,2-tetrachloroethane, 1,1,2,2-tetrachloroethane, and several model compounds on ferruginous smectite. The only product detected from the degradation of carbon tetrachloride was chloroform. There was no effect of pH on the rate of degradation. Transformation of 1,1,1,2-tetrachloroethane was primarily through reductive β -elimination to form 1,1-dichloroethylene, while transformation of 1,1,2,2-tetrachloroethane was through dehydrochlorination to produce TCE.

Nzengung et al. (2001) showed that PCE degraded on smectites to form TCE, and then *cis*-DCE, vinyl chloride, acetylene, ethylene, and ethane. In contrast to the behavior of carbon tetrachloride, Lee and Batchelor (2004) found that the rate constant for degradation of PCE on biotite increased with increasing pH. As pH increased from 5.5 to 8.1, the rate constant increased threefold, then the rate constant doubled between pH 8.1 and 8.5.

5.3 Rate Constants for Degradation of Chlorinated Alkenes

Table 5.1 provides rate constants available from the literature for the degradation of chlorinated alkenes on the phyllosilicate clays: biotite, montmorillonite, and vermiculite. The observed pseudo first-order rate constants are normalized to the surface area of the mineral presented to water in the suspension, and to the amount of structural iron in the minerals. The clays had been pretreated with dithionite to reduce the structural iron to iron(II). Lee and Batchelor (2004) found that the kinetics of degradation were biphasic, with an initial rapid phase that was followed by a transition to a slower phase. The kinetic parameters reported by Lee and Batchelor (2004) were used to calculate pseudo first-order rate constants for the initial rapid phase, which are reported in Table 5.1.

The first order rate constants normalized to the concentration of structural iron fell into a fairly narrow range, extending between 0.020 and 0.65 $M^{-1}d^{-1}$. The rates of degradation of PCE, TCE, *cis*-DCE, and vinyl chloride were comparable on a particular preparation of clay, but varied from clay to clay. On montmorillonite, the rate constants for degradation of the four chlorinated alkenes varied from 0.65 $M^{-1}d^{-1}$ for PCE to 0.33 $M^{-1}d^{-1}$ for vinyl chloride. On vermiculite, the rates varied from 0.020 $M^{-1}d^{-1}$ for PCE to 0.18 $M^{-1}d^{-1}$ for vinyl chloride.

The rate constants for degradation of the chlorinated alkenes on the phyllosilicate clays (after reduction of structural iron with dithionite) were comparable to the rate constant for degradation on pyrite, and exceeded the rate constant for degradation on magnetite (Table 5.1).

When the rate constant was normalized to the surface area of the clay mineral, the rate constants varied widely, depending on the clay mineral. The preparations of biotite, vermiculite, and montmorillonite used by Lee and Batchelor (2004) have specific surface areas of 1.9 m^2/g , 26.7 m^2/g and 488 m^2/g respectively. The

reactivity of the phyllosilicate clays was more influenced by the concentration of structural iron than by the surface area presented to water. As the specific surface area increased, the normalized rate of degradation decreased. The rate constants for the four chlorinated alkenes varied from 9.4 $L m^2 d^{-1}$ to 13.5 $L m^2 d^{-1}$ on biotite, from 0.062 $L m^2 d^{-1}$ to 0.67 $L m^2 d^{-1}$ on vermiculite, and from 0.0090 $L m^2 d^{-1}$ to 0.018 $L m^2 d^{-1}$ on montmorillonite.

5.4 Rate Constants for Degradation of Carbon Tetrachloride and Chlorinated Alkanes

Table 5.2 provides rate constants available from the literature for the degradation of carbon tetrachloride, 1,1,1-TCA, and 1,1,2,2-tetrachloroethane on phyllosilicate clays, including biotite, a ferruginous smectite, and vermiculite. When expressed on a surface area basis, the reactivity of the phyllosilicate clays was intermediate between pyrite and magnetite. Rate constants reported by Kriegman-King and Reinhard (1992) and Neumann et al. (2009), when normalized to the concentration of structural iron in their experiments, also indicate that reactivity of structural iron in biotite and vermiculite is comparable to the reactivity of structural iron in pyrite or magnetite. The rate constants for degradation of carbon tetrachloride on these clays were approximately ten to one-hundred times larger than the rate constants for the chlorinated alkenes (compare Table 5.2 and 5.1).

The rate constants for degradation of carbon tetrachloride on a preparation of ferruginous smectite was approximately one-hundred fold higher than rate constants for degradation on biotite and vermiculite. It is unclear whether this result comes from some difference in experimental procedure or approach, or represents a real difference in the behavior of carbon tetrachloride on these clays.

The rate constant for degradation of 1,1,1,2-tetrachloroethane was equivalent to the rate constants for degradation of carbon

tetrachloride, and the rate constant for degradation of 1,1,2,2-tetrachloroethane was three to fourfold faster.

5.5 Effect of Sorbed Iron (II) on the Rate of Degradation

The effect of sorbed iron(II) is modest. Lee and Batchelor (2004) compared the effect of sorbed iron on the kinetics of degradation of chlorinated alkenes on biotite. As sorbed iron(II) increased from zero to 0.15 mM g⁻¹, the rate of degradation on the clay surface increased 1.5 fold. Across a variety of experimental conditions, including a range of pH from 5.5 to 8.1, and for PCE, TCE, *cis*-DCE, and vinyl chloride reacting on biotite, vermiculite, and montmorillonite, the rate constant for reaction on the clay surface was generally less than twofold higher in the presence of 4.28 mM Fe(II).

5.6 Extrapolation of Rate Constants to the Field

Nzengung et al. (2001) reported that the rate constants for degradation of PCE on the clay minerals was not a linear function of the concentration of clay minerals. The rate of degradation in a 1% (weight/volume) suspension of clay was actually slower than the rate of degradation in a 0.5% suspension. Nzengung et al. (2001) explained this effect as being due to aggregation of the clay particles that reduced the surface area available to react with chlorinated organic compounds in water. Aggregation will be important for natural clays in aquifer sediment.

If the rate constants in Tables 5.1 and 5.2 are realized in aquifer material at field scale, they can make a substantial contribution to the destruction of these contaminants (Lee and Batchelor, 2004). However, the rate constants in Tables 5.1 and 5.2 are likely to be an upper boundary on the rates that might be achieved at field scale. This is particularly true because most of the experiments were done with clays that had been artificially reduced with dithionite. The rate constants in Tables 5.1 and 5.2 are probably not appropriate for aquifers that are

naturally aerobic. They may be appropriate for aquifers with ongoing sulfate reduction.

The rate constants presented in this section were developed for homogeneous samples of clays in laboratory experiments. To our knowledge, no one has published an estimate of structural iron in clay minerals in a sample of aquifer material, and related the concentration of structural iron to the rate of degradation of chlorinated organic contaminants. Because the reactivity of phyllosilicate clays is more directly related to the concentration of reactive structural iron in clay than to the total weight of clay or the surface area of clay, the total content of structural iron in clay, or perhaps the total content of structural iron(II) in clay, would be an appropriate parameter to predict abiotic degradation.

An estimate of total structural iron in the clay fraction of aquifer sediment is theoretically possible at the present state of practice, but making that estimate would require a complex series of extractions and digestions. To determine the concentration of structural iron in phyllosilicate clays, it would first be necessary to perform extractions to remove the exchangeable iron and iron oxide minerals. Depending on the redox status of the aquifer, it might be necessary to remove the chromium reducible sulfides to remove iron associated with mackinawite and pyrite. Presumably, the major portion of iron remaining in the sample would be structural iron associated with phyllosilicate clays. The final step will require digestion of the sample with 48% HF and 3.6 M H₂SO₄ and determination of iron using the 1,10-phenanthroline colorimetric method (Stucki, 1981; Komadel and Stucki, 1988).

The biphasic kinetics of degradation seen in laboratory experiments poses another impediment to extrapolation of the rate constants in Tables 5.1 and 5.2 to predict behavior in the field. Lee and Batchelor (2004) estimated the reductive capacity of individual samples of phyllosilicate clays to PCE, TCE, *cis*-DCE, and vinyl

chloride. Table 5.3 uses their data to estimate the total concentration of these chemicals that could be degraded by the clays when present at 10% of the total dry weight of aquifer sediment. This would be a high concentration of clay for a sediment that would readily transmit water and would function as a useful aquifer. Approximately 20 to 50 mg/L of chlorinated alkenes would be destroyed. Phyllosilicate clays can only be expected to make a significant contribution to the natural attenuation of relatively dilute plumes of chlorinated solvents.

The reactive iron in the phyllosilicate clays is a small fraction of the total structural iron in the clays. Lee and Batchelor (2003) found that only 1% of Fe(II) in the clay they examined could reduce PCE. Table 5.3 also expresses the specific initial reductive capacity of the clays examined by Lee and Batchelor (2004) on the basis of moles of chlorinated solvent destroyed per mole of total iron. Reductive dechlorination requires two electrons to remove one chlorine from the organic compound. Two moles of iron would be required to dechlorinate PCE, TCE, *cis*-DCE, or vinyl chloride to the next degradation product. A very small fraction of the total iron in the clays was available to reduce the chlorinated organic compounds.

Table 5.1 Rate constants for degradation of chlorinated alkenes on phyllosilicate clay minerals. Data for pyrite and magnetite are provided for comparison.

Compound	Mineral	pH	Other Conditions	Observed first order rate constant normalized to surface area of mineral	Observed first order rate constant normalized to concentration structural iron	Reference
				$L\ m^{-2}\ d^{-1}$	$M^{-1}\ day^{-1}$	
PCE	Pyrite	8	22 °C, 10 mM NaHCO ₃	2.4×10^{-5}	0.17	Lee and Batchelor (2002a)
PCE	Magnetite	7	22 °C, 10 mM NaHCO ₃	0.082×10^{-5}	0.0036	Lee and Batchelor (2002a)
PCE	Biotite reduced with dithionite	7	22 °C, 10 mM NaHCO ₃	13.5×10^{-5}	0.12	Lee and Batchelor (2004)
PCE	Montmorillonite reduced with dithionite	7	22 °C, 10 mM NaHCO ₃	0.018×10^{-5}	0.65	Lee and Batchelor (2004)
PCE	Montmorillonite reduced with dithionite	8.5	25 °C, 34.5 mM dithionite	1.5×10^{-5}	19	Nzungung et al. (2001)
PCE	Vermiculite reduced with dithionite	7	22 °C, 10 mM NaHCO ₃	0.074×10^{-5}	0.020	Lee and Batchelor (2004)
TCE	Biotite reduced with dithionite	7	22 °C, 10 mM NaHCO ₃	10×10^{-5}	0.092	Lee and Batchelor (2004)
TCE	Montmorillonite	7	22 °C, 10 mM NaHCO ₃	0.018×10^{-5}	0.64	Lee and Batchelor (2004)
TCE	Vermiculite reduced with dithionite	7	22 °C, 10 mM NaHCO ₃	0.062×10^{-5}	0.016	Lee and Batchelor (2004)
<i>cis</i> -DCE	Biotite reduced with dithionite	7	22 °C, 10 mM NaHCO ₃	9.4×10^{-5}	0.086	Lee and Batchelor (2004)
<i>cis</i> -DCE	Montmorillonite reduced with dithionite	7	22 °C, 10 mM NaHCO ₃	0.010×10^{-5}	0.37	Lee and Batchelor (2004)
<i>cis</i> -DCE	Vermiculite reduced with dithionite	7	22 °C, 10 mM NaHCO ₃	0.30×10^{-5}	0.079	Lee and Batchelor (2004)
VC	Biotite reduced with dithionite	7	22 °C, 10 mM NaHCO ₃	12×10^{-5}	0.111	Lee and Batchelor (2004)

Table 5.1 Continued.

Compound	Mineral	pH	Other Conditions	Observed first order rate constant normalized to surface area of mineral	Observed first order rate constant normalized to concentration structural iron	Reference
VC	Montmorillonite reduced with dithionite	7	22 °C, 10 mM NaHCO ₃	0.0090×10^{-5}	0.33	Lee and Batchelor (2004)
VC	Vermiculite	7	22 °C, 10 mM NaHCO ₃	0.67×10^{-5}	0.18	Lee and Batchelor (2004)

Table 5.2 Rate constants for degradation of carbon tetrachloride and chlorinated alkanes on phyllosilicate clay minerals. Data for pyrite and magnetite are provided for comparison.

Compound	Mineral	pH	Other Conditions	Observed first order rate constant normalized to surface area of mineral	Observed first order rate constant normalized to concentration structural iron	Reference
				L m ⁻² d ⁻¹	M ⁻¹ day ⁻¹	
carbon tetrachloride	Pyrite	6.5	25 °C, 1 M NaCl	1620 × 10⁻⁴	1.7	Kriegman-King and Reinhard (1994)
carbon tetrachloride	Magnetite	7.0	25 °C, 1 M NaCl	4.80 × 10⁻⁴	0.67	Danielsen and Hayes (2004)
carbon tetrachloride	Biotite	8.6	50 °C, 1 mM HS ⁻	33.2 × 10 ⁻⁴	4.4	Kriegman-King and Reinhard (1992)
carbon tetrachloride	Biotite	8.8	50 °C, 1 mM HS ⁻	23.1 × 10 ⁻⁴	3.1	Kriegman-King and Reinhard (1992)
carbon tetrachloride	Ferruginous Smectite	NR	5 mM NaCl	not reported	232	Cervini-Silva et al. (2001)
carbon tetrachloride	Ferruginous Smectite Reduced with dithionite	8.4	5 mM NaCl	not reported	483	Cervini-Silva et al. (2001)
carbon tetrachloride	Ferruginous Smectite reduced with dithionite	7.5	25 °C, 0.5 M NaCl	not reported	1.75	Neumann et al. (2009) from panel A, Figure S2
carbon tetrachloride	Vermiculite	8.3	50 °C, 1 mM HS ⁻	8.95 × 10 ⁻⁴	7.0	Kriegman-King and Reinhard (1992)
1,1,1,2-tetrachloroethane	Ferruginous Smectite	NR	5 mM NaCl	not reported	380	Cervini-Silva et al. (2001)
1,1,2,2-tetrachloroethane	Ferruginous Smectite	NR	5 mM NaCl	not reported	1,040	Cervini-Silva et al. (2001)

Table 5.3. Maximum quantity (C_{RC}^0) of chlorinated hydrocarbon that can be reduced by reactive iron in representative phyllosilicate clays. Calculated by multiplying the concentration of clay exposed to pore water (g/L) by the specific initial reductive capacity of the clay (S_R) as published in Lee and Batchelor (2004). Calculations assume a water filled porosity of 25% and a clay content of 10% of the total dry weight of sediment.

Clay	Chlorinated hydrocarbon	S_R	C_{RC}^0	Iron content of clay	C_{RC}^0 normalized to content of total iron	C_{RC}^0 normalized to content of total iron
		$\mu\text{M g}^{-1}$	mg L^{-1}	mg/g	$\frac{\text{mg}(\text{CH})}{\text{g}(\text{Total Iron})^{-1}}$	$\frac{\text{M}(\text{CH})}{\text{M}(\text{Total Iron})^{-1}}$
Biotite	PCE	0.4	52.7	117	0.57	1.9×10^{-4}
Biotite	TCE	0.482	50.4	117	0.54	2.3×10^{-4}
Biotite	<i>cis</i> -DCE	0.612	47.2	117	0.51	2.9×10^{-4}
Biotite	VC	1.06	52.7	117	0.57	5.1×10^{-4}
Vermiculite	PCE	0.177	23.3	56.7	0.52	1.7×10^{-4}
Vermiculite	TCE	0.188	19.6	56.7	0.44	1.9×10^{-4}
Vermiculite	<i>cis</i> -DCE	0.635	48.9	56.7	1.09	6.2×10^{-4}
Vermiculite	VC	1.01	50.2	56.7	1.11	9.9×10^{-4}
Montmorillonite	PCE	0.271	35.7	7.5	5.99	20×10^{-4}
Montmorillonite	TCE	0.282	29.5	7.5	4.94	21×10^{-4}
Montmorillonite	<i>cis</i> -DCE	0.318	24.5	7.5	4.11	24×10^{-4}
Montmorillonite	VC	0.353	17.5	7.5	2.94	26×10^{-4}

Methods to Characterize Sediments and Organic Contaminants

This section discusses methods that are currently available to predict or understand abiotic transformations of organic compounds in aquifer sediments.

6.1 *Isotopic Fractionation to Characterize Degradation of Organic Compounds*

Degradation of organic compounds either through abiotic processes or through biological processes can change the ratio of stable isotopes in the material that remains behind and has not been degraded. This process is called isotopic fractionation. In many cases it is possible to recognize degradation of organic contamination in field scale plumes from a change in the ratio of stable isotopes of carbon or hydrogen (Hunkeler et al., 2008). In some cases, it is possible to infer the extent of degradation from isotopic fractionation, and to separate the reduction in concentration caused by degradation from reductions in concentration caused by dilution and dispersion.

Commercial laboratories can determine the ratio of stable isotopes of carbon in chlorinated organic compounds such as PCE, TCE, and *cis*-DCE in water samples, even when the concentrations are as low as 5 to 10 $\mu\text{g/L}$. At the time of this writing, the cost is near \$300 per sample.

Reactions in which bond cleavage is the rate-limiting step can result in the enrichment of the heavier isotope (^{13}C) in the remaining parent compound (Bloom et al. 2000; Elsner et al. 2005; Zwank et al. 2005). The magnitude of isotope fractionation can be described by the bulk enrichment factor, ϵ_{bulk} , derived from the Rayleigh model (Liang et al. 2007). The more negative the value of ϵ_{bulk} , the greater the change in ratio of stable isotopes for a given amount of

degradation. For abiotic transformations, the magnitude depends on the mineral surface presented for reaction, and on the reaction pathway.

For biological transformations, the magnitude of isotope fractionation depends on various factors including temperature, bacterial species, structure of the organic compounds, and availability of nutrients (Bloom et al. 2000).

Readers who are not familiar with the use of stable isotope analysis to document the extent of degradation of organic compounds are directed to Hunkeler et al. (2008) for the definition of units, a discussion of analytical techniques, and example calculations.

6.1.1 *Isotopic Fractionation of Carbon Tetrachloride on Various Iron Minerals*

Zwank et al. (2005) compared the rate of degradation and the isotopic fractionation of carbon tetrachloride on a variety of iron minerals under comparable conditions. Minerals included magnetite (Fe_3O_4), mackinawite (FeS), goethite ($\alpha\text{-FeOOH}$), lepidocrocite ($\gamma\text{-FeOOH}$), hematite (Fe_2O_3), and siderite (FeCO_3). The pH was buffered to between 7.1 and 7.3. The minerals were suspended in a solution of 1 to 2.3 mM Fe^{2+} , and the surface area of the minerals in the suspension was approximately $50 \text{ m}^2 \text{ L}^{-1}$.

Zwank et al. (2005) found that the abiotic reductive dehalogenation of carbon tetrachloride was associated with substantial carbon isotopic enrichment. They found that the observed bulk enrichment factors (ϵ_{bulk}) correlated neither with the surface-normalized reaction rate constants nor with the type of products formed. However, the bulk enrichment factors fell into two distinctly different ranges for the two principal groups of minerals studied. With

iron (hydr)oxide minerals (goethite, hematite, lepidocrocite, and magnetite) and with siderite, the ϵ -values for carbon tetrachloride dehalogenation were remarkably similar (the range was $-29 \pm 3\text{‰}$). Because this value matched well with the theoretical estimates for the cleavage of an aliphatic C–Cl bond, they suggested that dissociative electron transfer to carbon tetrachloride controls the reaction rates for this group of iron minerals. Conversely, carbon tetrachloride transformation by different preparations of mackinawite was accompanied by a significantly lower carbon isotopic fractionation ($\epsilon_{\text{bulk}} = -15.9 \pm 0.3\text{‰}$), possibly due to the presence of nonfractionating rate-determining steps or a significantly different transition state structure of the reaction (Zwank et al. 2005).

Neumann et al. (2009) compared degradation of carbon tetrachloride on ferruginous smectite. The only product detected from the degradation of carbon tetrachloride was chloroform. The value of ϵ_{bulk} was -13.3‰ to -10.9‰ .

6.1.2 Isotopic Fractionation of PCE and TCE on Iron(II) Monosulfide

Liang et al. (2007) compared the enrichment of stable carbon isotopes during biological and nonbiological degradation of PCE and TCE. Significant carbon isotope fractionation was observed during FeS-mediated reductive dechlorination of tetrachloroethylene (PCE) and trichloroethylene (TCE). Bulk enrichment factors for PCE were $-30.2 \pm 4.3\text{‰}$ (pH 7), $-29.54 \pm 0.83\text{‰}$ (pH 8), and $-24.6 \pm 1.1\text{‰}$ (pH 9). For TCE, ϵ_{bulk} values were $-33.4 \pm 1.5\text{‰}$ (pH 8) and $-27.9 \pm 1.3\text{‰}$ (pH 9).

The bulk enrichment factors for abiotic degradation are substantial. Based on the uncertainty in the measurement, isotopic ratios in two different samples of PCE or TCE can usually be distinguished if the ratios differ by more than 2‰. If the bulk enrichment factor is near -30‰ , and as little as one-half the original material is degraded, the isotopic

shift would be 21‰. If degradation of PCE or TCE occurs through an abiotic reaction with FeS, then it should be possible to recognize degradation and predict the extent of degradation using stable carbon isotope analyses.

Bulk enrichment factors are also available for microbial reductive dechlorination by two isolated pure cultures [*Desulfuromonas michiganensis* strain BB1 (BB1) and *Sulfurospirillum multivorans* (Sm)] and a bacterial consortium [BioDechlor Inoculum (BDI)]. The ϵ_{bulk} values for biological PCE microbial dechlorination were $-1.39 \pm 0.21\text{‰}$ (BB1), $-1.33 \pm 0.13\text{‰}$ (Sm), and $-7.12 \pm 0.72\text{‰}$ (BDI), while those for TCE were $-4.07 \pm 0.48\text{‰}$ (BB1), $-12.8 \pm 1.6\text{‰}$ (Sm), and $-15.27 \pm 0.79\text{‰}$ (BDI) (Liang et al. 2007). In each case, the fractionation during abiotic transformation was substantially greater than the fractionation during biodegradation.

Because ϵ_{bulk} values for microbial reductive dechlorination of PCE and TCE are generally smaller in magnitude (less negative) than those for abiotic reductants, Zwank et al. (2005) suggested that differences in ϵ_{bulk} values could be used to distinguish abiotic and biotic reductive dechlorination of PCE, but not TCE, in model sulfate-reducing systems.

6.1.3 Isotopic Fractionation of EDB on Iron(II) Monosulfide

The isotopic enrichment factor for degradation of EDB on biogenic FeS as determined by Wilson et al. (2008) was $-20.2 \pm 2.23\text{‰}$ at 95% confidence. The enrichment of carbon isotopes during abiotic degradation of EDB during reaction with FeS (-20.2‰) is significantly greater than the enrichment during biodegradation (-5.7‰) (Wilson et al. 2008). This relationship has been observed for other halogenated organic compounds. The contrast in behavior of stable carbon isotopes in EDB during biodegradation and abiotic transformation parallels the behavior of PCE and TCE as observed by Liang et al. (2007).

6.1.4 Isotopic Fractionation of TCE on Green Rust

At this writing, there is only one value for ϵ_{bulk} associated with the degradation of a chlorinated hydrocarbon on green rust. Liang et al. (2009) reported a value of $-23.00 \pm 1.8\%$ for degradation of TCE on chloride green rust. This value is very similar to the fractionation of TCE on magnetite (Section 3) and on FeS (Liang et al. 2007; Zwank et al. 2005). Because the TCE is strongly fractionated, it should be possible to recognize abiotic transformation of TCE on sulfate green rust in the field (when it occurs) by an analysis of stable carbon isotopes.

6.1.5 Isotopic Fractionation of TCE and *cis*-DCE on Magnetite

Section 3 and Appendix B describe experiments conducted by staff at the Kerr Center on abiotic transformation of TCE and *cis*-DCE in sediments from two sites on the Twin Cities Army Ammunition Plant (TCAAP) north of St Paul, Minnesota. Sediment containing magnetite was collected from Site A and the Building 102 site.

As mentioned in Section 3 and Appendix B, there was no evidence of removal of PCE or TCE in sediment from Site A at the TCAAP; however, PCE and TCE were degraded in material from the site at Building 102. Figure 6.1 depicts the fractionation of stable carbon isotopes of TCE in pore water in the microcosms that were constructed with sediment from the site at Building 102. The fractionation of TCE was strong ($\epsilon = -39\% \pm 12\%$ at 95% confidence). This strong fractionation should make it possible to use stable carbon isotope analyses of TCE in ground water to recognize degradation of TCE at field scale.

In contrast to TCE, the fractionation of *cis*-DCE on magnetite is much weaker (Figure 6.2). Panel A of Figure 6.2 presents the data with an expanded y-axis, to facilitate comparison of differences. Panel B of Figure 6.2 plots the data on the same scale as Figure 6.1. The bulk isotopic enrichment factor (ϵ) extracted from

combined data from both Site A and the site at Building 102 is only -0.60% . The value is not different from zero at 90% confidence. The value of ϵ would have to be more negative than -1.4% to be different from zero at 95% confidence. Based on this limited data set, it will be difficult to use stable isotope fractionation to recognize degradation of *cis*-DCE at field scale.

The strong contrast in the isotopic enrichment factor between TCE and *cis*-DCE suggests that there are important differences in the mechanisms or pathways of degradation of TCE and *cis*-DCE on the surface of magnetite. This might explain why PCE and TCE did not degrade in microcosms constructed from sediment from Site A at TCAAP, but *cis*-DCE did degrade in microcosms made from sediment from Site A. The bulk isotopic enrichment factors for degradation of PCE and TCE in sediment from the Building 102 site are similar to the values reported by Liang et al. (2007) for degradation of PCE and TCE on FeS [$-29.54 \pm 0.83\%$ (for PCE at pH 8), and $-33.4 \pm 1.5\%$ (for TCE at pH 8)].

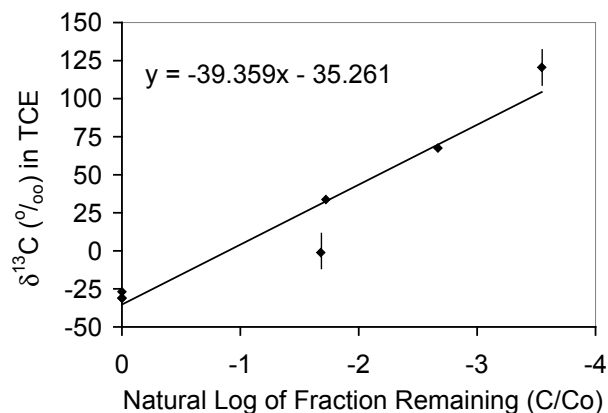


Figure 6.1. Fractionation of stable isotopes of carbon during abiotic degradation of TCE in aquifer sediment containing magnetite (site at Building 102 at TCAAP). The uncertainty in $\delta^{13}\text{C}$ is indicated by the vertical bars through the symbols.

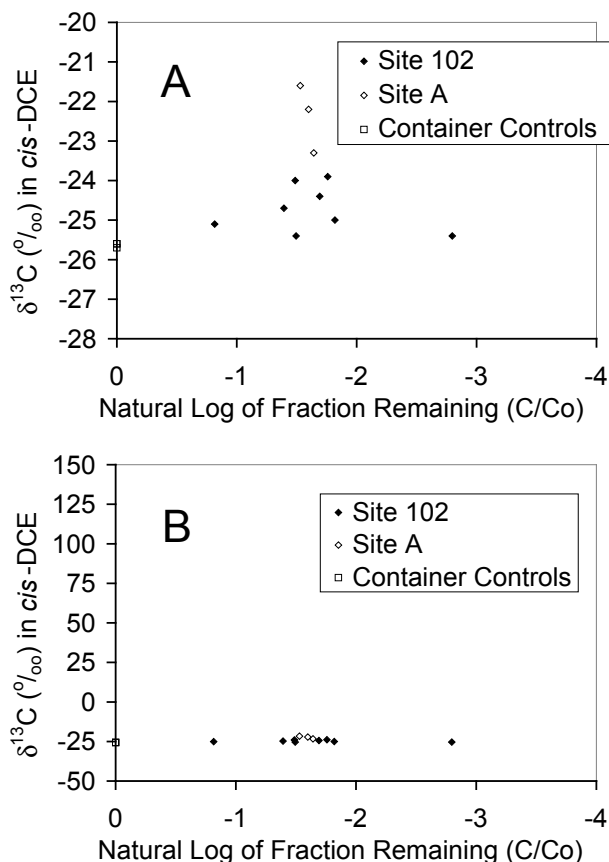


Figure 6.2. Fractionation of stable isotopes of carbon during abiotic degradation of *cis*-DCE in aquifer sediment containing magnetite.

6.1.6 Isotopic Fractionation of Chlorinated Alkanes on Phyllosilicate Clay

Neumann et al. (2009) also compared degradation of 1,1,1,2-tetrachloroethane and 1,1,2,2-tetrachloroethane on ferruginous smectite. Transformation of 1,1,1,2-tetrachloroethane was primarily through reductive β -elimination to form 1,1-dichloroethylene (ϵ_{bulk} , $-11.4\% \pm 2.0\%$ and $-14.9\% \pm 1.7\%$), while transformation of 1,1,2,2-tetrachloroethane was through dehydrochlorination to produce TCE (ϵ_{bulk} , $-24.0\% \pm 0.8\%$ and $-20.8\% \pm 2.2\%$).

6.2 Methods to Estimate the Quantity of Reactive Minerals

The essential components of a study to characterize reactive iron and sulfur minerals will include sample collection, sample fractionation (e.g., size or magnetic fractionation), determination of bulk elemental composition (e.g., total Fe and S), determination of chemical speciation of Fe and S, and determination of mineralogy.

There are two particular challenges related to the detection and measurement of the reactive iron-bearing minerals. The first challenge is that they are often sensitive to changes in the redox environment. Exposure to molecular oxygen from the atmosphere quickly destroys green rusts and iron(II) monosulfides. The second challenge is that the reactive iron and sulfur minerals are usually present in soil and aquifer sediment at low concentrations. Concentrations of mackinawite or green rust as low as 0.1% by weight, or concentrations of magnetite as low as 1% by weight, can transform chlorinated hydrocarbons at environmentally significant rates (Section 2 and Section 4 of this Report). These low, but environmentally relevant, concentrations can be difficult to characterize.

Amonette (2002) provides a recent description of the methods used to identify and quantify minerals in soils. As will be discussed below, established methods with adequate sensitivity and resolution are available to determine the bulk concentration of mackinawite and other iron(II) monosulfides, as well as, pyrite and other iron(II) disulfides. Established methods are not readily available to directly determine magnetite or green rusts at natural concentrations in environmental samples. However, magnetite can be easily concentrated by magnetic separation, and the bulk concentration of magnetite can be estimated from the magnetic susceptibility of the sample.

Established methods are not available to estimate the specific surface area of minerals in soils and aquifer materials. If the

minerals can be concentrated, the particle size can be estimated from the broadening of peaks in the X-ray diffraction spectrum, or by examination by scanning or transmission electron microscopy, and surface area can be calculated from the particle size distribution.

6.2.1 Characterization by Chemical Extraction Methods

Chemical extraction methods are perhaps the most frequently used techniques for establishing iron and sulfur partitioning in sediments and soils. Methods designed to differentiate iron minerals typically involve complexation and protonation reactions. The amount of iron extracted by hydrochloric acid, oxalic acid, ascorbic acid, and buffered sodium dithionite solutions is often used to distinguish mineral phases (Heron et al., 1994; Kostka and Luther, 1994). Methods for partitioning total sulfur in a sample among organic sulfur, acid-volatile sulfides (e.g., mackinawite), and chromium-reducible sulfur (e.g., pyrite and sulfur) are well established and sensitivity to 0.01% by weight is achievable for most sample types (e.g., Burton et al. 2008; Tack et al., 1997).

6.2.1.1 Sulfur Minerals in Soil and Sediments

Sulfur can generally be fractionated into sulfate, elemental sulfur, acid volatile sulfide (AVS), and chromium reducible sulfur (CrRS). In sediments, AVS and CrRS are the two most important fractions in regulating the behavior of contaminants. AVS is commonly used as a general estimate for FeS, and CrRS is an estimate for FeS₂ in sediment. Analysis of AVS and CrRS is commercially available from labs that support the AMIBA protocol (Aqueous and Mineral Intrinsic Bioremediation Assessment) as described in Kennedy et al. (2004). The labs can be located by using AMIBA or Aqueous and Mineral Intrinsic Bioremediation Assessment in a search engine on the internet.

AVS is operationally defined as sulfide that can be extracted with 1M HCl. The AVS extraction procedure is intended to digest labile sulfide

compounds, including iron monosulfides such as mackinawite (FeS). AVS measurements are generally considered to represent hydrogen sulfide released during the acid dissolution of iron monosulfides. AVS can also include sulfide associated with other acid-soluble sulfide minerals (e.g., poorly crystalline ZnS), residual pore-water sulfide (Morse and Rickard 2004), sulfide adsorbed to mineral or organic surfaces released at low pH, or sulfide associated with metal sulfide nanoparticles or clusters (Rickard and Morse 2005; Wilkin and Bischoff 2006).

CrRS is selective for inorganic S with an oxidation state less than +6 (Canfield et al. 1986). CrRS measurements are commonly used to determine the pyrite-sulfur content of sediments. CrRS is extracted with 0.5M CrCl₂ in 1M HCl which is usually prepared using a Jones reductor. CrRS can be analyzed in sequence after extraction and removal of AVS and elemental sulfur; or CrRS can be determined before removal of AVS and elemental sulfur. When this is done, the measured CrRS includes both AVS and elemental sulfur.

Qualitatively, the most common methods to determine the presence of iron sulfide components are X-ray diffraction (XRD), X-ray fluorescence (XRF), and scanning electron microscopy–energy dispersive spectroscopy (SEM–EDS). XRD can be used to detect certain minerals in a mixture without regard to their abundance; XRF can be used to determine the total elemental composition of a sample; and SEM–EDS can be used to visualize ultrastructures with subsequent estimation of their elemental composition. None of these methods however, are appropriate for quantitative analysis (Popa and Kinkle 2000).

There are several procedures available in the literature for quantitative determination of AVS and CrRS in sediment. Generally there are two ways to extract sulfide from sediment samples: diffusion (Hsieh et al. 2002; Ulrich et al. 1997) and purge and trap (Morse and Cornwell 1987). After the sulfide is extracted, the concentration

of sulfide can be measured several ways. These include coulometry (Oita 1983; Wilkin and Bischoff 2006), colorimetry (Allen et al. 1993; Cornwell and Morse 1987), gravimetric analysis (Di Toro et al. 1990; Leonard et al. 1993), sulfide ion-specific electrodes (Pesch et al. 1995), or gas chromatography with photoionization detection (Casas and Crecelius 1994; Lasorsa and Casas 1996; Leonard et al. 1999).

Lasorsa and Casas (1996) provide a detailed comparison of the advantages and disadvantages of some common analytical methods for AVS and CrRS measurements. The colorimetric method is relatively easy to use and is less time-consuming than the gravimetric method, and is cost effective in terms of consumables. It is also the most forgiving when extremely high or low levels of AVS are encountered, though dilution of the trapping solution is required to analyze high concentrations of AVS. Instrument failure and maintenance were seldom a problem. However, this method produced a relatively large volume of acid waste (approximately 280 mL per sample), and the mixed diamine reagent used in this method is the most hazardous of all of the reagents used in the available methods in terms of corrosivity and toxicity.

The gravimetric method was more time-intensive and complicated, and more expensive on a per-sample basis than the other methods. This is due to the expense of the silver nitrate reagent, as much as \$10 per sample. The cost for equipment is lower than the methods using photoionization or coulometric detectors. Only glassware and an accurate balance sensitive to 0.001 g are required. The method was not as forgiving when extremely high or low AVS concentrations were encountered, either due to uncertainty in weighing extremely small masses or the possibility of exhausting the silver reagent at very high concentrations of AVS. The volume of waste produced is significantly higher than that of the colorimetric method (approximately 500 mL) because of an extra trap to remove HCl and the larger volumes of trapping reagent.

The ion selective electrode method was the simplest to carry out and relatively inexpensive in terms of both consumable items and instrumentation. This method can be used over a wide range of concentrations without dilution of the trapping solution. It produced a volume of waste similar to that of the colorimetric method (approximately 280 mL).

The photoionization detection method is relatively simple, most cost effective in terms of consumables, and accurate at low concentrations. Difficulty may be experienced when extremely high AVS concentrations were encountered. The method works well when the NaOH-trapping step is eliminated, but since the photoionization detection method is linear to only about 1 pmole of H₂S, the NaOH-trapping step must be used with samples that have sulfide concentrations greater than 10 pmole/g.

A coulometric method was introduced by Wilkin and Bischoff (2006) to determine sulfur fractions in environmental samples. This method is simple, fast and sensitive, with a detection limit of 5 µg S g⁻¹ and average precision of 91% (Wilkin and Bischoff 2006). Only a small sample is required. The method can be applied to samples of sediments, soil, aquifer solids, and waste products. Another major advantage is the fact that the evolution of hydrogen sulfide gas is detected in-line. Chemical extraction end points can be precisely determined without need to set arbitrary time limits as in other methods. This method generates the smallest volume of waste (10 mL), but the coulometer is expensive. The anode and cathode solutions used in the measurement are highly toxic.

6.2.1.2 Interferences with Chemical Extraction Methods for Sulfur Minerals

Occasionally, when sediment samples are analyzed for sulfides by different methods, there are discrepancies between the concentrations that are reported. Some of the discrepancies are probably caused by inadequate treatment or preservation of the samples. Problems can

occur during collection and processing under N_2 or with precipitation of sulfides with zinc acetate, or oxidation after collection during shipment, or during steps involved in processing the samples such as washing or distillation. Alternatively, variations in the composition of the sample may be important (e.g., ferric iron interference, crystal size, and surface properties).

In the presence of acid-soluble ferric minerals, AVS can be underestimated using the hot distillation procedure (Pruden and Bloomfield, 1968; Berner, 1974; Cornwell and Morse, 1987). This underestimation is caused by the dissolution of ferric minerals in strong acid, presumably allowing soluble Fe(III) to oxidize sulfide (Hsieh et al. 2002). To minimize oxidation of AVS by Fe(III) during the hot distillation procedure, $SnCl_2$ has been added to the sample (Cornwell and Morse, 1987). However, Hsieh et al., (2002) found that the addition of 1 g $SnCl_2$ powder to their samples did not prevent the ferric interference on AVS. They also found that addition of 2 mL 1 M ascorbic acid to the sample effectively protects AVS from oxidation in the presence of 0.39 mmol acid-soluble Fe(III).

Another major interference is elemental sulfur which could interfere during the chromium reduction step in the determination of CrRS. This would result in an overestimation of FeS_2 (Popa and Kinkle 2000). Elemental sulfur (S^0_8) can be extracted by shaking the sediment with 20 mL of acetone for 24 h (Wieder et al., 1985), followed by a further 10 mL acetone rinse. The S (S^0_8) content of the acetone phase can then be determined by the Cr-reduction method.

6.2.2 Characterization of Chemical Identity by Spectroscopy or Diffraction

6.2.2.1 Characterization by X-ray Diffraction (XRD)

X-ray diffraction is generally the preferred method for mineral identification. X-ray diffraction patterns are diagnostic features that can be searched and matched with available software to confidently identify constituent minerals

contained in natural samples. One drawback with the method relates to the practical detection limit for particular minerals. In most situations, the mineral phases responsible for driving abiotic dechlorination reactions are typically expected to be less than one percent by weight of the total sediment. Detection limits using conventional powder X-ray diffraction techniques will vary depending on the sample matrix and on the degree of crystallinity of the component minerals, but quantitation limits of about 1 to 5 weight percent may be achieved for a given phase without pre-concentration. In natural samples, quartz usually overwhelms other minerals because it is abundant and because it diffracts more strongly than other minerals. For equivalent amounts of quartz and a mixture of other minerals, the strongest peaks will often be from quartz. Detection limit problems are consequently confounded by the fact that quartz is usually the major mineral component in ground-water aquifers.

As an example, mechanical mixtures of magnetite and quartz were prepared at three different dilutions ranging from 2% to 10% magnetite by weight. The mixed components were of comparable grain size (-325 mesh). For each sample, X-ray diffraction scans were collected in overnight runs to maximize sensitivity and increase the signal to noise ratio. The raw diffraction scans are shown on Figure 6.3 along with Powder Diffraction Files for magnetite (PDF 19-0629) and quartz (PDF 46-1045).

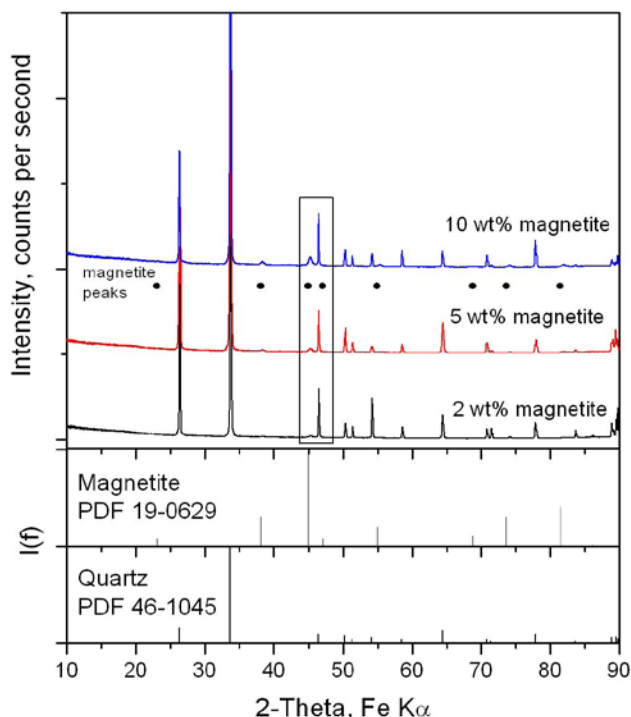


Figure 6.3. Powder X-ray diffraction scans of mixtures of magnetite and quartz.

As expected, quartz dominates the diffraction scans. The most prominent peak for magnetite is expected at 2-theta value (using Fe $K\alpha$ radiation) of about 45.3° . Peaks at this position are clearly observable in the 10% and 5% mixtures, and perhaps less obvious in the 2% mixture.

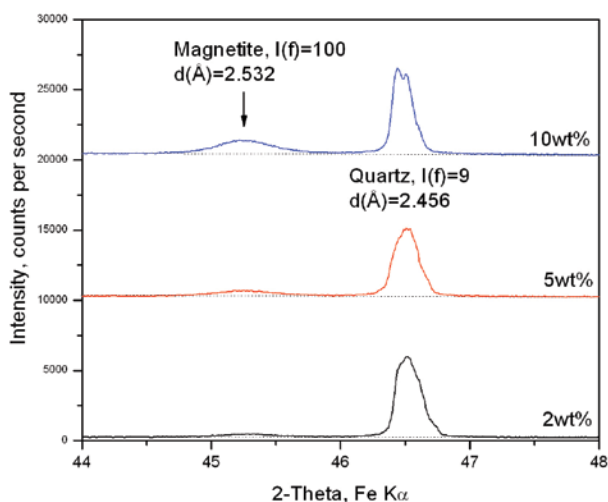


Figure 6.4. Blow-up of the 2-theta region from 44° to 48° , showing the most intense diffraction peak for magnetite at 45.2° .

A blow-up of the 2-theta region from 44° to 48° is shown in Figure 6.4. Judging from these data, a practical limit of detection for magnetite in polymineral mixtures is likely between about 2 and 5% on a weight basis. For any sample, detection limits can be improved by using pre-concentration steps such as magnetic separation or size fractionation.

6.2.2.2 Characterization of Green Rusts by X-ray Diffraction (XRD) and Atomic Force Microscopy (AFM)

Green rusts are particularly difficult to study because they oxidize within minutes of exposure to air. Special care must be taken to preserve green rust samples, both synthetic and natural. Some techniques have been developed that stabilize green rusts. Taylor (1982) handled and stored a synthetic carbonate green rust in a CO_2 atmosphere, such as might occur under natural anaerobic conditions in a soil below the groundwater table. For XRD examination, he placed a small amount of dry ice in the sample chamber of a vertical goniometer beneath a glass slide containing a smear of the sample. Recent practice of sample handling involves the use of an anaerobic glove box (4-6% H_2 in N_2) in which samples are processed. Glycerol is mixed with a sample to minimize air oxidation when making an XRD slide. For samples where the use of glycerol is not desirable, the XRD slide can be scanned on a miniature X-ray diffractometer that is housed inside an anaerobic glove box.

Christiansen et al. (2009) presented a sampling method for capturing green rust in groundwater without oxidation. Within 30 s of taking each water sample, a droplet that would cover about 1 cm^2 was deposited on a substrate (glass for XRD or mica for AFM) and covered with a platelet of the same material. The sample was left for a minute so particles in the solution could adhere; then the liquid was sucked away with a tissue. They tested several settling times (1/2 to 5 min), but detected no difference in the XRD patterns. For practical reasons, they chose 1 minute of settling time. In well under 5 minutes

from the time the water was taken from the flowing stream, the finished sample had been stored under a nitrogen atmosphere. The samples were transported to the laboratory in a nitrogen atmosphere and stored in an anaerobic chamber (4% H₂ in N₂). They imaged the samples with AFM in the glovebox. Reproducibility tests made with synthetic green rust proved that if it is dry, green rust fixed on Si-bearing substrates is stable in air for more than 24 hours. In this case, the powder XRD data were collected in air.

Green rusts form in soils and sediments when the level of oxygen is very low; in air they will transform to normal brown rust within a few minutes. This has prevented researchers from finding out exactly how and under what conditions they form. To overcome these problems, Christiansen and Stipp (2003) recreated the conditions conducive to green rust formation within the beamline of an X-ray machine. Using a complex chemical reaction cell, and with the unique power and intensity of the X-ray beam, they were able to gain a unique insight into the atomic scale formation and crystallization of green rust under conditions close to which it forms in contaminated land environments. Specifically, they used an AFM mounted inside a glove box to observe the formation and transformation of sulfate green rust and developed a method for obtaining XRD patterns from samples in an inert atmosphere. This avoids the use of glycerol and other treatments that may alter the crystal structure, making it possible to collect clearer patterns while avoiding any possibility of alteration. Some previously undefined XRD peaks from untreated sulfate green rust suggest internal ordering of sulfate and water. AFM evidence indicates that sulfate green rust can form from topotactic transformation of Fe(OH)₂ as the starting phase (Bernal et al., 1959).

Carbonate green rust was identified as a major Fe(0) corrosion product by XRD, even in simulated groundwater containing added sulfate and no added carbonate. Carbon dioxide diffusion from air provided carbonate for the formation of

carbonate green rust (Su and Puls, 2004). This suggests that carbonate green rust is either kinetically favored or thermodynamically more stable than sulfate green rust in the studied system.

Bearcock et al. (2006) used XRD to characterize green rust present in a 45-60 mm thick band which lay just below the surface (\approx 4 mm) of an ochreous deposit at an abandoned coal mine site. SEM imaging of the sample (presence of μ m-sized hexagonal crystals) and chemical analyses (Fe(II)/Fe(III) = 2:1) support the XRD identification of green rust either as pyroaurite (Powder Data File 01-070-2150) or GR2 (00-052-0163) (sulfate green rust). The sample contained 14.1 wt.% FeO.

In a recent study, Sumoondur et al. (2008) obtained direct evidence for the formation of magnetite via a green rust intermediate. The Fe(II) induced transformation of ferrihydrite, was quantified *in situ* and under O₂-free conditions using synchrotron-based time-resolved energy dispersive X-ray diffraction. At pH 9 and Fe(II)/Fe(III) ratios of 0.5 and 1, rapid growth (6 min) of sulfate green rust and its subsequent transformation to magnetite was observed. Electron microscopy confirmed these results, showing the initial rapid formation of hexagonal sulfate green rust particles, followed by the corrosion of the green rust as magnetite growth occurred, indicating that the reaction proceeds via a dissolution-reprecipitation mechanism. At pH 7 and a Fe(II)/Fe(III) ratio of 0.5, sulfate green rust was the stable phase, with no transformation to magnetite.

Information is lacking about the detection limit of green rusts using XRD for natural soil and sediment samples. Successful identification of green rusts with XRD is usually associated with a dark bluish green color in the sample.

XRD analysis is commercially available and the cost is reasonable.

6.2.2.3 Characterization of Green Rusts by Infrared Spectroscopy (IR)

IR can be used to determine the presence of anions in the green rust interlayers. For example, Ona-Nguema et al. (2004) used diffuse reflectance infrared Fourier transform spectroscopy to confirm the presence of intercalated carbonate and sulfate in the structure of biogenic green rust, in combination with XRD, TEM, and SEM. Su and Puls (2004) used FTIR-photoacoustic spectroscopy (interlayer carbonate stretching mode at $1352 - 1365 \text{ cm}^{-1}$) to identify carbonate green rust along with XRD and SEM as a major iron corrosion product in zerovalent iron-packed columns constructed for arsenic remediation. Commercial IR services are available and most research labs are equipped with IR.

6.2.3 Estimating Magnetite in Sediment from Magnetic Susceptibility

There is no direct chemical “test” that is specific for magnetite at its natural abundance in sediment. However, the magnetic susceptibility of magnetite can provide a useful estimate of the quantity of magnetite in aquifer sediment.

Magnetite is the most abundant mineral in natural sediments that exhibits magnetic behavior. Magnetism is an expression of the magnetic moments associated with the spin of unpaired electrons that are involved in chemical bonds. In magnetite the moments are highly aligned, but exist in two sets of opposing but unequal forces constrained by the crystal lattice of the mineral. As a result, when an external magnetic field is imposed on a sample of magnetite, the magnetic moments will align with the imposed field and add to the total magnetic field. The extent to which an imposed magnetic field is strengthened by the sample is termed the magnetization of the sample. The volume magnetic susceptibility of the sample is the ratio of the magnetization of the sample (the magnetic dipole moment per unit volume) measured in amperes per meter divided by the magnetic field strength, measured in amperes per meter.

As defined above, volume magnetic susceptibility is dimensionless. However, the actual value for volume magnetic susceptibility depends on how the magnetic permeability of free space is defined in the system of measurement. Unfortunately, two separate systems are in common use, the CGS system (centimeter gram second) with values reported as emu or e.m.u. for electromagnetic unit, and the International System of Units (abbreviated SI from the French *Le Système International d’Unités*) based on the meter, kilogram and second. This Report will use the SI system of measurement. A value for volume magnetic susceptibility in the CGS system can be converted to the SI system by multiplying by 4π . We will express measurements of magnetic susceptibility of aquifer sediment as the mass molecular susceptibility. The mass magnetic susceptibility is the volume magnetic susceptibility divided by the density of the sample in kg m^{-3} , and the unit for mass magnetic susceptibility in the SI system is $\text{m}^3 \text{ kg}^{-1}$.

Canfield and Berner (1987) studied the dissolution and pyritization of magnetite in marine sediments. Horneman et al. (2004) studied dissolution of arsenic from iron(II) minerals in anoxic aquifers in Bangladesh. As part of their studies they compared the mass magnetic susceptibility of their sediments to the mass of materials that could be separated from the sediment with a magnet. Their results are presented in Figure 6.5. The correlation of mass magnetic susceptibility with weight content of geological materials was roughly linear from less than 100 mg/kg to more than 10,000 mg/kg. However, there was significant scatter in the data. Individual measurements could vary by a factor of three from the regression line.

Figure 6.5 also presents the relationship between mass and mass magnetic susceptibility for four known materials. Magnetite Sample 1 was provided by Robert C. Thomas of Athens Georgia; its specific surface area is $18 \text{ m}^2 \text{ g}^{-1}$. Magnetite Sample 2 was purchased from Cerac Specialty Inorganics (particle size $5 \mu\text{m}$ or less, 99% pure). Magnetite Sample 3 was ground from magnetite

crystals. Finally, the Magnetite Calibration Standard in Figure 6.5 was the standard provided with a MS2 Magnetic Susceptibility System (Bartington Instruments Ltd., Oxford, England). The standard contained 1% by weight magnetite in silica. It was contained in a cylindrical sample pot with a capacity of 10 mL. As was the case with the natural sediment samples, the magnetic susceptibility of the magnetite standards varied from each other by a factor of three.

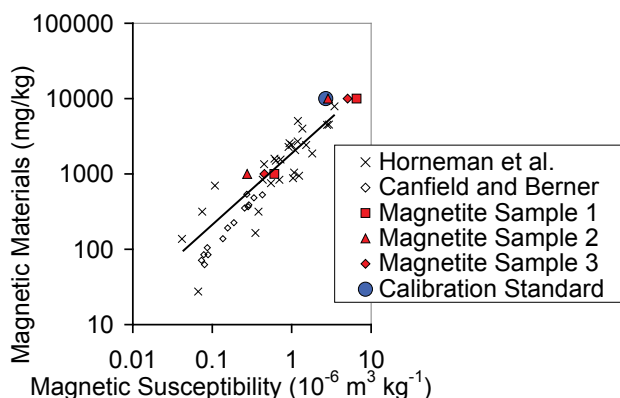


Figure 6.5. Relationship between the mass magnetic susceptibility of a sediment sample and the content of magnetic materials.

All the data on magnetic susceptibility in Section 3 and Appendix B were acquired with a MS2 Magnetic Susceptibility System using the MS2B detector (Bartington Instruments Ltd., Oxford, England). This unit is widely used by geologists and geochemists to characterize samples of rock and sediment. The Bartington Magnetic Susceptibility System claims good reproducibility down to $0.001 \times 10^{-6} \text{ m}^3 \text{ kg}^{-1}$. If the relationship in Figure 6.5 is extrapolated to this value, the content of magnetic materials would be near 1 mg/kg. This concentration is negligible. The estimation of magnetite in sediment is more likely to be limited by a spurious signal from another mineral, than by the sensitivity of the instrument.

The combined data of Horneman et al. (2004) and Canfield and Berner (1987) were used to extract a relationship between the mass

magnetic susceptibility of a sediment sample and the expected concentration of magnetic materials. A linear regression of the logarithm of the concentration of magnetic materials on the logarithm of the magnetic susceptibility of the sample produces equation 6.1.

$$\text{Log}(MM) = 1.0803 * \text{Log}(MS) + 9.7038$$

Equation 6.1

and equation 6.2,

$$MM = 10^{(1.0803 * \text{Log}(MS) + 9.7038)}$$

Equation 6.2

where MM is the concentration of magnetically separable materials (mg/kg) and MS is the mass magnetic susceptibility of the sample ($\text{m}^3 \text{ kg}^{-1}$).

Equation 6.2 was used to calculate the mass of magnetic material (assumed to be magnetite) exposed to pore water in the sediment samples in Table 3.1 and 3.2 in Section 3.

The reproducibility and linearity of magnetic susceptibility instruments such as the Bartington MS2 Magnetic Susceptibility System is good, generally much less than $\pm 10\%$ of the expected value. Error in predicting the content of magnetic materials from mass magnetic susceptibility will come from the natural variation in mass magnetic susceptibility of magnetite from one sample to another, and from the magnetic susceptibility of other minerals that might be in the sample. Hematite ($\alpha\text{-Fe}_2\text{O}_3$) and goethite ($\alpha\text{-FeOOH}$) are the only common iron minerals that have large enough mass magnetic susceptibilities to be confused with magnetite. The mass magnetic susceptibility of finely divided magnetite (particle diameter 12 nm to 69 nm) ranges from 500 to $1116 \times 10^{-6} \text{ m}^3 \text{ kg}^{-1}$, while the mass magnetic susceptibility of hematite and goethite range from 0.27 to $1.69 \times 10^{-6} \text{ m}^3 \text{ kg}^{-1}$ (Table 2.2, Dearing, 1999). The mass magnetic susceptibility of magnetite is one thousand-fold greater. If the iron content represented by the predicted concentration of magnetite is at least 1% of the total extractable iron, it is unlikely that the magnetic susceptibility of other iron minerals will cause significant error.

If it is necessary to do so, the chance of confusing another mineral with magnetite can be evaluated by comparing the total extractable iron concentration in a sample to the concentration of iron in magnetite that would be predicted from the mass magnetic susceptibility of the sample. For an example of this evaluation, compare data in Table 3.4 in Section 3. Equation 6.2 was used to calculate the concentration of magnetite that would be necessary to produce the mass magnetic susceptibility of the sediment. On a mass basis, magnetite is 72% iron by weight. To estimate the iron associated with magnetite, the concentration of magnetite in Table 3.4 was multiplied by 0.72. In sediments with detectable rates of abiotic removal of chlorinated organics, the amounts of iron that would be in the amounts of magnetite that were predicted from the mass magnetic susceptibility of the sediment varied from 16% to 83% of the total extractable iron.

6.3 Methods to Determine Oxidation Status

6.3.1 Characterization of Green Rusts by Mössbauer Spectroscopy

Mössbauer spectroscopy (MS) has often been used to characterize green rusts and to follow their Fe(II)/Fe(III) ratio during the process of oxidation of Fe(OH)₂ in the presence of aggressive anions such as Cl⁻, SO₄²⁻, CO₃²⁻. For example, Génin et al. (2002) studied chloride pitting of concrete reinforcing bars and the bacterial corrosion of cast iron in water pipes or steel sheet piles in harbors.

Refait et al. (2001) studied a green rust mineral extracted from hydromorphic soils in Fougères (France) by X-ray absorption spectroscopy (XAS) and transmission Mössbauer spectroscopy (TMS). The Mössbauer spectrum of the mineral, measured at 77 K, was composed of four quadrupole doublets: *D*₁ and *D*₂ due to Fe²⁺ [$\delta \cong 1.26$ mm/s and $\Delta EQ \cong 2.5$ and 2.9 mm/s, respectively] and *D*₃ and *D*₄ due to Fe³⁺ [$\delta \cong 0.46$ mm/s and $\Delta EQ \cong 0.5$ and 1.0 mm/s, respectively]. Finally, synthetic

Mg²⁺-Fe²⁺-Fe³⁺ hydroxycarbonates could be prepared by coprecipitation from Mg and Fe salts and lead to Mössbauer spectra similar to that of the mineral. In particular, the partial substitution of Fe²⁺ by Mg²⁺ proved to be consistent with the existence of the unusual doublet *D*₄.

Ona-Nguema et al. (2002b) obtained Mössbauer spectra measured at 77 K of precipitates that were sampled after 1 and 6 days of bioreduction. The spectra exhibited four quadrupole doublets (Figure 6.6, Panel a and b), the difference concerning only abundance areas. Doublets *D*₁, *D*₂, and *D*₃ are typical of a green rust spectrum at 77 K. *D*₃ is due to high-spin Fe³⁺ in octahedral sites with small values of isomer shift δ and quadrupole splitting Δ , whereas *D*₁ and *D*₂ with larger δ and Δ values are due to high-spin Fe²⁺ in octahedral sites. Doublet *D* _{γ} corresponds to Fe(III) with small δ and Δ values, as small as those found for ferric oxyhydroxide paramagnetic at 77 K, e.g., γ -FeOOH with $\Delta = 0.57$ mm s⁻¹.

Phases present after 6 days of bioreduction were also analyzed by TMS at 12 K (Figure 6.6, Panel c). The spectrum consisted of magnetically split components for γ -FeOOH and paramagnetic doublets for green rusts. Asymmetrically broadened absorption lines were fitted with three sextets; the main outer sextet *S* _{γ} had a field of 449 kOe. Doublet *D* _{γ} (Figure 6.6, Panel b) and sextet *S* _{γ} (Figure 6.6, Panel c) were both due to unreduced lepidocrocite. *D* _{γ} displayed a larger abundance after 1 day than after 6 days (Figure 6.6, Panel a and b) confirming the decrease of γ -FeOOH by reduction. Information is provided from spectra of Figure 6.6, Panel a and b concerning the Fe(II)/Fe(III) ratio inside the green rust. Assuming equal Lamb-Mössbauer factors *f* for all sites, the abundance of each iron site was proportional to the area under the peaks, and the Fe(II)/Fe(III) ratio was equal to ratio $\{D_1 + D_2\}/D_3$. The ratio was 32/33 and 44/41 for the samples obtained after 1 day and 6 days of bioreduction, respectively.

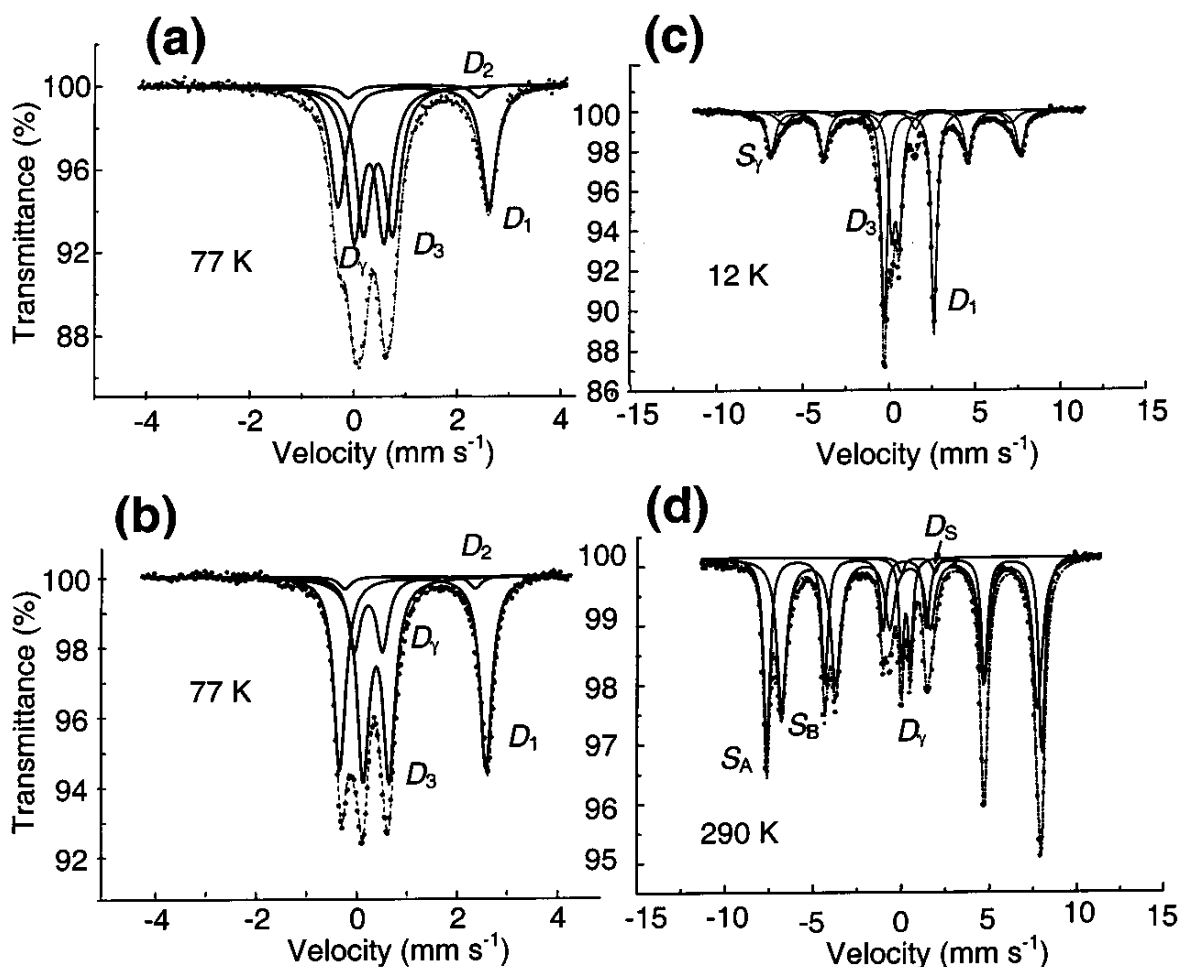


Figure 6.6. Mössbauer spectra of products obtained during reduction of γ -FeOOH (80 mM) with formate (75 mM) in the presence of AQDS (100 μ M) in bacterial cultures (initially 8×10^9 cells mL). Measurements at 77 K after (a) 1 and (b) 6 days of culture. (c) Measurement at 12 K after 6 days of culture. (d) Spectrum measured at 290 K of the products obtained by bioreduction of lepidocrocite during 30 h and after freezing (250 K) and thawing (295 K) of the mixture. (•), experimental curves; (---), global computed curves; —, elementary components (From Ona-Nguema et al., 2002b).

The high susceptibility towards oxidation is believed to be the major obstacle for the identification of green rust, and various procedures have been designed and demonstrated to stabilize synthetically prepared green rust at room temperature (Taylor, 1982; Hansen, 1989). Keeping the green rust at temperatures much below room temperature also inhibited the oxidation and permitted Mössbauer spectra to be obtained at these temperatures (Murad & Taylor, 1984, 1986; Cuttler et al., 1990).

Koch and Mørup (1991) reported the Mössbauer spectra of the greenish colored core of an ochre sludge aggregate (before and after partial oxidation) indicating the presence of green rust formed in a natural soil-like environment. Limitations of this technique include interference from other soil components and the low concentrations of green rust in samples. Samples from other natural environments containing green rust, may, for example, also contain ferrous layer-silicates that may have components with the same absorption lines and

that oxidize relatively easily. The presence of such components makes identification of green rust very difficult. However, in contrast to the ferric oxides, which are the final oxidation products of green rusts, most ferric components in layer-silicates may be expected to remain paramagnetic at temperatures above 12 K.

Another important factor facilitating detection of green rust in the ochre sludge aggregate was its relatively high concentration in the sample (Koch and Mørup, 1991). From the 80 K spectrum of the green core they estimated that Fe^{2+} amounts to ~6% of the total iron, and assuming a Fe^{2+} to Fe^{3+} ratio of 1.5 in the green rust, it was estimated that ~10% of the Fe in the sample is present in the green rust. The morphology of the green core, the sharp color transition, and the absence of Fe^{2+} in the freshly precipitated ochre indicate that the anaerobic transformation of organic matter plays a major role in the reduction of Fe^{3+} compounds necessary for the formation of green rust.

Feder et al. (2005) used a miniaturized Mössbauer spectrometer, adapted to the Earth's conditions from the instrument developed for Mars space missions, to study in situ variations of iron minerals in a gleysol. Mössbauer spectra were obtained over a depth interval from 15 to 106 cm. Measurements were repeated at the same depth at different times to follow mineralogical transformations over time. X-ray diffraction (XRD) and selective extraction techniques were performed on soil samples from the gleysol. The level of the water table was measured and the composition of the soil solution was monitored continuously in situ with an automatic multi-parameter probe.

All the Mössbauer spectra obtained are characteristic of the Fe(II)-Fe(III) green rust–fougerite, a natural mineral of the meixnerite group. The structural formula of this group is: $[\text{Fe}_{1-x}^{\text{II}} \text{Mg}_y \text{Fe}_x^{\text{III}} (\text{OH})_{2+2y}]^{x+} [xA \bullet m\text{H}_2\text{O}]^{x-}$, where x is the ratio $\text{Fe}^{3+}/\text{Fe}_{\text{tot}}$ and A is the intercalated anion. No other iron phases were detected from the

Mössbauer spectra or by XRD. About 90% of total iron was extractable by dithionite-citrate-bicarbonate, and 60% by citrate bicarbonate. In the horizons showing oximorphic properties that were in the upper part of the gleysol, the x ratio in fougerite, as deduced from Mössbauer spectra, was approximately 2/3. In the deepest horizons that show reductomorphic properties, the x ratio was only 1/3. Rapid mineralogical transformations were observed at well-defined points in the soil profile, as evidenced by variations in the x observed when Mössbauer spectra were acquired at different times at the same depth.

Mössbauer spectroscopy can provide information on the Fe bonding environment and the Fe(II)/Fe(III) ratio; however, the spectra are not unique for green rust. Common soil minerals such as chlorite and several Fe-bearing clays generate Mössbauer parameters at temperatures around 15 °C (Ballet et al., 1985; Feder et al., 2005) that are very similar to those of green rust (Gancedo et al., 1976; Cuttler et al., 1990). Definitive identification cannot be made by Mössbauer spectroscopy alone.

Analysis of samples by Mössbauer spectroscopy is commercially available from university laboratories. Billing is often on a per hour basis instead of a per sample basis. Fees in the range of \$500 to \$1000 per sample are typical.

6.3.2 Characterization of Green Rust by X-ray Adsorption Near Edge Spectroscopy (XANES)

X-ray adsorption near edge spectroscopy (XANES) is well-suited to identifying different oxidation states of an element. Because of the rich fine structure in the L-edge transition metal spectrum originating in crystal-field splitting multiple effects, the distribution of oxidation states in an inhomogeneous sample can be distinguished in a single spectrum. Two different methods are available for measuring the XANES; a total-electron yield method which detects the composition of the “near-surface” region, and a transmission method which

averages over the composition of the bulk of a thin section of material. Both methods lend themselves to spectroscopic imaging, using X-ray photoelectron emission microscopy (XPEEM) for near-surface spectro-microscopy, and scanning transmission x-ray microscopy (STXM) for the bulk measurements.

Kneedler et al. (1997) used a BL-7 Spectro-Microscopy Facility STXM and photoemission apparatus in their work. To produce green rust, a reaction was initiated between goethite (α -FeOOH) and a solution of FeCl₂. By halting the reaction prematurely, precipitates of green rust were obtained. After drying, the precipitates were mounted on a sample puck. Powders of two reference compounds were also mounted on the puck, FeCl₂ (Fe(II)) and goethite (Fe(III)) before insertion into an ultra-high vacuum chamber on the BL-7 instrument. To prevent contamination of the green rust sample, all stages of preparation and introduction into the analysis equipment were performed anaerobically, using an oxygen-free glove box and a sealed transport unit. To obtain XANES spectra for each specimen, the sample current to ground was measured as a function of incident photon energy through the Fe LII, III adsorption edge.

Figure 6.7 shows the XANES spectra for green rusts and two reference compounds. The distinction between Fe(II) and Fe(III) oxidation states is obvious from a comparison of the two reference compounds FeCl₂ and goethite (top and bottom, respectively). The green rust sample (second from top) has a distinct signature, which resembles most closely the Fe(II) spectrum, but contains a Fe(III) component; the characteristic peak of the Fe(III) signature is seen as a shoulder to the right of the main peak. Thus, the green rust can be regarded to first approximation as a superposition of Fe(II) and Fe(III) character. To establish the effect of oxygen contamination, the green rust was later exposed to air for 50 minutes, and reintroduced for a final XANES spectrum (third from top). While there is still a mixed Fe(II)/Fe(III) character

evident in the spectrum, the Fe(III) component now dominates, indicating a conversion of iron at the Fe(II) oxidation state to Fe(III).

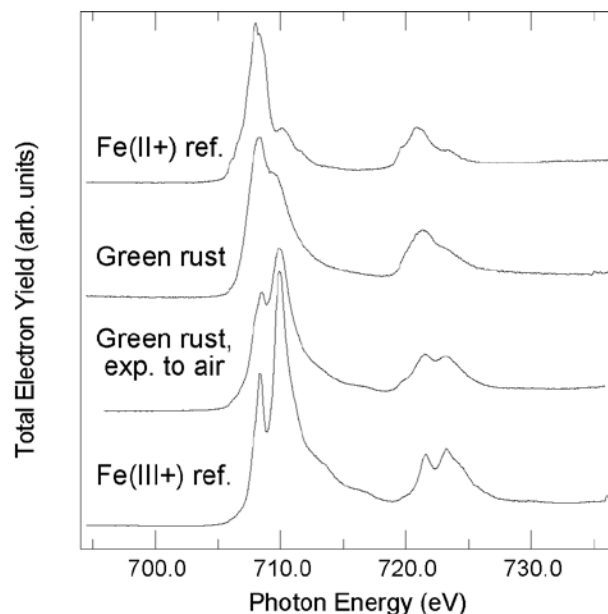


Figure 6.7. Total electron yield XANES measurements of the Fe-LII, III absorption edges for green rust and reference samples FeCl₂ (II+) and goethite (III+). Spectra are normalized to constant background increase through the edges (From Kneedler et al., 1997).

Refaat et al. (2001) extracted a green rust mineral from hydromorphic soils in Fougères (France) and characterized it by X-ray absorption spectroscopy (XAS) and transmission Mössbauer spectroscopy (TMS). The XAS spectrum at the Fe K absorption edge of this mineral proved to be very similar to that of synthetic green rusts. However, the radial distribution function obtained for the green rust mineral proved to be intermediate between those of carbonate green rust and pyroaurite, that is between the Fe²⁺-Fe³⁺ and Mg²⁺-Fe³⁺ hydroxycarbonates. Consequently, a partial substitution of Fe²⁺ by Mg²⁺ occurs, leading to the general formula of [Fe_{(1-x)}²⁺Mg_{y}}²⁺Fe_{x}}³⁺(OH)_{(2+2y)]^{x+} [x/n Aⁿ⁻ • m H₂O]^{x-} where Aⁿ⁻ is the interlayer anion. The Mössbauer spectrum of the green rust mineral, measured at 77 K, was composed of four quadrupole doublets: D₁ and D₂ due to Fe²⁺ [$\delta \approx 1.26$ mm/s and}}

$\Delta E_Q \approx 2.5$ and 2.9 mm/s, respectively] and D_3 and D_4 due to Fe^{3+} [$\delta \approx 0.46$ mm/s and $\Delta E_Q \approx 0.5$ and 1.0 mm/s, respectively]. Finally, synthetic Mg^{2+} - Fe^{2+} - Fe^{3+} hydroxycarbonates could be prepared by coprecipitation from Mg and Fe salts which produced Mössbauer spectra similar to that of the mineral. In particular, the partial substitution of Fe^{2+} by Mg^{2+} proved to be consistent with the existence of the unusual doublet D_4 .

A variety of analytical instruments is usually required to study and identify green rusts. Suzuki et al. (2008) used XANES, the extended X-ray absorption fine structure (EXAFS) and XRD measurements to characterize the effect of the addition of copper sulfate ions on the chemical state and local structure of sulfate green rust. The Fe K edge XANES spectra showed that Fe(II) in green rust was partially oxidized by the addition of the copper sulfate solution. The Cu K edge XANES spectra showed that the copper sulfate ions in the green rust suspension were reduced to zerovalent copper. Radial structural functions indicated that the green rust was composed of edge sharing FeO_6 octahedral units, and that the structure was changed by the oxidation of Fe(II). In addition, it was found that the green rust was partially oxidized to α - FeOOH by the addition of copper ions.

A limitation of the XANES technique is that the XAS spectra of various green rusts proved to be independent of the interlayer anion, and the nature of the anions present in the mineral green rust could not be determined by the XANES method. XAS analyses are conducted in national labs and are not available in commercial labs.

6.4 Methods to Estimate the Specific Surface Area of Minerals

Abiotic degradation of organic compounds on reactive minerals is a heterogeneous reaction. As a consequence, the rate of reaction is strongly influenced by the surface area of the mineral presented to the organic compound. Finely divided minerals with high specific surface area will be more reactive. As a practical matter, information

on the specific surface area is rarely available for specific minerals in aquifer sediments. When this information is available, it was obtained at considerable cost using specialized equipment.

6.4.1 Surface Area from Peak Broadening during X-ray Diffraction

Laboratory studies of chemically synthesized reactive minerals usually report the specific surface area of the mineral preparation as determined by Brunauer-Emmett Teller (BET) analysis. This approach determines a sorption isotherm for nitrogen gas, and thus measures the entire surface in a sample, regardless of its mineralogical composition. This approach is not applicable for reactive minerals that are present as a minor component of sediments.

If magnetite is separated and enriched from sediment by magnetic separation, it may be possible to estimate magnetite particle size from the broadening of characteristic peaks during XRD analysis, as was done by Vikesland et al. (2007) and Ferrey et al. (2004).

6.4.2 Surface Area from Electron Microscopy

If the magnetite is separated and enriched, it may also be possible to estimate particle size distribution using electron microscopy, as was done by Vikesland et al. (2007) and Ferrey et al. (2004). He et al. (2008) used Electron Microscopy to estimate the particle size distribution of pyrite and FeS in complex natural materials. The dimensions and geometry of the particles as revealed from electron microscopy are used to calculate the ratio of surface area to volume (m^2/m^3) for typical particles of the reactive mineral. Then the concentration of the mineral in the sample (g/g) is determined by XRD or chemical extraction methods, or from magnetic susceptibility. Then the specific surface area for the mineral in the bulk sediment (m^2/g) is calculated by multiplying the concentration of the mineral in the sediment by the ratio of surface area to volume, then dividing by the bulk density of the mineral (g/m^3).

Jeong et al. (2008) used electron microscopy to characterize the specific surface area of synthetic mackinawite, and compared the specific surface area as estimated from crystal size and shape to surface area as estimated by peak broadening during XRD analysis, and a method based on the weight associated with a mono-layer of ethylene glycol monoethyl ether. The method based on electron microscopy estimated lower values for specific surface, probably because of aggregation of the crystals of mackinawite.

6.4.3 Characterization of Green Rusts by Scanning/Transmission Electron Microscopy

Both scanning electron microscopy (SEM) and transmission electron microscopy (TEM) have been used to help identify green rusts. The SEM image of a naturally occurring green rust (fougerite) sample showed hexagonal crystals about 0.5 μm size (Trolard et al., 2007). The SEM image of synthetic carbonate green rust showed a particle size range from 0.1 to 0.3 μm (Su and Wilkin, 2005). Ona-Nguema et al. (2002b) showed that after incubation of lepidocrocite in an iron reducing bacterial culture for 6 days, the TEM image of the particles (Figure 6.8) showed large hexagonal crystals of carbonate green rust, measuring about 10 μm . The electron diffraction pattern of [001] zone (caption to Figure 6.8), indexed in the hexagonal representation of $R3m$ space group, yielded the same parameter a as that obtained by XRD.

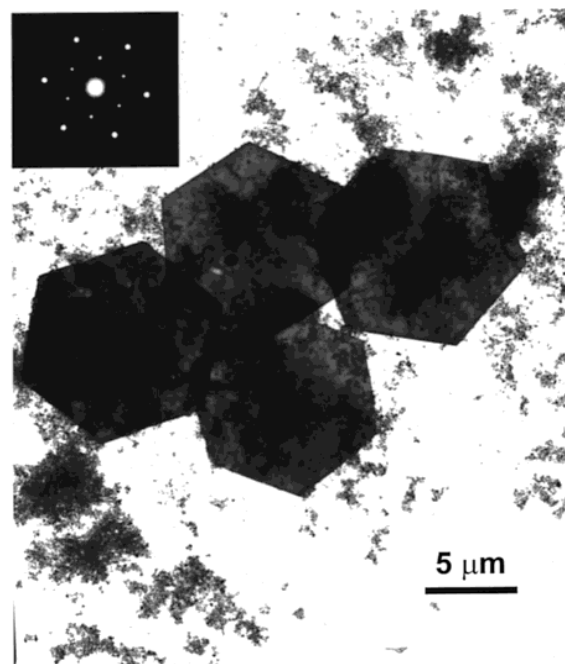


Figure 6.8. TEM image and corresponding electron diffraction pattern of carbonate green rust hexagonal crystals mixed with a minor fine-grained phase ($\gamma\text{-FeOOH}$) obtained after 6 days of bacterial reduction of lepidocrocite (initially 80 mM $\gamma\text{-FeOOH}$, 75 mM formate, and 100 μM AQDS). Electron diffraction pattern along [001] zone axis (From Ona-Nguema et al., 2002b).

The limitation of microscopy in detecting green rusts is that the hexagonal morphology is not unique to green rusts; many clay-sized minerals show similar hexagonal features. Thus, caution is needed in image interpretation. SEM and TEM analyses can be performed via commercial labs; however, the analysts should be well familiar with the nature of the samples because the morphology of crystals can change when the samples are prepared for examination. Imaging of samples by SEM and TEM is commercially available from university laboratories. Billing is often on a per hour basis instead of a per sample basis. Fees in the range of \$500 to \$1000 per sample are typical.

6.5 Collection and Handling of Samples

Because many iron and sulfur minerals are sensitive to oxidation, extreme caution should be taken in handling these samples to ensure that they reflect the actual conditions in contaminated subsurface environments. Upon exposure to air, iron(II) monosulfides, as measured by acid volatile sulfide (AVS), are destroyed by chemical oxidation. When this happens, the concentration of AVS that is determined in the sample can grossly underestimate the true concentration of AVS in the material in the environment. The process of oxidation begins when the sediments are brought up from depth during sampling. Because the process continues during handling, storage, and analysis, it is crucial for the accurate measurement of AVS in anoxic sediment to use techniques for sampling, handling and analysis that minimize the effects of oxidation (Lasorsa and Casas 1996).

Duan et al. (1997) found that AVS in their samples was largely oxidized to the level of elemental sulfur unless they protected their samples by in situ treatment with zinc acetate. However, Lasorsa and Casas (1996) used zinc acetate for sample preservation, and found it to be ineffective.

Several studies (Di Toro et al. 1990; Lasorsa and Casas 1996; Ulrich et al. 1997) show that sulfide levels are best maintained when samples are handled under a nitrogen atmosphere, stored at 4 °C or frozen at -20 °C and analyzed within 2 weeks of collection. When sampling conditions make it impossible to handle the samples under an inert atmosphere, it is recommended that the samples be handled as quickly as possible and then frozen until analysis within 2 weeks of collection. Wilkin and Bischoff (2006) found that freezing sediment samples in the field immediately after collection, shipping the samples frozen on dry ice, and thawing and processing the samples in an anaerobic glove box protected reduced iron and arsenic species in the sample from oxidation. The

process of collecting, storing, and handling materials prior to characterization is critical. Minerals containing ferrous iron and sulfide are typically sensitive to air exposure. Freezing of materials and storage under oxygen-free conditions will generally minimize the oxidation of redox-sensitive minerals (Wilkin, 2006). Core samples should be frozen with liquid nitrogen or dry ice in the field immediately after they are acquired. In some cases, it is possible to freeze the sample in-situ with liquid nitrogen, and then retrieve the sample in the frozen state (He et al. 2008). Samples should be kept frozen during shipment and storage, and should be thawed for analysis under an anaerobic atmosphere.

Size separation and magnetic separation can be particularly useful to isolate reactive minerals in aquifer materials; however, it must be emphasized that fractionation procedures should be carried out under an anaerobic atmosphere to prevent oxidation.

Recommendations for Future Research

We offer a few specific suggestions and recommendations for future research.

7.1 Further Explore the Role of Phyllosilicate Clays

Despite promising laboratory experiments, we are not aware of any field work that has attempted to associate removal of PCE, TCE, *cis*-DCE, or vinyl chloride in ground water to reaction of these contaminants with phyllosilicate clays. A good place to start would be contamination in aquifers containing glauconitic clays (green-sand) as described in Brown et al. (2007).

7.2 Reexamine the Role of Pyrite

Pyrite as it develops in anaerobic ground water aquifers may be more reactive than is currently acknowledged in conventional wisdom. The available laboratory work on reactions with pyrite was done with specimens of hydrothermal pyrite that was ground to an appropriate particle size, instead of using biogenic pyrite. Biogenic pyrite that accumulates in contaminated aquifers has a complex crystal shape (framboids, see He et al., 2008) that may have a greater specific surface area, or present a more reactive surface, than the pyrite used in laboratory experiments.

7.3 Determine if Geochemical Models Can Be a Useful Surrogate to Predict the Rates of Abiotic Degradation at Field Scale

The acquisition of aquifer material and characterization of the material for reactive minerals can be expensive and time consuming. It may be possible to empirically associate rate constants for abiotic degradation in field scale plumes to hydrologic parameters of the aquifer and geochemical parameters of the ground water. This could be done by characterizing field scale plumes to extract a rate constant

for abiotic degradation, then using statistical methods to attempt to correlate the field scale rate to pertinent geochemical parameters.

7.4 Use Geochemical Models to Improve Estimates of Degradation on Mineral Surfaces

At the present state of practice, geochemical models are used to predict the mineral phases that might occur in contact with ground water, but are not used to refine the estimates of rate of reaction on the surfaces of mineral phase that are recognized and determined by chemical extraction techniques, or XRD, or magnetic susceptibility. It may be possible to refine an estimate of the field scale rate degradation by assigning a rate constant to an important mineral phase that is appropriate for the particular geochemical environment in that ground water under consideration.

7.5 Characterize Isotopic Fractionation of *cis*-DCE and Vinyl Chloride on Reactive Minerals

In many chlorinated solvent plumes, there is evidence of natural anaerobic biodegradation of PCE and TCE based on accumulation of *cis*-DCE; however, vinyl chloride, the expected transformation product of *cis*-DCE, does not accumulate to an appreciable extent. In the past, this has been interpreted as a failure of *cis*-DCE to further degrade (*cis* stall) even though transport and fate models of the evolution of the plume indicate that a sink for *cis*-DCE is necessary to model the disposition of *cis*-DCE in the plume. There is increasing success in using stable isotopes to explain the behavior of *cis*-DCE and vinyl chloride in ground water. Work is needed to determine the carbon isotopic enrichment factor for degradation of *cis*-DCE on iron(II) mono-

sulfides, and enrichment factors of all the chlorinated alkenes on phyllosilicate clays.

7.6 Characterize the Role of Manganese Oxides

Manganese oxides can be an important component of aquifer matrix material. A variety of organic compounds have been shown to react with manganese oxide (MnO_2). Cheney et al. (1998) reported a rapid reaction of atrazine with synthetic δ - MnO_2 to produce N-dealkylated forms of atrazine. The rate of dealkylation was rapid compared to rates of biological degradation of atrazine. Barrett and McBride (2005) showed that glyphosate and its degradation product aminomethylphosphonate reacted with birnessite (a manganese oxide mineral) to produce ortho-phosphate. Mihelcic and Luthy (1988) showed that α -naphthol was rapidly degraded by manganese oxide. Ko et al. (2007) found that 4-chlorophenol degraded on manganese oxide. The rate of degradation was at a maximum at pH near the zero point of charge for the manganese dioxide (pH 4 to 5). Petrie et al. (1995) showed that addition of manganese oxide to soil poisoned with mercuric chloride and sodium azide showed significant reductions in the concentration of pentachlorophenol compared to poisoned soil without addition of manganese oxide.

Despite literature that documents rapid reaction of chlorinated aromatic organic compounds with manganese oxide, to our knowledge, nothing has been published concerning the rate of abiotic degradation of chlorinated alkenes or alkanes on manganese oxides.

- Allen, H.E., G. Fu, and B. Deng. Analysis of acid-volatile sulfide (AVS) and simultaneously extracted metals (SEM) for estimation of potential toxicity in sediments. *Environmental Toxicology Chemistry* 12: 1441-1453 (1993).
- Amonette, J.E. Methods for determination of mineralogy and environmental availability. In *Soil Mineralogy with Environmental Applications* (eds. J. Dixon and D. Schulze), Soil Science Society of America, Madison, WI (2002).
- Amonette, J.E., D.J. Workman, D.W. Kennedy, J.S. Fruchter, and Y.A. Gorby. Dechlorination of carbon tetrachloride by Fe(II) associated with goethite. *Environmental Science & Technology* 34: 4606-4613 (2000).
- Arakaki, T. and J.W. Morse. Coprecipitation and adsorption of Mn(II) with mackinawite (FeS) under conditions similar to those found in anoxic sediments. *Geochimica et Cosmochimica Acta* 57: 9-14 (1993).
- Arnold, W.A. and A.L. Roberts. Pathways of chlorinated ethylene and chlorinated acetylene reaction with Zn(0). *Environmental Science & Technology* 32: 3017-3025 (1998).
- Arnold, W.A. and A.L. Roberts. Pathways and kinetics of chlorinated ethylene and chlorinated acetylene reaction with Fe(0) particles. *Environmental Science & Technology* 34: 1794-1805 (2000).
- Assaf-Anid, N. and K.Y. Lin. Carbon tetrachloride reduction by Fe²⁺, S²⁻, and FeS with vitamin B₁₂ as organic amendment. *Journal of Environmental Engineering* 128: 94-99 (2002).
- Ayala-Luis, K.B., C.B. Koch, and H.C.B. Hansen. The standard Gibbs energy of formation of Fe(II)Fe(III) hydroxide sulfate green rust. *Clays and Clay Minerals* 56: 633-644 (2008).
- Ballet, O., J.M.D. Coey, K.J. Burke. Magnetic properties of sheet silicates; 2:1:1 layer minerals. *Physics and Chemistry of Minerals* 12: 370-378 (1985).
- Barbash, J.E. and M. Reinhard. Abiotic dehalogenation of 1,2-dichloroethane and 1,2-dibromoethane in aqueous solution containing hydrogen sulfide. *Environmental Science & Technology* 23: 1349-1358 (1989).
- Barrett, K.A. and M.B. McBride. Oxidative degradation of glyphosate and aminomethylphosphonate by manganese oxide. *Environmental Science & Technology* 39: 9223-9228 (2005).
- Bearcock, J.M., W.T. Perkins, E. Dinelli, and S.C. Wade. Fe(II)/Fe(III) 'green rust' developed within ochreous coal mine drainage sediment in South Wales, UK. *Mineralogical Magazine* 70: 731-741 (2006).
- Bebie, J., M.A.A. Schoonen, M. Fuhrmann and D.R. Strongin. Surface charge development on transition metal sulfides: An electrokinetic study. *Geochimica et Cosmochimica Acta* 62: 633-642 (1998).
- Behrends, T. and P. Van Cappellen. Transformation of hematite into magnetite during dissimilatory iron reduction – conditions and mechanisms. *Geomicrobiology Journal* 24: 403-416 (2007).
- Benner, S.G., D.W. Blowes, W.D. Gould, R.B. Herbert, Jr., and C.J. Ptacek. Geochemistry of a permeable reactive barrier for metals

- and acid mine drainage. *Environmental Science & Technology* 33: 2793-2799 (1999).
- Benning, L.G., R.T. Wilkin and H.L. Barnes. Reaction pathways in the Fe-S system below 100°C. *Chemical Geology* 167: 25-51 (2000).
- Bernal, J.D., D.R. Dasgupta, and A.L. Mackay. The oxides and hydroxides of iron and their structural interrelationships. *Clay Mineral Bulletin* 4: 15-30 (1959).
- Berner, R.A. Electrode studies of hydrogen sulfide in marine sediments. *Geochimica et Cosmochimica Acta* 27: 563-575 (1963).
- Berner, R.A. Iron sulfides in Pleistocene deep Black Sea sediments and their paleo-oceanographic significance. In, *The Black Sea—Geology, Chemistry and Biology*, eds. E. T. Degens, D. A. Ross. Am. Assoc. Pet. Geol., Mem., 20: 524-531 (1974).
- Berner, R.A. Sedimentary pyrite formation. *American Journal of Science* 268: 1-23 (1970).
- Billon, G., B. Ouddane, J. Laureyns and A. Boughriet. Analytical and thermodynamic approaches to the mineralogical and compositional studies on anoxic sediments. *Journal of Soils and Sediments* 3:180-187 (2003).
- Bloom, Y., R. Aravena, D. Hunkeler, E. Edwards and S.K. Frape. Carbon isotope fractionation during microbial dechlorination of trichloroethene, *cis*-1,2-dichloroethene, and vinyl chloride: Implications for assessment of natural attenuation. *Environmental Science & Technology* 34: 2768-2772 (2000).
- Bocher, F., A. Géhin, C. Ruby, J. Ghanbaja, M. Abdelmoula, J.-M.R. Génin. Coprecipitation of Fe(II-III) hydroxycarbonate green rust stabilised by phosphate adsorption. *Solid State Sciences* 6: 117-124 (2004).
- Bond, D.L. and S. Fendorf. Kinetics and structural constraints of chromate reduction by green rusts. *Environmental Science & Technology* 37: 2750-2757 (2003).
- Bourrié, G., F. Trolard, J. Génin, A. Jaffrezic, V. Maître and M. Abdelmoula. Iron control by equilibria between hydroxy-green rusts and solutions in hydromorphic soils. *Geochimica Cosmochimica Acta* 63: 3417-3427 (1999).
- Boursiquot, S., M. Mullet, M. Abdelmoula, J.-M. Génin and J.-J. Ehrhardt. The dry oxidation of tetragonal FeS_{1.4} mackinawite. *Physics and Chemistry of Minerals* 28: 600-611 (2001).
- Bouwer, E.J. and P.L. McCarty. Ethylene dibromide transformation under methanogenic conditions. *Applied and Environmental Microbiology* 50: 527-528 (1985).
- Bradley, P.M. History and ecology of chloroethene biodegradation: a review. *Bioremediation Journal* 7: 81-109 (2003).
- Brown, R.A., J.T. Wilson and M. Ferrey. Monitored natural attenuation forum: the case for abiotic MNA. *Remediation Journal* 17: 127-137 (2007).
- Burris, D.R., C.A. Delcomyn, M.H. Smith and A.L. Roberts. Reductive dechlorination of tetrachloroethylene and trichloroethylene catalyzed by vitamin B₁₂ in homogeneous and heterogeneous systems. *Environmental Science & Technology* 30: 3047-3052 (1996).
- Burton, E.D., L.A. Sullivan, R.T. Bush, S.G. Johnston and A.F. Keene. A simple and inexpensive chromium-reducible sulfur method for acid-sulfate soils. *Applied Geochemistry* 23: 2759-2766 (2008).
- Butler, E.C. and K.F. Hayes. Effects of solution composition and pH on the reductive dechlorination of hexachloroethane by iron sulfide. *Environmental Science & Technology* 32: 1276-1284 (1998).
- Butler, E.C. and K.F. Hayes. Factors influencing rates and products in the transformation

- of trichloroethylene by iron sulfide and iron metal. *Environmental Science & Technology* 35: 3884-3891 (2001).
- Butler, E.C. and K.F. Hayes. Kinetics of the transformation of halogenated aliphatic compounds by iron sulfide. *Environmental Science & Technology* 34: 422-429 (2000).
- Butler, E.C. and K.F. Hayes. Kinetics of the transformation of trichloroethylene and tetrachloroethylene by iron sulfide. *Environmental Science & Technology* 33: 2021-2027 (1999).
- Butler, E.C. and K.F. Hayes. Reductive Transformation of Halogenated Aliphatic Pollutants by Iron Sulfide. Chapter 6, In: *Chemicals in the Environment: Fate, Impacts, and Remediation*, eds., R. L. Lipnick, R. P. Mason, M. L. Phillips, and C. U. Pittman, American Chemical Society Symposium Series No. 806, Washington, DC (2002).
- Butler, I.B. and D. Rickard. Framboidal pyrite formation via the oxidation of iron(II) monosulfide by hydrogen sulfide. *Geochimica et Cosmochimica Acta* 64: 2665-2672 (2000).
- Campbell, T.J., D.R. Burris, A.L. Roberts and J.R. Wells. Trichloroethylene and tetrachloroethylene reduction in a metallic iron-water-vapor batch system. *Environmental Toxicology and Chemistry* 16: 625-630 (1997).
- Canfield, D.E. and R.A. Berner. Dissolution and pyritization of magnetite in anoxic marine sediments. *Geochimica et Cosmochimica Acta* 51: 645-659 (1987).
- Canfield, D.E., R. Raiswell, J.T. Westrich, C.M. Reaves and R. A. Berner. The use of chromium reduction in the analysis of reduced inorganic sulfur in sediments and shales. *Chemical Geology* 54: 149-155 (1986).
- Casas, A. and E.A. Crecelius. Relationship between acid volatile sulfide and the toxicity of zinc, lead and copper in marine sediments. *Environmental Toxicology and Chemistry* 13: 529-536 (1994).
- Cervini-Silva, J., R.A. Larson, J. Wu and J.W. Stucki. Transformation of chlorinated aliphatic compounds by ferruginous smectite. *Environmental Science & Technology* 35: 805-809 (2001).
- Charlet, L., D. Bosbach and T. Peretyashko. Natural attenuation of TCE, As, Hg linked to heterogeneous oxidation of Fe(II): an AFM study. *Chemical Geology* 190: 303-319 (2002).
- Cheney, M.A., J.Y. Shin, D.E. Crowley, S. Alvey, N. Malengreau and G. Sposito. Atrazine dealkylation on a manganese oxide surface. *Colloids and Surfaces A: Physicochemical and Engineering Aspects* 137: 267-273 (1998).
- Choi, J.Y. Degradation of perchloroethylene and nitrate by high-activity modified green rusts. Doctoral Dissertation. 150 pp. Texas A&M University (2005).
- Choi, J., K. Choi and W. Lee. Effects of transition metal and sulfide on the reductive dechlorination of carbon tetrachloride and 1,1,1-trichloroethane by FeS. *Journal of Hazardous Materials* 162: 1151-1158 (2009).
- Choi, J., and W. Lee. Enhanced degradation of tetrachloroethylene by green rusts with platinum. *Environmental Science & Technology* 42: 3356-3362 (2008).
- Christiansen, B.C. and S.L.S. Stipp. Structure and reactivity of green rust. Geophysical Research Abstracts, Vol. 5, 00644, European Geophysical Society (2003).
- Christiansen, B.C., T. Balic-Zunic, K. Dideriksen, and S.L.S. Stipp. Identification of green rust in groundwater. *Environmental*

- Science & Technology* 43: 3436–3441 (2009).
- Chun, C.L., R.M. Hozalski, and W.A. Arnold. Degradation of disinfection byproducts by carbonate green rust. *Environmental Science & Technology* 41: 1615–1621 (2007).
- Clesceri, L.S., A.E. Greenberg and A.D. Eaton (editors). Standard methods for the examination of water and wastewater, American Public Health Association, American Water Works Association, Water Environment Federation, 20th edition, Washington DC, USA (1999).
- Cohn, C.A., S. Mueller, E. Wimmer, N. Leifer, S. Greenbaum, D.R. Strongin and M.A.A. Schoonen. Pyrite induced hydroxyl radical formation and its effect on nucleic acids. *Geochemical Transactions* 7: 3. Published online 2006 April 4. doi: 10.1186/1467-4866-7-3 (2006).
- Conway, B.E., J.C.H. Ku and F.C. Ho. The electrochemical surface reactivity of iron sulfide, FeS₂. *Journal of Colloid Interface Science* 75: 357-372 (1980).
- Cornwell, J.C. and J.W. Morse. The characterization of iron sulfide minerals in anoxic marine sediments. *Marine Chemistry* 22: 193-206 (1987).
- Criddle, C.S. and P.L. McCarty. Electrolytic model system for reductive dehalogenation in aqueous environments. *Environmental Science & Technology* 25: 973-978 (1991).
- Cuttler, A.H., V. Man, T.E. Cranshaw, and G. Longworth. A Mössbauer study of green rust precipitates: I. Preparation from sulphate solutions. *Clay Minerals* 25: 289-301 (1990).
- Danielsen, K., and K.F. Hayes. pH dependence of carbon tetrachloride reductive dechlorination by magnetite. *Environmental Science & Technology* 38: 4745-4752 (2004).
- Darlington, R., L. Lehmicke, R.G. Andrachek and D.L. Freedman. Biotic and abiotic anaerobic transformations of trichloroethene and *cis*-1,2-dichloroethene in fractured sandstone. *Environmental Science & Technology* 42(12): 4323-4330 (2008).
- Dearing, J. *Environmental Magnetic Susceptibility, Using the Bartington MS2 System*. Chi Publishing, Kenilworth, England ISBN 0 9523409 0 9 (1999).
- Devlin, J.F. and D. Müller. Field and laboratory studies of carbon tetrachloride transformation in a sandy aquifer under sulfate reducing conditions. *Environmental Science & Technology* 33: 1021-1027 (1999).
- Di Toro, D.M., J.D. Mahony, D.J. Hansen, K.J. Scott, M.B. Hicks, S M. Mayr and M.S. Redmond. Toxicity of cadmium in sediments: the role of acid volatile sulfide. *Environmental Toxicology and Chemistry* 9: 1487-1502 (1990).
- Doong, R.-A. and S.-C.Wu. Reductive dechlorination of chlorinated hydrocarbons in aqueous solutions containing ferrous and sulfide ions. *Chemosphere* 24: 1063-1075 (1992).
- dos Santos Afonso, M. and W. Stumm. Reductive dissolution of iron (III) (hydr) oxides by hydrogen sulfide. *Langmuir* 8: 1671-1675 (1992).
- Drissi, S.H., P. Refait, M. Abdelmoula and J.M.R. Génin. The preparation and thermodynamic properties of Fe(II)-Fe(III) hydroxide-carbonate (green rust 1); Pourbaix diagram of iron in carbonate-containing aqueous media. *Corrosion Science* 37: 2025-2041 (1995).
- Duan, W.-M., M.L. Coleman, and K. Pye. Determination of reduced sulphur species in sediments-an evaluation and modified technique. *Chemical Geology* 141: 185-194 (1997).

- Elsner, M., S.B. Haderlein, T. Kellerhals, S. Luzi, L. Zwank, W. Angst and R.P. Schwarzenbach. Mechanisms and products of surface-mediated reductive dehalogenation of carbon tetrachloride by Fe(II) on goethite. *Environmental Science & Technology* 38: 2058-2066 (2004a).
- Elsner, M., R.P. Schwarzenbach, and S.B. Haderlein. Reactivity of Fe(II)-bearing minerals toward reductive transformation of organic contaminants. *Environmental Science & Technology* 38: 799-807 (2004b).
- Elsner, M., L. Zwank, D. Hunkeler and R.P. Schwarzenbach. A new concept linking observable stable isotope fractionation to transformation pathways of organic pollutants. *Environmental Science & Technology* 39: 6896-6916 (2005).
- Erbs, M., H.C.B. Hansen and C.E. Olsen. Reductive dechlorination of carbon tetrachloride using iron(II) iron(III) hydroxide sulfate (green rust). *Environmental Science & Technology* 33: 307-311 (1999).
- Feder, F., F. Trolard, G. Klingelhöfer, and G. Bourrié. In situ Mössbauer spectroscopy: Evidence for green rust (fougerite) in a gleysol and its mineralogical transformations with time and depth. *Geochimica et Cosmochimica Acta* 69: 4463-4483 (2005).
- Fennelly, J.P. and A.L. Roberts. Reaction of 1,1,1-trichloroethane with zero-valent metals and bimetallic reductants. *Environmental Science & Technology* 32: 1980-1988 (1998).
- Ferrey, M.L., R.T. Wilkin, R.G. Ford and J.T. Wilson. Non-biological removal of *cis*-dichloroethylene and 1,1-dichloroethylene in aquifer sediment containing magnetite. *Environmental Science & Technology* 38: 1746-1752 (2004).
- Furukawa, Y., J. Kim, J. Watkins and R.T. Wilkin. Formation of ferrihydrite and associated iron corrosion products in permeable reactive barriers of zero-valent iron. *Environmental Science & Technology* 36: 5469-5475 (2002).
- Gancedo, J.R., M.L. Martinez and J.M. Oton. Mössbauer spectroscopy study of corrosion products of iron with ammonium nitrate in aqueous solutions. *Journal of Physics Colloquium C6*:297-299 (1976).
- Gander, J.W., G.F. Parkin and M.M. Scherer. Kinetics of 1,1,1-trichloroethane transformation by iron sulfide and a methanogenic consortium. *Environmental Science & Technology* 36: 4540-4546 (2002).
- Génin, J.-M. R., G. Bourrie, F. Trolard, M. Abdelmoula, A. Jaffrezic, P. Refait, V. Maitre, B. Humbert, and A. Herbillon. Thermodynamic equilibria in aqueous suspensions of synthetic and natural Fe(II)-Fe(III) green rusts: occurrences of the mineral in hydromorphic soils. *Environmental Science & Technology* 32: 1058-1068 (1998).
- Génin J.-M.R., P. Refait, and M. Abdelmoula. Green rusts and their relationship to iron corrosion; a Key Role in Microbially Influenced Corrosion. *Hyperfine Interactions* 139: 119-131 (2002).
- Gillham, R.W., and S.F. O'Hannesin. Enhanced degradation of halogenated aliphatics by zero-valent iron. *Ground Water* 32: 958-967 (1994).
- Gregory, K.B., P. Larese-Casanova, G.F. Parkin and M.M. Scherer. Abiotic transformation of hexahydro-1,3,5-trinitro-1,3,5-triazine by FeII bound to magnetite. *Environmental Science & Technology* 38: 1408-1414 (2004).
- Hanoch, R.J., H. Shao and E.C. Butler. Transformation of carbon tetrachloride by bisulfide treated goethite, hematite, magnetite, and kaolinite. *Chemosphere* 63: 323-334 (2006).
- Hansel, C.M., S.G. Benner and S. Fendorf. Competing Fe(II)-induced mineralization

- pathways of ferrihydrite. *Environmental Science & Technology* 39: 7147-7153 (2005).
- Hansen, H.C.B. Composition, stabilization, and light absorption of Fe(II)Fe(III) hydroxycarbonate (green rust). *Clay Minerals* 24: 663-669 (1989).
- Hansen, H.C.B. Environmental chemistry of iron(II)-iron(III) LDHs. In *Layered Double Hydroxides* (ed. V. Rives). pp. 413-434. Nova Science Publisher, Huntington, NY (2001).
- Hansen, H.C.B., S. Guldborg, M. Erbs and C.B. Koch. Kinetics of nitrate reduction by green rusts-effects of interlayer anion and Fe(II):Fe(III) ratio. *Applied Clay Science* 18: 81-91 (2001).
- Hansson, E.B., M.S. Odziemkowski and R.W. Gillham. Influence of Na₂S on the degradation kinetics of CCl₄ in the presence of very pure iron. *Journal of Contaminant Hydrology* 98: 128-134 (2008).
- Hashsham, S.A., R. Scholze and D.L. Freedman. Cobalamin-enhanced anaerobic biotransformation of carbon tetrachloride. *Environmental Science & Technology* 29: 2856-2863 (1995).
- He, Y.T., J.T. Wilson, and R.T. Wilkin. Impact of iron sulfide transformation on trichloroethylene degradation. *Geochimica et Cosmochimica Acta* 74: 2025-2039 (2010).
- He, Y.T., J.T. Wilson and R.T. Wilkin. Transformation of reactive iron minerals in a permeable reactive barrier (biowall) used to treat TCE in groundwater. *Environmental Science & Technology* 42: 6690-6696 (2008).
- Henderson, J.K., D.L. Freedman, R.W. Falta, T. Kuder and J.T. Wilson. Anaerobic biodegradation of ethylene dibromide and 1,2-dichloroethane in the presence of fuel hydrocarbons. *Environmental Science & Technology* 42: 864-870 (2008).
- Henneke, E., G.W. Luther, G.J. de Lange and J. Hoefs. Sulphur speciation in anoxic hypersaline sediments from the eastern Mediterranean Sea. *Geochimica et Cosmochimica Acta* 61: 307-321 (1997).
- Herbert, R.B., S.G. Benner and D.W. Blowes. Solid phase iron-sulfur geochemistry of a reactive barrier for treatment of mine drainage. *Applied Geochemistry* 15: 1331-1343 (2000).
- Herbert, R.B., S.G. Benner, A.R. Pratt and D.W. Blowes. Surface chemistry and morphology of poorly crystalline iron sulfides precipitated in media containing sulfate-reducing bacteria. *Chemical Geology* 144: 87-97 (1998).
- Heron, G., C. Crouzet, A.C. Bourg and T.H. Christensen. Speciation of Fe(II) and Fe(III) in contaminated aquifer sediments using chemical extraction techniques. *Environmental Science & Technology* 28:1698-1705 (1994).
- Horneman, A., A. van Geen, D.V. Kent, P.E. Mathe, Y. Zheng, R.K. Dhar, S. O'Connell, M.A. Hoque, Z. Aziz, Z., M. Shamsudduha, A.A. Seddique and K.M. Ahmed. Decoupling of As and Fe release to Bangladesh groundwater under reducing conditions. Part I: Evidence from sediment profiles. *Geochimica et Cosmochimica Acta*. 68: 3459-3473 (2004).
- Hsieh, Y.P., S.-W. Chung, Y.-J. Tsau and C.-T. Sue. Analysis of sulfides in the presence of ferric minerals by diffusion methods. *Chemical Geology* 182: 195-201 (2002).
- Hunger, S. and L.G. Benning. Greigite: a true intermediate on the polysulfide pathway to pyrite. *Geochemical Transactions* 8: 1-20 (2007).
- Hunkeler, D., R.U. Meckenstock, B. Sherwood Lollar, T.C. Schmidt and J.T. Wilson. *A Guide for Assessing Biodegradation and Source Identification of Organic Ground*

- Water Contaminants using Compound Specific Isotope Analysis (CSIA)*. EPA 600/R-08/148 (2008).
- Hurtgen, M.T., T.W. Lyons, E.D. Ingall and A.M. Cruse. Anomalous enrichments of iron monosulfide in euxinic marine sediments and the role of H₂S in iron sulfide transformations: Examples from Effingham Inlet, Orca basin, and the Black Sea. *American Journal of Science* 299: 556-588 (1999).
- Jeong, H.Y. and K.F. Hayes. Impact of transition metals on reductive dechlorination rate of hexachloroethane by mackinawite. *Environmental Science & Technology* 37: 4650-4655 (2003).
- Jeong, H.Y. and K.F. Hayes. Reductive dechlorination of tetrachloroethylene and trichloroethylene by mackinawite (FeS) in the presence of metals: reaction rates. *Environmental Science & Technology* 41: 6390-6396 (2007).
- Jeong, H.Y., H. Kim and K.F. Hayes. Reductive dechlorination pathways of tetrachloroethylene and trichloroethylene and subsequent transformation of their dechlorination products by mackinawite (FeS) in the presence of metals. *Environmental Science & Technology* 41: 7736-7743 (2007).
- Jeong, H.Y., J.H. Lee and K.F. Hayes. Characterization of synthetic nanocrystalline mackinawite: Crystal structure, particle size, and specific surface area. *Geochimica et Cosmochimica Acta* 72: 493-505 (2008).
- Karim, Z. Formation of ferrihydrite by inhibition of green rust structures in the presence of silicon. *Soil Science Society of America Journal* 50: 247-250 (1986).
- Kennedy, L., J.W. Everett and J. Gonzales. Aqueous and mineral intrinsic bioremediation assessment: natural attenuation. *Journal of Environmental Engineering* 130: 942-950 (2004).
- Kennedy, L.G., J.W. Everett and J. Gonzales. Assessment of biogeochemical natural attenuation and treatment of chlorinated solvents, Altus AFB, Altus, Oklahoma. *Journal of Contaminant Hydrology* 83: 221-236 (2006).
- Kenneke, J.F. and E.J. Webber. Reductive dehalogenation of halomethanes in iron- and sulfate-reducing sediments, 1. Reactivity pattern analysis. *Environmental Science & Technology* 37: 713-720 (2003).
- Klausen, J., S.P. Troeber, S.B. Haderlein and R.P. Schwarzenbach. Reduction of substituted nitrobenzenes by Fe(II) in aqueous mineral suspensions. *Environmental Science & Technology* 29: 2396-2404 (1995).
- Kneedler, E.M., J. Rothe, K.W. Weissmahr, K. Pecher, and B.P. Tonner. Identification of green rust in environmental compounds using XANES of Fe-L_{II, III} Edges. (1997). <http://www.als.lbl.gov/als/compendium/AbstractManager/uploads/Kneedler1.pdf> (accessed September 22, 2009).
- Ko, S.-O., S.-Y. Jun, D.-H. Lee, J. Park and W.-S. Shin. Effects of oxidative coupling reaction of 4-chlorophenol with manganese oxide on the phenanthrene sorption. *Journal of Environmental Science and Health Part A* 42:257-263 (2007).
- Koch, C.B. and S. Mørup. Identification of green rust in an ochre sludge. *Clay Minerals* 26: 577-582 (1991).
- Komadel, P. and J. W. Stucki. Quantitative assay of minerals for Fe²⁺ and Fe³⁺ using 1,10-phenanthroline: III. A rapid photochemical method. *Clays and Clay Minerals* 36: 379-381 (1988).
- Kostka, J.E. and G.W. Luther. Partitioning and speciation of solid phase iron in saltmarsh

- sediments. *Geochimica et Cosmochimica Acta* 58: 1701-1710 (1994).
- Kriegman-King, M. and M. Reinhard. Transformation of carbon tetrachloride by pyrite in aqueous solution. *Environmental Science & Technology* 28: 692-700 (1994).
- Kriegman-King, M.R. and M. Reinhard. Transformation of carbon tetrachloride in the presence of sulfide, biotite, and vermiculite. *Environmental Science & Technology* 26: 2198-2206 (1992).
- Kuder, T., Y. He, J.T. Wilson and R.P. Philp. Reactions of 1,2-dibromoethane in FeS-hydrogen sulfide systems: kinetics and isotope fractionation. *Environmental Science & Technology* (In Prep.).
- Lasorsa, B. and A. Casas. A comparison of sample handling and analytical methods for determination of acid volatile sulfides in sediment. *Marine Chemistry* 52: 211-220 (1996).
- Lee, W. and B. Batchelor. Abiotic reductive dechlorination of chlorinated ethylenes by iron-bearing soil minerals. 1. Pyrite and magnetite. *Environmental Science & Technology* 36: 5147-5154 (2002a).
- Lee, W. and B. Batchelor. Abiotic reductive dechlorination of chlorinated ethylenes by iron-bearing soil minerals. 2. Green rust. *Environmental Science & Technology* 36: 5348-5354 (2002b).
- Lee, W. and B. Batchelor. Abiotic reductive dechlorination of chlorinated ethylenes by iron-bearing phyllosilicates. *Chemosphere* 56: 999-1009 (2004).
- Lee, W. and B. Batchelor. Reductive capacity of natural reductants. *Environmental Science & Technology* 37: 535-541 (2003).
- Lennie, A.R., S.A.T. Redfern, P.E. Champness, C.P. Stoddart, P.F. Schofield and D.J. Vaughan. Transformation of mackinawite to greigite: An in situ X-ray powder diffraction and transmission electron microscope study. *American Mineralogist* 82: 302-309 (1997).
- Lennie, A.R., S.A.T. Redfern, P.F. Schofield and D.J. Vaughan. Synthesis and Rietveld crystal structure refinement of mackinawite, tetragonal FeS. *Mineralogical Magazine* 59: 677-683 (1995).
- Leonard, E.N., V.R. Mattson, D.A. Benoit, R.A. Hoke and G.T. Ankley. Seasonal variation of acid volatile sulfide concentration in sediment cores from three northeastern Minnesota lakes. *Hydrobiologia* 271: 87-95 (1993).
- Leonard, E.N., D.R. Mount and G.T. Ankley. Modification of metal partitioning by supplementing acid volatile sulfide in freshwater sediments. *Environmental Toxicology and Chemistry* 18: 858-864 (1999).
- Liang, X., Y. Dong, T. Kuder, L.R. Krumholz, R.P. Philp and E.C. Butler. Distinguishing abiotic and biotic transformation of tetrachloroethylene and trichloroethylene by stable carbon isotope fractionation. *Environmental Science & Technology* 41: 7094-7100 (2007).
- Liang, X., R.P. Philp, and E.C. Butler. Kinetic and isotope analyses of tetrachloroethylene and trichloroethylene degradation by model Fe(II)-bearing minerals. *Chemosphere* 75: 63-69 (2009).
- Lipczynska-Kochany, E., S. Harms, R. Milburn, G. Sprah and N. Nadarajah. Degradation of carbon tetrachloride in the presence of iron and sulphur containing compounds. *Chemosphere* 29: 1477-1489 (1994).
- Liu, X.M., P. Peng, J.M. Fu and W.L. Huang. Effects of FeS on the transformation kinetics of γ -hexachlorocyclohexane. *Environmental Science & Technology* 37: 1822-1828 (2003).

- Liu, Y., S.A. Majetich, R.D. Tilton, D.S. Sholl and G.V. Lowry. TCE dechlorination rates, pathways, and efficiency of nanoscale iron particles with different properties. *Environmental Science & Technology* 39: 1338-1345 (2005).
- Loyaux-Lawniczak, S., P. Refait, J.-J. Ehrhardt, P. Lecomte, and J.-M. R. Génin. Trapping of Cr by formation of ferrihydrite during the reduction of chromate ions by Fe(II)–Fe(III) hydroxysalt green rusts. *Environmental Science & Technology* 34: 438– 443 (2000).
- Maithreepala, R.A. and R.A. Doong. Enhanced dechlorination of chlorinated methanes and ethenes by chloride green rust in the presence of copper(II). *Environmental Science & Technology* 39: 4082-4090 (2005).
- McCormick, M.L., and P. Adriaens. Carbon tetrachloride transformation on the surface of nanoscale biogenic magnetite particles. *Environmental Science & Technology* 38: 1045-1053 (2004).
- McCormick, M.L., E.J. Bouwer and P. Adriaens. Carbon tetrachloride transformation in a model iron reducing culture: Relative kinetics of biotic and abiotic reactions. *Environmental Science & Technology* 36: 403-410 (2002).
- MDH. *Public Health Assessment Baytown Township Groundwater Contamination Site Washington County, Minnesota*. EPA Facility ID: MND982425209. Prepared by: Minnesota Department of Health under Cooperative Agreement with the Agency for Toxic Substances and Disease Registry (September 14, 2004). <http://www.health.state.mn.us/divs/eh/hazardous/sites/washington/baytown/baytownpha.pdf> (accessed 06-07-2009).
- Mihelcic, J.R. and R.G. Luthy. Degradation of polycyclic aromatic hydrocarbon compounds under various redox conditions in soil-water systems. *Applied and Environmental Microbiology* 54: 1182-1187 (1988).
- Morse, J.W. and J.C. Cornwell. Analysis and distribution of iron sulfide minerals in recent anoxic marine sediments. *Marine Chemistry* 22: 55-69 (1987).
- Morse, J.W. and D. Rickard. Chemical dynamics of sedimentary acid volatile sulfide. *Environmental Science & Technology* 38: 131A-136A (2004).
- Murad, E. and R.M. Taylor. The Mössbauer spectra of hydroxycarbonate green rusts. *Clay Minerals* 19: 77–83 (1984).
- Murad, E. and R.M. Taylor. The oxidation of hydroxycarbonate green rusts. pp. 585-593. In *Industrial Applications of the Mössbauer Effect*, G.J. Long and J.G. Stevens (eds), Plenum Press, New York, NY (1986).
- Myneni, S.C.B., T.K. Tokunaga, and G.E. Brown, Jr. Abiotic selenium redox transformations in the presence of Fe(II,III) oxides. *Science* 278: 1106–1109 (1997).
- Neal, A.L., S. Techkarnjanaruk, A. Dohnalkova, D. McCready, B.M. Peyton and G.G. Geesey. Iron sulfides and sulfur species produced at hematite surfaces in the presence of sulfate-reducing bacteria. *Geochimica et Cosmochimica Acta* 65: 223-235 (2001).
- Neumann, A., T.B. Hofstetter, M. Skarpeli-Liati and R.R. Schwarzenbach. Reduction of polychlorinated ethanes and carbon tetrachloride by structural Fe(II) in smectites. *Environmental Science & Technology* 43: 4082-4089 (2009).
- Neumann, A., T.B. Hofstetter, M. Lüssi, O.A. Cirpka, S. Petit and R.P. Schwarzenbach. Assessing the redox reactivity of structural iron in smectites using nitroaromatic compounds as kinetic probes. *Environmental Science & Technology* 42: 8381-8387 (2008).

- Nooten, T.V., D. Springael and L. Bastiaens. Positive impact of microorganisms on the performance of laboratory-scale permeable reactive iron barriers. *Environmental Science & Technology* 42: 1680-1686 (2008).
- Nzungu, V.A., R.M. Castillo, W.P. Gates and G.L. Mills. Abiotic transformation of perchloroethylene in homogeneous dithionite solution and in suspensions of dithionite-treated clay minerals. *Environmental Science & Technology* 35: 2244-2251 (2001).
- O'Loughlin, E.J. and D.R. Burris. Reduction of halogenated ethanes by green rust. *Environmental Toxicology and Chemistry* 23: 41-48 (2004).
- O'Loughlin, E.J., K.M. Kemner and D.R. Burris. Effects of Ag^I, Au^{III}, and Cu^{II} on the reductive dechlorination of carbon tetrachloride by green rust. *Environmental Science & Technology* 37: 2905-2912 (2003).
- O'Loughlin, E., P. Larese-Casanova, M. Scherer, and R. Cook. Green Rust Formation from the Bioreduction of γ -FeOOH (Lepidocrocite): Comparison of Several Shewanella Species. *Geomicrobiology Journal* 24: 211-230 (2007).
- Oita, I.J. Coulometric determination of sub-part-per-million levels of sulfur in volatile liquids. *Analytical Chemistry* 55: 2434-2436 (1983).
- Ona-Nguema G., M. Abdelmoula, F. Jorand, O. Benali, A. Géhin, J.-C. Block, and J.-M. R. Génin. Iron(II,III) hydroxycarbonate green rust formation and stabilization from lepidocrocite bioreduction. *Environmental Science & Technology* 36: 16-20 (2002b).
- Ona-Nguema G., M. Abdelmoula, F. Jorand, O. Benali, A. Géhin A., J.-C. Block, and J.-M. R. Génin. Microbial reduction of lepidocrocite γ -FeOOH by Shewanella putrefaciens; the formation of green rust. *Hyperfine Interactions* 139: 231-237 (2002a).
- Ona-Nguema, G., C. Carteret, O. Benali, M. Abdelmoula, J.-M.R. Génin, and F. Jorand. Competitive formation of hydroxycarbonate green rust 1 versus hydroxysulphate green rust 2 in Shewanella putrefaciens cultures. *Geomicrobiology Journal* 21: 79-90 (2004).
- Ostwald, J. A note on occurrences of nickeliferous and cupriferous mackinawite. *Mineralogical Magazine* 42: 516-517 (1978).
- Park, S., S. Kim, J. Kim, S. Choi, H.I. Inyang and S. Tokunaga. Particle surface hydrophobicity and the dechlorination of chloro-compounds by iron sulfides. *Water, Air, and Soil Pollution* 6: 97-110 (2006).
- Pecher, K., S.B. Haderlein and R.P. Schwarzenbach. Reduction of polyhalogenated methanes by surface-bound Fe(II) in aqueous suspensions of iron oxides. *Environmental Science & Technology* 36: 1734-1741 (2002).
- Pesch, C.E., D.J. Hansen, W.S. Boothman, W.J. Berry and J.D. Mahony. The role of acid volatile sulfide and interstitial water metal concentrations in determining bioavailability of cadmium and nickel from contaminated sediments to the marine polychaete *Neanthes arenaceodentata*. *Environmental Toxicology and Chemistry* 14: 129-141 (1995).
- Petrie, R.A., J.E. McLean and R.C. Sims. Treatment of pentachlorophenol with manganese oxide addition to biotic and abiotic sediments. *Hazardous Waste & Hazardous Materials* 12: 271-281 (1995).
- Pham, H.T., M. Kitsuneduka, J. Hara, K. Suto and C. Inoue. Trichloroethylene transformation by natural mineral pyrite: The deciding role of oxygen. *Environmental Science & Technology* 42: 7470-7475 (2008).

- Phillips, D.H., B. Gu, D.B. Watson, Y. Roh, L. Liang and S.Y. Lee. Performance evaluation of a zerovalent iron reactive barrier: Mineralogical characteristics. *Environmental Science & Technology* 34: 4169-4176 (2000).
- Popa, R. and B.K. Kinkle. Discrimination among iron sulfide species formed in microbial cultures. *Journal of Microbiological Methods* 42: 167-174 (2000).
- Posfai, M., P.R. Buseck, D.A. Bazylinski and R.B. Frankel. Iron sulfides from magnetotactic bacteria: Structure, composition, and phase transitions. *American Mineralogist* 83: 1469-1481 (1998a).
- Posfai, M., P.R. Buseck, D.A. Bazylinski and R.B. Frankel. Reaction sequence of iron sulfide minerals in bacteria and their use as biomarkers. *Science* 280: 880-883 (1998b).
- Poulton, S.W. Sulfide oxidation and iron dissolution kinetics during the reaction of dissolved sulfide with ferrihydrite. *Chemical Geology* 202: 79-94 (2003).
- Poulton, S.W., M.D. Krom and R. Raiswell. A revised scheme for the reactivity of iron (oxyhydr)oxide minerals towards dissolved sulfide. *Geochimica et Cosmochimica Acta* 68: 3703-3715 (2004).
- Pruden, G. and C. Bloomfield. The determination of ferrous sulfide in soil in the presence of ferric oxide. *Analyst* (London) 93: 532-534 (1968).
- Pyzik, A.J. and S.E. Sommer. Sedimentary iron monosulfides: Kinetics and mechanisms of formation. *Geochimica et Cosmochimica Acta* 45: 687-698 (1981).
- Raiswell, R. and D.E. Canfield. Rates of reaction between silicate iron and dissolved sulfide in Peru Margin sediments. *Geochimica et Cosmochimica Acta* 60: 2777-2787 (1996).
- Randall, S.R., D.M. Sherman, and K. Vala Ragnarsdottir. Sorption of As(V) on green rust ($\text{Fe}_4(\text{II})\text{Fe}_2(\text{III})(\text{OH})_{12}\text{SO}_4 \cdot 3\text{H}_2\text{O}$) and lepidocrocite ($\gamma\text{-FeOOH}$): Surface complexes from EXAFS spectroscopy. *Geochimica et Cosmochimica Acta* 65: 1015-1023 (2001).
- Refaat, P., M. Abdelmoula, F. Trolard, J.-M. R. Génin, J.J. Ehrhardt, and G. Bourrié. Mössbauer and XAS study of a green rust mineral; the partial substitution of Fe^{2+} by Mg^{2+} . *American Mineralogist* 86: 731-739 (2001).
- Rickard, D. Kinetics of pyrite formation by the H_2S oxidation of iron(II) monosulfide in aqueous solutions between 25 and 125°C: the rate equation. *Geochimica et Cosmochimica Acta* 61: 115-134 (1997).
- Rickard, D. The solubility of FeS. *Geochimica et Cosmochimica Acta* 70: 5779-5789 (2006).
- Rickard, D. and G.W. Luther. Chemistry of iron sulfides. *Chemical Review* 107, 514-562 (2007).
- Rickard, D. and G.W. Luther. Kinetics of pyrite formation by the H_2S oxidation of iron(II) monosulfide in aqueous solutions between 25 and 125°C: the mechanism. *Geochimica et Cosmochimica Acta* 61: 135-147 (1997).
- Rickard, D. and J.W. Morse. Acid volatile sulfide (AVS). *Marine Chemistry* 97 (2005) 141-197 (2005).
- Rimstidt, J.D. and D.J. Vaughan. Pyrite oxidation: a-state-of-the-art assessment of the reaction mechanism. *Geochimica et Cosmochimica Acta* 67: 873-880 (2003).
- Roberts, A.L., L.A. Totten, W.A. Arnold, D.R. Burris and T.J. Campbell. Reductive elimination of chlorinated ethylenes by zerovalent metals. *Environmental Science & Technology* 30: 2654-2659 (1996).
- Scherer, M.M., E. O'Loughlin, G.F. Parkin, R. Valentine, H. Al-Hosney, R. Handler, C. Just, P. Larese-Casanova, T. Pasakarnis, S. L. Smith. *Sustainability of long-term abiotic*

- attenuation of chlorinated ethenes*. Final Report, SERDP Project ER-1369. (28 September 2007).
- Schoonen, M.A.A. Mechanisms of sedimentary pyrite formation. In *Sulfur Biogeochemistry: Past and Present*. Geological Society of America, Special Paper 379, Boulder, CO (2004).
- Schoonen, M.A.A. and H.L. Barnes. Reactions forming pyrite and marcasite from solution: II. via FeS precursors below 100°C. *Geochimica et Cosmochimica Acta* 55: 1505-1514 (1991).
- Schoonen, M.A. and D.R. Strongin. Catalysis of Electron Transfer Reactions at Mineral Surfaces. In: *Environmental Catalysis*, by V.H. Grassian, Taylor and Francis, pages 37-60, 2005.
- Schwarzenbach, R.P., W. Giger, C. Schaffner and O. Wanner. Groundwater contamination by volatile halogenated alkanes: abiotic formation of volatile sulfur compounds under anaerobic conditions. *Environmental Science & Technology* 19: 322-327 (1985).
- Shao, H. and E.C. Butler. Influence of soil minerals on the rates and products of abiotic transformation of carbon tetrachloride in anaerobic soils and sediments. *Environmental Science & Technology* 43: 1896-1901 (2009).
- Shen, H. and J.T. Wilson. Trichloroethylene removal from groundwater in flow-through columns simulating a permeable reactive barrier constructed with plant mulch. *Environmental Science & Technology* 41: 4077-4083 (2007).
- Sivavec, T.M. and D.P. Horney. Reduction of chlorinated solvents by Fe (II) minerals. In: *Preprints of Papers Presented at the 213th ACS National Meeting*, vol. 37. American Chemical Society: San Francisco, CA, pp. 115-117 (1997).
- Stucki, J. W. The quantitative assay of minerals for Fe²⁺ and Fe³⁺ using 1,10-phenanthroline. II. A photochemical method. *Soil Science Society of America Journal* 45: 638-641 (1981).
- Su, C. and R.W. Puls. Significance of iron(II, III) hydroxycarbonate green rust in arsenic remediation using zerovalent iron in laboratory column tests. *Environmental Science & Technology* 38: 5224-5231 (2004).
- Su, C. and R.T. Wilkin. Arsenate and arsenite sorption on and arsenite oxidation by iron(II,III) hydroxycarbonate green rust. *American Chemical Society Symposium Series* 915: 25-40 (2005).
- Sumoondur, A., S. Shaw, I. Ahmed, and L.G. Benning. Green rust as a precursor for magnetite: An *in situ* synchrotron based study. *Mineralogical Magazine* 72: 201-204 (2008).
- Suzuki, S., K. Shinoda, M. Sato, S. Fujimoto, M. Yamashita, H. Konishi, T. Doi, T. Kamimura, K. Inoue, and Y. Waseda. Changes in chemical state and local structure of green rust by addition of copper sulphate ions. *Corrosion Science* 50: 1761-1765 (2008).
- Szecsody, J.E., J.S. Fruchter, M.D. Williams, V.R. Vermeul and D. Sklarew. In situ chemical reduction of aquifer sediments: Enhancement of reactive iron phases and TCE dechlorination. *Environmental Science & Technology* 38: 4656-4663 (2004).
- Tack, F.M., F. Lapauw and M.G. Verloo. Determination and fractionation of sulphur in a contaminated dredged sediment. *Talanta* 44: 2185-2192 (1997).
- Tandoi, V., T.D. DiStefano, P.A. Bowser, J.M. Gossett and S.H. Zinder. Reductive dehalogenation of chlorinated ethenes and halogenated ethanes by a high-rate anaerobic enrichment culture *Environmental Science & Technology* 28: 973-979 (1994).

- Taylor, L. A. and L. W. Finger. Structural refinement and composition of mackinawite. *Carnegie Institute of Washington Geophysical Laboratory Annual Report* 69: 318-322 (1970).
- Taylor, R.M. Crystal structures of some double hydroxide minerals. *Mineralogical Magazine* 39: 377-389 (1973).
- Taylor, R.M. Formation and properties of Fe(II)/Fe(III) hydroxy-carbonate and its possible significance in soils. *Clay Minerals* 15: 369-382 (1980).
- Taylor, R.M. Stabilization of colour and structure in the pyroaurite-type compounds Fe(II) Fe(III)-hydroxycarbonates. *Clay Minerals* 17: 369-372 (1982).
- Tobler, N.B., T.B. Hofstetter, K.L. Straub, D. Fontana and R.P. Schwarzenbach. Iron-mediated microbial oxidation and abiotic reduction of organic contaminants under anoxic conditions. *Environmental Science & Technology* 41: 7765-7772 (2007).
- Trolard, F., G. Bourrié, M. Abdelmoula, P. Refait, and F. Feder. Fougerite, a new mineral of the pyroaurite-iowaite group: Description and crystal structure. *Clays and Clay Minerals* 55: 323-334 (2007).
- Ulrich, G.A., L.R. Krumholz and J.M. Sufliata. A rapid and simple method for estimating sulfate reduction activity and quantifying inorganic sulfides. *Applied and Environmental Microbiology* 63: 1627-1630 (1997).
- Vaughan, D.J. and J.R. Craig. *Mineral Chemistry of Metal Sulfides*. Cambridge, MA, Cambridge University Press, 1978.
- Vaughan, D.J. and M.S. Ridout. Mössbauer studies of some sulphide minerals. *Journal of Inorganic Nuclear Chemistry* 33: 741-746 (1971).
- Vikesland, P.J., A.M. Heathcock, R.L. Rebodos and K.E. Makus. Particle size and aggregation effects on magnetite reactivity toward carbon tetrachloride. *Environmental Science & Technology* 41: 5277-5283 (2007).
- Vogel, T.M., C.S. Criddle and P.L. McCarty. Transformations of halogenated aliphatic compounds. *Environmental Science & Technology* 21: 722-736 (1987).
- Vogel, T.M. and P.L. McCarty. Abiotic and biotic transformations of 1,1,1-trichloroethane under methanogenic conditions. *Environmental Science & Technology* 21: 1208-1213 (1987).
- Wang, Q. and J.W. Morse. Pyrite formation under conditions approximating those in anoxic sediments: I. Pathway and morphology. *Marine Chemistry* 52: 99-121 (1996).
- Weerasooriya, R. and B. Dharmasena. Pyrite-assisted degradation of trichloroethene (TCE). *Chemosphere* 42: 389-396 (2001).
- Wiedemeier, T.H., M.A. Swanson, D.E. Moutoux, E.K. Gordon, J.T. Wilson, B.H. Wilson, D.H. Kampbell, P.E. Haas, R.N. Miller, J.E. Hansen and F.H. Chapelle. *Technical Protocol for Evaluating Natural Attenuation of Chlorinated Solvents in Ground Water*. EPA/600/R-98/128 (1998).
- Wieder, R.K., G.E. Lang and V.A. Granus. An evaluation of wet chemical methods for quantifying sulfur fractions in freshwater wetland peat. *Limnology and Oceanography* 30: 1109-1115 (1985).
- Wilkin, R.T. *Ground Water Issue: Mineralogical Preservation of Solid Samples Collected from Anoxic Subsurface Environments*. EPA/600/R-06/112 (2006).
- Wilkin, R.T. and K.J. Bischoff. Coulometric determination of total sulfur and reduced inorganic sulfur fractions in environmental samples. *Talanta* 70: 766-773 (2006).
- Wilkin, R.T. and R.W. Puls. *Capstone Report on the Application, Monitoring, and*

- Performance of Permeable Reactive Barriers for Ground-Water Remediation, Volume 1: Performance Evaluations at Two Sites*, EPA Report, EPA/600/R-03/045a, 156 pp. (2003).
- Williams, A.G.B and M.M. Scherer. Kinetics of Cr(VI) reduction by carbonate green rust. *Environmental Science & Technology* 35: 3488–3494 (2001).
- Williams, A.G.B. and M.M. Scherer. Spectroscopic evidence for Fe(II)-Fe(III) electron transfer at the iron oxide-water interface. *Environmental Science & Technology* 38: 4782-4790 (2004).
- Wilson, J.T., K. Banks, R.C. Earle, Y.T. He, T. Kuder and C. Adair. *Natural attenuation of the lead scavengers 1,2-dibromoethane (EDB) and 1,2-dichloroethane (1,2-DCA) at motor fuel release sites and implications for risk management*. USEPA, EPA 600/R-08/107, Ada, OK (2008).
- Wilson, J.T., D.H. Kampbell, M. Ferrey and P. Estueta. *Evaluation of the Protocol for the Natural Attenuation of Chlorinated Solvents: Case Study at the Twin Cities Army Ammunition Plant*. EPA/600/R-01/025, 2001.
- Wolthers, M., S.J. Van der Gaast and D. Rickard. The structure of disordered mackinawite. *American Mineralogist* 88: 2007-2015 (2003).
- Zegeye, A., G. Ona-Nguema, C. Carteret, L. Huguet, M. Abdelmoula, F. Jorand. Formation of hydroxysulphate green rust 2 as a single iron(II-III) mineral in microbial culture. *Geomicrobiology Journal* 22: 389–399 (2005).
- Zegeye, A, C. Ruby, and F. Jorand. Kinetic and thermodynamic analysis during dissimilatory γ -FeOOH reduction: Formation of green rust 1 and magnetite. *Geomicrobiology Journal* 24: 51–64 (2007).
- Zwank, L., M. Elsner, A. Aeberhard, R.P. Schwarzenbach. and S.B. Haderlein. Carbon isotope fractionation in the reductive dehalogenation of carbon tetrachloride at iron (hydr)oxide and iron sulfide minerals. *Environmental Science & Technology* 39: 5634-5641 (2005).

Appendix A

Iron Sulfides

A.1 *Experimental Details Related to TCE Degradation by FeS*

FeS was synthesized by mixing a solution of Fe²⁺ (prepared with ferrous ammonium sulfate) and a solution of NaHS inside an anaerobic glovebox. The mixed solution contained equal molar concentrations of iron and sulfide. NaHS was prepared by reacting N₂-sparged NaOH with 10% H₂S (g/g). The mixed FeS suspension was allowed to settle overnight before removing supernatant. Then, the FeS suspension was transferred into a dialysis bag and dialyzed against filtered tap water that had been sparged with oxygen-free nitrogen gas. The dialysis water was amended with Na₂S to a S²⁻ concentration of approximately 100 mg/L. Based on prior experiments using deionized water, a total of seven washes over three to four days were sufficient to remove all the ions except sodium and sulfide in the synthesized FeS suspension. However, washing with tap water would result in Na⁺, S²⁻ and ions in the tap water being transferred to the solution. After dialysis, the FeS suspension was stored in a glass bottle inside an anaerobic glovebox until use. The content of solid FeS in the suspension was determined gravimetrically.

Filtered tap water was used for dialysis because of its capacity to buffer pH. The tap water was naturally buffered with a bicarbonate buffer system (alkalinity 320 mg/L). Biological buffers were avoided in this study because Danielsen et al. (2005) and other studies have shown that biological buffers have significant impact on the rate of TCE degradation.

FeS directly from the FeS suspension after dialysis was described as non-freeze dried FeS (ND FeS). To prepare freeze dried FeS (FD FeS), the dialyzed FeS suspension was freeze dried with a LABCONCO® Freeze Dry System.

Filtered tap water sparged with oxygen-free nitrogen was used to prepare a ¹³C-labeled TCE stock solution. Experimental incubations were carried out in glass serum vials with a measured volume of 21 mL. To begin an incubation, 20 mL of well mixed suspension containing 20 g/L FeS was transferred to each vial, then 1.05 mL of ¹³C-labeled TCE stock solution was added, and then the vial was sealed without headspace with a Teflon-faced septum and a crimp cap. Controls were prepared with filtered tap water without FeS. Triplicates of control and FeS treatment were prepared for each time interval. To determine the effect of pH, the FeS suspensions were adjusted to pH 5.4, 6.2, 7.2 and 8.4 using 1 M HCl or 1 M NaOH before adding the TCE stock solution. Samples were incubated for different time periods on a Stovall® Low Profile Roller in the dark at room temperature.

A suspension of freeze dried FeS was prepared by sparging filtered tap water with oxygen-free nitrogen, then adding freeze dried FeS to produce a final solid FeS content of 20 g/L. Then the pH was adjusted to 7.2 with 1 M NaOH or 1 M HCl.

To generate a sample for analysis of TCE and daughter products, 0.2-mL samples of the pore water in the experimental systems were added to 20.0 mL filtered tap H₂O (preserved with 2 drops of concentrated HCl) in a glass vial with crimp seal. The diluted sample was contained in a 21-mL glass serum vial that was sealed with a Teflon faced septum and crimp cap. To generate a sample for isotope analysis, 2 mL of original sample were added to 18 mL of filtered tap water in a sealed vial. One original replicate experimental system was used directly to sample for dissolved gases. A helium headspace was created in the vial (2 mL). The vial was shaken to distribute dissolved gasses to the headspace, and

then the headspace was sampled for analysis of methane, ethane, ethylene, and acetylene. The appropriate Henry's Law Constant was used to calculate the original concentration in the water in the experimental system. In addition, pH, Fe²⁺, and S²⁻ concentrations were measured after filtering samples with 0.2- μ m Millipore[®] filter.

Concentrations of [1,2-¹³C] TCE, along with *cis*-DCE, *trans*-DCE, 1,1-DCE, and vinyl chloride were analyzed using gas chromatography/mass spectrometry (GC/MS) according to a modification of the procedures established in EPA Method 5021A, "Volatile Organic Compounds in Various Sample Matrices using Equilibrium Headspace Analysis," in conjunction with EPA Method 8260C, "Volatile Organic Compounds by Gas Chromatography/Mass Spectrometry (GC/MS)". The method detection limit for each compound was 0.001 μ M in the diluted sample, or 0.1 μ M in the original experimental system. Methane, ethylene, ethane, and acetylene were analyzed by injecting headspace gases into a HP Series P200H GC Chromatograph. The detection limit for each hydrocarbon was below 0.076 μ M in the liquid phase. Dissolved organic carbon (DOC) and dissolved inorganic carbon (DIC) in water was analyzed using a Dohrman DC-80 Carbon Analyzer. The method detection limit was 15 μ M. Stable isotope ratios were analyzed by Isotech Laboratories, Inc. (Champaign, IL). The precision of the analyses was 0.1%. Sulfide and Fe²⁺ in water samples were analyzed with a spectrophotometer (Hach DR/2010) using the methylene blue method and the 1,10-phenanthroline method, respectively. The pH was measured using a BNC pH Testr10[®] pH meter.

A.2 Experimental Details Related to EDB Degradation by FeS

The FeS was synthesized the same way as described in Section A.1. An EDB stock solution was prepared in filtered tap water that had been sparged with oxygen-free nitrogen gas. The EDB microcosms in FeS suspension were prepared in serum vials as described above with

the preparation of TCE microcosms. The pH of the FeS suspensions was adjusted to pH 5.4, 6.2, 7.2, and 8.4 using 1M HCl or 1 M NaOH before adding EDB stock solution. The experimental systems were incubated for different time periods on a Stovall[®] Low Profile Roller in the dark at room temperature.

To analyze EDB and daughter products, the 0.2 mL original sample was added to 20.0 mL filtered tap H₂O (preserved with 2 drops of concentrated HCl) in a crimp sealed vial. For isotope analysis, 2 mL of original sample were added to 18 mL of filtered tap water in crimp sealed vial. For dissolved gases measurement, 2 mL of original sample were added into 18 mL of filtered tap water in crimp sealed vial. In addition, pH, Fe²⁺, and S²⁻ concentration were measured after filtering samples with 0.2- μ m Millipore[®] filter. EDB analytical methods followed procedures in appendix D of Wilson et al. (2008).

Experiments described in Section A.1 and Section A.2 were conducted at the Kerr Environmental Research Center.

Appendix B

Magnetite

At the time of this writing (summer 2009), Ferrey et al. (2004) provides the only published information on the rates of degradation of chlorinated organic compounds on naturally occurring magnetite in an aquifer sediment. This appendix describes additional microcosm studies done at the Kerr Center. The microcosms were constructed with sediment from aquifers contaminated with chlorinated solvents.

B.1 Building 102 Site and Site A on the TCAAP, North of St. Paul, Minnesota

The Building 102 site is located in the shallow water table aquifer on the west side of the Twin Cities Army Ammunition Plant (TCAAP) (See Ferrey et al., 2004 and Wilson et al., 2001 for background on the TCAAP). The water table occurs in sand approximately 1.2 to 2.4 m below ground surface. The horizontal ground water velocity was estimated to be 230 m yr⁻¹. The contamination flowed to the north, resulting in a plume that was approximately 40 m wide and 140 m long (Compare Table B.1 and Figure B.1). The contaminants are essentially depleted in 72 m of travel from the most contaminated well. The contaminated ground water is oxygenated much of the time, with some traces of reduced iron and reduced manganese.

Site A was also in the shallow water table aquifer. It is located on the northwest side of the TCAAP. Ground water at Site A was 3 to 6 m below ground surface, with the aquifer ranging in thickness from 3 m near the source area to 9 m to the west. The aquifer sediments are composed of lacustrine silt and fine or medium sands. The ground water seepage velocity is estimated to be 60 m yr⁻¹ at Site A. The area near well 01U108 is considered the primary source of contaminants to the aquifer (Figure B.2). The wells depicted in Figure B.2 have been sampled annually for over 15 years. Over time, the plume is shrinking back toward the source. The ground water at Site A is anoxic. PCE and TCE are reduced to *cis*-DCE, but the concentrations of vinyl chloride are low (Table B.2).

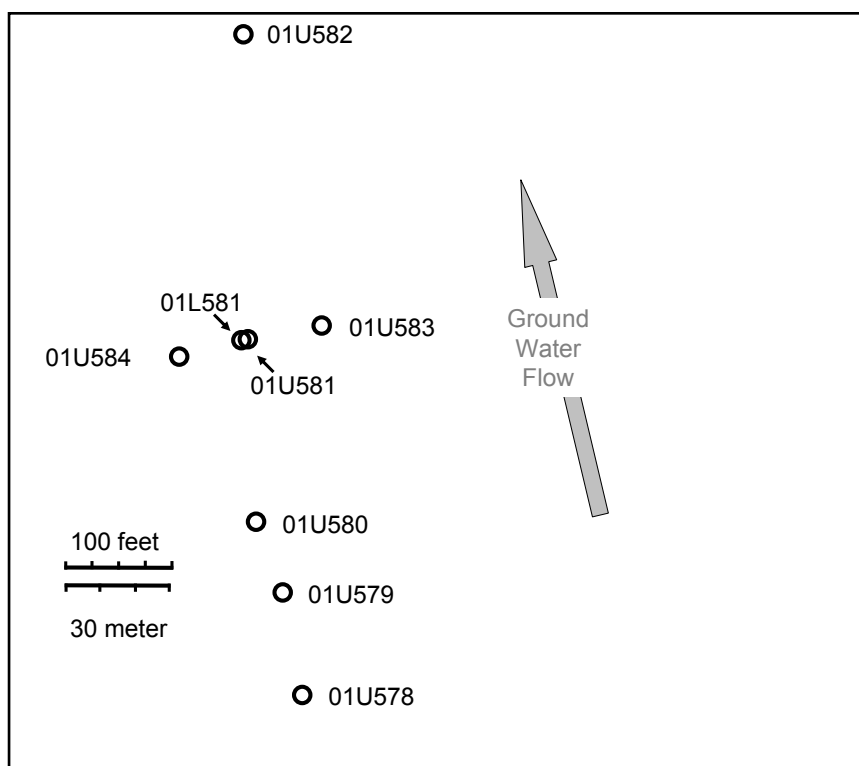


Figure B.1. Orientation of monitoring wells at the Building 102 site on the TCAAP.

Table B.1. Distribution of chlorinated organic compounds and geochemical parameters in ground water at the Building 102 site on the TCAAP in 2005.

Building 102 Site	Distance from source	PCE	TCE	<i>cis</i> -DCE	Vinyl Chloride	O ₂	Fe ²⁺	pH
	m	μg/L	μg/L	μg/L	μg/L	mg/L	mg/L	S.U.
01U578	Background	<1	<1	<1	<1	1.7	1	6.5
01U579	0.0	<1	380	520	6.9	1.6	ND	6.4
01U580	21.3	1	17000	4400	19	2.6	ND	6.6
05U581	71.6	0.4	1.3	8.8	<1	1.7	ND	6.2
05L581	71.6	<1	9.1	7.6	<1	0.7	ND	6.7
01U584	71.6	<1	<1	<1	<1	1.3	ND	6.6
01U583	74.7	1.2	<1	<1	<1	2.3	1.1	6.1
01U582	156.1	<1	<1	<1	<1	4.6	ND	6.6

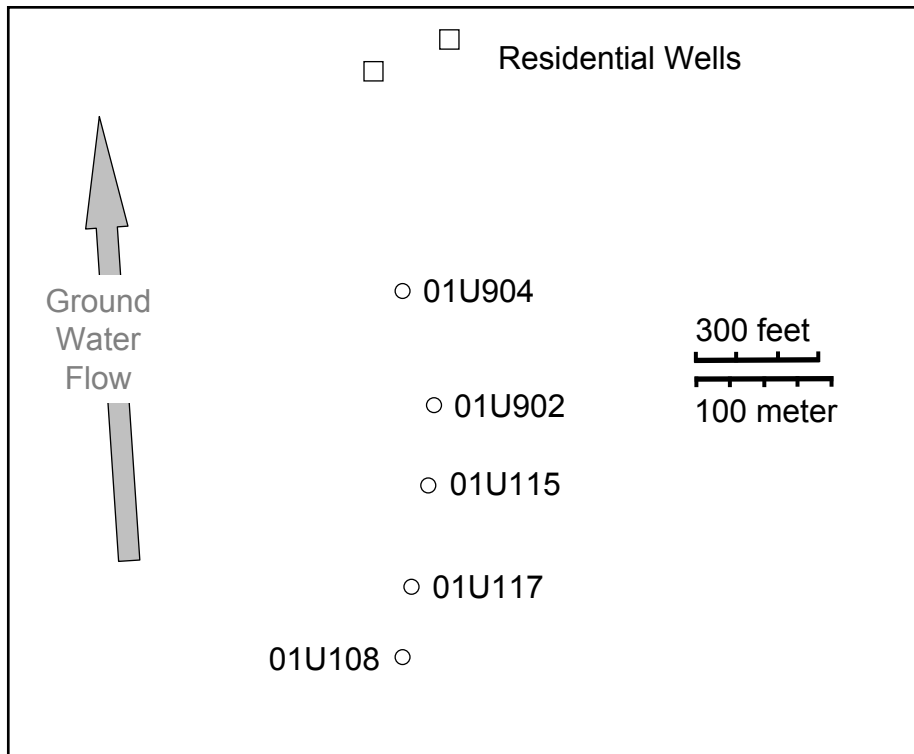


Figure B.2. Orientation of monitoring wells at Site A on the TCAAP.

Table B.2. Distribution of chlorinated organic compounds and geochemical parameters in ground water at Site A on the TCAAP in 1998.

Site A	Distance from source	PCE	TCE	<i>cis</i> -DCE	Vinyl Chloride	O ₂	Fe ²⁺	pH
	m	µg/L	µg/L	µg/L	µg/L	mg/L	mg/L	S.U.
01U067	Background	<1	<1	<1	<1	5.3	<0.1	-
01U108	0	1100	750	800	<1.9	<1	0.4	6.8
01U117	61	78.2	47	200	<1	<1	0.06	7
01U115	137	1.2	13	50	<1	<1	<0.1	7
01U904	293	1.7	71	48	<1	<1	<0.1	-

Sediment was acquired from the Building 102 site and Site A in an acetate sleeve within a coring device that was pushed into the ground water sediment below the water table. The sediments were used to construct a laboratory study of degradation and isotopic fractionation of PCE, TCE, and *cis*-DCE in sediment containing magnetite. To preclude biodegradation of the organics by bacteria that use the chlorinated organic compounds as an electron acceptor, or by iron reducing bacteria that can degrade *cis*-DCE, the sediments were dried to a powder, then autoclaved over night, and then used to construct microcosms. Aseptic technique was used to construct the microcosms. Microcosms were constructed in January 2006.

In previous microcosm experiments, there was one to two mL of water standing above the sediment in each microcosm. These conditions confound experiments intended to monitor isotopic fractionation, because the chlorinated organic compounds in the standing water in the microcosm are not exposed to the reactive minerals, and as a result, the chlorinated organic compounds in the standing water are not fractionated (personal communication Tomasz Kuder, U. Oklahoma, see discussion in Hunkeler et al., 2008).

To construct the microcosms, approximately 35 g of sediment was added to a 25-mL serum bottle, leaving 3 mL of headspace. Then 1.0 mL of water containing the dose of PCE, TCE, or *cis*-DCE was added. The microcosm was sealed and vortexed to mix the dose into the pore water of the microcosm. Then the sediment in the microcosm was allowed to settle, the microcosm was opened, and the standing water was removed. Then the microcosm was sealed using a flat Teflon-coated, grey, butyl rubber septum and crimp cap. To sample the microcosm, the septum was removed and 2.5 mL of RO water was added to the microcosm. The microcosm was resealed, vortexed to mix the water, and then opened for sampling. One mL of standing water was transferred to 14 mL of RO water in

a 20 mL serum bottle, preserved with two drops of HCl, sealed with a septum and crimp cap, and analyzed for volatile organic compounds as described in Ferrey et al. (2004). An additional 1 mL aliquot of standing water was transferred to 14 mL of RO water in a 20-mL serum bottle, preserved with two drops of HCl, sealed with a septum and crimp cap, and analyzed for the ratio of stable carbon isotopes by Tomasz Kuder in Paul Philp's lab at the University of Oklahoma.

Container controls were prepared by adding the dose solutions to sterile RO water in 25-mL serum bottles, and sealing the bottles with the same Teflon faced septa and crimp caps.

Figures B.3, B.4, and B.5 present the removal of PCE, TCE and *cis*-DCE respectively in sediment from the Building 102 site and Site A. Although PCE and TCE were removed in microcosms constructed with sediment from the Building 102 site, the removal of PCE and TCE in the sediment from Site A was significantly slower than the removal in the container controls. The rates of removal of PCE and TCE in the Site A sediment were 0.21 ± 0.15 per year and 0.29 ± 0.10 per year respectively, while that in the container control was 0.80 ± 0.21 per year.

The microcosms were incubated on their sides with wet sand against the septum. The sand would have reduced the surface area available at the septum for diffusion of the organic compounds from water into the septum. Because pore water occupied only 25% to 30% of the total porosity in the sediment, the surface area available for diffusion may have been reduced by a factor of three. In addition, convection currents in the water controls may have allowed fresh water to be presented to the Teflon faced septum that sealed the controls, while mass transfer limitations imposed during diffusion through pore water in the sand in the microcosms may have further reduced loss of TCE from the microcosms. The sediment from Site A on the TCAAP and the sediment from the nearby Baytown Superfund site were similar in texture.

The rate of removal of PCE and TCE in microcosms constructed with sediment from Site A was not used in the calculations which appeared in Section 3, Tables 3.2 and 3.4. However, the rates of removal of PCE and TCE in the microcosms constructed with sediment from Site A were probably better controls on losses from the container than the formal container controls. The rates of removal of PCE and TCE in microcosms constructed with sediment from the Building 102 site were used in calculations in Tables 3.2 and 3.4 without correction for removal in the container controls.

In contrast to the behavior of PCE and TCE, *cis*-DCE was degraded in microcosms constructed with sediment from both sites (Figure B.5).

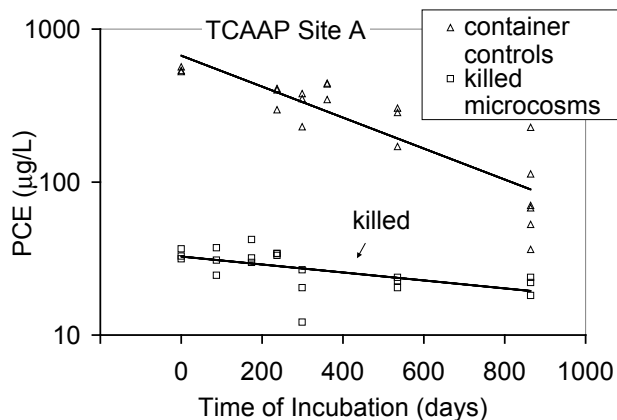
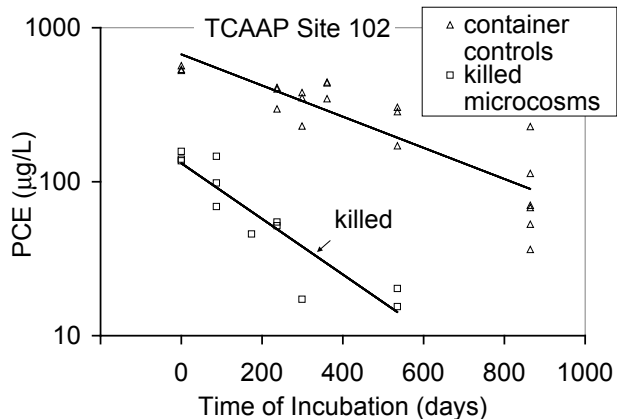


Figure B.3 Removal of PCE in autoclaved sediment from the Building 102 Site and Site A on the former TCAAP, north of St. Paul, MN.

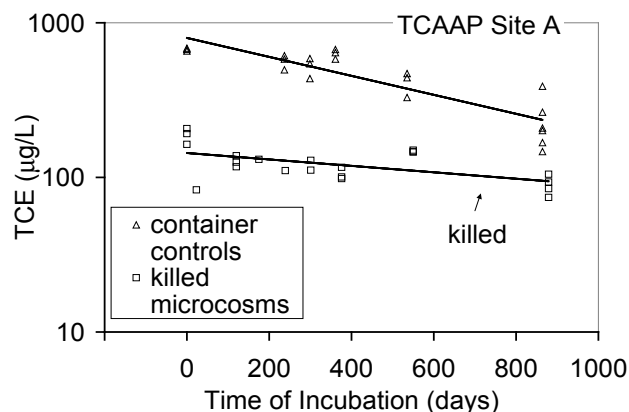
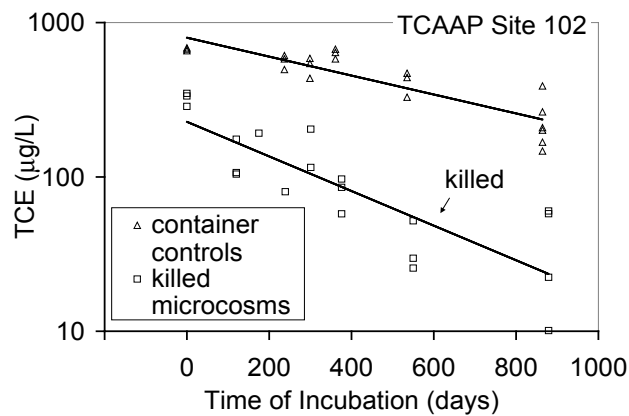


Figure B.4. Removal of TCE in autoclaved sediment from the Building 102 Site and Site A on the former TCAAP, north of St. Paul, MN.

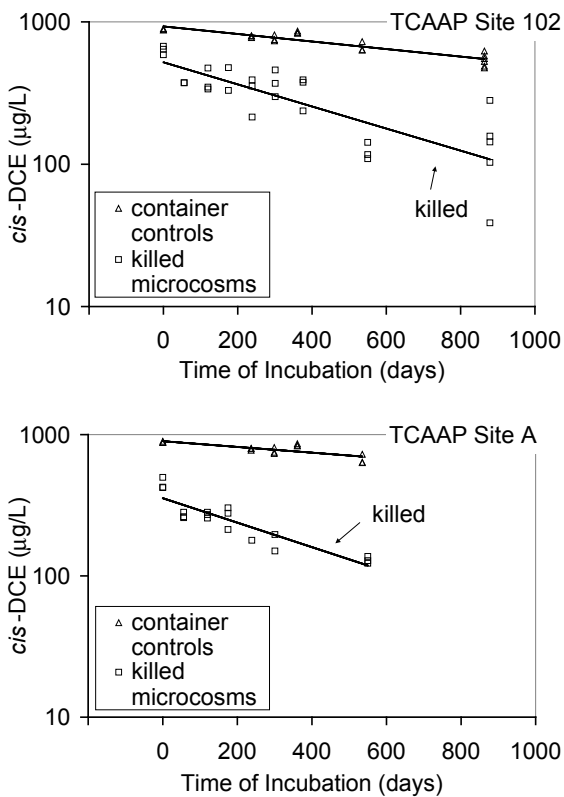


Figure B.5. Removal of *cis*-DCE in autoclaved sediment from the Building 102 Site and Site A on the former TCAAP, north of St. Paul, MN.

B.2 Baytown Superfund Site, Minnesota

TCE releases from a former metal manufacturing shop have contaminated water supply aquifers in portions of Baytown and West Lakeland Townships, and portions of the cities of Baytown and Lake Elmo, in Minnesota. The source of the TCE plume was discovered in 2004. At the source, the water table was in sands and gravels in glacial drift overlying the water supply aquifers in the Prairie du Chien dolomite and underlying Jordan Sandstone. There was up to 50 mg/L TCE in ground water at the source. A hollow stem auger rig and a split spoon sampler were used to acquire sandy sediment from the glacial drift, at a location down gradient from the source of contamination near monitoring well

10B (see Figure B.6) from a depth interval 4.5 to 6.0 meters below the water table. The microcosm study was constructed in January 2004. The microcosms were constructed following procedures described in Ferrey et al. (2004).

Figure B.6 depicts the distribution of TCE in the Prairie du Chien aquifer, and the locations of the source area, and monitoring wells down gradient of the release. Table B.3 compares the concentrations of TCE, *cis*-DCE, and dissolved oxygen along the flow path. Concentrations of oxygen in the ground water were high. There was very little evidence of reductive dechlorination of TCE in the monitoring wells.

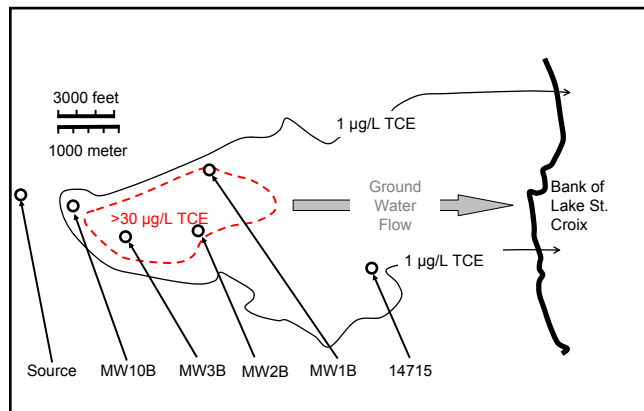


Figure B.6. Relationship between monitoring wells in Table B.3 and TCE contamination in the underlying Prairie Du Chien Aquifer at Baytown Township, MN. TCE concentration contours redrawn from Figure 5a of Minnesota Department of Health (2004).

Table B.3. Distribution of chlorinated organics and dissolved oxygen in the ground water in the Baytown TCE plume.

Location	2003		2005		
	TCE	TCE	<i>cis</i> -DCE	Dissolved Oxygen	pH
	μg/L	μg/L	μg/L	mg/L	S.U.
MW10B	100 to 130	224	0.29	6.0	
MW3B	80	90.7	<0.2	5.8	7.8
MW1B	29 to 38	0.75	<0.2	7.7	
MW2B	20		<0.2		
14715	4	3.29	<0.2		

Figure B.7 compares removal of TCE in the microcosm study conducted with the sediment from Baytown. There was more removal of TCE in the living microcosms than in the autoclaved killed microcosms. To be conservative, the rate of removal of TCE in the autoclaved sediment was taken as the best estimate of removal from abiotic processes. The first order rate constants and the 95% confidence interval on the rate constants are presented in Tables 3.2 and 3.4. There was a small increase in removal of TCE in the killed microcosms over the water control. As discussed previously for sediment from Site A and Site 102 at the TCAAP, the loss of TCE from the water controls probably overestimated loss from the microcosms. The removal of TCE in the killed Baytown microcosms was 0.98 ± 0.49 per year at 95% confidence. The sediment from Baytown and Site A on the TCAAP were similar in texture. The removal of TCE in the Site A sediment was 0.29 ± 0.10 per year at 95% confidence. The removal in the killed microcosms was used in calculations in Tables 3.2 and 3.4 without correction for removal in the water controls.

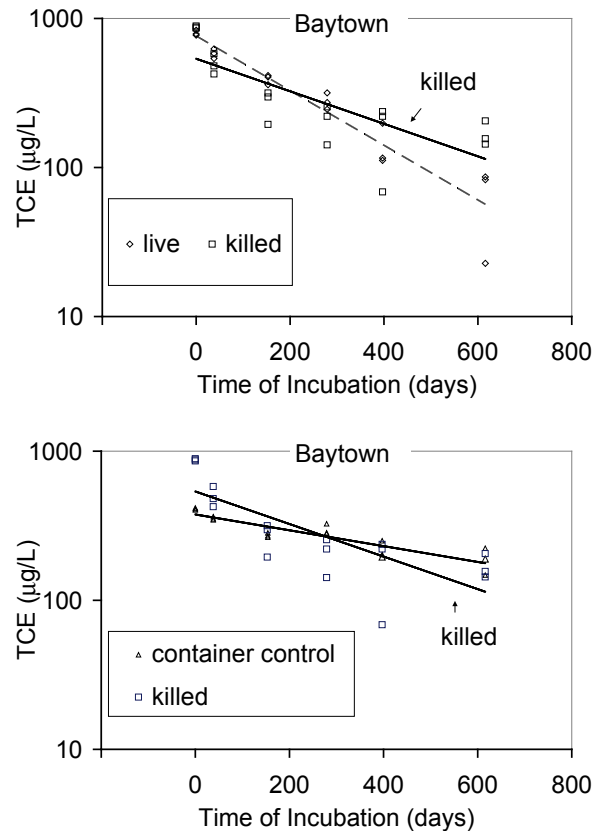


Figure B.7. Removal of TCE in sediment from the Baytown Site, north of St. Paul, Minnesota.

B.3 Thermo-Chem Site, East of Muskegon, Michigan

At the Thermo-Chem site, wastes from a solvent recycling facility had been disposed to a lagoon, resulting in ground water contamination from a mixed NAPL containing petroleum hydrocarbons and chlorinated solvents. The water table aquifer is in glacial outwash sand. The plume of contamination extended to the south toward Black Creek (Figure B.8). The plume discharged from the glacial outwash sand, and entered the sediments in the flood plain of Black Creek, and eventually ground water discharged to Black Creek. Sediment was collected from the bed sediments on the north side of Black Creek. A Geoprobe rod was driven to a depth of 6 meters below land surface. The rod contained a knockout point. The point was dislodged, and

then the rod was pulled back a few centimeters. Sediment and ground water was pumped from the bottom of the rod with plastic tubing and a peristaltic pump. The sediment was retained in a jar as water was allowed to overflow until the jar was filled with sediment.

The sediment was used to construct a microcosm study following the procedures in Ferrey et al. (2004). The microcosm study began in December 2003.

Figure B.8 depicts the distribution of the plume when the sediment sample was collected in 1998. By the time the plume reached the bank of Black Creek, most of the PCE and TCE had been reduced to *cis*-DCE. There was relatively little vinyl chloride detected at the site. The ground water was anoxic and iron-reducing (Table B.4).

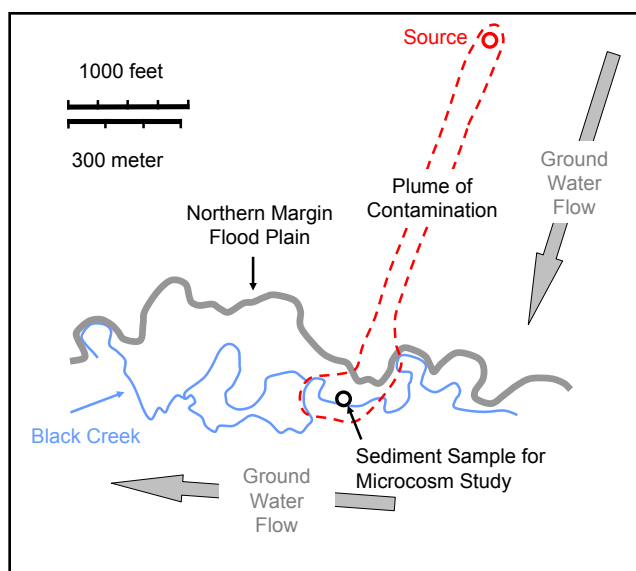


Figure B.8. Location of sediment used for microcosms in the plume of contamination at Thermo-Chem site near Muskegon, Michigan.

Table B.4. Distribution of chlorinated organic compounds and geochemical parameters in ground water on the bank of Black Creek at the Thermo-Chem site in Michigan.

Date	Depth below land surface	PCE	TCE	<i>cis</i> -DCE	Vinyl Chloride	O ₂	Fe ²⁺	pH
	m	µg/L	µg/L	µg/L	µg/L	mg/L	mg/L	S.U.
April 1998	3.5	150	30.4	1100	350	0.2	1.6	
April 1998	4.4	6.6	9	6920	94.9	0.2	1.9	
April 1998	6.2	6	4	8580	17	0	1.65	
Oct 1998	1.7	17.6	0	1.3	3.1	0.5	1.0	6.8
Oct 1998	2.6	43.7	9.4	31.4	65.8	0.32	0.8	7
Oct 1998	3.5	9.4	11.9	1340	235	0.3	2.7	7.4
Oct 1998	4.4	3.7	5.6	7500	135	0.17	6.75	7.1

Removal of *cis*-DCE in sediment from Black Creek in Michigan was similar to removal in sediment from Minnesota. The rate of removal was the same in both living and autoclaved sediments. No vinyl chloride was detected in the microcosms (data not shown).

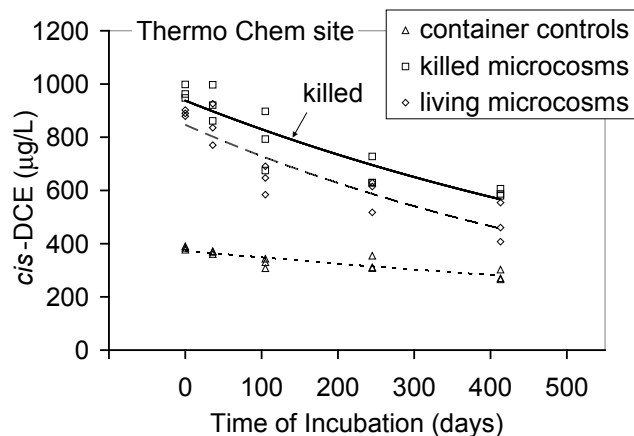


Figure B.9. Removal of *cis*-DCE in sediment from the Thermo-Chem site, east of Muskegon, Michigan.

B.4 Products of Degradation of *cis*-DCE in Sediment from TCAAP Minnesota Site

In an attempt to identify the products of abiotic degradation of *cis*-DCE in the autoclaved sediment described in Ferrey et al. (2004), the experiment was repeated using freshly collected sediment from near monitoring well 03U094 on the TCAAP. The sediment was collected from an interval approximately 1 m below the water table. The sediment corresponded to the “shallow” sediment in Ferrey et al. (2004). One treatment repeated the procedure in Ferrey et al. (2004). The other treatment added ^{14}C -*cis*-DCE to autoclaved sediment and sterile container controls. Figure B.10 presents the time course of removal of *cis*-DCE in the microcosm experiment with unlabelled *cis*-DCE. The microcosm experiment began in December 2003.

After one day and after 375 days of incubation, the contents of the microcosms containing ^{14}C -*cis*-DCE were stirred with a vortex mixer,

and three microcosms and three container controls were opened and the pore water was sampled and distributed for analysis. Two ml of the standing water was preserved with HCl and shipped to Paul Bradley with the U.S.G.S. District Office at Columbia, South Carolina, for analysis of radioactivity in volatile components by gas chromatography and a proportional counter. One ml of the standing water was analyzed for label remaining using a liquid scintillation counter.

In the parallel study using microcosms that were dosed with *cis*-DCE that was not radioactive (see Figure B.10, Table 3.1), the first order rate of disappearance that would be expected for ^{14}C -*cis*-DCE in the microcosms is 0.82 ± 0.39 per year at 95% confidence. At this rate of transformation, after 375 days of incubation, only about 43% of the original ^{14}C label should remain as ^{14}C -*cis*-DCE and about 57% would be transformed to something else. At 95% confidence, from 37% to 81% of the original label should be transformed to something else.

Results are presented in Table B.5. In three microcosms, from 14% to 34% of the total volatile label was recovered as carbon dioxide. The balance of the volatile label was ^{14}C -*cis*-DCE. No other labeled products were detected. In two of three container controls, no carbon dioxide was detected, but in one control, 24% of the total label was recovered as carbon dioxide. The production of carbon dioxide in this one container control has not been explained.

Table B.5. Distribution of ^{14}C from ^{14}C -*cis*-DCE in microcosms and container controls.

Microcosm	Carbon Dioxide	<i>cis</i> -DCE
	Percent of total ^{14}C recovered as a vapor	
2-T5	14	86
7-T5	34	66
11-T5	24	76
Container Control (sterile water, no sediment)		
90W	0	100
100W	24	76
108W	0	100

The only labeled product identified in this study was carbon dioxide, but the yield of ^{14}C label in carbon dioxide was less than would be expected from the transformation of *cis*-DCE. It is likely that other materials were produced in the microcosms, similar to the materials described as non-strippable residue in the microcosm experiments of Darlington et al. (2008).

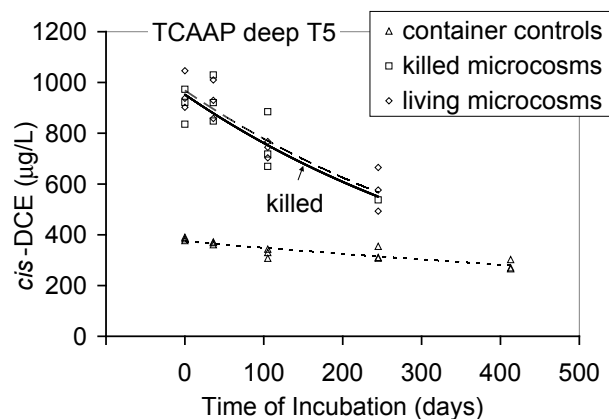


Figure B.10. Removal of *cis*-DCE in autoclaved sediment from the former TCAAP, north of St. Paul, MN.

B.5 Removal of Vinyl Chloride in Sediment from TCAAP Minnesota Site

Figure B.11 presents data on the removal of vinyl chloride in sediment from the TCAAP site. The data was collected as part of the data set for Ferrey et al. (2004), but was not included in

that manuscript because a container control was not done for vinyl chloride. There was a trend toward lower rates of removal in the container controls with fewer chlorine atoms on the parent molecule. The rate of removal of PCE in the container controls was 0.80 ± 0.21 per year, the rate of removal of TCE was as much as 0.49 ± 0.12 per year, and rate of removal of *cis*-DCE was as much as 0.26 ± 0.08 per year (Table 3.1 and 3.2). Based on this trend in the rate of removal of PCE, TCE and *cis*-DCE, the rate of removal of vinyl chloride should be less than the rate of removal of *cis*-DCE. In any case, the removal of vinyl chloride in container controls should not be any faster than the removal of *cis*-DCE.

Work presented in this appendix shows that the removal of PCE from sediment microcosms can be as much as fourfold lower in microcosms filled with sediment compared to the container controls, and the removal of TCE could be twofold lower than removal in container controls (Table 3.2). The true removal of vinyl chloride through diffusion out of the microcosm is probably on the order of 0.13 per year or less. The removal of vinyl chloride in sediment microcosms was 0.311 ± 0.12 per year. The values for vinyl chloride in Tables 3.2 and 3.4 (Section 3) were not corrected for removal in the container controls.

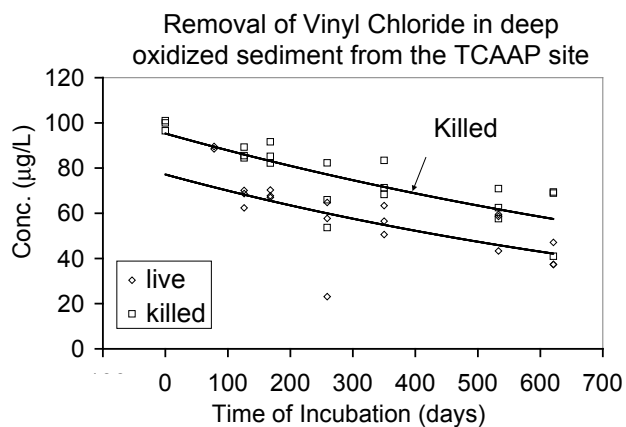


Figure B.11. Removal of vinyl chloride in sediment from the former TCAAP, north of St. Paul, MN.

Appendix C

Materials and Methods for Laboratory Studies of Abiotic Transformation of TCE and Carbon Tetrachloride by Green Rusts

Stoichiometric carbonate green rust and sulfate green rust were synthesized by precipitation of ferrous ions in sulfate-containing solution using ferrous sulfate heptahydrate, sodium hydroxide, sodium carbonate, and sodium bicarbonate followed by oxidation using air bubbles (Su and Wilkin, 2005). After synthesis, green rust suspensions were stored inside an anaerobic glovebox (3-6% H₂ in N₂) before use. The solid concentrations of green rusts in suspensions were determined gravimetrically after washing off dissolved salts with deionized water and drying the solids inside the glovebox. Green rust mineralogy was confirmed by X-ray diffraction. Samples were mixed with glycerol to minimize oxidation during handling and XRD analysis. It was found that carbonate green rust was not stable as it changed to magnetite and Fe(OH)₂ within 48 hours. Therefore, fresh samples were used in the dechlorination tests.

The surface area of the preparation of green rust was measured by the BET N₂ gas adsorption method. Approximately 7 mL of the suspension of sulfate green rust was filtered through a 0.22 μm membrane and then rinsed with 10 mL of deionized and N₂-purged water in the anaerobic glovebox (humidity = 35 to 60%). The sample was then ground to desired fineness by rolling the sample with a Teflon roller for 7 minutes. Samples were then transferred to a Coulter 3100 surface area analyzer in a portable anaerobic chamber to maintain anaerobic conditions. The samples were then out-gassed at 80°C for 15 min before N₂ adsorption took place. Exposure time of the sample to the atmosphere was less than 45 seconds during the procedure. The measured surface area was 28.4 m² g⁻¹.

In the microcosm study involving TCE, appropriate amounts of suspensions of synthetic carbonate green rust or sulfate green rust (0.25 g equivalent dry mass) were added to 60-mL glass serum bottles, then approximately 50 mL of degassed and deionized water was added. Appropriate amounts of a 1000 mg L⁻¹ TCE stock solution were added to create desired initial TCE concentrations (2 to 10 mg L⁻¹) followed by addition of degassed and deionized water to fill the bottles leaving no headspace. The electrolyte concentrations in the 60-mL serum bottles were 0.037 M Na₂SO₄ + 0.030 M Na₂CO₃ (or NaHCO₃) in the carbonate green rust experiments and 0.074 M Na₂SO₄ in the sulfate green rust experiments. The bottles were sealed with Teflon-lined septa and aluminum caps, and then they were removed from the glovebox and shaken on a shaker at 100 rpm in the dark at 23 ± 1°C for up to 30 days.

To evaluate the effect of Fe(II) sorbed to the green rust on TCE degradation, ferrous sulfate was added to some of the suspensions of green rust two hours before TCE addition to bring about a total dissolved Fe(II) concentration of 35 mM. To evaluate the catalytic effect of copper ions, appropriate amounts of a 0.1 M CuSO₄ stock solution were added to make final Cu(II) concentrations at 0.5 to 10 mM to some of the suspensions of green rust, with or without a Trizma buffer (pH 8) two hours before the addition of TCE.

Batch tests involving carbon tetrachloride (initial concentrations near 2 mg L⁻¹) were performed in 60-mL serum bottles with 0.25 g of sulfate green rust at different pH levels

(adjusted with H_2SO_4 and NaOH) in the presence or absence of added CuSO_4 solution over a wide range of time periods up to 15 days.

At pre-set time intervals, the bottles were centrifuged at 3600 rpm for 30 minutes and then they were moved inside the anaerobic glovebox. The clear supernatant solution was transferred using a glass syringe into a 43-mL glass bottle and capped without headspace for analysis of TCE and carbon tetrachloride and their degradation products (dichloroethylene isomers, vinyl chloride, chloroform, chloride, acetylene, ethylene, and ethane). The pH and redox potential were measured on the remaining solution. Dissolved chlorinated hydrocarbons were determined using gas chromatography-mass spectroscopy and dissolved non-chlorinated hydrocarbons by gas chromatography. Finally, 15 mL of solution was filtered through a 0.22- μm membrane and the filtrates were acidified with HCl for total dissolved elements (Fe, B, Si) analyses using Inductively-Coupled Plasma–Optical Emission Spectrometry (ICP-OES).

Data on ratioed concentrations were fitted by linear regression to a pseudo first order rate equation ($\text{Ln } C/C_0 = -kt$), where C is the concentration at reaction time t (h), C_0 is the initial concentration, and k is the rate constant (h^{-1}).

Appendix D

Quality Assurance Documentation

D.1 Analysis of Halogenated Organic Compounds in Water Samples

Concentrations of Carbon Tetrachloride, TCE, ¹³C- labeled TCE, *cis*-DCE, ¹³C-labeled *cis*-DCE, Vinyl Chloride and EDB were determined by headspace gas chromatography/mass spectrometry (GC/MS) using a modification of EPA Method 5021A, "Volatile Organic Compounds in Various Sample Matrices using Equilibrium Headspace Analysis," June 2003. Samples were collected for analysis with an automated static headspace sampler. Analytes were determined by gas chromatography/mass spectrometry using an Ion Trap Detector. The quantitation limit for Carbon Tetrachloride, TCE, ¹³C- labeled TCE, *cis*-DCE, ¹³C-labeled *cis*-DCE and Vinyl Chloride was 1.0 µg/L; the quantitation limit for EDB was 5.0 µg/L.

These are the quantitation limits in the samples provided for analysis to the in-house analytical contractor. In most cases, the samples were acquired from small microcosms, and the samples were diluted before they were delivered to the analyst. Samples for Section 2 were diluted one hundredfold, samples from Section 3 were diluted fifteenfold, and samples from Section 4 were not diluted.

The quality assurance parameters for measurements of data presented in Section 2 are compiled in Tables D.1 and D.2. The symbols under the column labeled "parameter" in the table are as follows. The Continuing Calibration Check (CCC) standards are determined at beginning of each set of samples, after every 20 samples and end of each sequence of samples. The purpose of the CCC standards is to check for changes in the sensitivity of the instrument over time during the analytical run.

A method blank (MB) is determined at the beginning and end of each set of samples. The blank is acquired from the same source of water used to prepare standards and dilute samples to bring them into the range of the calibration curve. The purpose is to determine if there is any background contribution of the analyte of interest from the analytical procedures.

The Matrix Spike (MS) is an analysis of a specially prepared replicate of a sample that has already been analyzed. It is spiked with a known amount of the analyte, and then the total concentration of analyte is determined. The difference between the concentration determined in the sample and the concentration determined in the spiked sample is compared to the concentration that was spiked into the sample. The purpose is to determine if there is a change in the recovery of the analyte from the sample in preparation or analysis of sample. The agreement between the measured increase in concentration with the spike and the expected increase in concentration is an estimate of the accuracy of the determination.

The Secondary Standards (SS) are determined at the beginning of the sample set. They are freshly prepared from some other source of material than the source that was used to prepare the standards used to calibrate the instrument, and CCC standards. Their purpose is to provide an independent check on the standards used to calibrate the instrument.

Duplicates are replicate analyses of the same sample. They are usually prepared by diluting a sample, and then splitting and preparing the sample for duplicate determination of concentrations. Results are expressed as the relative percent difference (RPD), which is the difference between the two separate determinations,

divided by the average of the two determinations, expressed as a percentage. Agreement between duplicates is an expression of analytical precision of the determination.

The column labeled “No.” in the tables is the number of determinations performed for that particular quality parameter. For duplicates, the table reports the number of determinations with results above the method detection limit out of the total number of determinations performed.

Table D.1. Quality of Data on Concentrations of Halogenated Organic Compounds as Determined in Experiments Described in Section 2.

Analyte	Parameter	Acceptable Value, Concentration or Range of Values			Max	Min	No.
		Relative Percent Difference (%)	µg/L	% Expected Value			
Section 2, Figures 2.1 and 2.2.							
¹³ C TCE	CCC			120 to 80	104	92	19
¹³ C TCE	MB		≤0.10		≤0.10		20
¹³ C TCE	MS			130 to 70	109	71	11
¹³ C TCE	SS			120 to 80	96		1
¹³ C TCE	Duplicates	≤25			19.8	2.3	8 of 10
TCE	CCC			120 to 80	117	90	22
TCE	MB		≤0.10		≤0.10		20
TCE	MS			130 to 70	112	88	11
TCE	SS			120 to 80	113	71	15
TCE	Duplicates	≤25			25		1 of 10
¹³ C <i>c</i> -DCE	CCC			120 to 80	Not	Done	
¹³ C <i>c</i> -DCE	MB		≤0.10		≤0.10		14
¹³ C <i>c</i> -DCE	MS			130 to 70	Not	Done	
¹³ C <i>c</i> -DCE	SS			120 to 80	Not	Done	
¹³ C <i>c</i> -DCE	Duplicates	≤25			<MDL		0 of 6
<i>c</i> -DCE	CCC			120 to 80	118	97	22
<i>c</i> -DCE	MB		≤0.10		≤0.10		20
<i>c</i> -DCE	MS			130 to 70	106	91	11
<i>c</i> -DCE	SS			120 to 80	111	100	15
<i>c</i> -DCE	Duplicates	≤25			18.5		1 of 10
Section 2, Figures 2.3 and 2.4.							
EDB	CCC			120 to 80	108	83	13
EDB	MB		≤0.18		≤0.18		13
EDB	MS			130 to 70	111	71	8
EDB	SS			120 to 80	107	83	13
EDB	Duplicates	≤25			11.2	0.49	7 of 8

Table D.2. Quality of Data on Concentrations of Acetylene as Determined in Experiments Described in Section 2.

Analyte	Parameter	Acceptable Value, Concentration or Range of Values			Max	Min	No.
		Relative Percent Difference (%)	ppm (v/v)	% Nominal Value			
Section 2 Figure 2.1							
C ₂ H ₂	CCC			115 to 85	103	91	11
C ₂ H ₂	MB		≤1.63		≤1.63		10
C ₂ H ₂	SS			115 to 85	101	94	5
C ₂ H ₂	Duplicates	≤20			13.8	0	8 of 15

All the quality parameters for concentrations of halogenated organic compounds and acetylene were within the acceptance limits, and data from all of the samples in the experiments were used in the figures and in calculations.

The quality assurance parameters for measurements of data presented in Section 3 are compiled in Table D.3. As indicated by the * in the table, the Duplicates were out of range

for determination of PCE, and both the MS and Duplicates were out of range for determination of TCE in three sample sets. Data from these sample sets were not used in the figures and in calculations. The quality parameters for concentrations of halogenated organic compounds in all of the other sample sets were within the acceptance limits, and data from all of the other sample sets in the experiments were used in the figures and in calculations.

Table D.3. Quality of Data on Concentrations of Halogenated Organic Compounds as Determined in Experiments Described in Section 3 and Appendix B.

Analyte	Parameter	Acceptable Value, Concentration or Range of Values			Max	Min	No.
		RPD (%)	µg/L	% Nominal Value			
Appendix B, Site A and Site 102, Figures B.3, B.4, and B.5.							
PCE	CCC			120 to 80	119	9192	45
PCE	MB		≤0.10		≤0.10		37
PCE	MS			130 to 70	112	82	15
PCE	SS			120 to 80	110	91	20
PCE	Duplicates	≤25			63*	5	12 of 19
TCE	CCC			120 to 80	107	93	45
TCE	MB		≤0.10		≤0.10		37
TCE	MS			130 to 70	106	57*	15
TCE	SS			120 to 80	105	91	20
TCE	Duplicates	≤25			64*	3	11 of 10
<i>c</i> -DCE	CCC			120 to 80	110	86	45
<i>c</i> -DCE	MB		≤0.10		≤0.10		37
<i>c</i> -DCE	MS			130 to 70			11
<i>c</i> -DCE	SS			120 to 80	114	82	15
<i>c</i> -DCE	Duplicates	≤25			17	2.4	11 of 19
Appendix B, Baytown Site, Figures B.7 and B.8.							
TCE	CCC			120 to 80	117	92	12
TCE	MB		≤0.10		≤0.10		16
TCE	MS			130 to 70	117	96	6
TCE	SS			120 to 80	118	96	13
TCE	Duplicates	≤25			15	5.7	6 of 6
Appendix B, Thermo Chem and TCAAP5 Site, Figures B.9 and B.10.							
<i>c</i> -DCE	CCC			120 to 80	104	97	7
<i>c</i> -DCE	MB		≤0.10		≤0.10		11
<i>c</i> -DCE	MS			130 to 70	109	96	5
<i>c</i> -DCE	SS			120 to 80	108	91	12
<i>c</i> -DCE	Duplicates	≤25			21	0.4	5 of 5
Appendix B, TCAAP deep, Figure B.11							
VC	CCC			120 to 80	115	82	15
VC	MB		≤0.10		≤0.10		8
VC	MS			130 to 70	113	93	2
VC	Duplicates	≤25			<MDL		0 of 2

* Determinations of PCE and TCE in container controls corresponding to 60, 96, and 174 days of incubation are not included in the figures or data analysis.

The quality assurance parameters for measurements of data presented in Section 4 are compiled in Table D.4. All the quality parameters for concentrations of halogenated

organic compounds were within the acceptance limits, and data from all of the samples in the experiments were used in the figures and in calculations.

Table D.4. Quality of Data on Concentrations of Halogenated Organic Compounds as Determined in Experiments Described in Section 4.

Analyte	Parameter	Acceptable Value, Concentration or Range of Values			Max	Min	No.
		RPD (%)	µg/L	% Expected Value			
Section 4							
CCl ₄	CCC			120 to 80	112	81	85
CCl ₄	MB		≤0.10		≤0.10		75
CCl ₄	MS			130 to 70	111	93	25
CCl ₄	SS			120 to 80	113	86	59
CCl ₄	Duplicates	≤25			<MDL		0 of 23
TCE	CCC			120 to 80	120	89	85
TCE	MB		≤0.10		≤0.10		75
TCE	MS			130 to 70	124	76	25
TCE	SS			120 to 80	111	91	59
TCE	Duplicates	≤25			9.8	0.91	23 of 23

D.2 Analysis of Ratio of Stable Isotopes of Carbon in TCE and *cis*-DCE

The compound-specific stable isotope analysis (CSIA) of TCE, and *cis*-DCE in water was conducted in the Stable Isotope Laboratory of the University of Oklahoma. Because the method has not been published elsewhere, it is described in detail in this section. The method combines purge-and-trap (PT) extraction and gas chromatography–isotope ratio mass spectrometry (GC–IRMS) for chromatographic separation of the analytes and determination of their isotope ratios.

The TCE and *cis*-DCE are extracted from the water by a PT unit (either model OI 4560 or OI

4660). The GC–IRMS instrument is a combination of a Varian 3410 GC and a Thermo Finnigan MAT 252 IRMS. The purge and trap transfer line connects to a polar-phase pre-column that is used to separate water prior to LN₂ cryofocusing. Analytes eluting from the pre-column are focused on a liquid nitrogen trap and then the analytes are separated on a non-polar GC column prior to isotope ratio determination. The two columns, cryofocuser and the transfer line are interfaced through a 6-port switching valve resulting in splitless refocusing of the PT effluent.

After GC separation, the analytes are converted to CO₂ in an inline combustion reactor

containing Ni-Pt kept at 940°C. An auxiliary O₂ stream is mingled with carrier gas upstream of the reactor to facilitate more efficient combustion of the analytes. Combustion to CO₂ does not affect chromatographic resolution.

The CO₂ peaks are introduced into the IRMS for determination of carbon isotope ratios. Raw output of the IRMS consists of three simultaneously acquired signal channels, corresponding to CO₂ with variable C and O isotope substitution. Integration of the individual channel outputs over the peak's retention time window provides ¹³C/¹²C ratios of each GC peak.

Rather than measuring the absolute ratios of isotope species, IRMS technique relies on data normalization relative to internal standard of known isotopic composition. A number of pulses of standard gas (CO₂) are introduced into the IRMS's source during the run to provide a reference ¹³C/¹²C signal to compare to the signal derived from the analytical sample. This configuration permits high-precision determination of δ¹³C (the total analytical error of δ¹³C is ± 0.5‰ or better) in chlorinated ethenes at concentrations as low 2 to 3 µg/l in a 25 ml sample.

The analysis was conducted using the following parameters.

The analytes were purged from a 25-ml water sample. The purge gas was helium. The water sample was purged at a flow rate of 40 ml/min for 12 min. The sample temperature was 50 °C. The trap was a Vocab 3000. The temperature program that was used is the manufacturer's default for this type of sorbent. After the sample was purged, dry helium was delivered to the trap for 3 min. The PT trap was then desorbed for 5 min using helium at a flow rate of 6 to 8 ml min.

The pre-column was a 0.5 µm film DB-Carbowax column, 25m × 0.25mm. The flow rate of helium carrier gas was 6 to 8 ml/min., isothermal at 40° C for 6 minutes

with LN2 cryofocusing. The final separation on analytes was on a DB-MTBE, 60m × 0.32mm column. The flow rate of helium carrier gas was 1.8 ml/min. The GC column was held isothermal at 40 °C for 9 min, and then ramped at 6 °C/min. After elution of the last peak of interest, the columns were cleaned by baking them at 240 °C for 15 min.

The MAT 252 IRMS was operated at 8kV, focused for "high linearity." Due to sample size limitations, some of the data were obtained with the IRMS focused for "high sensitivity." Tuning for "high sensitivity" permitted analysis of lower concentrations in samples but required a more stringent QAQC procedure in the samples to assure that their respective peak sizes were matched. The concentrations of the spiked compounds in the external standard runs were very close to the target analyte concentrations.

Method bias associated with sample preparation and analytical reproducibility were determined daily by analysis of an external standard (water spiked with DCE, TCE, and PCE of known isotope composition) that was run through the PT-GCIRMS cycle, using identical method parameters as the analyzed samples. The external standard is the equivalent of a CCC standard as discussed above. At regular intervals, the external samples are checked against a known reference sample (Vienna PDB, provided by the International Atomic Energy Agency in Vienna, Austria). The V-PDB sample serves as the SS standard.

The quality assurance parameters for measurements of data presented in Section 3 are compiled in Table D.5. The acceptance value for replicate analyses of the external standards was a sample standard deviation of ± 0.5‰ or less. All three sample sets were within the acceptance level (Table D.5). The determined values in the analytical samples were corrected for the bias associated with sample preparation in their particular sample set, before they were plotted in figures or used in calculations.

Duplicate analyses for $\delta^{13}\text{C}$ of *cis*-DCE were performed on 4 out of 14 samples. Duplicates differed from each other in a range of 0.2‰ to 0.6‰. This was within the expected agreement between duplicates of 1‰. Duplicate analyses for $\delta^{13}\text{C}$ of TCE were performed on 3 out of 14 samples. Two of the sets of duplicates (analyzed

in “high linearity” mode) differed from each other at 0.2‰ and 0.8‰. One of the set of duplicates was analyzed in “high sensitivity” mode. The agreement was 0.1‰. Two samples depicted in Figure 3.7 were analyzed in “high sensitivity” mode. The two samples with greater uncertainty were identified in the figure.

Table D.5. Quality parameters for analysis of $\delta^{13}\text{C}$ in TCE and *cis*-DCE.

TCE				<i>cis</i> -DCE	
Set 1		Set 2		Set 1	
10/10/2008 to 10/14/2008		10/14/2008 to 10/16/2008		10/8/2008 to 10/17/2008	
Run #	$\delta^{13}\text{C}$	Run #	$\delta^{13}\text{C}$	Run #	$\delta^{13}\text{C}$
	‰		‰		‰
4164	-30.0	4184	-30.4	4143	-24.8
4165	-30.2	4190	-31.3	4144	-24.7
4171	-30.6	4191	-30.3	4150	-24.9
4172	-30.2	4197	-31.2	4153	-24.8
4178	-30.6	4198	-30.6	4159	-25.3
4179	-30.2	4202	-30.8	4164	-25.2
4181	-30.1	4206	-30.6	4165	-24.8
4182	-30.1			4171	-24.8
				4172	-24.6
average	-30.3	average	-30.7	average	-25.0
stdev	0.2	stdev	0.4	stdev	0.3
reference $\delta^{13}\text{C}$	-30.7	reference $\delta^{13}\text{C}$	-30.7	reference $\delta^{13}\text{C}$	-26.1
bias correction	-0.4	bias correction	0.0	bias correction	-1.1
average	-30.3	average	-30.7	average	-25.0
stdev	0.2	stdev	0.4	stdev	0.3

D.3 Analysis of Total Iron in Sediment

Samples of the sediment used to construct the microcosms were extracted in nitric acid by microwave digestion using a CEM Corporation Microwave Accelerated Reaction System, Model MARS5. Samples were digested at approximately 175°C in 10% nitric acid. The extracts

were analyzed for the concentration of total iron by Inductively Coupled Plasma-Atomic Emission Spectroscopy using a Perkin Elmer Optima 3000DV emission spectroscope. All the quality parameters for concentrations of total iron in nitric acid digests were within the acceptance limits, and data from all of the samples in the experiments were used in the calculations.

Table D.6. Quality of Data on Concentrations of Total Iron in Sediment as Determined in Experiments Described in Section 3.

Analyte	Parameter	Acceptable Value, Concentration or Range of Values			Max	Min	No.
		RPD (%)	mg/L	% Expected Value			
Total Iron	CCC			110 to 90	102	99.5	8
Total Iron	MB		≤0.10		≤0.10		9
Total Iron	MS			110 to 90	108	90	4
Total Iron	SS			110 to 90	106	101	4
Total Iron	Duplicates	≤20			8.4	0.1	7

D.4 Analysis of Sodium, Potassium, Calcium, Magnesium, and Iron in Water Samples

Water samples were analyzed for the concentration of total iron by Inductively Coupled Plasma-Atomic Emission Spectroscopy using a Perkin Elmer Optima 3000DV emission spectroscope. If concentrations of iron in samples collected in November 2008 were below the detection limit for Inductively Coupled Plasma-Atomic Emission Spectroscopy, they were analyzed by Inductively Coupled Plasma Mass Spectrometry on a Thermo Elemental PQExcell Plasma Mass Spectrometer.

The quality assurance parameters for measurements of data presented in Section 1 are compiled in Table D.7. One of the method blanks for sodium was slightly over twice the acceptable value according to the relevant SOP. The value in the blank was 0.2 mg/L and the values

returned from the field were all in excess of 300 mg/L. The presence of sodium in the blank at 0.2 mg/L has no effect on the data quality for sodium.

The MS samples were routinely spiked to increase the concentration of analyte by 2 mg/L. The concentration of calcium and magnesium in the matrix spikes were less than the concentration determined in the sample. The concentrations in the samples were greater than 300 mg/L for calcium and greater than 100 mg/L for magnesium. The spiked concentration was too low to allow adequate resolution over the ambient concentrations. All the other quality parameters for concentrations of sodium, potassium, calcium, magnesium, and iron in water were within the acceptance limits, and data from all of the samples in the experiments were used in the calculations.

Table D.7. Quality of Data on Concentrations of Sodium, Potassium, Calcium, Magnesium and Iron used in the Geochemical Modeling in Section 1.

Analyte	Parameter	Acceptable Value, Concentration or Range of Values			Max	Min	No.
		RPD (%)	mg/L	Expected Value (%)			
Sodium	CCC			110 to 90	102	98.6	4
Sodium	MB		≤0.091		0.217*		10
Sodium	MS			110 to 90	Not	Done	
Sodium	SS			110 to 90	102	98.8	5
Sodium	Duplicates	≤20			1.47	0.95	5 of 5
Potassium	CCC			110 to 90	105	100	4
Potassium	MB		≤0.092		≤0.092		10
Potassium	MS			110 to 90	Not	Done	
Potassium	SS			110 to 90	101	98.2	5
Potassium	Duplicates	≤20			8.3	1.15	5 of 5
Calcium	CCC			110 to 90	104	99	8
Calcium	MB		≤0.001		≤0.001		10
Calcium	MS			110 to 90	NA		1
Calcium	SS			110 to 90	100	98.6	5
Calcium	Duplicates	≤20			1.92	0.45	5 of 5
Magnesium	CCC			110 to 90	106	97.5	
Magnesium	MB		≤0.023		≤0.023		10
Magnesium	MS			110 to 90	NA		1
Magnesium	SS			110 to 90	99.8	97.4	5
Magnesium	Duplicates	≤20			1.42	0	3 of 5
Inductively Coupled Plasma-Atomic Emission Spectroscopy							
Iron	CCC			110 to 90	100	97.5	10
Iron	MB		≤0.008		≤0.008		10
Iron	MS			110 to 90	106	96.5	4
Iron	SS			110 to 90	103	100	5
Iron	Duplicates	≤20			1.39	1.03	2 of 5
Inductively Coupled Plasma Mass Spectrometry							
Iron	CCC			110 to 90	108	99.1	3
Iron	MB		≤0.0003		≤0.0003		3
Iron	MS			110 to 90	100		1
Iron	SS			110 to 90	100		1
Iron	Duplicates	≤20			5.17		1

* One sample out of acceptable range.

D.5 Analysis of Sulfate and Chloride in Water Samples

Concentrations of sulfate and chloride were determined by capillary ion electrophoresis with indirect UV detection using a Quanta 4000 Capillary Ion Analyzer.

One of the SS samples was slightly out of range. All the other quality parameters for concentrations of chloride and sulfate in water were within the acceptance limits, and data from all of the samples in the experiments were used in the calculations.

Table D.8. Quality of Data on Concentrations of Sulfate and Chloride used in the Geochemical Modeling in Section 1.

Analyte	Parameter	Acceptable Value, Concentration or Range of Values			Max	Min	No.
		RPD (%)	mg/L	% Expected Value			
Sulfate	CCC			110 to 90	105	90.8	18
Sulfate	MB		≤0.137		≤0.137		10
Sulfate	MS			120 to 80	101	84.7	7
Sulfate	SS			110 to 90	98.4	92	6
Sulfate	Duplicates	≤20			2.08	0	13
Chloride	CCC			110 to 90	105	92.6	18
Chloride	MB		≤0.113		≤0.113		10
Chloride	MS			120 to 80	100	87.8	7
Chloride	SS			110 to 90	95.1	88.6*	6
Chloride	Duplicates	≤20			2.1	0	13

*One sample out of acceptable range.

D.6 Analysis of Sulfide in Water Samples

Sulfide concentrations in water samples as described in Table 1.2 and Figure 1.3 were measured with a spectrophotometer (Hach DR/2010) at wavelength 665 nm using the methylene blue method (Standard Method 4500 D, Clesceri et al., 1999). Many of the samples exceeded 100 mg/L sulfide. If a sample was out of range, it was diluted in oxygen free distilled water to bring it into range.

D.7 Determination of Magnetic Susceptibility

In each sample set, the nominal value of the Magnetic Susceptibility of the calibration standard ($2.66 \times 10^{-6} \text{ m}^3 \text{ kg}^{-1}$) was compared to the actual reading. For five sets of samples, the relative percent difference (RPD) between the measured value of the calibration standard and the nominal value of the calibration standard ranged from 0.02% to 0.53%. Each sediment sample was determined in duplicate, and sometimes in triplicate. In the case of triplicate analyses, the

RPD was calculated between the first and second replicate, and the first and third replicate. For 24 duplicate determinations on sediment samples, the RPD varied between 1.2% and 21.5%. The median value of RPD was 6.4%.

The sediment cores were blended by hand before they were used to construct microcosms, and were sampled for determination of mass magnetic susceptibility. The RPD included error in the measurement of the mass magnetic susceptibility as well as variation in the content of magnetic materials from one 10 cm³ sample to the next. It is likely that most of the variability from sediment sample to sediment sample in the material used to construct each of the treatments of the microcosm studies reflected variation in the concentration of magnetite in the sediment.

D.8 Scintillation Counting

The following applies to the experiments in Section B.5. Liquid Scintillation Counting was used to estimate the amount of ¹⁴C radio-label that was associated with pore water in the microcosms or container controls, and with sediment solids in the microcosms.

The solution of ¹⁴C *cis*-DCE that was used to spike the microcosms and container controls and to prepare standards was prepared from neat ¹⁴C *cis*-DCE that was supplied by American Radiolabeled Chemicals, Inc. The specific activity was 2.0 mCi/mMole. The ¹⁴C *cis*-DCE was provided without a carrier such as ethanol, and without a stabilizer. The liquid contents of the glass ampoule (approximately 6.5 μL) were taken up into a 10 μL syringe, and transferred to 70 ml of RO water in a glass serum bottle. The bottle was sealed with a Teflon faced septum, and stirred over night with a magnetic stir bar to dissolve the ¹⁴C *cis*-DCE. This became the stock solution used to dose the microcosms and container controls, and to estimate the counting efficiency of the scintillation counter. Each microcosm or container control received 1.0 ml of stock solution. The ¹⁴C in the stock solution produced 3.49×10^6 dpm/ml.

The counting efficiency of the water samples was determined by counting a ¹⁴C Standard Spike of the stock solution. To prepare the ¹⁴C Standard Spike, 100 μl of the *cis*-DCE dissolved in 900 μl of autoclaved RO water was transferred to 6 ml of Beckman Ready Safe Scintillation Cocktail. Samples were calculated against the efficiency of this known standard by counting 1 ml of water from the microcosms in 6 ml Beckman Ready Safe Scintillation Cocktail. Program A2 was used on the LKB Liquid Scintillation Counter with a count time of 60 minutes. The Error Range was 0.744% to 1.33%. The sample counts used in calculations were corrected for counting efficiency.

Soil samples were counted as follows: 0.2 g soil was suspended in 8 ml Beckman Ready Value Scintillation Cocktail and 7 ml autoclaved RO water in a 20 ml scintillation vial (the vial was vigorously shaken to suspend the soil particles for scintillation counting). Program 3 on the Beckman LS5000TD Liquid Scintillation Counter was used for counting. The count time was 60 minutes. The counting efficiency for soil gel samples was 70% to 81%. Sample counts used in calculations were corrected for counting efficiency.

ISSUE
PERMIT



PRESORTED STANDARD
POSTAGE & FEES PAID
EPA
PERMIT NO. G-35

Office of Research and Development (8101R)
Washington, DC 20460

Official Business
Penalty for Private Use
\$300

Identification and Characterization Methods for Reactive Minerals Responsible for Natural Attenuation of Chlorinated Organic Compounds

